Contract No. DACA67-00-D-2002, Task Order No. 1
Seismic Ground Motion Study for
Skookumchuck Dam
Lewis County, Washington

March 2001

Submitted To:
Seattle District
U.S. Army Corps of Engineers
P. O. Box 3755
Seattle, Washington 98124-2255

By:
Shannon & Wilson, Inc.
400 N 34th Street, Suite 100
Seattle, Washington 98103

21-1-08920-001

SHANNON & WILSON, INC.
GEOTECHNICAL AND ENVIRONMENTAL CONSULTANTS

SEATTLE
RICHLAND
FAIRBANKS
ANCHORAGE
DENVER
SAINT LOUIS
BOSTON

March 5, 2001

Department of the Army
Seattle District, Corps of Engineers
P.O. Box 3755
Seattle, WA 98124-2255

Attn: CENWS-EC-TB-GE
Lawrence V. Mann

RE: CONTRACT NO. DACA67-00-D-2002, TASK ORDER NO. 1, SEISMIC GROUND MOTION STUDY FOR SKOOKUMCHUCK DAM PROJECT, LEWIS COUNTY, WASHINGTON

Please find enclosed twenty copies of our final report for the referenced project. This report presents the final results of our ground motion study.

If you have any questions or require further information, please contact me or Bill Perkins at (206) 632-8020.

Sincerely,

SHANNON & WILSON, INC.

Gerard J. Buechel, P.E.
Vice President

RAM:GJB/ram

Enclosure: Twenty Copies of Seismic Ground Motion Study Report

21-1-08920-001-R2-L1/WP/MGI

400 NORTH 34TH STREET · SUITE 100
P.O. BOX 300303
SEATTLE, WASHINGTON 98103
206·632·8020 FAX 206·695·6777
TDD: 1·800·833·6388

TABLE OF CONTENTS

Page

LIST OF TABLES

Table No.

LIST OF FIGURES

Figure No.

LIST OF FIGURES (cont.)

Figure No.

LIST OF FIGURES (cont.)

Figure No.

LIST OF APPENDICES

Appendix No.

CONTRACT NO. DACA67-00-D-2002, TASK ORDER NO. 1
SEISMIC GROUND MOTION STUDY FOR
SKOOKUMCHUCK DAM SITE
LEWIS COUNTY, WASHINGTON

1.0 INTRODUCTION

1.1 PURPOSE AND SCOPE

This report presents the results of our seismic ground motion study for the Skookumchuck Dam. The objective of this study is to develop peak ground motions, duration, spectra and three component time histories for an Operating Basis Earthquake (OBE), Intermediate Design Earthquake (IDE), and Maximum Credible Earthquake (MCE) as outlined in the revised Statement of Work (SOW) dated February 10, 2000 by the Department of the Army, Seattle District, Corps of Engineers. A summary description of these events is as follows:

- OBE – An event with a 50 percent probability of exceedance during the service life of the structures, and assuming a service life of 100 years, this event will correspond to a return period of 144 years.
- IDE – An event with a 500-year recurrence interval.
- MCE – The greatest earthquake that can reasonably be generated by a specific source.

The specific ground motion parameters (deliverables) outlined in the SOW for each of the events consist of the following:

- Peak Ground Acceleration (PGA)
- Peak Ground Velocity (PV)
- Peak Ground Displacement (PD)
- Duration of shaking at levels exceeding 0.05g
- Horizontal and vertical response spectra at 2, 5, 10, and 20 percent damping
- One set of time histories consisting of 2 horizontal orthogonal motions and 1 vertical motion

For the MCE, the median and median-plus-one-standard-deviation estimates of the PGA, PV, PD, and response spectra are required. The median and median-plus-one-standard-deviation ground motions are intended to represent the greatest ground motions that can reasonably be expected at the dam site.

To provide the ground motions parameters outlined in the SOW, the scope of work includes the following tasks.

- Characterizing the significant seismic sources in the region of the dam. Seismic sources are characterized in terms of the location, geometry, maximum earthquake magnitude, and earthquake recurrence rate.
- Performing probabilistic seismic hazard analyses (PSHA) and developing hazard curves (ground motion amplitude versus frequency of exceedance curves) for PGA and response spectral values.
- Performing deterministic seismic hazard analyses (DSHA) and developing PGA and response spectral values.
- Developing three sets of three-component (two horizontal and one vertical) time histories, one each for the OBE, IDE, and MCE.

1.2 SITE DESCRIPTION

The Skookumchuck dam is located in western Washington on the Skookumchuck River, approximately 11 kilometers upstream (east) of Bucoda and 19 kilometers northeast of Centralia at approximately 122.72 degrees west longitude and 46.78 degrees north latitude (Figure 1-1). The dam is a rolled earthfill structure consisting of a silt core and sandy gravel shells with a vertical height of approximately 160 feet above the original streambed. At the crest, the dam is approximately 1,340 feet long (north-south) with width of approximately 30 feet. An ungated spillway, excavated into rock, is located at the south abutment. Both abutments, the entire dam south of the original river channel, and the core north of the channel are founded on rock; the outer shells north of the original river channel in alluvial deposits.

1.3 ACKNOWLEDGEMENTS

The compilation of this report involved the participation of many individuals. We acknowledge Dr. Steve Kramer who provided specific input to the earthquake source zone characterization and seismic hazard analysis. Dr. Walt Silva of Pacific Engineering and Analysis performed the finite fault modeling of the Cascadia Subduction Zone, developed vertical time histories, and provided valuable seismological input for the study.

Many members of the staff of Shannon & Wilson, Inc. contributed significantly to the effort of preparing this report. The project is under the overall direction of Mr. Gerard Buechel who is the Project Manager.

1.4 LIMITATIONS

Within the limitations of scope, schedule, and budget, the analyses, conclusions, and recommendations presented in this report were prepared in accordance with generally accepted professional geotechnical engineering principles and practices in this area at the time this report was prepared. We make no other warranty, either express or implied. The conclusions and recommendations are based on our understanding of the project as described in this report and the site conditions as observed at the time of the field explorations. This report was prepared for the exclusive use of the Department of the Army, Corps of Engineers.

2.0 SITE GEOLOGY

Geologic maps of the region (Schasse, 1987; Walsh et al., 1987) indicate that the dam site is located in Eocene-age Northcraft Formation, which is described as porphyrtic augite basaltic andesite, andesite, and olivine-augite basalt lava flows, flow breccia, and sills; interbedded with pyroclastic rocks and feldspathic sandstone. Geologic explorations conducted for the design of the dam and subsequent construction observations (Bechtel, 1971) indicated that the Northcraft Formation on which the dam is founded consists of moderately hard to very hard, 10- to 30-foot-thick, interbedded basalt, flow breccias, and tuffs, with a dip of about 10 to 15 degrees to the northwest.

3.0 TECTONIC SETTING AND SEISMICITY

3.1 INTRODUCTION

The tectonic regime of western Washington and Oregon is dominated by the Cascadia Subduction Zone (CSZ) in which the Juan de Fuca plate is subducting beneath the North American plate. This tectonic regime gives rise to a number of potential seismic sources that are generally divided into three categories: (1) crustal, (2) intraslab, and (3) interplate. Characterization of the geometries, potential magnitudes, and recurrence behavior of each of these sources, and the uncertainty inherent in each, is described in the following sections.

3.2 TECTONICS

The tectonics and seismicity of the region are the result of ongoing, oblique, relative northeastward subduction along the CSZ of the Juan de Fuca Plate beneath the North American

Plate. The convergence of these two plates not only results in east-west compressive strain (Lisowski, 1993), but also results in dextral shear, clockwise rotation, and north-south compression of accreted crustal blocks that form the leading edge of the North American Plate (Wells et al., 1998). As in most active convergence zones, the CSZ contains a continental fore-arc consisting of accreted sedimentary and volcanic rocks in front of a landward mountainous, active volcanic arc. Unlike most active subduction zones, there is a conspicuous absence of an oceanic trench that normally delineates subduction between two plates.

Within the framework of the subduction zone, the region is divided into four primary tectonic provinces: (1) the Juan de Fuca Plate, (2) the continental fore-arc on the western edge of the North American Plate, (3) the landward continental volcanic arc (Cascade Mountains), and (4) the back arc east of the Cascade Mountains. The three provinces on the North American Plate in and adjacent to western Washington (fore-arc, volcanic arc, and back arc) are illustrated on Figure 3-1. The Juan de Fuca Plate is located at depth below the crustal provinces shown on Figure 3-1. As shown on Figure 3-1, the crustal tectonic provinces can be further subdivided into regional terrains.

The dam is situated on the boundary between the continental fore-arc (province 2) and the Cascade Mountains (province 3) and is underlain at depth by the subducted portion of the Juan de Fuca Plate (province 1). Because of the dam's location within, near, or above these tectonic provinces, the following provides a brief description of these provinces as a basis for discussion of seismicity and earthquake sources that could significantly affect the site.

3.2.1 Province 1, Juan De Fuca Plate

Province 1 is the Juan de Fuca Plate basaltic oceanic crust. This province can be divided into two subprovinces: the portion of the plate west of the subduction zone and the portion of the slab subducted beneath the North American Plate. Of the subducted portion of the Juan de Fuca Plate, the shallower western part is undergoing north-south compression to accommodate the angular geometry of the North American Plate and subduction zone in the region (Weichert and Hyndman, 1983). The north-south compression produces an arch or an east-west-trending, east-plunging anticlinal structure in the subducting plate. The crest of the arch corresponds approximately with the center of the Olympic Mountains in the overlying continental crust. As the plate dives deeper to the east, downdip (i.e., east-west) tensional forces dominate.

3.2.2 Province 2, Fore-Arc

Province 2, the fore-arc region on the western edge of the North American Plate, is composed of imbricated slabs of Tertiary oceanic sediment and basaltic crust that have been accreted or underplated onto the leading edge of the continental crust. The rock is exposed in the coastal mountains, including the Olympic Mountains and the Willapa Hills. These mountains are composed of Tertiary basalt and sedimentary rocks with a core of Tertiary metamorphic rock exposed in the Olympic Mountains. The accretion and underplating at the continental margin is particularly well illustrated in the Olympic Mountains, which contain sequences of steeply dipping and overturned, thrust-faulted sedimentary and volcanic rock around the metamorphic core.

Geophysical and geologic evidence support the hypothesis that the fore-arc (western leading edge of the North American Plate) can be divided into two primary crustal blocks that are being dragged and pulled to the north parallel to the arc (Wells et al., 1998). These blocks include the coastal areas of Oregon and Washington and extend east to the Cascade Mountains. The southern block, consisting of the Coast Range and Willamette Lowland terrains in Oregon and southern Washington, is translating to the north and rotating clock-wise relative to a pole or pivot point located in eastern Washington. This motion translates into north-south compression and dextral shear in the Olympic Mountains, Willapa Hills and Puget Sound Basin terrains as they are compressed between the Oregon block to the south and the relatively stationary, Canadian Coastal Mountains to the north. It is estimated that the compression rate across the terrains in Washington are about 0.07 to 0.09 centimeter per year, and it is postulated that most of the compression and shearing is occurring within the more fractured, Puget Sound Basin terrain immediately north of the site (Wells et al., 1998). This hypothesis is supported by the observation that the rate of historical shallow crustal seismicity is much greater in the Puget Sound Basin terrain than in the Willapa Hills or Olympic Mountain terrains. In addition, no evidence of Quaternary movement has been found on mapped faults in the Willapa Hills, while there is substantial evidence for Quaternary movement on structures with the Puget Sound Basin.

While the bedrock structure of the Puget Sound Basin terrain is largely concealed by thick Quaternary deposits and repeated glaciation, it has been the subject of recent and on-going scientific research in the area (e.g., Gower et al., 1985; Johnson et al., 1994, 1996, and 1999; Ma et al., 1996; Pratt et al., 1997; Yount and Gower, 1991; and Yount et al., 1985). Faults and structures in and adjacent to the Lowland are shown on Figure 3-2. This on-going research suggests that the north-south compression of the this terrain is being accommodated primarily beneath the Lowland by a series of west and northwest trending faults or structures that extend to a decollement at a depth of about 14 to 20 kilometers. These structures extend from the Doty Fault near Chehalis, north to the Darrington-Devils Mountain Fault near Anacortes and include the Black Hills structure, the Tacoma structure, Seattle Fault, Kingston Arch and South Whidbey Fault (see Figure 3-2). However, geologic or geophysical evidence of Holocene movement has only been observed to date for the Seattle Fault with some evidence for Late Quaternary (possibly Holocene) movement on the South Whidbey and Puget Sound Faults.

The west to northwest trending structures are presumably bounded by strike-slip or shear zones (Coast Range Boundary Fault) located on the east near and within the Cascade Mountains (province 3) and on the west along Hood Canal at the foot of the Olympic Mountains (Hood Canal Fault). South and east of the basin, active shear zones are observed in en-echelon, northwest-southeast trending zones around Mount St. Helens and Mount Rainier (see Figure 3-2). It is postulated that these shear zones are connected to the south Whidbey Fault farther to the north by a Coast Range Boundary Fault or faults. However, no direct geologic or geophysical evidence of the existence or location of the Coast Range Boundary Fault or faults have been published. Dextral shear may also be accommodated with the Lowland as recent explorations (Johnson et al., 1999) indicated that dextral shear zones or strike-slip faults (Puget Sound Fault) may be present beneath Puget Sound, extending from south of Vashon Island to north of Kingston.

3.2.3 Province 3, Volcanic Arc

Province 3, the landward continental volcanic arc, is the Cascade Mountains, and is further divide into a North Cascades terrain of mostly Metamorphosed Cretaceous and older rocks, intruded by igneous rocks, and South Cascades terrain of younger sedimentary and igneous rocks that are predominate in the Cascades south of Snoqualmie Pass. Superimposed on this mountain range are relatively young volcanoes, resulting from partial melting of the subducted oceanic crust beneath. Cascade volcanoes in Washington include Mount Rainier, Mount Baker, Mount St. Helens, Mount Adams, and Glacier Peak.

As previously indicated, two zones of observed historically seismicity delineate two, en-echelon, northwest-southeast trending zones around Mount St. Helens and Mount Rainier (see Figure 3-2). However, outside of the Mount St Helens zone, there is little evidence on Quaternary movement on mapped faults within this province.

3.3 SEISMICITY

The project site is located in a moderately active tectonic region that has been subjected to numerous earthquakes of low to moderate strength and occasionally to strong shocks during the brief 170-year historical record in the Pacific Northwest. The following presents a brief review of historical seismicity and characterization of the source zones.

In discussing the historical seismicity, both earthquake magnitude and intensity are used. Prior to the 1940's, historical events were primarily recorded using the Modified Mercalli intensity scale. Roman numerals are used exclusively with the Modified Mercalli scale. Magnitude reported prior to the 1940s in the northwest is typically estimated from the Modified Mercalli intensity. Since the 1940s, earthquakes have generally been reported using magnitude scales. Earthquake magnitudes may correspond to several different scales, including surface waves (M_s) body waves (m_b) and local magnitude (M_L). All earthquake magnitude scales use Arabic numerals to represent the size of the event.

3.3.1 Historical Seismicity

The largest historic earthquakes felt in Washington are listed on Table 3-1. Table 3-2 lists earthquakes of magnitude 4 or larger that have occurred in Western or adjacent regions in British Columbia, Canada and Oregon. Figure 3-3 shows the locations of the earthquakes listed in Table 3-2.

The largest historic earthquakes to affect the site include the magnitude (M_s) 7.1 Olympia earthquake of April 13, 1949, and the magnitude (m_b) 6.5 Seattle-Tacoma earthquake of April 29, 1965. These events were located (epicentral distance) approximately 36 kilometers (1949) and 73 kilometers northeast (1965) of the dam site. Ground shaking in the Chehalis/Tenino/Bucoda area near the dam was reported as Modified Mercalli intensity VIII (1949) and VII to VI (1965). The 1949 and 1965 events were located in the subducted Juan de Fuca slab beneath the Lowland (province 1) at depths of 54 and 63 kilometers, respectively. The level of ground shaking that occurred during these two events at the dam site is likely the maximum vibratory ground motion that would have occurred at the project site during the 170 years of historical record.

Other large historic earthquakes felt in western Washington include the 1872 North Cascades earthquake and two other events in western British Columbia, Canada. The North Cascades earthquake of December 15, 1872, appears to have been one of the largest crustal earthquakes in the Pacific Northwest, with an estimated magnitude of 7+ and a maximum intensity of VIII. Although the epicentral location of this event is uncertain, owing to the sparse population of the area at that time, it apparently was a shallow crustal event located about 200 to 250 kilometers (epicentral distance) northeast of the dam site, however somewhere in the same tectonic province as the dam (province 2) in the north Cascades-Okanogan region. In Canada, major earthquakes occurred on Vancouver Island on June 23, 1946, and in the Queen Charlotte Islands on August 21, 1949 (Coffman and von Hake, 1973). These events had magnitudes of 7.3 and 8.1, respectively. Because of the large distance of these earthquakes from the dam site (over 250 kilometers), there were no reports of significant damage in the area.

3.3.2 Evidence for Cascadia Subduction Zone Earthquakes

Evidence has been found by several researchers to support the potential occurrence of earthquakes on the CSZ. Without direct evidence of the occurrence of large earthquakes, paleoseismological investigations have revealed compelling evidence of a number of instances of sudden coastal subsidence at numerous locations along the length of the CSZ (e.g. Atwater, 1987,1992; Grant, 1989; Darienzo and Peterson, 1990; Clarke and Carver, 1992; Atwater and Hemphill-Haley, 1997). Other evidence includes the presence of turbidites in deep-sea channels off the coast of Washington and Oregon (Adams, 1990, 1996; Weichert and Adams, 1995), the presence of buried soils at Humboldt Bay (Clarke and Carver, 1992) and in northern Oregon (Darienzo and Peterson, 1995; Peterson and Darienzo, 1996), interbedded peat and mud at Coos Bay, Oregon (Nelson et al., 1996), buried scarps near Willapa Bay (Meyers et al., 1996), and buried soils at Grays Harbor (Shennan et al., 1996). Taken together, these different observations represent strong evidence that the CSZ has produced, and remains capable of producing, strong earthquakes.

3.3.3 Evidence for Seattle Puget Sound Fault Earthquakes

Until recently, crustal seismicity generally had neither been correlated with known or inferred structures within the fore-arc, nor had surface expression of Holocene fault ground surface rupture within the Willapa Hills or Puget Sound Basin been observed. Until the late 1980's, it had generally been accepted that shallow crustal events within the Willapa Hills and Puget Sound Basin would have a maximum magnitude of about 6. However, geologic evidence developed during the 1990's (Bucknam et al., 1992; Atwater and Moore, 1992; Karlin and Abella, 1992; Schuster et al., 1992; Jacoby et al., 1992; Johnson et al., 1996; Pratt et al., 1997; Johnson et al., 1999) and tectonic models (Wells et al., 1998) suggest that the geophysical lineament/crustal block boundary beneath Seattle (Seattle Fault) is seismogenic and capable of producing shallow crustal events of magnitudes up to 7.6.

Evidence of recent movement on the Seattle Fault includes raised bedrock terraces south of the inferred Seattle Fault, tsunami deposits north of the fault, and landslide deposits into Lake Washington which have correlative dates of about 1,100 years before present ((Bucknam et al., 1992; Atwater and Moore, 1992; Karlin and Abella, 1992; Schuster et al., 1992; and Jacoby et al., 1992). It has been postulated that these events were the result of reverse movement of the Seattle Fault, with the south side moving up approximately 7 meters relative to the north.

Recent analyses of seismic reflection data (Pratt et al., 1997; Johnson et al., 1999) provide additional evidence of recent movement on the Seattle Fault. Johnson et al. (1999) analyzed high-resolution and conventional industry marine seismic reflection data and subsequently characterized the Seattle Fault as a 4 to 6 kilometer-wide (north-south) zone consisting of a series of east-west trending, south dipping strands as shown on Figure 3-4. Folds in the Quaternary section of the seismic reflection profile indicate that movement has occurred on at least some of the strands through the Holocene. Johnson et al. (1999) also identify a north trending strike-slip zone in the center of Puget Sound (Puget Sound Fault) that offsets the east-west trending strands of the Seattle Fault (see Figure 3-4). Based on the observed offset of the Seattle Fault, Johnson et al. (1999) indicate that the Puget Sound Fault is also likely to be active.

Fault trenching studies by the U.S. Geological Survey (USGS) on the Toe Jam Hill Strand of the Seattle Fault on Bainbridge Island also indicate that movement on the Seattle Fault has ruptured the ground surface during the Holocene. While these studies are not yet complete, the trenching studies completed thus far seem to indicate that at least 3 to 4 events ruptured the ground surface on this strand of the fault over the last 12,000 years (Nelson, 2000).

4.0 EARTHQUAKE SOURCES

This section summarizes the characteristics of the seismic sources that are included in the probabilistic seismic hazard analysis (PSHA) and the deterministic seismic hazard analysis (DSHA). The earthquake sources can generally be described by considering three factors:

identification of the source's geometry and direction of slip, maximum potential size of the earthquake, and the rate of recurrence.

Within the present understanding of the regional tectonics and historical seismicity, three broad seismogenic source zones have been identified. These include the interplate portion of the CSZ, the intraslab portion of the CSZ, and the crustal source zone. Fault and areal sources are discussed within the crustal source zone section.

4.1 CASCADIA SUBDUCTION ZONE

The CSZ is an active subduction zone off the western coast of North America that extends over a length of some 1,100 kilometers from southern British Columbia in the north to northern California in the south (Figure 4-1). Over most of the CSZ, the Juan de Fuca plate is subducting beneath the North American plate, but the northern and southern portions involve subduction of the Explorer and Gorda plates, respectively. The plates converge in a generally northeasterly direction at a rate of 2 to 4 centimeters per year.

Subduction zones can produce thrust events on the interface between the subducting and overriding plates. Such interplate earthquakes can release large amounts of energy. The lack of observed interplate earthquakes on the CSZ raises questions about its potential for producing large magnitude events. This behavior can alternatively be interpreted as characteristic of weak coupling between the plates that allows convergence to take place continuously (and aseismically), or as a quiet period in which strain energy is accumulating in a locked zone between the occurrence of large earthquakes.

Earthquakes can also originate within the subducting plate. Such intraslab earthquakes are extensional events that occur within the subducting Juan de Fuca plate. As the Juan de Fuca plate subducts beneath the North American plate, stress and physical changes in the subducting plate produce high-angle normal faulting earthquakes such as the 1949 Olympia and 1965 Seattle-Tacoma events.

Figure 4-2 shows a cross section that identifies these two earthquake sources through the central Puget Sound Basin, approximately 100 kilometers north of the dam, based on Hyndman and Wang (1995) and Stanley et al., (1999). Figure 4-3 shows a similar cross section of the approximate latitude of the dam.

4.1.1 Interplate Source

4.1.1.1 Geometry

As illustrated in Figure 4-4(a), the geometry of the northern subducting portion of the CSZ has previously been characterized on the basis of hypocentral locations of intraslab events (Crosson and Owens, 1987). More recently, local earthquake tomography has been used (Stanley et al., 1999) to develop a P-wave velocity model of the region that, combined with geological, paleoseismic, gravity, magnetic, magnetotelluric, deformation, seismicity, focal mechanism, and geodetic data, provides a somewhat different interpretation of interplate source geometry (Figure 4-4[b]).

The seismogenic portion of the CSZ is bounded in both the updip and downdip directions. Because no direct measurements of the boundaries of the seismogenic portion are available, their positions must be estimated from indirect evidence.

Updip Extent. At depths shallower than the updip boundary, relative plate motion occurs aseismically due to the presence of stable subducted clays such as illites and smectites (Wang, et al., 1980; Vrolijk, 1990), relatively weak, unconsolidated accretionary wedge sediments (Byrne et al., 1988), and potential high pore pressures (Dragert et al., 1994). Hyndman and Wang (1993) used temperature considerations to conclude that brittle behavior would be associated with the dehydration of stable sliding clays above temperatures of 100°C to 150° C; thermal modeling suggested that the updip boundary of the CSZ is near the deformation front (Figure 4-2 and 4-5).

Using geophysical data to map folds and faults along the CSZ in north central Oregon, Goldfinger et al. (1992) defined a slope break located approximately 30 kilometers east of the deformation front, which was postulated as representing the updip boundary. Comparisons with the Nankai subduction zone of southwest Japan, which shows several similarities to the CSZ, support an updip boundary located 30 to 60 kilometers east of the deformation front (Figure 4-2 and 4-5).

For the seismic hazard analysis, the following two updip boundaries were considered:

1. An updip boundary corresponding to the deformation front.

2. An updip boundary corresponding to the slope break identified by Goldfinger et al. (1992).

Downdip Extent. Crustal uplift and subsidence deformations measured preceding and following interface earthquakes in other parts of the world offer information on the downdip extent of rupture. The accumulation and eventual release of strain energy in a locked zone produces a pattern of surface uplift and subsidence that has been correlated to the spatial extent of rupture. The "zero isobase," or boundary between regions of surface uplift and subsidence (Plafker and Kachedoorian, 1969; Dragert et al., 1994) has been shown to approximate the downdip extent of rupture in past subduction earthquakes. Geomatrix (1995) also considered this alternative for modeling the downdip boundary of the CSZ. The landward extent of the zero isobase boundary is shown on Figure 4-5.

At depths greater than those corresponding to the downdip boundary, temperatures are high enough that the rock behaves in a ductile manner that accommodates plate motion aseismically. The transition between brittle and ductile behavior typically occurs at temperatures of 350° C to

450°C for metamorphosed sedimentary rocks (Hyndman and Wang, 1993). Tichelaar and Ruff (1993) used thermal characteristics and maximum rupture depths from worldwide subduction zones to infer that the brittle-ductile transition occurs at approximately 400°C for silicic upper plate rock and about 550°C when the upper plate contains mafic rock. Hyndman and Wang 1993; 1995) modeled the thermal regime along the CSZ and concluded that the subduction zone was locked at temperatures less than 350°C and uncoupled at temperatures above 450°C with a transition zone at intermediate temperatures (Figure 4-2). The transition zone (at temperatures between 350°C and 450°C) was considered to be incapable of nucleating rupture but remained capable of propagating rupture. Geomatrix (1995) modeled the downdip boundary of the CSZ at the midpoint of this transition zone. Analysis of the Ryukyu-Kyushu arc and Japan trench suggests that moderate to large-sized earthquakes occurred at depths between 20 and 30 kilometers where temperatures are expected to be in the range of 300°C and 600°C. The landward extent of the assumed boundary for the midpoint of the transition is shown on Figure 4-5.

Stanley et al. (1999) recently developed a three-dimensional velocity model of western Washington that indicated the presence of a high-velocity zone at the bottom of the North American plate beneath the Puget Sound Basin. The high velocity zone had a generally flat upper surface beginning at depths of about 14 to 16 kilometers and a monotonically dipping lower surface from 18 kilometers on the southwest to about 33 kilometers on the northeast; the across-strike width was about 50 kilometers. A high velocity feature had previously been detected beneath Vancouver Island (Spence et al., 1985) and was considered to represent accreted mafic, and perhaps ultramafic, rock (Clowes et al., 1987). Stanley et al. (1999) interpret the high velocity zone as consisting of voluminous mafic and ultramafic rock, and conclude that the serpentinite minerals in the body could support brittle rupture at temperatures of 400°C to 600°C. This interpretation implies that the downdip boundary of the seismogenic portion of the CSZ could extend to depths of approximately 40 kilometers rather than the maximum depth of about 25 kilometers that corresponds to the midpoint of the transition zone. Stanley et al. (1999) provides detailed discussions of several factors that support and contradict this interpretation. The extent of the assumed boundary for the mafic zone is shown on Figure 4-5.

For the seismic hazard analysis, the following three downdip boundaries were considered:

1. A downdip boundary corresponding to the zero isobase.

2. A downdip boundary corresponding to the midpoint of the transition zone defined by Hyndman and Wang (1993, 1995).

3. A downdip boundary corresponding to the eastern edge of the mafic zone identified by Stanley et al. (1999) at locations where the mafic zone is in contact with the Juan de Fuca plate, and to points halfway between the zero isobase and midpoint of the transition zone elsewhere.

4.1.1.2 Maximum Magnitude

The maximum magnitude of a CSZ interplate event can be obtained from the estimated geometry of the rupture surface using correlations based on actual observations in past earthquakes. Correlations between magnitude and rupture length, and between magnitude and rupture area, were used. All correlations are based on the assumption that rupture occurs over the entire seismogenic width of the CSZ.

Maximum Width. The maximum width of the CSZ depends on the locations of the updip and downdip boundaries of the seismogenic zone discussed in the previous section. The previously discussed updip and downdip CSZ boundaries give rise to the six estimated maximum widths shown below:

TABLE 4-1
ESTIMATED CSZ RUPTURE WIDTHS

Boundary Locations	Average Updip boundary width at deformation front	Average Updip boundary width at slope break
Downdip boundary at zero isobase	90 km	65 km
Downdip boundary at midpoint of transition zone	75 km	50 km
Downdip boundary at edge of mafic zone	120 km	95 km

The widths indicated for the zero isobase and transition zone downdip boundaries shown above were obtained by averaging the variable width of the CSZ over its entire length. The width for the mafic zone downdip boundary was obtained by adding 45 kilometers to the widths associated with the midpoint of the transition zone. The additional 45 kilometers represents the downdip length of the high-velocity mafic body in central Puget Sound. The six postulated updip and downdip boundaries are shown on Figure 4-6.

Maximum Length. Maximum rupture lengths were estimated using a process similar to that employed by Geomatrix (1995). The lack of interplate activity on the CSZ requires that maximum rupture length be estimated by indirect means such as paleoseismic data, fault segmentation, and empirical aspect ratio interpretation.

Paleoseismic investigations have identified geologic evidence of large earthquakes at numerous locations along the length of the CSZ. Dating of these features is imprecise, however, and a significant error band is associated with the times at which the event producing each feature is estimated to have occurred. The error bands are wide enough, and overlap so significantly, that evaluation of temporal/spatial patterns in paleoseismic evidence does not provide estimates of the rupture lengths of individual events.

Rupture lengths may be constrained by structural factors such as bends and discontinuities in fault geometry. Geomatrix (1995) reviewed previous fault segmentation studies and identified seven segmentation boundaries along the Juan de Fuca plate. The evidence for segmentation includes changes in strike and dip, variations in seismicity, topographic variations, and other factors. Changes in strike and dip of the subducting plate are more pronounced on the northern portion of the CSZ (i.e. adjacent to Washington) than the southern (adjacent to Oregon, which was the focus of the Geomatrix (1995) investigation). The identified segmentation boundaries define eight segments with an average length of approximately 135 kilometers (Figure 4-7).

Observations of worldwide interplate ruptures indicate an empirical relationship between their lengths and widths. Because the width of the CSZ is known more accurately than segment lengths, an estimate of rupture length can be obtained using the anticipated width and historical length-to-width, or aspect ratios. Geomatrix (1993) compiled a database of 53 interplate events of $M > 7$ with well-defined source parameters and aftershock-based information on rupture lengths and widths; this database indicates that the average aspect ratio was 2.4 and that most interplate events had aspect ratios less than 4. The weighted average of the potential CSZ widths shown above is 75 kilometers. Using this width, the average length would be on the order of 180 kilometers, and most events would be expected to have lengths less than 300 kilometers.

Comparing the segmentation-based average length of 135 kilometers with the aspect ratio-based average length of 180 kilometers suggests that an average segment length of 150 kilometers is reasonable. To account for the fact that more than one segment could rupture at a given time, four possible rupture lengths were considered in the seismic hazard analysis:

1. A 150-kilometer rupture length that corresponds to the rupture of a single segment. The aspect ratio of 2 for such an event would be consistent with the average aspect ratio observed in worldwide subduction earthquakes.

2. A 250-kilometer rupture length that represents the average length of the rupture of two adjacent segments. The aspect ratio of about 3 for such an event would be greater than most of the aspect ratios that have been observed in similar environments.

3. A 450 kilometer rupture that represents the average length of the rupture of three adjacent segments. The aspect ratio of 6 for a 450-kilometer rupture would be among the largest that have been observed worldwide.

4. A 1,100 kilometer rupture that represents the entire length of the CSZ. The aspect ratio of such an event would be approximately 14, which would be larger than any that has previously been observed.

The four rupture lengths are consistent with those identified by Geomatrix (1995) for their evaluation of seismic hazards in Oregon.

Determination of M_{max}. Maximum magnitudes were determined in a manner that considered the various potential rupture lengths described above and maintained consistency with best estimates of the recurrence rates of CSZ earthquakes. Analysis of available recurrence data suggests that large CSZ interplate earthquakes occur at an average recurrence interval of 600 years (Section 4.1.1.3).

As discussed previously, earthquake magnitude can be correlated to both rupture length and rupture area. Both approaches to maximum magnitude determination were used in this PSHA. The rupture length-based correlations of Wells and Coppersmith (1994) were used to estimate magnitudes for the four potential rupture lengths described in above. The length-based estimates of maximum magnitude ranged from 7.7 (150-kilometer rupture length) to 8.7 (1,100-kilometer rupture length).

Area-based maximum magnitude estimates depend on both rupture length and rupture width. Assuming that such large earthquakes involve rupture along the entire length of the CSZ, area-based empirical correlations can be used to estimate the maximum magnitude for each of the six updip/downdip boundary pairs. Assuming that these earthquakes occur at an average recurrence interval of 600 years and making a reasonable estimate of the rigidity of the CSZ rock (Atwater and Hemphill-Haley, 1997), equivalent slip rates can be computed for each of these cases. These slip rates are based on average rates of recurrence over several thousand years and, therefore, may not match current slip rate measurements. Using these slip rates and conserving the overall moment rate, maximum magnitudes were computed for different recurrence intervals and rupture widths. For the assumed recurrence rates (Section 4.1.1.3) and various updip/downdip boundary pairs, area-based maximum magnitudes ranged from 8.0 (150-kilometer rupture length) to 9.0 (1,100-kilometer rupture length).

4.1.1.3 Earthquake Recurrence

In other parts of the world, subduction zone interplate earthquakes appear to occur within a relatively narrow range of magnitudes. This fact, coupled with the fact that small-moderate interplate earthquakes have not been observed on the CSZ, suggests that the characteristic earthquake model is most appropriate for this source. The recurrence interval of characteristic CSZ earthquakes can be estimated from the results of recent paleoseismic investigations.

Atwater and Hemphill-Haley (1997) summarized the results of several investigations conducted at different locations along the CSZ, specifically at Gray's Harbor, Willapa Bay, and Long Beach in Washington; in deep-sea channels, Coos Bay, and a series of northern bays in Oregon; and at Humboldt Bay in Northern California. At each site, time-datable evidence of a discrete number of different events was recorded and used to compute an average recurrence interval. Uncertainty in the assigned dates led Atwater and Hemphill-Haley (1997) to report ranges of recurrence intervals for each location. Assuming a symmetric, triangular probability distribution for each reported interval and weighting each site equally, the average recurrence interval (standard deviation) for large CSZ earthquakes based on geologic evidence along the entire CSZ is 657 (204) years.

Adams (1990) reported age ranges for a series of Holocene turbidites assumed to have been derived from failures of canyon heads some 50 kilometers west of Willapa Bay (Griggs and Kulm, 1970), an area directly above the probable area of shallow rupture on the CSZ (Hyndman and Wang, 1995). Adams interpreted the ages of the turbidites from the relatively uniform thicknesses of pelagic clay layers deposited between the turbidites. The estimated ages of five distinct events were 250-360 years, 570-830 years, 1,000-1,400 years, 1,730-2,640 years, and 2,270-3,300 years. By assuming that the ages of each of these events could be represented by symmetric, triangular probability distributions, a probability distribution for recurrence interval could be computed. This distribution indicated an average recurrence interval (standard deviation) of 620 (290) years.

Atwater and Hemphill-Haley (1997) also reported ranges of age for seven distinct events based on buried soils in Willapa Bay. The estimated ages of these events were 290-310 years, 900-1,300 years, 1,110-1,350 years, 1,500-1,700 years, 2,390-2,780 years, 2,800-3,320 years, and 3,320-3,500 years. Again assuming triangularly distributed ages for each event; a probability distribution for recurrence interval based on buried soils at Willapa Bay was computed. This distribution indicated an average recurrence interval (standard deviation) of 520 (300) years.

The three data sets for recurrence intervals yielded the statistics shown in the table below. Considering the proximity of the turbidite- and buried soil-based recurrence intervals to the Skookumchuck dam site, the mean, coefficient of variation, and skew coefficients of each data set were averaged. The resulting average statistics were then utilized in a point-estimation procedure to obtain weighted, discrete recurrence intervals that produced the same average statistics.

The point estimation procedure produced two recurrence intervals that were considered in the seismic hazard analysis: 410 years and 985 years.

TABLE 4-2
COMPUTED RECURRENCE INTERVAL STATISTICS.

	Mean (years)	Standard Deviation (years)	Coefficient of Variation	Skew Coefficient
Geologic evidence	657	204	0.311	1.06
Turbidite evidence	619	292	0.472	0.80
Buried soil evidence	524	301	0.574	0.29
Average values	600	-	0.452	0.72

4.1.2 Intraslab Source

The intraslab source represents extensional events that occur within the subducting Juan de Fuca plate. As the Juan de Fuca plate subducts beneath the North American plate, stress and physical changes in the subducting plate produce high-angle normal faulting earthquakes such as the 1949 Olympia and 1965 Seattle-Tacoma events.

4.1.2.1 Geometry

Because numerous intraslab earthquakes have been recorded, the geometry of the intraslab source is relatively well defined in Washington state. Most of these earthquakes are relatively small, but are useful for imaging the geometry of the intraslab source. Based on numerous such events, Crosson and Owens (1987) determined that the CSZ is arched, or curved, beneath Washington state (Figure 4-4[a]). The axis of the arch, as determined by Crosson and Owens (1987) runs in a generally east-west direction. More recently, a three-dimensional velocity model developed on the basis of local earthquake tomography (Stanley et al., 1999) indicated a somewhat different arch shape with an axis that trends toward the northeast (Figure 4-4[b]). An overlay of the Crosson and Owens and Stanley et al. geometries is shown on Figure 4-8.

4.1.2.2 Maximum Magnitude

Because intraslab events involve high-angle normal faulting, the area of the rupture surface is strongly dependent on the thickness of the subducting slab. Young subduction zones, such as the CSZ, generally have relatively thin subducting slabs. Thermal modeling of the CSZ (Hyndman and Wang, 1993) and the observed geometry of the Wadati-Benioff zone (Jarrard, 1986) confirm the likelihood that the subducting slab is relatively thin.

Worldwide observations indicate that the largest intraslab earthquakes are on the order of magnitude 7-1/2, with the largest of these occurring in older subducting slabs. The 1949 Olympia earthquake had a magnitude of 7.1. Based on these observations, the recorded intraslab seismicity of the CSZ, and the thin nature of the Juan de Fuca plate, maximum intraslab earthquake magnitudes are judged to be in the range of 7.1 to 7.5.

4.1.2.3 Earthquake Recurrence

Recurrence relationships for CSZ intraslab earthquakes were based on historical seismicity, and were modeled using a truncated exponential (Gutenberg-Richter) recurrence law as described in Section 5.1.1.2.

4.2 CRUSTAL SOURCES

Both areal source zones and discrete faults are used to characterize crustal sources. Areal source zones are used to model much of the crustal seismogenic potential because, as previously noted, evidence of Quaternary movement on faults in the Willapa Hills and South Cascades (outside the Mount St. Helens and Mount Rainier Zones) has not been found, and the bedrock structure of most of the Puget Lowland is concealed by thick Quaternary deposits and repeated glaciation.

Crustal faults identified within the Puget Lowland with evidence of Late Pleistocene or Holocene (e.g., Seattle Fault, Puget Sound Fault) are considered discrete sources. The Mount St. Helens and Mount Rainier zones are also considered as discrete zones.

4.2.1 Regional Areal Crustal Source Zones

The tectonic terrains described by McCrumb et al. (1989) within the fore-arc and volcanic arc (Figure 3-1) were used as the basis for developing the regional areal crustal zones. Based on historical seismicity rates, the Olympic Mountains, Willapa Hills, and Coast Range terrains were combined into a single areal source zone. The resulting areal source zones used in the seismic hazard analysis are shown on Figure 4-9.

Recurrence relationships for the crustal source zone earthquakes were based on historical seismicity, and were modeled using a truncated Gutenberg-Richter (exponential) recurrence law.

It was assumed that the maximum depth to which shallow crustal earthquakes would propagate is 20 kilometers. Both Pratt et al. (1997) and Parsons et al. (1999) suggest that a decollement is present in the crust beneath the Lowland between a depth of 14 to 20 kilometers.

Estimates of the maximum magnitude for all areal source zones except the Mt. St. Helens and Western Mt. Rainier zones range from approximately 7.0 to 7.5. The upper value was selected as it is about ¼ to ½ a magnitude larger than the 1872 North Cascades event (magnitude 7+), which is the largest historic crustal earthquake in any of the areal source zones adjacent to the Central Puget Sound zone (Figure 4-9). It is also near the maximum magnitude estimated for the Seattle Fault (i.e., magnitude 7.6). The lack of evidence of Late Pleistocene or Holocene movement (e.g., ground surface rupture) would generally tend to indicate smaller maximum earthquake magnitudes. However, considering the thick mantle of Quaternary sediment, the repeated glaciation, and the generally thick vegetative cover in the region, it is plausible that such evidence of ground rupture has been obscured. This larger magnitude also allows for the possibility of other large structures within the fore-arc and volcanic arc (e.g., Kingston Arch, South Whidbey Fault, Arlington-Devils Mountain Fault, Hood Canal Fault, Olympia Fault and Doty Fault) to be seismogenic despite the current lack of information (e.g., slip rates, recurrence intervals) required for explicit, individual modeling of specific structures in a PSHA.

The Mount St. Helens and Western Mount Rainier Seismic zones are located with the larger South Cascades areal source zone and are shown on Figure 4-9. These zones of increased seismicity above the background South Cascades zone have been identified and studied by various investigators (e.g., Weaver and Smith, 1983; Stanley et al., 1996; Moran et al., 1999), with depths of observed seismicity between 2 and 20 kilometers. Estimated maximum earthquake magnitudes for the Mount St. Helens zone range from about 6 to 7, with the range determined by assumptions regarding potential segmentation/non-segmentation of the zone. Estimated maximum earthquake magnitude for the Western Rainier zone is approximately 5.5.

4.2.2 Fault Specific Sources

In addition to the areal crustal zones, fault specific sources are also considered. The Seattle and Puget Sound Fault were modeled in the PSHA explicitly because there is evidence of Holocene movement on these structures with estimates of slip rates and geologic evidence that, though preliminary, provide indications of possible recurrence intervals. Other capable crustal faults within 100 kilometers of the dam but with insufficient data to explicitly model in the PSHA include the Hood Canal and Legislature or Olympia Faults (Figure 3-2). However, these faults are considered in the DSHA.

Work by Johnson et al. (1996) indicates that there is evidence of late Quaternary (possibly Holocene) movement on the South Whidbey Fault. Potential maximum earthquake magnitudes between 7.0 and 7.3 are estimated for this fault. However, Johnson et al. (1996) also indicate that the existing data is not sufficient for rigorous quantification of the seismic hazard associated with this fault, and we note that the dam site is located 125 kilometers or more south-southwest of the fault. Consequently, this fault was not explicitly modeled in the PSHA. Rather, as previously indicated, the maximum earthquake magnitude in the areal source zone in which the fault is located is 7.5 to allow for large earthquakes on unknown or uncertain faults.

4.2.2.1 Seattle Fault

The location of the Seattle Fault used in the seismic hazard analysis is shown on Figure 4-10, the southern extent of the fault is located approximately 60 kilometers north of the dam. The maximum fault rupture length is estimated to be approximately 65 kilometers (Pratt et al., 1997). Johnson et al. (1999) indicate the north-south trending Puget Sound Fault appears to segment the Seattle Fault, resulting in an approximately 40-kilometer-long east segment and 25-kilometer-long west segment. However, they also indicate that geologic evidence associated with rupture on this fault, approximately 1,100 years before present, suggests that this segmentation does not limit rupture length (i.e., rupture occurs on both segments).

The most recently published model showing the downdip extent of the Seattle Fault is by Pratt et al. (1997), which indicates that the Seattle Fault is a thrust fault dipping to the south at an angle of about 20 degrees, steepening to about 45 degrees in the near surface. An approximately north-south cross-section illustrating this model is shown on Figure 4-11. Johnson et al. (1999) show the Seattle Fault steepening to about 60 to 85 degrees within 3 kilometers of the surface. In the model by Pratt et al. (1997), the 30 to 40 kilometer-long "Tacoma Fault" (Gower et al., 1985, Rogers et al., 1996) that defines the north edge of the Tacoma basin is re-interpreted as the south end of the Seattle Fault. This geometry results in a down dip width of approximately 32 to 43 kilometers. Based on the relationship between rupture area and magnitude by Wells and Coppersmith (1994), the estimated mean maximum magnitude may be about 7.4; maximum earthquake magnitudes corresponding to mean plus and minus one standard deviation from the mean are 7.2 and 7.6, respectively.

Slip rates on the Seattle Fault have been estimated from marine seismic reflection data (Johnson et al., 1999) and reported between 0.07 and 0.11 centimeters per year. Fault trenching studies by the USGS on the Toe Jam Hill Strand of the Seattle Fault on Bainbridge Island, while preliminary, begin to provide some indication of recurrence intervals on the fault. The trenching studies completed thus far seem to indicate that at least 3 to 4 events ruptured the ground surface on this strand of the fault over the last 12,000 years (Nelson, 2000) or roughly a recurrence rate of 3,000 to 4,000 years for an event large enough to result in ground surface rupture (about magnitude 6.5+). The lack of observed uplifted terraces and similar geologic evidence used to infer the movement on the Seattle Fault 1,100 years ago suggest longer recurrence intervals on the order of 6,000 years (Bucknam, 2000).

There appears to be reasonable agreement between the slip rate, recurrence, and maximum magnitude assuming a characteristic earthquake recurrence model and rupture across the entire fault (i.e., no segmentation). Assuming a slip rate of 0.11 centimeters per year and characteristic earthquake magnitudes of 7.4 and 7.6, the corresponding recurrence interval is approximately 1,600 years to 3,600 years respectively, which is in general agreement with the preliminary estimated recurrence rates determined from the geologic evaluation of the Toe Jam Hill Fault trenches. A slip rate of 0.07 centimeters per year and characteristic earthquake magnitudes of 7.4 and 7.6 correspond to recurrence intervals of approximately 2,600 years to 5,600 years respectively.

It has also been postulated that the Seattle Fault and the “Tacoma Fault” are two separate, relatively high angle faults. However, the observed slip rates and preliminary estimated recurrence rates on the Toe Jam Fault do not appear to be consistent with this model. Specifically, using the non-segmented fault length depicted by Pratt et al. (1997), and assuming a similar length at depth, the estimated mean maximum magnitude is about 7.2 based on the relationship by Wells and Coppersmith (1994); fault lengths indicated by Gower et al. (1985) and Rogers et al. (1996) give mean maximum magnitude estimates of 7.0 and 7.1, respectively. For slip rates of 0.07 and 0.11 centimeters per year and assuming a characteristic earthquake recurrence model, recurrence intervals for the calculated maximum magnitudes range from about 1,100 to 2,200 years and are generally shorter than that inferred from existing geologic evidence.

4.2.2.2 Puget Sound Fault

This fault zone reported by Johnson et al. (1999) is a north-south trending zone of near vertical strike-slip fault strands. The location of the fault used in the seismic hazard analysis is shown on Figure 4-10, the southern end of the fault is located approximately 65 kilometers north of the site. The total length of this zone mapped by Johnson et al. (1999) is about 55 kilometers. While this fault may be segmented, it appears in offsets of the east-west trending Seattle fault, such that segmentation may not limit rupture length. Johnson et al. (1999) do not indicate a maximum depth, but their seismic reflection data indicate a minimum depth of at least 6 kilometers. It would be reasonable to assume that the fault extends to the decollement at a depth of about 14 to 20 kilometers. Based on the relationship between rupture length and magnitude by Wells and Coppersmith (1994), and assuming a rupture length of 55 kilometers (i.e., no segmentation), the mean maximum magnitude is estimated to be about 7.1; maximum earthquake magnitudes corresponding to mean plus and minus one standard deviation from the mean are 6.8 and 7.4, respectively.

Slip rates on the Puget Sound Fault estimated from marine seismic reflection data are reported between 0.03 and 0.08 centimeters per year. Assuming a characteristic earthquake recurrence model and a mean maximum magnitude of 7.1 (i.e., no segmentation), recurrence intervals range from about 3,000 years to 8,000 years.

4.2.2.3 Hood Canal Fault

The Hood Canal Fault, located approximately 75 kilometers northwest of the site (see Figure 3-2), is a capable structure. While no evidence of Holocene or late Pleistocene movement has been observed, nor does historical macro seismicity seem to occur along this structure, it is associated with the much smaller East and West Saddle Mount Faults on which Holocene movement has occurred (Wilson et al., 1979). These two small faults that are approximately 4 kilometers combined length are roughly parallel to the Hood Canal Fault and are located approximately 3 to 5 kilometers west of the south end of the Hood Canal Fault. This structure was also considered capable in the seismic hazard assessment for the WNP-3 site at Satsop, Washington (Geomatrix, 1988).

As shown on Figure 3-2, the length of the Hood Canal Fault is approximately 100 kilometers. Based on surface rupture length and magnitude by Wells and Coppersmith (1994) maximum earthquake magnitudes on the order of 7.5 could result from strike-slip rupture along the entire length of the fault. It is possible that the fault is segmented resulting in smaller maximum magnitudes, however, no studies have been completed addressing potential segmentation and magnitude.

4.2.2.4 Legislature Fault

The Legislature or Olympia Fault, located approximately 9.3 kilometers northeast of the site (see Figure 3-2) is a capable structure. Gower et al. (1985) locate this structure at the northeast side of a positive gravity anomaly that may represent a northeast dipping homocline of Eocene basalt, with a length of 78 kilometers. This structure was indicated to be 88 kilometers long and considered capable in the seismic hazard assessment for the WNP-3 site at Satsop, Washington (Geomatrix, 1988). Rogers et al. (1996) identify this structure as an 82 kilometer long structure with potential Quaternary movement. Stanley et al. (1999) postulate that this fault dips steeply down to the southwest and forms the southern boundary of the Seattle-Tacoma Basins and thereby associated with the active Seattle Fault within the basin. Sherrod (1999) provides evidence of approximately 1 meter of rapid subsidence and liquefaction in the south Puget Sound area in the vicinity of Olympia occurring approximately 1,100 years ago. He postulates that movement on the Legislature fault could be an explanation for the observed subsidence and liquefaction. This evidence is sufficiently compelling that the USGS will conduct seismic reflection studies in fiscal year 2002 to further evaluate the seismogenic potential of this fault.

For this study, it is assumed that the length of the Legislature Fault is approximately 80 kilometers long. Based on rupture length and magnitude by Wells and Coppersmith (1994) mean maximum earthquake magnitudes on the order of 7.2 could result from rupture of the entire fault. It is possible that the fault is segmented resulting in smaller maximum magnitudes. However, geologic evidence associated with the Seattle Fault indicates that rupture along the entire length of the fault and across the width of the basin is likely. Because of the Legislatures Fault's association with the basin and Seattle Fault, it may be possible for the entire length of the Legislature Fault to rupture also.

5.0 SEISMIC HAZARD ANALYSIS

Horizontal and vertical ground motions will be developed for the OBE and IDE using probabilistic seismic hazard analysis (PSHA). Ground motions for the MCE will be developed using the results of the deterministic seismic hazard analysis (DSHA) including finite fault simulations of rupture of the CSZ Interplate source. The following provides the results of the PSHA and DSHA, including the finite fault simulation.

5.1 PROBABILISTIC SEISMIC HAZARD ANALYSIS

5.1.1 Methodology

The PSHA considers uncertainties in potential earthquake location, recurrence, and effects to produce rock uniform hazard spectra for development of the OBE and IDE ground motions. The seismic hazard at the dam site is calculated using the program EZ-FRISK (Risk Engineering, Inc. 1998). EZ-FRISK calculates seismic hazard using the methodology for probabilistic hazard analysis developed by Cornell (1968), McGuire (1976, 1978), and Der Kiureghian and Ang (1975, 1977). The basic assumption of the model is that the spatial locations of earthquakes within a given source zone are completely random, and that they occur independently in time (i.e., as a Poisson process). Kramer (1996) provides a good description of the concepts and calculations involved in a PSHA.

Three basic inputs to the PSHA include source geometry, earthquake recurrence behavior, and ground motion attenuation behavior. Alternative models for these three inputs were considered using a logic tree approach. Uncertainties are typically associated with characterizing seismic source geometry, earthquake recurrence, and ground motion attenuation, and multiple alternatives for each of these basic inputs may be appropriate to consider. A logic tree approach allows for consideration of multiple alternative models, each of which is assigned a weighting factor that is interpreted as the relative likelihood of that model being correct. This is done by assessing potential models for each input into the PSHA and assigning a weighting factor to each model considered. A logic tree consists of a series of nodes and branches, with each branch representing a potential model at the node. A weighting factor or probability that a model is correct is assigned to each branch at a node, and the sum of the weighting factors at any node must equal 1. Multiple nodes and branches make up the logic tree. The probability that the complete model described by a series of nodes and branches across the entire tree is the product of the probability assigned to the branches that describe the model. The program EZ-FRISK was used to calculate the ground motions for each complete model (series of nodes and branches across the entire logic tree). Once each model was calculated, it is multiplied by the probability calculated for that model. The final calculated ground motions is then the sum of the ground motions calculated for each complete branch of the logic tree, each complete branch of which has been multiplied by the probability assigned to model the branch represents.

5.1.1.1 Source Geometry

The earthquake source zones considered in the Skookumchuck dam PSHA thus far are presented in Section 4.0. These zones included the two deep sources (Interplate CSZ and Intraslab CSZ) and the 13 shallow sources (Vancouver Island, Olympic Mountains, Willapa Hills, Coast Range, Willamette Lowland, North Puget Sound, Central Puget Sound, North Cascades, South Cascades, Mt. St. Helens, Western Rainier, Seattle Fault, and Puget Sound Fault). Figures 4-6, 4-8, 4-9, and 4-10 show the geometries of the zones and faults that are considered in the PSHA.

The geometries of the interplate, intraslab, Seattle Fault, and Puget Sound Fault were modeled using the geometric convention of EZ-FRISK in which faults are represented as planar surfaces defined by two dip angles and three depths. The shallowest depth corresponds to the minimum depth of energy release for the fault. The intermediate depth corresponds to the location where a change in dip can occur. The greatest depth is set at the maximum depth of energy release.

The fault geometry model of EZ-FRISK produces fault zones of constant width. To obtain the desired fault rupture lengths and maintain consistency with the various CSZ geometry models, the principle of superposition was used to model sources of variable width. In this procedure, the hazard for a variable width source was taken as that obtained for a large zone with constant width approximately equal to the greatest width of the CSZ, minus the hazard contribution of smaller, constant width strip zones that occupied the space between the large source zone and the actual CSZ. The assumption of constant width was reasonable for the remaining fault sources. Crustal areal source zones were modeled as horizontal planar regions at constant depth.

5.1.1.2 Recurrence

The recurrence equations used for each of the source zones describe the expected distribution of the magnitudes of earthquakes produced by that source zone. Two forms of the recurrence equation were considered: the truncated exponential (Gutenberg-Richter) distribution and the characteristic earthquake distribution.

The Gutenberg-Richter model is typically applied to zones where the observed seismicity includes contributions from multiple sources. The basic Gutenberg-Richter recurrence equation expresses the average number of earthquakes per year, N, that exceed some magnitude, M, using the form:

$$\log \mathbf{N} = \mathbf{a} - \mathbf{b}M,$$

where **a** is equal to the annual number of earthquakes of M > 0 and **b** describes the relative likelihood of large and small earthquakes. The values of **a** and **b** were determined by regression analysis using historical seismicity data, which was obtained from the Pacific Northwest Seismic Network located at the University of Washington, and from the National Geophysical Data Center. The seismicity catalog contained pre-instrumental and instrumental seismicity between 1841 and January 2000. Duplicate records and dependent events, such as foreshocks and aftershocks, were removed from the catalog, and the catalog was corrected for completeness prior to determination of the Gutenberg-Richter parameters.

Plots of the Gutenberg-Richter recurrence equations and the data from which they were obtained are shown in Figures 5-1 through 5-10. The Gutenberg-Richter equation is commonly modified to consider earthquakes above some minimum magnitude (taken as M = 4.0 in this study) and below some maximum value (Section 5.1.1.4). The Gutenberg-Richter relations were used to describe the earthquake recurrence for the crustal areal zones and the intraslab zone.

Recent studies have shown that individual faults tend to produce repeated earthquakes of similar magnitude. This behavior is described by the characteristic earthquake model, the magnitude distribution of which is generally applied to specific faults. In this study, the characteristic magnitude distribution of Youngs and Coppersmith (1985) was used to describe earthquake recurrence for the Interplate CSZ, Seattle Fault, and Puget Sound Fault.

5.1.1.3 Ground Motion Attenuation Relationships

Ground motion attenuation relationships describe the amplitude of various ground motion parameters. The following subsections describe the ground motion attenuation relationships used in the PSHA.

Deep CSZ Earthquakes. Few attenuation relationships that apply to deep events such as interplate and intraslab subduction zone earthquakes have been developed. The limited number of attenuation relations results from the limited availability of strong motion records from such events. A single empirical attenuation relationship (Youngs et al., 1997) is available for peak ground acceleration and spectral accelerations on soft rock (i.e., typical west coast rock condition) due to interplate and intraslab subduction earthquakes. This relationship is based primarily on recorded ground motions in Japan, Mexico, and the Solomon Islands, and predicts spectral accelerations over a period range of 0 to 3 seconds. To compensate for the lack of recorded large CSZ earthquakes, Wong et al. (2000) used stochastic ground motion modeling to develop an attenuation relationship that would be specifically applicable to CSZ interplate earthquakes. Because it is based on simulations, the Wong et al. (2000) attenuation relationship extends to periods of over 10 seconds. This relationship was also used in the PSHA.

Shallow Crustal Earthquakes. Many more empirical attenuation relationships are available for shallow than deep earthquakes. Selection of appropriate relationships for the PSHA involved careful consideration of the consistency between the attenuation database and shallow crustal sources in the Pacific Northwest and the range of periods over which spectral acceleration predictions can be made. These considerations eliminated the use of several common attenuation relationships due to the inclusion of unrepresentative events in their database and/or their limitation to relatively short periods. To characterize the attenuation of ground motion on typical west coast or soft rock from shallow crustal earthquakes, two empirical attenuation relationships were used: the relationships developed by Abrahamson and Silva (1997) and Sadigh et al. (1997). Both attenuation relationships, which are widely used to characterize the ground motions produced by shallow earthquakes, are based primarily on California strong motion data with additional selected records from Mexico, Iran, USSR, and other countries. To account for uncertainty in which attenuation model is most appropriate for shallow sources in the Pacific Northwest, multiple attenuation relationships were used in the PSHA.

5.1.1.4 Logic Tree

Uncertainty in the source parameters (e.g. geometry, updip and downdip extent, recurrence rate, etc.) are incorporated into the PSHA through the use of a logic tree approach (Figure 5-9). The logic tree approach considers potential alternative source parameters and assigns an associated weighting factor to the potential alternative. The weighting factor represents the likelihood that the parameter considered is the actual value. EZ-FRISK is used to calculate spectral ground motions (e.g., peak ground acceleration and spectral accelerations for 0.01, 0.02, 0.03, 0.05, at 0.075-, 0.1-, 0.2-, 0.3-, 0.5-, 0.75-, 1.0-, 2.0-, and 3.0-second periods) for each model represented by the end of each branch of the logic tree. The probability that the ground motions calculated by a given model is the "correct" motion is the product of the weighting factors along the entire length of a given branch. The final ground motion (e.g., peak ground acceleration or other spectral acceleration) is the sum of the ground motions calculated at the end of each branch of the logic tree after they have been factored by their respective probabilities of being "correct."

Figure 5-11 presents the logic tree used for the Skookumchuck Dam PSHA. The main branches of the logic tree describe modeling of hazards from the interplate, intraslab, and crustal earthquake sources. In many cases, the parameters represented by the branches of the logic tree at a particular node are assigned equal weights. This uniform distribution of weighting factors was used when the available evidence did not indicate that one model was preferred to the others. Specific branches of the logic tree where data suggest alternative distributions are discussed below.

Interplate Downdip Extent. Unequal weights are assigned to the different models for potential locations of the downdip extent of the CSZ interplate source. The weighting factor for the zero isobase downdip extent is set higher than those of the other two alternatives because of its basis in empirical observations from past subduction zone earthquakes. The weighting factor for the transition zone boundary is higher than that of the mafic zone boundary because of the additional uncertainty involved in the assumption of the mafic composition and thermo-mechanical behavior of the high-velocity region. Three potential downdip boundary locations and the weighting factors assigned to them are:

1. A downdip boundary corresponding to the center of the transition zone defined by Hyndman and Wang (1993, 1995). This boundary is assigned a weight of 0.33.

2. A downdip boundary corresponding to the zero isobase. This boundary is assigned a weight of 0.5.

3. A downdip boundary corresponding to the eastern edge of the high-velocity body identified by Stanley et al. (1999). This boundary is assigned a weight of 0.17.

Interplate Recurrence. The point estimation procedure produced two recurrence intervals that are treated as branches of a logic tree: 410 years (weighting factor = 0.67) and 985 years (weighting factor = 0.33). These recurrence intervals and the weighting factors produce mean, coefficient of variation, and skew coefficients equal to the average of those based on geologic evidence, turbidite evidence, and buried soil evidence (Section 4.1.1.3).

Interplate Rupture Length. To account for the fact that more than one segment could rupture at a given time, four possible rupture lengths are considered. The four rupture lengths are consistent with those identified by Geomatrix (1995) for their evaluation of seismic hazards in Oregon. The weighting factors used in the investigation give greater weight to longer ruptures than those used by Geomatrix (1995) in view of the increased evidence of very large CSZ earthquake that has been identified since the time of the Geomatrix study. The potential maximum rupture lengths and weighting factors assigned to each are:

1. A 150-kilometer rupture length that corresponds to the rupture of a single segment. The aspect ratio of such an event would be consistent with the average aspect ratio observed in worldwide subduction earthquakes. This rupture length is assigned a weight of 0.1.

2. A 250-kilometer rupture length that represents the average length of the rupture of two adjacent segments. The aspect ratio of such an event would be greater than most of the aspect ratios that have been observed in similar environments. This rupture length is assigned a weight of 0.3.

3. A 450 kilometer rupture that represents the average length of the rupture of three adjacent segments. The aspect ratio of a 450-kilometer rupture would be among the largest that have been observed worldwide. This rupture length is assigned a weight of 0.3.

4. A 1,100 kilometer rupture that represents the entire length of the CSZ. The aspect ratio of such an event would be approximately 14, which would be larger than any that has previously been observed. This rupture length is assigned a weight of 0.3.

Intraslab Geometry. Intraslab earthquakes are modeled using two different intraslab geometries – that of Crosson and Owens (1987) with a weighting factor of 0.75 and that of

Stanley et al. (1999) with a weighting factor of 0.25. The Crosson and Owens (1987) geometry is weighted more heavily due to its basis in actual measured earthquake hypocentral locations.

Intraslab Maximum Magnitude. For the PSHA, three different maximum intraslab magnitudes are considered: M7.1 (weighting factor = 0.25), M7-1/4 (weighting factor = 0.50), and M7-1/2 (weighting factor = 0.25). The weighting factors are selected using judgment and a review of other PSHAs.

Seattle Fault Maximum Magnitude. Three different maximum magnitudes are considered: M7.2 (weighting factor = 0.20), M7.4 (weighting factor = 0.6), M7.6 (weighting factor = 0.20). Based on rupture area, the mean maximum magnitude is estimated at 7.4 and is therefore given the greatest weight. Magnitudes 7.2 and 7.6 are minus and plus one standard deviation, respectively, around the estimated mean maximum magnitude and are given a lower weight.

Seattle Fault Slip Rate. The two slip rates used in the PSHA correspond to the estimated upper and lower bound slip rates from Johnson et al. (1999). The lower slip rate (0.07 centimeters per year) is given a higher weighting (0.7) as this slip rate resulted in recurrence intervals for characteristic events which are more consistent with the preliminary estimated recurrence rates determined from the geologic evaluation of the Toe Jam Hill Fault trenches.

Puget Sound Fault Activity. Prior to work by Johnson et al. (1999), this fault had not been identified by any other researchers, and additional work has not yet been published to further substantiate the existence of this fault. Consequently, we have assigned a weighting factor of 0.7 to the assumption of it being a seismogenic source.

Puget Sound Fault Maximum Magnitude. Three different maximum magnitudes are considered: M7.1 (weighting factor = 0.20), M6.9 (weighting factor = 0.6), M7.3 (weighting factor = 0.20). Based on rupture area, the mean maximum magnitude is estimated at 7.1 using the rupture area/magnitude relationship by Wells and Coppersmith (1994) and is therefore given the greatest weight. Magnitudes 6.9 and 7.1 (slightly less than plus/minus one standard deviation around the estimated mean maximum magnitude) are given a lower weight.

Crustal Source Zones Maximum Magnitude. Except for the Mt. St. Helens and Western Mt. Rainier zones, three different maximum magnitudes are considered: M7.0 (weighting factor = 0.20), M7.25 (weighting factor = 0.6), M7.5 (weighting factor = 0.20). These magnitudes and weighting factors are selected to be at least as large as the largest crustal event in historically observed in these zones (1872 North Cascades magnitude 7+ event) but not larger than the maximum magnitude assumed on the Seattle Fault (magnitude 7.6). For the Mount St. Helens Zone, maximum earthquake magnitudes considered are M6.0 (weighting factor = 0.2), M6.5 (weighting factor = 0.6), and M7.0 (weighting factor = 0.2). For the Western Mount Rainier Zone, maximum earthquake magnitudes considered are M5.25 (weighting factor = 0.2), M5.5 (weighting factor = 0.6), and M5.75 (weighting factor = 0.2).

Crustal Source Zones Depth. Except for the Mt. St. Helens and Western Mt. Rainier zones, three different depths for earthquakes within the source zones are considered: 12 kilometers (weighting factor = 0.20), 15 kilometers (weighting factor = 0.60), 18 kilometers (weighting factor = 0.20). Most of the historical shallow crustal seismicity is distributed between these depths. Consequently, a distribution about a depth of 15 kilometers is assumed by using lower weighting factors at depths of 15-kilometers-plus/minus-3-kilometers. This distribution is also consistent with a decollement between depths of 14 and 20 kilometers. In the Mount St. Helens and Western Mount Rainier Zones, historic seismicity has typically been observed throughout depths of 2 to 20 kilometers. Consequently depths of 2, 11, and 20 kilometers are assumed in the analysis with equal weighting factors of 0.33.

5.1.2 Results

The probabilistic seismic hazard for the Skookumchuck dam is estimated for peak horizontal acceleration and horizontal spectra acceleration for oscillator periods up to 3 seconds.

The soft rock (typical west coast rock conditions) uniform hazard spectra (UHS) for the OBE and IDE that are obtained by incorporating results as described above are shown for spectral acceleration, spectral velocity, and spectral displacement in Figures 5-12 through 5-14, respectively. Contributions of the various seismic sources to the mean hazard for peak horizontal acceleration, 1.0 second period and 3.0 second period are shown on Figures 5-15 through 5-17, respectively. The intraslab zone can be seen to dominate the peak acceleration hazard curve (Figure 5-15) for return periods greater than 100 years. At 1.0 second period (Figure 5-16) the crustal zone dominates the hazard for a 144-year return period with a significant contribution from the interslab and a smaller contribution from the interplate zone. For a 500-year return period, the intraslab and crustal source zones are still the highest sources of hazard; however, the contribution from the interplate is much greater and significant to the total hazard. At 3 seconds (Figure 5-17), the crustal zones are the highest sources of hazard for 144- and 500-year return periods, with significant contributions from the intraslab and interplate sources.

Deaggregation of the PSHA results for peak ground acceleration indicates that at 144 years, the distribution of the ground motion hazard is somewhat bimodal. Some of the ground motion hazard at the OBE level is from magnitude 5.25 to 5.75 events at distances of 10 to 30 kilometers; the majority of the contribution to the hazard is centered about a distance of 50 to 60 km and a magnitude of 5.0 to 7.0 (Figure 5-18 for PGA and Figure 5-19 for 1 second period). For the 500-year IDE level, the ground motion hazard is generally dominated by magnitude 6.75 to 7.75 events at distances of 40 to 70 kilometers with a some contribution from magnitude 8+ events at distances of 60 to 70 kilometers for periods greater than about 0.3 seconds (Figures 5-20 through 5-24).

5.2 DETERMINISTIC SEISMIC HAZARD ANALYSIS

Development of MCE ground motions is based on deterministic analyses. MCEs are selected based on the largest ground motions that may occur at the site from capable seismogenic sources. Two MCE sources were determined, namely the Cascadia Subduction Zone Interplate and the Legislature Fault.

5.2.1 Cascadia Subduction Zone Interplate

The maximum magnitude associated with the Cascadia Subduction Zone Interplate is M_w 9.0, which requires rupture of nearly the entire subduction zone. Based on the mafic wedge model of Stanley, et al. (1999), the closest approach of the seismogenic rupture approaches to within 51 kilometers of the site. The depth to the rupture surface is estimated at a depth of 45 kilometers. The corresponding distance from the dam to the closest point of rupture is 68 kilometers. Horizontal peak ground acceleration and response spectra were estimated for the site using the empirical attenuation relationship of Youngs et al. (1997), which was also used in the PSHA. The response spectrum is shown on Figure 5-25.

5.2.2 Legislature Fault

The maximum mean magnitude estimated for the Legislature fault is M_w 7.2, which assumes no segmentation or rupture across all segments of the fault. The closest distance from the dam to the fault trace is 9.3 kilometers. Because signs of surface ground rupture have not been observed, it was assumed that the fault could rupture to within 2 kilometers of the ground surface. The corresponding distance from the dam to the closest point of rupture is 9.5 kilometers. Horizontal peak ground acceleration and response spectra were estimated for the site using the empirical attenuation relationship of Abrahamson and Silva (1997), which was also used in the PSHA. The response spectrum is shown on Figure 5-26.

6.0 RECOMMENDED GROUND MOTIONS

Earthquake ground motion parameters required in the SOW include mean PGA, PGV, PGD, duration of shaking exceeding 0.05g (bracketed duration), horizontal and vertical response spectra at 2, 5, 10, and 20 percent damping for the ground motion levels considered. One set of time histories consisting of 2 horizontal orthogonal motions and 1 vertical motion for the OBE, IDE, and each MCE is also required. In addition, median and median-plus-one-standard-deviation motions for the MCEs are also required.

6.1 PEAK GROUND MOTIONS, SPECTRA AND DURATION

Table 6-1 lists the PGAs, PV's, PD's and bracketed duration for each design earthquake. Five percent damped horizontal and vertical spectra for the MCE are shown on Figures 6-1 through 6-3. Vertical spectra were computed from the horizontal component rock outcrop spectra by applying empirical frequency-dependant vertical/horizontal (V/H) ratios by Silva et al. (1999). Spectra for other damping levels (2, 10, and 20 percent) can be scaled from the 5 percent spectra by using the scaling factors in Table 6-2.

6.2 EARTHQUAKE TIME HISTORIES

Synthetic horizontal and vertical rock motions were developed to match the UHS response spectra for the MCE spectra shown in Figures 6-1 and 6-2. In addition to the synthetic time histories, recorded time histories were scaled to match the PGA of the OBE and IDE horizontal and vertical rock UHS spectra. The process to develop the time histories included the following:

1. Select appropriate earthquake time histories (i.e., selection time histories recorded on rock for similar magnitude, type of faulting, distance from fault, and duration).

2. Develop initial rock time histories compatible to OBE, IDE, and MCE rock UHS spectra. The rock UHS spectra are designated as "target" spectra. The initial MCE time histories are developed using the program RASCAL (Silva et al., 1987) to match the target spectra and the phase spectra from the selected earthquake time histories. The selected time histories for the OBE and IDE are scaled to match the PGA of the corresponding target rock UHS spectra

3. Baseline correct the initial rock time histories to minimize velocities and displacements at the end of the time history, using the program BASECOR (Abrahamson, 1994).

Table 6-3 lists the earthquake time histories that were selected in step 1 above. Because of the relatively few existing subduction zone histories, finite fault rupture simulations of the CSZ Interplate were conducted to develop synthetic earthquake time histories that would have the appropriate duration and phase. The finite fault simulation was conducted by Pacific Engineering and Analysis, under subcontract to Shannon & Wilson, Inc., and a detailed description of the simulation procedure is provided in Appendix A. Plots of the original seed time histories used in the development of the synthetic ground motions for the MCE are shown on Figure 5-27 and 5-28.

The three component time histories for the OBE, IDE, and MCEs are provided on a CD-ROM that accompanies this report. Plots of the acceleration, velocity, and displacement time histories; and response spectra for each component are presented in Appendix B. The peak ground motion parameters for each time history are shown on the time history plots in Appendix B.

SHANNON & WILSON, INC.

ROBERT A. MITCHELL
STATE OF WASHINGTON
35200
REGISTERED PROFESSIONAL ENGINEER
EXPIRES 8/17/01

REGISTERED PROFESSIONAL
OREGON
WILLIAM J. PERKINS
No. G1650
GEOLOGIST

Robert A. Mitchell, P.E. Principal Engineer	William J. Perkins, R.P.G Senior Principal Engineering Geologist

Gerard J. Buechel, P.E.
Vice President

RAM:WJP:GJB/wjp

7.0 REFERENCES

Abrahamson, N.A. (2000). BASECOR, baseline correction program.

Abrahamson, N.A. and Silva, W.J. (1997). "Empirical Response Spectral Attenuation Relations for Shallow Crustal Earthquakes," *Seismological Research Letters*, v. 68, No. 1, January/February, p. 94-127.

Adams, J. (1990). "Paleoseismicity of the Cascadia Subduction Zone: Evidence from Turbidites off the Oregon-Washington Margin," *Tectonics*, v. 9, No. 4, p. 569-583.

Adams, J. (1996). Great Earthquakes Recorded by Turbidites off the Oregon-Washington Coast, *in* Rogers, A.M., Walsh, T.J., Kockelman, W.J., and Priest, G.R., eds., Assessing Earthquake Hazards and Reducing Risk in the Pacific Northwest, U.S. Geological Survey Professional Paper 1560, pp. 147-158.

Atkinson, G.M. (1996). "The High-Frequency Shape of the Source Spectrum for Earthquakes in Eastern and Western Canada." *Bulletin of the Seismological Society of America* 86(1A), 106-112.

Atwater, B.F. (1987). "Evidence for Great Holocene Earthquakes along the Outer Coast of Washington State," *Science*, v. 236, p. 942-944.

_____ (1992). "Geologic Evidence for Earthquakes During the Past 2000 years along the Copalis River, Southern Coastal Washington," *Journal of Geophysical Research*, v. 97, p. 1901-1919.

Atwater, B.F. and Moore, A.L. (1992). "A Tsunami about 1000 years Ago in Puget Sound, Washington," *Science*, v. 236, p. 942-944.

Atwater, B.F. and Hemphill-Haley, E. (1997). "Recurrence Intervals for Great Earthquakes of the past 3500 years at Northeastern Willapa Bay, Washington," U.S. Geological Survey Professional Paper 1576.

Bechtel, 1971,

Boore, D.M., Joyner, W.B., and Fumal, T.E. (1997). "Equations for Estimating Horizontal Response Spectra and Peak Acceleration from Western North American Earthquakes: A Summary of Recent Work," *Seismological Research Letters*, v. 68, No. 1, January/February, p. 128-153.

Bucknam, R.C., Hemphill-Haley, E., and Leopold, E.B. (1992). "Abrupt Uplift within the Past 1700 Years of the Southern Puget Sound, Washington," *Science*, v. 258, p. 1611-1613.

Bucknam, R.C. (2000). Personal communication.

Byrne, D., Davies, D., and Sykes, L. (1988). “Loci and Maximum Size of Thrust Earthquakes and the Mechanics of the Shallow Region of Subduction Zones,” *Tectonics*, v. 7, p. 833-857.

Campbell, K.W. (1997). “Empirical Near-Source Attenuation Relationships for Horizontal and Vertical Components of Peak Ground Acceleration, Peak Ground Velocity, and Pseudo-Absolute Acceleration Response Spectra,” *Seismological Research Letters*, v. 68, No. 1, January/February, p. 154-179

Clarke, S.H., Jr. and Carver, G.A. (1992). “Late Holocene Tectonics and Paleoseismicity, Southern Cascadia Subduction Zone,” *Science*, v. 255, p. 188-192.

Clowes, R.M., Brandon, M.T., Green, A.G., Yorath, C.J., Brown, A.S., Kanasewich, E. R., and Spencer, C. (1987). LITHOPROBE--Southern Vancouver Island: Cenozoic Subduction Complex Images by Deep Seismic Reflections,” *Canadian Journal of Earth Sciences*, v. 24, p. 31-51.

Coffman, J.L. and von Hake, C.A. (1973). “Earthquake History of the United States,” (revised, ed.), U.S. National Oceanic and Atmospheric Administrative Publication 41-1.

Cohee, B.P., P.G. Somerville and N.A. Abrahamson (1991). “Simulated Ground Motions for Hypothesized M_w = 8 Subduction Earthquakes in Washington and Oregon.” *Bulletin of the Seismological Society of America*, 81(1), 28-56.

Cornell, C.A. (1968). “Engineering Seismic Risk Analysis,” *Bulletin of the Seismological Society of America*, v. 58, pp. 1583-1606.

Crosson, R.S. and Owens, T.J. (1987). “Slab Geometry of the Cascadia Subduction Zone Beneath Washington from Earthquake Hypocenters and Teleseismic Converted Waves,” *Geophysical Research Letters*, v. 14, p. 824-827.

Darienzo, M. and Peterson, C. (1990). “Investigation of Coastal Neotectonics and Paleoseismicity of the Southern Cascadia Margin as Recorded in Coastal Marsh Systems,” *in* Jacobson, M.L. ed., National Earthquake Hazards Reduction Program, Summaries of Technical Reports, Volume XXXI, U.S. Geological Survey Open File Report 90-680, p. 131-139.

Darienzo, M.E. and Peterson, C.D. (1995). “Magnitude and Frequency of Subduction-zone Earthquakes at Four Estuaries in Northern Oregon,” *Journal of Coastal Research*, Vol. 10, pp. 850-876.

Der Kiureghian, A. and Ang, A.H.S. (1975). “A Line Source Model for Seismic Risk Analysis,” University of Illinois Technical Report, UILU-ENG-75-2023, Urbana, 134 p. October.

Der Kiureghian, A. and Ang, A.H.S. (1977). "A Fault-Rupture Model for Seismic Risk Analysis," *Bulletin of the Seismological Society of America*, v. 67, No. 4, p. 1173-1194.

Dragert, H., Hyndman, R.D., Rogert, G.C., and Wang, K. (1994). "Current Deformations and the Width of the Seismogenic Zone of the Northern Cascadia Subduction Thrust," *Journal of Geophysical Research*, v. 99, p. 653-668.

EduPro Civil Systems (1999). ProShake.

Geomatrix Consultants (1993). "Seismic Margin Earthquake for the Trojan Site," Final unpublished report prepared for Portland General Electric Trojan Nuclear Plant, Rainier, Oregon.

_____, (1995). "Seismic Design Mapping, State of Oregon Final Report," prepared for Oregon Department of Transportation, Personal Services Contract 11688, Project No. 2442, January.

Goldfinger, C., Kulm, L.D., Yeats, R.S., Mitchell, C., Weldon, R.E., Peterson, C., Darienzo, M., Grant, W., and Priest, G. (1992a). "Neotectonic Map of the Oregon Continental Margin and Adjacent Abyssal Plain," Oregon Department of Geology and Mineral Industries, Open File report O-92-4, 17p.

Goldfinger, C., Kulm, L.D., Yeats, R.S., Applegate, B., MacKay, M.E., and Moore, G.F. (1992b). "Transverse Structural Trends along the Oregon Convergent Margin," *Geology*, v. 20, p.141-144.

Gower, H.D., Yount, J.D., and Crosson, R.S. (1985). "Seismotectonic Map of the Puget Sound Region, Washington," U.S. Geological Survey Miscellaneous Investigations Series Map I-1613, scale 1:250,000.

Grant, W.C. (1989). "More Evidence from Tidal-Marsh Stratigraphy for Multiple Late Holocene Subduction Earthquakes along the Northern Oregon Coast, " *Geological Society of America* Abstracts with Programs, v. 21, No. 4, p. 86.

Griggs, G.B. and Kulm, L.D. (1970). "Sedimentation in Cascadia deep-sea channel," *Geological Society of America Bulletin*, Vol. 81, pp. 1361-1384.

Hyndman, R.D. and Wang, K. (1993). "Thermal Constraints on the Zone of Major Thrust Earthquake Failure: the Cascadia Subduction Zone," *Journal of Geophysical Research*, v. 98, p.2039-2060.

_____, K. (1995). "The Rupture Zone of Cascadia Great Earthquakes from Current Deformation and the Thermal Regime," *Journal of Geophysical Research*, v. 100, No. 22, p. 133-154.

Jacoby, G.C., Williams, P.L., and Buckley, B.M. (1992). "Tree Ring Correlation Between Prehistoric Landslides and Abrupt Tectonic Events in Seattle, Washington," *Science*, v. 258, p. 1621-1623.

Jarrard, R.D., (1986). "Relations among Subduction Parameters," *Review of Geophysics*, v. 24, No. 2, p. 217-284.

Johnson, S.Y., Potter, C.J., and Armentrout, J.M. (1994). "Origin and Evolution of the Seattle Basin and Seattle Fault," *Geology*, v. 22, p. 71-74.

Johnson, S.Y., Potter, C.J., Armentrout, J.M., and others, (1996). "The Southern Whidbey Island Fault, an Active Structure in the Puget Lowland, Washington," *Geological Society of America Bulletin*, v. 108, p. 334-354.

Johnson, S.Y., Dadisman, S.V., Childs, J.R., and Stanley, W.D. (1999). "Active Tectonics of the Seattle Fault and Central Puget Sound, Washington--Implications for Earthquake Hazards," *Geological Society of America Bulletin*, v. 111, No. 7, p. 1042-1053, July.

Jones, M.A. (1996). "Thickness of Unconsolidated Deposits in the Puget Sound Lowland, Washington and British Columbia," U.S. Geological Survey Water-Resources Investigations Report 94-4133.

Karlin, R.E. and Arbella, S.E.B. (1992). "Paleoearthquakes in the Puget Sound Region Recorded in Sediments from Lake Washington, USA," *Science*, v. 258, p. 1617-1620.

Kramer, S.L. (1996). *Geotechnical Earthquake Engineering*, Prentice-Hall.

Lisowski, M. (1993). "Geodetic Measurements of Strain Accumulation in the Puget Sound Basin," *in* Large Earthquakes and Actives Faults in the Puget Sound Region, a Conference Sponsored by the Quaternary Research Center and U.S. Geological Survey, Seattle, Washington, Program Notes, 8 p.

Ma, L., Crosson, R.S., and Ludwin, R.S. (1996). "Western Washington Focal Mechanisms and their Relationship to Regional Tectonic Stress," U.S. Geological Survey Professional Paper 1560, p. 257-284.

McCrumb, D.R., Galster, R.W., West, D.O., Crosson, R.S., Ludwin, R.S., Hancock, W.E., and Mann, L.V. (1989). "Tectonics, Seismicity, and Engineering Seismology" in Washington, *in* Galster, Richard W., Engineering geology in Washington, v.1: Washington Division of Geology and Earth Resources Bulletin 78, p.97-120.

McGuire, R.K. (1976). "FORTRAN Computer Program for Seismic Risk Analysis," U.S. Geological Survey Open-File Report 76-67, 90 p.

_____, (1978). "FRISK: Computer Program for Seismic Risk Analysis Using Faults as Earthquake Sources," U.S. Geological Survey Open-File Report 78-1007, 70 p.

Meyers, R.A., Smith, D.G., Jol, H.M., and Peterson, C.D. (1996). "Evidence for Eight Great Earthquake-Subsidence Events Detected with Ground-Penetrating Radar, Willapa Barrier, Washington," Geology, v. 24, p. 99-102.

Nelson, A.R. (2000). Personal communication.

Nelson, A.R., Shennan, I., and Long, A.J. (1996). "Identifying Coseismic Subsidence in Tidal-Wetland Stratigraphic Sequences at the Cascadia Subduction Zone of Western North America," *Journal of Geophysical Research*, v. 101, pp. 6115-6135.

Parsons, T., Wells, E.W., and Fisher, M.A. (1999). "Three-Dimensional Velocity Structure of Siletzia and Other Accreted Terranes in the Cascadia Forearc of Washington," *Journal of Geophysical Research*, v. 104, no. B8, p.18,015-18,039.

Peterson, C.D., and Darienzo, M.E. (1996). "Discrimination of Climatic, Oceanic, and Tectonic Mechanisms of Cyclic Marsh Burial, Alsea Bay, Oregon," *in* Rogers, A.M., Walsh, T.J., Kockelman, W.J., and Priest, G.R., eds., Assessing earthquake hazards and reducing risk in the Pacific Northwest, U.S. Geological Survey Professional Paper 1560, pp. 115-146.

Plafker, G. and Kachadoorian, R. (1969). "Geologic Effects of the March 1964 Earthquake and Associated Seismic Sea Waves on Kodiak and Nearby Islands of Alaska," U.S. Geological Survey Professional Paper 543-D, 46 p.

Pratt, T.L., Johnson, S.Y., Potter, C.J., and others, (1997). "Seismic-reflection Images Beneath Puget Sound, Western Washington State," *Journal of Geophysical Research*, v. 102, p. 469-490.

Risk Engineering, (1998). EZ-FRISK, version 4.1

Rogers, W.P. (1970). "A Geological and Geophysical Study of the Central Puget Sound Lowland," Ph.D. thesis, University of Washington, Seattle, Washington, 123 p.

Rogers, A.M., Walsh, T.J., Kockelman, W.J., and Priest, G.R. (1996). "Earthquake Hazards in the Pacific Northwest--An Overview," *in* A.M. Rogers, T.J. Walsh, W.J. Kockelman and G.R. Priest (eds.), Assessing Earthquake Hazards and Reducing Risk in the Pacific Northwest, U.S. Geological Survey Professional Paper 1560, v. 1, p. 1-54.

Sadigh, K., Chang, C.-Y., Egan, J.A., Makdisi, F., Youngs, R.R. (1997). "Attenuation Relationships for Shallow Crustal Earthquakes Based on California Strong Motion Data," *Seismological Research Letters*, v. 68, No. 1, January/February, p. 180-189.

Schasse, Henry W. (1987) “Geologic Map of the Centralia Quadrangle, Washington” Washington Department of Natural Resources Open File Report 87-11, scale 1:250,000.

Schuster, R.L., Laiger, R.L., and Pringle, P.T. (1992). “Prehistoric Rock Avalanches in the Olympic Mountains, Washington,” *Science*, v. 258, p. 1620-1621.

Shennan, I., Long, A.J., Rutherford, M.M., Green, F.M., Innes, J.B., Lloyd, J.M., Zong, Y., and Walker, K.J. (1996). Tidal marsh stratigraphy, sea-level change and large earthquakes, I: a 5000 year record in Washington, USA, *Quaternary Science Reviews*, Vol. 15, pp. 1023-1059.

Silva, W.J. (1997). “Characteristics of vertical Strong ground motions for applications to engineering design.” Proc. Of the FHWA/NCEER Workshop on the Nat’l Representation of Seismic, I.M. Friedland, M.S Power and R. L. Mayes eds., *Technical Report NCEER*-97-0010.

Silva, W.J. and Lee, K. (1987). “State-of-the-art for Assessing Earthquake Hazards in the United States, Report 24, WES RASCAL Code for Synthesizing Earthquake Ground Motions,” US Army Corps of Engineers, Miscellaneous Paper S-73-1, May.

Silva, W.J., N. Abrahamson, G. Toro, C. Costantino (1997). “Description and validation of the stochastic ground motion model.” Submitted to Brookhaven National Laboratory, Associated Universities, Inc. Upton, New York.

Silva, W. J. R. McGuire, and C. Costantino. (1999). “Comparison of Site Specific Soil UHS to Soil Motions Computed with Rock UHS,” Proc. of the BNL, NEA/CSNI/R(2000)2.

Spence, G.D., Clowes, R.M., and Ellis, R.M. (1985). “Seismic Structure across the Active Subduction Zone of Western Canada:,” *Journal of Geophysical Research*, v. 90, p. 6754-6722.

Stanley, D., Villasenor, A., and Benz, H. (1999). “Subduction Zone and Crustal Dynamics of Western Washington: A Tectonic Model for Earthquake Hazards Evaluation,” U.S. Geological Survey Open-File Report 99-311 on-line edition, 66 p.

Tichelaar, B.W. and Ruff, L.J. (1993). “Depth of Seismic Coupling along Subduction Zones,” *Journal of Geophysical Research*, v. 98, p. 2017-2037.

Vrolijk, P. (1990). “On the Mechanical Role of Smectite in Subduction Zones,” *Geology*, v. 18, p. 703-707.

Walsh, Timothy J. (1987) “Geologic Map of the south half of the Tacoma Quadrangle, Washington.” Washington Department of Natural Resources Open File Report 87-3, scale 1:250,000.

Weaver, C.S. and Smith, S.W. (1983). "Regional Tectonic and Earthquake Hazard Implications of a Crustal Fault Zone in Southwestern Washington," *Journal of Geophysical Research*, v. 88, No. B12, pp. 10371-10383.

Weichert, D.H. and Hyndman, R.D. (1983). "A Comparison of the Rate of Seismic Activity and Several Estimates of Deformation in the Puget Sound Area," *in* Proceedings of Workshop XIV, Earthquake Hazards of the Puget Sound Region," U.S. Geological Survey Open-File Report 83-19, p. 105-130.

Wells, D.L. and Coppersmith, K.J. (1994). "New Empirical Relationships Among Magnitude, Rupture Length, Rupture Width, Rupture Area, and Surface Displacement," *Bulletin of the Seismological Society of America*, v. 84, No. 4, p. 974-1002.

Wells, R.E., Weaver, C.S., and Blakeley, R.J. (1998). "Fore-arc Migration in Cascadia and its Neotectonic Significance," *Geology*, v. 26, p. 759-762.

Williams, R. (2000). Personal communication (USGS).

Wong, I., Silva, W., Bott, J., Wright, D, Thomas, P., Gregor, N., Li, S., Mabey, M., Sojourner, A., and Wang, Y. (2000). "Earthquake Scenario and Probabilistic Ground Shaking Maps for the Portland, Oregon, Metropolitan Area," Interpretive Map Series IMS-16, State of Oregon Dept. of Geology and Mineral Industries.

Youngs, R.R., Chiou, S.-J., Silva, W.J., and Humphrey, J.R. (1997). "Strong Ground Motion Attenuation Relationships for Subduction Zone Earthquakes," *Seismological Research Letters*, v. 68, No. 1, January/February, p. 58-73.

TABLE 3-1
LARGEST HISTORIC EARTHQUAKES FELT IN WASHINGTON

99 Year	Date	Time (PST)	North Latitude	West Longitude	Depth (km)	Mag (felt)[1]	Mag (inst)[2]	Maximum Modified Mercalli Intensity	Felt Area (sq km)	Location
1872	Dec. 14	21:40	48° 48'00"	121° 24'00"	Shallow	7.3	None	IX	1,010,000	North Cascades
1877	Oct. 12	13:53	45° 30'00"	122° 30'00"	Shallow	5.3	None	VII	48.000	Portland, Oregon
1880	Dec. 12	20:40	47° 30'00"	122° 30'00"	?	?	None	VII	?	Puget Sound
1891	Nov. 29	15:21	48° 00'00"	123° 30'00"	?	?	None	VII	?	Puget Sound
1893	Mar. 06	17:03	45° 54'00"	119° 24'00"	Shallow	4.7	None	VII	21,000	Southeastern Washington
1896	Jan. 03	22:15	48° 30'00"	122° 48'00"	?	5.7	None	VII	?	Puget Sound
1904	Mar. 16	20:20	47° 48'00"	123° 00'00"	?	5.3	None	VII	50,000	Olympic Peninsula, eastside
1909	Jan. 11	15:49	48° 42'00"	122° 48'00"	Deep	6.0	None	VII	150,000	Puget Sound
1915	Aug. 18	06:05	48° 30'00"	121° 24'00"	?	5.6	None	VI	77,000	North Cascades
1918*	Dec. 06	00:41	49° 37'00"	125° 55'00"	?	7.0	7.0	VIII	650,000	Vancouver Island
1920	Jan. 23	23:09	48° 36'00"	123° 00'00"	?	5.5	None	VII	70,000	Puget Sound
1932	July 17	22:01	47° 45'00"	121° 50'00"	Shallow	5.2	None	VII	41,000	Central Cascades
1936	July 15	23:08	46° 00'00"	118° 18'00"	Shallow	6.4	5.75	VII	270,000	Southeastern Washington
1939	Nov. 12	23:46	47° 24'00"	122° 36'00"	Deep	6.2	5.75	VII	200,000	Puget Sound
1945	April 29	12:16	47° 24'00"	121° 42'00"		5.9	5.5	VII	128,000	Central Cascades
1946	Feb. 14	19:18	47° 18'00"	122° 54'00"	40	6.4	6.3	VII	270,000	Puget Sound
1946*	June 23	09:13	49° 48'00"	125° 18'00"	Deep	7.4	7.3	VIII	1,096,000	Vancouver Island
1949	April 13	11:55	47° 06'00"	122° 42'00"	54	7.0	7.1	VIII	594,000	Puget Sound
1949*	Aug. 21	20:01	53° 37'20"	133° 16'20"		7.8	8.1	VIII	2,220,000	Queen Charlotte Is, B.C.
1959	Aug. 05	19:44	47° 48'00"	120° 00'00"	35	5.5	5.0	VI	64,000	North Cascades, east side
1959*	Aug. 17	22:37	44° 49'59"	111° 05'	10-12	7.6	7.5	X	1,586,00	Hebgen Lake, Montana
1962*	Nov. 05	19:36	45° 36'30"	122° 35'54"	18	5.3	5.5	VII	51,000	Portland, Oregon
1965	April 29	07:28	47° 24'00"	122° 24'00"	63	6.8	6.5	VIII	500,000	Puget Sound
1981	Feb. 13	22:09	46° 21'01"	122° 14'66"	7	5.8	5.5	VII	104,000	South Cascades
1983*	Oct. 28	06:06	44° 03'29"	113° 51'25"	14	7.2	7.3	VII	800,000	Borah Peak, Idaho
1995	Jan. 28	07:11	47° 23'17"	122° 21'54"	16	--	5.0	V	--	Robinson Point, Washington
1996	May 2	20:04	47° 45'36"	121° 52'34"	7	--	5.1	V	--	Duvall, Washington
1997	June 23	11:13	47° 35'56"	122° 32'26"	7	--	4.9	VI		Bremerton, Washington
1999	July 2	05:43	47° 04'33"	123° 46'35"	41	--	5.9	VII	--	Satsop, Washington

[1] Mag (felt) = an estimate of magnitude, based on felt area; unless otherwise indicated, it is calculated from Mag (felt) = -1.88+1.53 logA, where A is the total felt area; from Toppozada 1975.
[2] Mag (inst) = instrumentally determined magnitude; refer to reference listed in the original Table 2 of Noson et al (1988) (or NGDC (1999) [post 1983]).
* Earthquake occurred outside the state of Washington.

Reference: Noson et al. (1988) and NGDC (1999)

TABLE 3-2
HISTORIC EARTHQUAKES IN OR NEAR WESTERN WASHINGTON, M ≥ 4[1]

Year	Month	Day	Time (GMT)	North Latitude (degrees)	West Longitude (degrees)	Depth (kilometers)	Magnitude[2]	Source
1841	12	2	16:00:00	45.6	122.7	–	4.3	GSC
1859	4	2	02:30:00	47	123	–	4.3	GSC
1864	10	29	18:10:00	48.5	123.5	–	5	GSC
1865	8	25	21:00:00	48.5	123.5	–	5	GSC
1872	12	15	05:37:00	48.6	121.4	–	7.4	GSC
1877	10	12	17:00:00	45.5	122.5	–	5.33	DNA
1885	10	9	08:00:00	47	123	–	4.3	GSC
1885	12	8	22:40:00	47.5	122.5	–	4.3	GSC
1891	9	21	13:00:00	48	123.5	–	4.3	OSU
1891	9	22	03:40:00	48	123.5	–	4.3	GSC
1891	11	29	23:21:00	48.11	123.45	–	5	OSU
1892	2	3	20:30:00	45.5	122.8	–	5	GSC
1892	4	17	14:50:00	47	123	–	5	GSC
1895	2	25	04:47:00	46.5	122.4	–	4.3	GSC
1895	4	16	00:02:00	48	123	–	4.6	GSC
1896	2	6	21:55:00	48.3	124.3	–	5	GSC
1896	4	2	03:17:00	45.3	123.3	–	5	GSC
1896	4	2	11:17:00	45.2	123.2	–	5	OSU
1903	3	14	02:15:00	47.7	122.2	–	4.3	GSC
1904	3	17	04:21:00	47.5	124	–	5.3	GSC
1909	1	11	23:49:00	48.7	122.8	–	6	DNA
1909	5	24	17:20:00	47.6	120	–	4	GSC
1911	9	29	02:39:00	48.8	122.7	–	4.3	GSC
1913	7	29	16:15:00	47	122	–	4.3	GSC
1913	12	25	14:40:00	47.7	122.5	–	4.3	GSC
1914	9	5	09:35:00	47	123	–	4.3	GSC
1915	5	18	19:00:00	45.5	122.7	–	4.3	GSC
1915	5	20	03:00:00	45.5	122.7	–	4.3	GSC
1915	8	18	14:05:00	48.53	121.43	–	5.5	GSC
1915	8	18	18:00:00	48.5	121.4	–	4.3	GSC
1916	1	2	00:52:00	47.3	122.3	–	4.3	GSC
1916	2	22	11:45:00	48.8	122.6	–	4.3	GSC
1917	3	28	17:05:00	46.8	122	–	4.3	GSC
1917	6	9	14:30:00	46.8	122	–	4.3	GSC
1917	11	12	10:47:00	46.8	121.8	–	4.3	GSC
1918	2	28	23:45:00	46.5	120.5	–	4.3	GSC
1918	6	21	06:47:00	46.5	121.7	–	4.3	GSC
1920	1	24	07:10:00	48.7	123	–	5	GSC
1923	2	12	18:30:00	49	122.7	–	4.3	GSC
1926	9	17	23:14:40	49	124	–	5.5	GSC

TABLE 3-2 (CONT.)
HISTORIC EARTHQUAKES IN OR NEAR WESTERN WASHINGTON

Year	Month	Day	Time (GMT)	North Latitude (degrees)	West Longitude (degrees)	Depth (kilometers)	Magnitude[2]	Source
1926	12	4	13:55:00	48.5	123	–	4.3	GSC
1926	12	30	17:57:00	47.7	120.2	–	5	DNA
1928	2	2	12:52:00	47.8	121.7	–	5	DNA
1930	7	19	02:38:00	45	123.2	–	5	DNA
1931	4	18	03:55:00	48.7	122.2	–	5	DNA
1931	12	31	15:25:00	47.5	123	–	5	DNA
1932	1	5	23:13:00	48	121.8	–	4.3	GSC
1932	7	18	06:01:00	48	121.8	–	5.7	DNA
1932	8	6	22:16:00	47.7	122.3	–	5	DNA
1934	5	5	04:06:00	48	123	–	4.3	GSC
1934	9	18	08:00:00	47	121	–	4.3	GSC
1934	9	27	00:15:00	47	121	–	4.3	GSC
1934	10	20	07:31:00	47	121	–	4.3	GSC
1934	11	1	15:28:00	47	121	–	4.3	GSC
1934	11	2	23:17:00	47	121	–	4.3	GSC
1934	11	3	14:50:00	48	121	–	4	GSC
1935	7	9	21:45:00	47.7	120	–	4.3	GSC
1938	1	6	13:11:00	47.8	122.4	–	4.3	GSC
1939	11	13	07:45:54	47.4	122.6	–	6.2	DNA
1940	10	27	22:29:18	47.2	123.4	–	4.6	GSC
1941	12	29	18:37:00	45.535	122.62	–	5	DNA
1942	10	14	11:30:00	48.3	120.6	–	4.3	GSC
1943	4	24	00:10:46	47.3	120.6	–	5	DNA
1943	11	29	00:43:00	48.4	122.9	–	5	DNA
1944	3	5	13:00:00	45	123.41	–	4.3	OSU
1944	3	31	22:15:00	47	123	–	4.3	GSC
1944	10	31	12:34:00	47.8	120.6	–	4.3	GSC
1944	12	7	04:48:00	46.977	123.89	–	5	DNA
1945	1	28	05:06:08.1	48.242	122.377	–	5	DNA
1945	4	29	20:16:17	47.4	121.7	–	5.7	DNA
1945	4	30	07:45:45	47.4	121.7	–	5	DNA
1945	5	1	20:46:00	47.4	121.7	–	4.3	GSC
1945	6	15	22:24:21	49	123.5	–	4.2	GSC
1945	11	12	04:05:00	48	122.5	–	5	DNA
1946	2	15	03:17:47	47.3	122.9	25	5.8	DNA
1946	2	15	12:17:15	46.87	122.268	–	5	DNA
1946	2	23	08:54:53	47.045	122.89	–	5	DNA
1948	9	24	22:35:00	47.855	122.587	–	5	DNA
1949	4	13	19:55:43	47.1	122.75	54	7.1	DNA
1949	6	1	08:23:15	47.5	124.5	–	4	GSC

TABLE 3-2 (CONT.)
HISTORIC EARTHQUAKES IN OR NEAR WESTERN WASHINGTON

Year	Month	Day	Time (GMT)	North Latitude (degrees)	West Longitude (degrees)	Depth (kilometers)	Magnitude[2]	Source
1950	4	14	11:03:48	48	122.5	–	5	DNA
1950	12	3	01:57:00	48	122.3	–	4.3	GSC
1952	8	6	17:32:17	47.5	122.4	–	4.3	GSC
1953	12	16	04:32:12	45.5	122.7	–	5	DNA
1954	3	16	15:56:00	47.1	121.8	–	4.3	GSC
1954	4	23	19:19:26	45.1	122.9	–	4	GSC
1954	5	5	01:42:00	47.3	122.4	–	4.3	GSC
1954	5	15	13:02:32	47.4	122.5	–	5	DNA
1955	3	26	06:56:51	48.1	122	–	5	DNA
1957	1	26	01:16:07.4	48.29	122.6	–	5	DNA
1957	2	11	17:05:56	47.5	121.7	–	5	DNA
1957	11	1	10:12:02	46.7	121.5	–	4.2	GSC
1957	11	16	22:00:00	45.3	123.8	–	5	GSC
1957	11	17	06:00:29	45.3	123.8	–	5	DNA
1958	4	12	22:37:11	48	120	–	5	DNA
1958	5	22	20:13:01	48.02	121.6	–	4.2	GSC
1958	10	7	05:07:56	46.7	124	–	5	DNA
1959	8	4	23:53:30	45.68	122.27	–	4.7	GSC
1959	11	23	18:15:25	46.67	121.75	–	4.8	GSC
1959	12	12	06:24:17	48.7	123.3	–	4.5	DNA
1960	9	10	15:06:34	47.7	123.15	–	5.2	DNA
1961	9	16	03:24:58	46	122.2	–	4.3	GSC
1961	9	17	15:55:55.9	46.023	122.122	7	5.1	DNA
1961	10	31	02:35:00	48.4	120	–	4.3	GSC
1961	11	7	01:29:08.4	45.7	122.866	–	5.1	DNA
1961	11	7	21:30:00	45.5	122.6	–	4.3	GSC
1962	1	15	05:29:13	47.833	120.216	–	4.4	DNA
1962	8	11	16:53:00	46	123.5	–	5	OSU
1962	11	6	03:36:43	45.608	122.598	18	5.5	DNA
1962	12	31	20:49:30.8	47.25	122.08	2	5.2	DNA
1963	1	24	21:43:09.8	47.57	122.03	–	5.1	DNA
1963	12	27	02:36:22.5	45.78	123.35	35	5	DNA
1964	1	15	23:06:36.2	45.9	120	33	4.2	PDE
1964	1	26	21:41:00	46.1	122.4	–	4.3	GSC
1964	4	26	01:42:49	48.7	120.5	–	4.4	DNA
1964	7	14	15:50:03.3	48.9	122.5	–	5	DNA
1964	10	1	12:31:24.6	45.7	122.8	–	4.5	DNA
1964	10	12	04:31:00	45.7	122.8	–	4.3	GSC
1964	10	14	06:33:00	47.7	122.1	–	4.3	GSC
1964	10	15	14:32:37.7	47.6	122.1	–	4.4	DNA

TABLE 3-2 (CONT.)
HISTORIC EARTHQUAKES IN OR NEAR WESTERN WASHINGTON

Year	Month	Day	Time (GMT)	North Latitude (degrees)	West Longitude (degrees)	Depth (kilometers)	Magnitude[2]	Source
1965	4	29	15:28:43.3	47.4	122.4	57	6.5	DNA
1965	10	23	16:27:59.3	47.5	122.4	–	4.8	DNA
1967	1	18	06:58:21	47.295	122.571	22	4	DNA
1967	3	7	03:51:8.8	47.84	122.68	34	4.5	DNA
1967	5	16	01:01:00	49	122.5	–	4	DNA
1967	5	25	23:22:34.5	48.2	122.81	33	4.5	DNA
1967	8	5	01:11:54.7	46.1	120	33	4.4	DNA
1968	1	27	08:28:23.7	45.61	122.605	34	4	DNA
1968	6	19	05:51:43	47.2	122.5	–	4.69	DNA
1968	9	6	12:16:30.8	48.1	122.76	34	4.7	DNA
1968	11	30	14:40:11	46.68	122.4	13	4.1	DNA
1969	2	14	8:33:36.1	48.94	123.07	52	4.7	DNA
1969	6	11	21:45:08	48.8	122.1	33	4	DNA
1969	10	9	17:07:55	46.766	121.716	–	4.3	DNA
1969	11	1	15:44:24.4	47.89	121.81	5	4.5	DNA
1969	11	10	07:38:44.7	48.55	121.51	33	5.1	DNA
1969	11	28	09:51:32.6	47.4	122.7	33	4.1	DNA
1970	5	18	05:29:54	48.6	122.7	18	4	GSC
1970	10	24	22:32:08.4	47.34	122.374	13	4.2	DNA
1971	11	23	02:12:17.3	48.178	121.37	18	4.14	DNA
1971	12	28	07:50:00.8	47.576	122.216	20	4.1	DNA
1972	11	9	04:19:19.9	48.394	123.23	42	4.12	DNA
1973	7	18	21:58:05.9	46.827	121.814	6	4	DNA
1974	4	20	03:00:10.3	46.774	121.567	–	4.9	DNA
1974	5	16	13:04:36.9	48.101	122.974	49	4.33	DNA
1974	12	13	03:28:54.2	45.265	121.599	22	4	DNA
1974	12	13	03:30:39	45.37	121.707	5	4.1	DNA
1975	4	16	19:09:29.4	47.548	122.909	42	4	DNA
1975	4	23	01:03:42.7	47.082	122.672	45	4.5	DNA
1976	4	13	00:47:15	45.154	120.861	15	4.8	DNA
1976	4	13	00:47:17.1	45.221	120.771	15	4.8	PDE
1976	4	17	02:11:46	45.168	120.801	15	4.2	DNA
1976	5	16	08:35:15	48.8	123.351	60	5.1	DNA
1976	9	2	13:36:11.4	48.193	122.768	20	4.5	DNA
1976	9	8	08:21:02	47.379	123.098	46	4.5	DNA
1976	10	14	21:39:18.2	46.697	122.384	5	4	DNA
1977	6	17	06:16:02.4	47.761	122.72	18	4	DNA
1977	7	10	07:19:30.2	48.583	122.398	13	4.3	DNA
1978	3	5	18:13:36.5	48.054	122.954	53	4	DNA
1978	3	11	15:52:11.6	47.422	122.718	24	4.8	DNA

TABLE 3-2 (CONT.)
HISTORIC EARTHQUAKES IN OR NEAR WESTERN WASHINGTON

Year	Month	Day	Time (GMT)	North Latitude (degrees)	West Longitude (degrees)	Depth (kilometers)	Magnitude[2]	Source
1978	3	31	08:03:00.4	47.42	122.721	23	4.2	DNA
1978	8	19	01:51:19	48.63	123.55	32	4.3	DNA
1978	8	23	10:37:19	48.349	123.212	18	4.4	DNA
1978	12	31	03:23:46.9	47.595	121.847	19	4.1	DNA
1979	3	11	14:39:33.2	46.444	122.406	17	4.2	DNA
1979	11	9	16:02:09	48.82	124.66	16	4.3	DNA
1979	11	26	23:18:27.3	48.549	122.396	17	4.1	DNA
1980	3	20	23:47:43.4	46.192	122.204	1	4.2	SEA
1980	3	22	22:22:42.5	46.204	122.221	–	4.2	SEA
1980	3	24	21:56:49.4	46.199	122.173	–	4.4	SEA
1980	3	25	07:08:46.1	46.197	122.183	–	4.1	SEA
1980	3	25	21:50:51.2	46.202	122.205	–	4.1	SEA
1980	3	25	22:53:01.6	46.2	122.18	–	4.3	SEA
1980	3	26	01:06:29.9	46.202	122.189	–	4	SEA
1980	3	26	02:03:18.3	46.206	122.206	–	4.4	SEA
1980	3	26	02:35:59.9	46.202	122.187	–	4.1	SEA
1980	3	26	05:00:04.3	46.203	122.184	–	4.3	SEA
1980	3	26	05:13:40.4	46.205	122.196	–	4.1	SEA
1980	3	26	05:30:09.8	46.2	122.195	–	4.2	SEA
1980	3	26	05:30:26.4	47.563	122.061	–	4	ISC
1980	3	26	07:17:21.8	46.205	122.183	–	4.1	SEA
1980	3	26	09:10:07.8	46.206	122.176	–	4.1	SEA
1980	3	26	09:44:02.5	46.201	122.169	–	4.4	SEA
1980	3	26	14:47:26.1	46.256	122.177	–	4.1	SEA
1980	3	26	17:07:10.8	46.192	122.206	2	4.4	SEA
1980	3	26	20:37:49	46.209	122.187	–	4	SEA
1980	3	27	03:40:05.6	46.218	122.18	–	4.2	SEA
1980	3	27	03:48:58.4	46.209	122.188	–	4.1	SEA
1980	3	27	04:26:10.3	46.194	122.182	4	4	SEA
1980	3	27	06:33:23.8	46.197	122.218	–	4.3	SEA
1980	3	27	07:39:15.5	46.207	122.178	–	4	SEA
1980	3	27	14:55:54.5	46.205	122.191	–	4.3	SEA
1980	3	27	15:55:03.7	46.209	122.201	1	4	SEA
1980	3	27	18:55:44.8	46.205	122.192	–	4	SEA
1980	3	27	20:16:43	46.204	122.186	–	4.3	SEA
1980	3	27	22:00:05.4	46.215	122.194	–	4.7	SEA
1980	3	28	01:51:12.6	46.206	122.187	2	4.3	SEA
1980	3	28	03:35:50.8	46.203	122.19	–	4	SEA
1980	3	28	08:28:25.6	46.214	122.178	–	4.9	SEA
1980	3	28	12:51:19.3	46.209	122.18	1	4.4	SEA

TABLE 3-2 (CONT.)
HISTORIC EARTHQUAKES IN OR NEAR WESTERN WASHINGTON

Year	Month	Day	Time (GMT)	North Latitude (degrees)	West Longitude (degrees)	Depth (kilometers)	Magnitude[2]	Source
1980	3	28	13:59:38.4	46.207	122.189	–	4.1	SEA
1980	3	28	15:18:43.2	46.205	122.204	–	4	SEA
1980	3	28	22:50:28.4	46.21	122.201	2	4.1	SEA
1980	3	29	05:48:47.3	46.205	122.193	2	4.4	SEA
1980	3	29	08:36:56.7	46.203	122.176	1	4.4	SEA
1980	3	29	10:34:40.3	46.214	122.185	–	4.3	SEA
1980	3	29	11:51:48.1	46.203	122.196	2	4.4	SEA
1980	3	29	13:01:50.7	46.199	122.204	–	4.3	SEA
1980	3	29	15:05:24.7	46.202	122.187	–	4.5	SEA
1980	3	29	15:35:39.6	46.214	122.176	1	4.4	SEA
1980	3	29	19:01:01.7	46.215	122.178	–	4	SEA
1980	3	29	20:55:51.8	46.207	122.19	–	4.4	SEA
1980	3	29	23:20:40.5	46.204	122.189	–	4.3	SEA
1980	3	30	02:56:19.6	46.211	122.192	–	4.3	SEA
1980	3	30	03:53:55	46.192	122.169	–	4.4	SEA
1980	3	30	07:42:17.1	46.206	122.183	–	4.1	SEA
1980	3	30	09:16:53.1	46.203	122.193	2	4.5	SEA
1980	3	30	12:39:57.6	46.21	122.177	–	4.1	SEA
1980	3	30	13:32:25.3	46.21	122.193	–	4.6	SEA
1980	3	30	17:55:10	46.208	122.183	–	4.6	SEA
1980	3	30	22:47:11.7	46.211	122.195	–	4.7	SEA
1980	3	31	02:44:6.1	46.208	122.193	–	4.5	SEA
1980	3	31	05:13:22.3	46.235	122.113	–	4.1	ISC
1980	3	31	07:49:42	46.21	122.188	–	4.7	SEA
1980	3	31	08:12:51.9	46.213	122.199	–	4.2	SEA
1980	3	31	11:34:9.8	46.21	122.194	–	4.6	SEA
1980	3	31	14:49:01.2	46.215	122.191	–	4.5	SEA
1980	3	31	14:49:01.2	46.212	122.193	–	4.5	SEA
1980	3	31	19:29:11.3	46.224	122.171	–	4.2	SEA
1980	4	1	04:24:30.5	46.215	122.18	–	4.9	SEA
1980	4	1	08:54:25.4	46.213	122.187	–	4.9	SEA
1980	4	1	12:30:46.6	46.208	122.182	1	4.9	SEA
1980	4	1	23:14:38.5	46.209	122.193	–	4.9	SEA
1980	4	2	09:37:12.9	46.21	122.191	–	4.9	SEA
1980	4	2	18:48:20.6	46.208	122.183	–	4.6	SEA
1980	4	3	02:43:19.3	46.208	122.189	–	4.8	SEA
1980	4	3	09:35:26.8	46.227	122.172	–	5.1	SEA
1980	4	3	15:30:20.1	46.203	122.186	–	4.3	SEA
1980	4	3	21:51:58.5	46.212	122.181	–	4	SEA
1980	4	3	23:57:51.9	46.212	122.187	–	5	SEA

TABLE 3-2 (CONT.)
HISTORIC EARTHQUAKES IN OR NEAR WESTERN WASHINGTON

Year	Month	Day	Time (GMT)	North Latitude (degrees)	West Longitude (degrees)	Depth (kilometers)	Magnitude[2]	Source
1980	4	4	09:42:35.3	46.212	122.206	1	4.3	SEA
1980	4	4	09:49:56.1	46.221	122.193	–	4	SEA
1980	4	4	13:45:05.6	46.209	122.181	–	4.9	SEA
1980	4	4	21:40:44.7	46.222	122.186	–	4.9	SEA
1980	4	5	06:39:3.1	46.204	122.183	–	4.3	SEA
1980	4	5	08:49:17.3	46.21	122.177	1	4.4	SEA
1980	4	5	10:58:49.2	46.203	122.191	–	4.1	SEA
1980	4	5	13:46:55.9	46.206	122.2	1	4.5	SEA
1980	4	5	16:42:05.5	46.216	122.2	2	4.7	SEA
1980	4	6	06:58:04.3	46.211	122.187	–	5.1	SEA
1980	4	6	17:18:46.6	46.213	122.174	–	4	SEA
1980	4	6	20:26:12.2	46.201	122.194	–	4.1	SEA
1980	4	6	23:22:56	46.205	122.174	–	4	SEA
1980	4	6	23:26:00.8	46.206	122.192	–	4.4	SEA
1980	4	7	01:57:44.8	46.207	122.196	–	4.1	SEA
1980	4	7	04:52:53.9	46.185	122.168	2	4	SEA
1980	4	7	06:45:18.9	46.213	122.182	–	4.8	SEA
1980	4	7	09:42:01.5	46.213	122.176	–	4	SEA
1980	4	7	11:32:31.6	46.21	122.177	–	4	SEA
1980	4	7	11:51:43.5	46.205	122.178	–	4	SEA
1980	4	7	15:05:32.7	46.217	122.182	3	5.1	SEA
1980	4	8	02:18:46.8	46.202	122.189	–	4	SEA
1980	4	8	04:46:58.2	46.211	122.178	–	4.1	SEA
1980	4	8	06:07:04.5	46.206	122.18	–	4.8	SEA
1980	4	8	13:42:26.9	46.201	122.183	–	4.1	SEA
1980	4	8	19:29:02.9	46.21	122.196	–	5.1	SEA
1980	4	8	22:10:15.2	46.225	122.188	–	4.2	SEA
1980	4	8	22:13:49.8	46.203	122.193	–	4.4	SEA
1980	4	9	05:40:50.6	46.481	122.324	–	4.2	ISC
1980	4	9	09:01:44.2	46.202	122.184	2	4.5	SEA
1980	4	9	10:13:19.8	46.192	122.185	–	4.7	SEA
1980	4	9	18:19:26.9	46.214	122.173	–	4.7	SEA
1980	4	9	22:29:03.3	46.207	122.183	–	4.1	SEA
1980	4	10	00:25:47.8	46.215	122.168	–	4.8	SEA
1980	4	10	00:25:51.8	46.332	122.099	4	4.3	ISC
1980	4	10	00:44:15.5	46.222	122.185	–	4.9	SEA
1980	4	10	00:44:18.7	46.309	122.075	4	4.8	ISC
1980	4	10	14:16:15.1	46.209	122.183	–	4.7	SEA
1980	4	10	21:08:26	46.206	122.18	–	4.2	SEA
1980	4	11	04:45:22	46.218	122.178	1	4.7	SEA

TABLE 3-2 (CONT.)
HISTORIC EARTHQUAKES IN OR NEAR WESTERN WASHINGTON

Year	Month	Day	Time (GMT)	North Latitude (degrees)	West Longitude (degrees)	Depth (kilometers)	Magnitude[2]	Source
1980	4	11	07:42:01.6	46.207	122.195	–	4.1	SEA
1980	4	11	14:52:25	46.209	122.188	–	4.1	SEA
1980	4	11	18:01:10.3	46.205	122.183	–	4.3	SEA
1980	4	11	19:15:08.3	46.2	122.152	–	4.1	SEA
1980	4	11	21:56:30.9	46.208	122.18	–	4	SEA
1980	4	11	23:51:59.8	46.208	122.168	–	5	SEA
1980	4	12	05:16:22.2	46.217	122.174	–	4.7	SEA
1980	4	12	15:08:11.7	46.204	122.186	–	4.3	SEA
1980	4	12	20:45:33.9	46.208	122.191	–	4	SEA
1980	4	12	20:47:42	46.213	122.18	–	4	SEA
1980	4	12	22:29:12	46.219	122.198	1	4.6	SEA
1980	4	13	01:25:55.9	46.203	122.189	–	4.2	SEA
1980	4	13	03:03:22.7	46.245	122.188	–	4	SEA
1980	4	13	04:45:26.9	46.208	122.186	–	4	SEA
1980	4	13	06:13:18.4	46.204	122.188	–	4.2	SEA
1980	4	13	08:36:18.7	46.212	122.18	1	4.8	SEA
1980	4	13	09:40:46.3	46.213	122.185	–	4	SEA
1980	4	13	12:06:20.5	46.207	122.195	–	4.1	SEA
1980	4	13	17:35:41.6	46.204	122.193	–	4.5	SEA
1980	4	13	18:58:21.6	46.21	122.183	–	4.9	SEA
1980	4	14	03:01:02.4	46.203	122.188	–	4.1	SEA
1980	4	14	06:53:38.8	46.215	122.178	–	4.3	SEA
1980	4	14	06:59:22.3	46.21	122.192	2	4.9	SEA
1980	4	14	12:28:43.5	46.212	122.187	1	4.4	SEA
1980	4	14	13:49:03.7	46.203	122.197	1	5.2	SEA
1980	4	14	15:30:30.6	46.207	122.189	–	4	SEA
1980	4	14	22:28:53.1	46.214	122.2	–	4	SEA
1980	4	15	00:37:5.3	46.209	122.184	2	4.5	SEA
1980	4	15	02:26:17.9	46.197	122.196	–	4.3	SEA
1980	4	15	06:58:22.2	46.211	122.201	1	4.7	SEA
1980	4	15	07:15:31.8	46.201	122.19	1	4	SEA
1980	4	15	11:53:53.9	46.207	122.188	1	4.1	SEA
1980	4	15	16:12:04.6	46.207	122.187	–	4.1	SEA
1980	4	15	17:54:54.1	46.213	122.181	–	5	SEA
1980	4	15	21:55:49	46.427	121.929	5	4	DNA
1980	4	16	04:58:57.4	46.205	122.184	1	4	SEA
1980	4	16	11:47:28.6	46.203	122.189	1	4.1	SEA
1980	4	16	15:22:05.5	46.212	122.186	–	4.8	SEA
1980	4	16	15:40:23.5	46.214	122.176	3	4.6	SEA
1980	4	16	22:46:24.7	46.207	122.188	–	4.2	SEA

TABLE 3-2 (CONT.)
HISTORIC EARTHQUAKES IN OR NEAR WESTERN WASHINGTON

Year	Month	Day	Time (GMT)	North Latitude (degrees)	West Longitude (degrees)	Depth (kilometers)	Magnitude^2	Source
1980	4	17	04:26:15.9	46.208	122.182	–	4.7	SEA
1980	4	17	07:06:47.3	46.193	122.202	2	4	SEA
1980	4	17	17:43:22.5	46.213	122.186	–	5	SEA
1980	4	18	00:51:05.7	46.208	122.187	–	4	SEA
1980	4	18	00:53:40.4	46.213	122.184	–	4.7	SEA
1980	4	18	00:53:43.6	46.389	122.119	2	4.7	ISC
1980	4	18	02:24:37.4	46.287	121.596	3	4.1	ISC
1980	4	18	09:23:38.9	46.201	122.188	–	4	SEA
1980	4	18	10:45:22.2	46.201	122.184	1	4	SEA
1980	4	18	13:03:55.2	46.212	122.178	–	4.2	SEA
1980	4	18	13:08:29.3	46.204	122.186	–	4	SEA
1980	4	18	19:16:25.3	46.205	122.184	2	4	SEA
1980	4	18	21:16:02.1	46.208	122.183	–	5	SEA
1980	4	18	22:27:14.4	46.208	122.178	1	4.6	SEA
1980	4	19	02:37:26.1	46.203	122.185	–	4.1	SEA
1980	4	19	06:03:12.4	46.204	122.193	–	4.1	SEA
1980	4	19	08:07:17.9	46.206	122.189	–	4.3	SEA
1980	4	19	14:53:14.2	46.207	122.182	–	4	SEA
1980	4	19	17:48:35.5	46.216	122.174	–	4.4	SEA
1980	4	19	22:28:28.2	46.21	122.181	1	4.8	SEA
1980	4	20	00:13:42.6	46.243	122.408	4	4	ISC
1980	4	20	04:53:02.4	46.206	122.185	–	4.1	SEA
1980	4	20	05:04:50.2	46.209	122.192	1	4	SEA
1980	4	20	08:08:08.5	46.218	122.192	–	4	SEA
1980	4	20	10:25:25	46.209	122.181	1	4.3	SEA
1980	4	20	17:53:34	46.202	122.191	–	4	SEA
1980	4	20	19:19:32.8	46.211	122.179	1	5.1	SEA
1980	4	20	22:03:48.7	46.211	122.176	–	4.4	SEA
1980	4	21	03:23:33.6	46.203	122.189	–	4.1	SEA
1980	4	21	05:17:52.1	46.209	122.181	–	4.3	SEA
1980	4	21	15:13:54.6	46.208	122.174	–	4.8	SEA
1980	4	21	19:52:08.5	46.211	122.167	–	4.4	SEA
1980	4	22	03:11:33	46.203	122.184	–	4	SEA
1980	4	22	6:11:55.8	46.211	122.181	1	4.4	SEA
1980	4	22	06:46:20	46.221	122.194	–	4	SEA
1980	4	22	10:25:05.4	46.209	122.189	–	4.4	SEA
1980	4	22	16:36:17.9	46.204	122.186	–	4	SEA
1980	4	22	19:28:18.7	46.203	122.182	–	5	SEA
1980	4	22	22:04:11	46.206	122.17	2	4.4	SEA
1980	4	23	13:08:15.3	46.207	122.202	1	4	SEA

TABLE 3-2 (CONT.)
HISTORIC EARTHQUAKES IN OR NEAR WESTERN WASHINGTON

Year	Month	Day	Time (GMT)	North Latitude (degrees)	West Longitude (degrees)	Depth (kilometers)	Magnitude[2]	Source
1980	4	23	15:18:01	46.208	122.18	–	4.5	SEA
1980	4	24	09:50:9.4	46.209	122.179	–	4.4	SEA
1980	4	24	10:50:42.6	46.212	122.191	–	4	SEA
1980	4	24	13:32:07.7	46.196	122.18	2	4.1	SEA
1980	4	24	17:34:10.3	46.213	122.183	–	4.8	SEA
1980	4	24	23:07:53.5	46.211	122.182	–	4.2	SEA
1980	4	25	00:27:57.5	46.202	122.205	–	4	SEA
1980	4	25	11:00:21.7	46.203	122.188	–	4.1	SEA
1980	4	25	23:20:27.9	46.257	122.18	5	4.6	DNA
1980	4	26	04:11:00.4	46.485	122.028	–	4.3	ISC
1980	4	26	12:16:55.6	46.204	122.187	–	4	SEA
1980	4	26	14:26:00.2	46.212	122.179	–	4	SEA
1980	4	26	15:53:59.7	46.207	122.183	–	4.1	SEA
1980	4	27	01:15:41.6	46.207	122.189	1	4.3	SEA
1980	4	27	01:15:45.5	46.443	122.104	4	4.2	ISC
1980	4	27	01:59:56	46.205	122.187	–	4.2	SEA
1980	4	27	07:15:17.4	46.203	122.186	3	4	SEA
1980	4	27	07:26:21	46.211	122.179	–	4.9	SEA
1980	4	27	12:34:37.3	46.208	122.188	–	4	SEA
1980	4	27	14:48:20.2	46.21	122.178	–	4.2	SEA
1980	4	28	03:49:33.5	46.208	122.189	1	4.9	SEA
1980	4	28	05:15:53.9	46.215	122.181	–	4.4	SEA
1980	4	28	12:30:54.6	46.199	122.188	–	4	SEA
1980	4	28	12:39:38.5	46.209	122.19	–	4.1	SEA
1980	4	28	15:09:07.5	46.202	122.182	–	4.1	SEA
1980	4	28	23:52:35.4	46.206	122.181	–	4.1	SEA
1980	4	29	04:24:30	46.214	122.18	1	4.8	SEA
1980	4	29	06:22:38.5	46.216	122.183	–	4.6	SEA
1980	4	29	12:41:36.3	46.21	122.18	–	4.2	SEA
1980	4	30	00:34:10.3	46.193	122.16	–	4.2	SEA
1980	4	30	00:34:15.8	46.478	121.921	1	4.2	ISC
1980	4	30	05:09:02.5	46.21	122.172	–	4.9	SEA
1980	4	30	05:09:02.5	46.211	122.169	–	4.9	SEA
1980	4	30	07:42:09.1	46.211	122.184	1	4.5	SEA
1980	4	30	07:42:09.2	46.212	122.189	1	4.5	SEA
1980	4	30	07:54:58.9	46.204	122.171	–	4	SEA
1980	4	30	20:50:38.4	46.202	122.186	–	4	SEA
1980	5	1	04:46:15.4	46.209	122.182	–	4.6	SEA
1980	5	1	04:46:15.4	46.207	122.182	–	4.6	SEA
1980	5	1	06:18:32.1	46.203	122.189	–	4.1	SEA

TABLE 3-2 (CONT.)
HISTORIC EARTHQUAKES IN OR NEAR WESTERN WASHINGTON

Year	Month	Day	Time (GMT)	North Latitude (degrees)	West Longitude (degrees)	Depth (kilometers)	Magnitude[2]	Source
1980	5	1	10:59:03.5	46.192	122.196	1	4	SEA
1980	5	1	19:27:15.6	46.189	122.199	–	4.6	SEA
1980	5	1	21:31:09.4	46.21	122.175	–	4.1	SEA
1980	5	2	05:12:18.9	46.209	122.183	2	4.4	SEA
1980	5	2	08:36:31.4	46.202	122.196	–	4.1	SEA
1980	5	2	12:52:17.7	46.206	122.176	6	4.3	SEA
1980	5	2	13:02:29.4	46.215	122.19	–	4.8	SEA
1980	5	3	05:00:46.4	46.204	122.179	–	4.5	SEA
1980	5	3	05:05:30.2	46.21	122.19	–	4.4	SEA
1980	5	3	06:47:50.5	46.2	122.187	–	4.1	SEA
1980	5	3	15:40:57	46.207	122.2	–	4.2	SEA
1980	5	3	20:45:37.8	46.199	122.173	–	4.2	SEA
1980	5	4	11:58:27.4	46.217	122.186	1	4.9	SEA
1980	5	4	21:39:22	46.201	122.189	–	4	SEA
1980	5	5	01:53:30.3	46.207	122.194	–	4	SEA
1980	5	5	05:43:04	46.21	122.179	1	4.7	SEA
1980	5	5	07:27:30.3	46.196	122.182	–	4	SEA
1980	5	5	09:12:54.4	46.211	122.18	1	4.3	SEA
1980	5	5	13:19:08.4	46.211	122.19	4	4	SEA
1980	5	5	16:13:51.9	46.213	122.176	–	4	SEA
1980	5	6	00:03:31.5	46.209	122.18	–	4.3	SEA
1980	5	6	08:15:01.6	46.206	122.198	–	4	SEA
1980	5	6	15:30:44.8	46.383	121.9	1	4	PDE
1980	5	6	17:04:49.1	46.21	122.174	1	4.6	SEA
1980	5	6	17:53:13.2	46.221	122.247	–	4	SEA
1980	5	6	19:22:28.3	46.211	122.178	1	4.4	SEA
1980	5	7	03:44:42.6	46.204	122.188	–	4.2	SEA
1980	5	7	08:52:32.9	46.205	122.187	–	4	SEA
1980	5	7	11:09:17.9	46.217	122.195	1	4.7	SEA
1980	5	7	12:33:20.8	46.204	122.181	–	4	SEA
1980	5	8	01:19:58.8	46.2	122.187	–	4.2	SEA
1980	5	8	07:46:50	46.207	122.191	1	4.4	SEA
1980	5	8	07:48:46.2	46.21	122.177	–	4.7	SEA
1980	5	8	08:47:55.4	46.203	122.191	–	4	SEA
1980	5	8	09:03:39.9	46.214	122.179	1	4.6	SEA
1980	5	8	10:05:38	46.206	122.193	–	4.3	SEA
1980	5	9	00:55:2.3	46.201	122.187	1	4	SEA
1980	5	9	04:31:58	46.203	122.179	–	4	SEA
1980	5	9	07:01:01.1	46.216	122.174	–	4.7	SEA
1980	5	9	14:10:37.2	46.207	122.182	1	4	SEA

TABLE 3-2 (CONT.)
HISTORIC EARTHQUAKES IN OR NEAR WESTERN WASHINGTON

Year	Month	Day	Time (GMT)	North Latitude (degrees)	West Longitude (degrees)	Depth (kilometers)	Magnitude[2]	Source
1980	5	9	18:06:26.5	46.214	122.174	1	4.6	SEA
1980	5	9	21:29:35.6	46.201	122.181	–	4	SEA
1980	5	10	01:14:10.5	46.204	122.187	1	4	SEA
1980	5	10	05:50:3.9	46.206	122.19	1	4.1	SEA
1980	5	10	09:25:55.3	46.18	122.119	–	4.1	SEA
1980	5	10	11:15:54.8	46.207	122.183	–	4	SEA
1980	5	10	12:31:47.5	46.213	122.178	1	4.5	SEA
1980	5	10	17:35:20.5	46.207	122.191	2	4.3	SEA
1980	5	11	01:19:29.4	46.202	122.189	2	4.1	SEA
1980	5	11	04:00:17.9	46.211	122.179	2	4.6	SEA
1980	5	11	08:09:48.3	46.203	122.185	1	4.1	SEA
1980	5	11	13:29:53.9	46.211	122.18	1	4.4	SEA
1980	5	11	15:00:52.1	46.199	122.166	1	4	SEA
1980	5	11	22:46:24.4	46.207	122.191	1	4.3	SEA
1980	5	12	12:11:25.2	46.207	122.194	–	4.2	SEA
1980	5	12	16:26:29.6	46.209	122.177	1	4.3	SEA
1980	5	12	16:46:50.2	46.203	122.182	1	4.3	SEA
1980	5	12	17:24:11.7	46.206	122.191	–	4.1	SEA
1980	5	12	18:42:09.9	46.211	122.17	–	4	SEA
1980	5	12	20:33:39.6	46.212	122.176	–	4.8	SEA
1980	5	13	01:30:50.1	46.217	122.173	–	4.4	SEA
1980	5	13	11:12:12.8	46.184	122.194	5	4.1	SEA
1980	5	14	02:18:57.7	46.213	122.177	1	4.6	SEA
1980	5	14	09:43:51.7	46.203	122.186	1	4.2	SEA
1980	5	14	14:08:16.3	46.21	122.171	1	4.1	SEA
1980	5	14	18:48:01.8	46.196	122.178	–	4.1	SEA
1980	5	14	23:45:58.4	46.203	122.181	–	4	SEA
1980	5	15	06:48:24.6	46.199	122.183	1	4.1	SEA
1980	5	15	17:29:16.7	46.207	122.167	1	4	SEA
1980	5	16	03:31:04.6	46.199	122.182	–	4.3	SEA
1980	5	16	12:34:54.1	46.213	122.197	1	4.7	SEA
1980	5	16	13:27:13.5	46.2	122.184	1	4.1	SEA
1980	5	16	14:22:00.2	46.207	122.179	1	4.3	SEA
1980	5	16	16:17:44.4	46.198	122.196	–	4.1	SEA
1980	5	17	08:31:53	46.197	122.205	3	4.2	SEA
1980	5	17	21:42:07.4	46.209	122.177	2	4.3	SEA
1980	5	18	01:50:52	46.198	122.184	2	4.1	SEA
1980	5	18	14:36:10.7	46.205	122.182	2	4.1	SEA
1980	5	18	15:32:11.4	46.207	122.188	2	5.7	SEA
1980	5	18	20:24:05.3	46.166	122.162	–	4.1	SEA

TABLE 3-2 (CONT.)
HISTORIC EARTHQUAKES IN OR NEAR WESTERN WASHINGTON

Year	Month	Day	Time (GMT)	North Latitude (degrees)	West Longitude (degrees)	Depth (kilometers)	Magnitude[2]	Source
1980	5	18	21:07:11.5	46.202	122.21	5	4.3	SEA
1980	5	18	21:10:06.9	46.203	122.194	3	4	SEA
1980	5	18	21:52:14.1	46.205	122.188	3	4.1	SEA
1980	5	18	21:54:40.9	46.203	122.176	2	4	SEA
1980	5	18	21:59:00.9	46.203	122.192	2	4	SEA
1980	5	18	22:18:08.8	46.199	122.177	1	4.1	SEA
1980	5	18	22:27:12.7	46.189	122.198	6	4.1	SEA
1980	5	18	22:35:49.9	46.209	122.207	10	4.2	SEA
1980	5	18	22:37:08	46.203	122.186	2	4	SEA
1980	5	18	22:38:34.2	46.195	122.189	1	4.1	SEA
1980	5	18	22:48:08.9	46.164	122.194	12	4.2	SEA
1980	5	18	22:49:04.4	46.199	122.191	2	4.2	SEA
1980	5	18	22:50:54.9	46.182	122.211	5	4.3	SEA
1980	5	18	22:54:01.3	46.227	122.18	–	4.5	SEA
1980	5	18	22:59:04.3	46.201	122.192	3	4.2	SEA
1980	5	18	23:00:49.9	46.208	122.193	6	4	SEA
1980	5	18	23:03:17.6	46.204	122.179	1	4	SEA
1980	5	18	23:07:21.5	46.127	122.15	–	4.3	SEA
1980	5	18	23:09:41.3	46.149	122.171	27	4.1	SEA
1980	5	18	23:14:19.5	46.211	122.184	3	4.1	SEA
1980	5	19	00:18:02.7	46.204	122.187	1	4	SEA
1980	5	19	00:58:02.6	46.626	121.788	–	4.1	ISC
1980	5	21	16:02:31.8	46.196	122.205	14	4.3	SEA
1980	5	24	23:01:23.6	46.333	122.213	2	4.1	SEA
1980	5	28	14:15:31.6	46.336	122.213	1	4.1	SEA
1980	5	28	14:18:30.2	46.335	122.206	3	4	SEA
1980	6	8	22:40:10.6	47.968	123.017	48	4.2	SEA
1981	2	2	01:23:18.3	46.263	120.989	1	4	SEA
1981	2	14	06:09:27.2	46.349	122.236	7	5.2	SEA
1981	2	18	06:09:38.7	47.197	120.893	3	4.2	SEA
1981	5	13	05:00:36.1	46.363	122.248	10	4.5	SEA
1981	5	28	08:56:02.5	46.53	121.398	2	4.6	SEA
1981	5	28	09:10:45.9	46.525	121.394	3	5	SEA
1982	3	1	17:40:04.7	46.346	122.247	11	4.4	SEA
1983	10	31	21:47:58.8	47.337	123.243	43	4.3	SEA
1984	4	11	03:07:42	47.535	120.186	8	4.3	SEA
1987	12	2	07:12:57.4	46.675	120.684	18	4.1	SEA
1987	12	2	09:02:24.2	46.679	120.673	17	4.3	SEA
1988	3	11	10:01:26	47.191	122.322	65	4.3	PDE
1988	7	29	04:59:47	46.855	121.914	11	4.1	SEA

TABLE 3-2 (CONT.)
HISTORIC EARTHQUAKES IN OR NEAR WESTERN WASHINGTON

Year	Month	Day	Time (GMT)	North Latitude (degrees)	West Longitude (degrees)	Depth (kilometers)	Magnitude[2]	Source
1989	2	14	21:41:10	48.429	122.228	–	4	SEA
1989	3	5	06:42:00	47.813	123.357	46	4.5	SEA
1989	3	6	03:09:54	48.429	122.231	1	4.2	SEA
1989	6	18	20:38:37.3	47.41	122.776	45	4.4	PDE
1989	9	12	10:57:02	46.2	122.4	33	4	NAO
1989	12	24	08:45:58	46.65	122.116	18	4.9	SEA
1990	4	2	11:13:22	48.832	122.188	–	4.3	SEA
1990	4	3	02:18:20	48.836	122.175	2	4	SEA
1990	4	14	05:33:26	48.845	122.161	12	5	SEA
1990	4	14	05:40:07	48.822	122.189	3	4	SEA
1990	6	9	17:12:16	46.268	122.055	10	4	SEA
1990	6	11	11:44:90	48.268	121.761	4	6	SEA
1990	12	20	22:16:12	46.201	122.186	1	6	SEA
1990	12	21	02:45:33	46.204	122.187	–	5	SEA
1991	5	3	23:12:36	46.267	122.21	7	6	SEA
1993	3	25	13:34:35	45.035	122.607	20	5.6	SEA
1994	6	15	08:22:19.8	47.411	123.161	45	4	SEA
1994	6	18	07:01:07.3	47.621	121.27	–	4.3	SEA
1995	5	20	12:48:48.2	46.881	121.943	13	4.1	SEA
1996	5	3	04:04:22	47.76	121.88	4	5.5	PDE
1997	6	23	19:13:27	47.6	122.57	7	5	PDE
1997	6	24	14:23:12	48.38	119.89	7	4.6	PDE
1998	10	9	16:43:08	46.2	120.7	3.2	4	PNSN
1999	7	3	01:43:54	47.08	123.46	40	5.9	PDE-W

Notes:

[1] Data from National Geographic Data Center, Boulder, Colorado

[2] M_S, M_L, m_b or based on felt area or Maximum Modified Mercalli Intensity. Maximum reported magnitudes are listed on the table

TABLE 4-1
ESTIMATED CSZ RUPTURE WIDTHS

Boundary Locations	Average Updip boundary width at deformation front	Average Updip boundary width at slope break
Downdip boundary at zero isobase	90 km	65 km
Downdip boundary at midpoint of transition zone	75 km	50 km
Downdip boundary at edge of mafic zone	120 km	95 km

TABLE 4-2
COMPUTED RECURRENCE INTERVAL STATISTICS.

	Mean (years)	Standard Deviation (years)	Coefficient of Variation	Skew Coefficient
Geologic evidence	657	204	0.311	1.06
Turbidite evidence	619	292	0.472	0.80
Buried soil evidence	524	301	0.574	0.29
Average values	600	-	0.452	0.72

TABLE 6-1
PEAK GROUND MOTION PARAMETERS

Earthquake	Magnitude	Depth (km)	Horizontal Distance To Rupture (km)	Distance To Rupture (km)	Peak Ground Acceleration (g)		Peak Ground Velocity (cm/sec)		Peak Ground Displacement (cm)		Bracketed Duration (Sec)[1]
					Horizontal[1]	Vertical	Horizontal[1]	Vertical	Horizontal[1]	Vertical	
OBE	n/a	n/a	n/a	n/a	0.12	0.09	5.04	2.01	0.48	0.33	2
IDE	n/a	n/a	n/a	n/a	0.22	0.19	29.08	25.93	13.5	33.2	24
CSZ MCE (median)	9	45	51.0	68.0	0.21	0.18	18.6	14.6	17.3	18.8	129
CSZ MCE (median+1s)	9	45	51.0	68.0	0.41	0.35	36.9	20.7	26.9	22.1	217
Legislature Fault MCE (median)	7.2	2	9.3	9.5	0.40	0.21	36.9	22.8	23.0	22.5	43
Legislature Fault MCE (median+1s)	7.2	2	9.3	9.5	0.65	0.47	64.4	52.0	24.5	25.1	81

Notes:
[1] Peak ground parameters and duration obtained from the larger of the two horizontal components.
CSZ = Cascadia Subduction Zone
IDE = Intermediate Design Earthquake
km = kilometers
MCE = Maximum Credible Earthquake
OBE = Operating Basis Earthquake
n/a = Not applicable

TABLE 6-2
RESPONSE SPECTRA SCALING FACTORS FOR DAMPING

Damping (Percent)	Spectral Acceleration Scaling Factor	Spectral Velocity Scaling Factor	Spectral Displacement Scaling Factor
2	1.29	1.23	1.17
5	1.00	1.00	1.00
10	0.77	0.83	0.86
20	0.65	0.65	0.73

Note:
Scaling factors are after Newmark and Hall, 1982.

TABLE 6-3
EARTHQUAKE TIME HISTORY SOURCES

Design Event	Historic Earthquake	Magnitude	Station	Closest Approach Distance (km)[3]
OBE	1957 San Francisco	5.3	Golden Gate Park[1]	12
IDE	1949 Olympia	7.1	Olympia Hwy Test Lab[1]	54
CSZ MCE	Finite Fault Sim.	9	n/a	n/a
Legislature Fault MCE	1992 Landers	7.3	Lucerne[2]	1

Notes:
1. The recorded earthquake time history from this station was scaled to the PGA of the corresponding rock UHS.
2. The phase spectra from this recorded earthquake time history and the corresponding rock UHS were used as inputs to the spectral matching program.
3 Closest Approach Distance between Historic Earthquake and referenced station. This distance should not be considered directly related to the Skookumchuck PSHA deaggregation analysis.

CSZ = Cascadia Subduction Zone
IDE = Intermediate Design Earthquake
Km = kilometer
MCE = Maximum Credible Earthquake
n/a = Not applicable
OBE = Operating Basis Earthquake

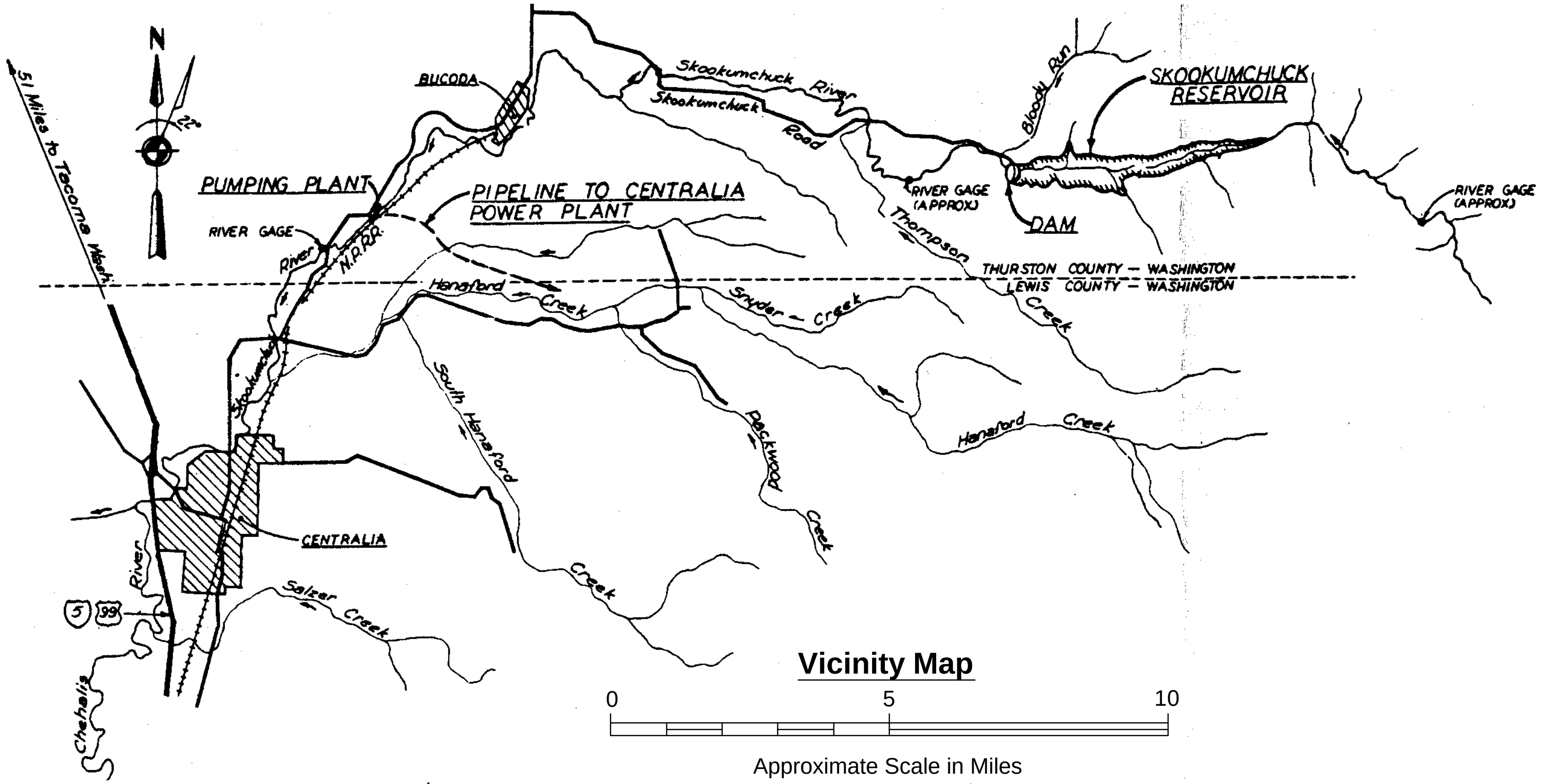

Vicinity Map

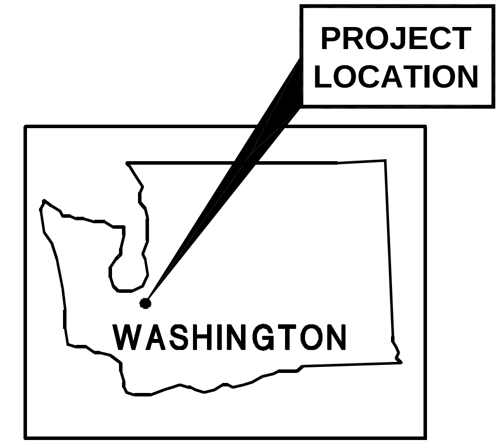

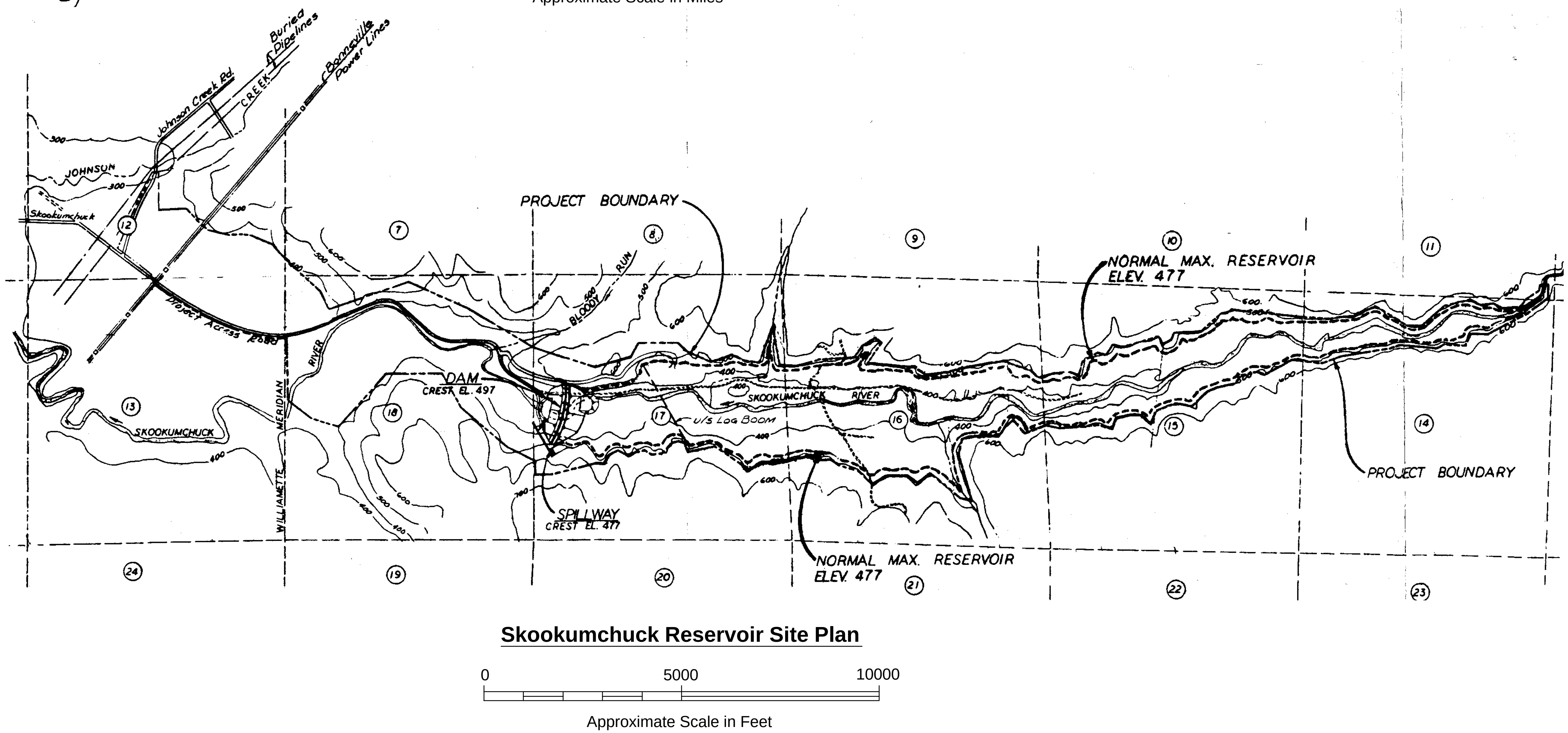

Skookumchuck Reservoir Site Plan

NOTE

1. Vicinity Map and Site Plan from "Project Location and Reservoir Map" dated 2/5/69, final revision 5/20/71 by Bechtel Corporation.
2. Vertical Datum, U.S. Coast & Geodetic Survey, North American 1947 Adjustments.

Seismic Ground Motion Study Skookumchuck Dam Lewis County, Washington	
VICINITY MAP AND SITE PLAN	
July 2000	21-1-08920-001
SHANNON & WILSON, INC. Geotechnical and Environmental Consultants	**FIG. 1-1**

File: I:\Drafting\211\08920-001\21-1-08920-001 Fig 4-2.dwg Date: 03-05-2001 Author: LR

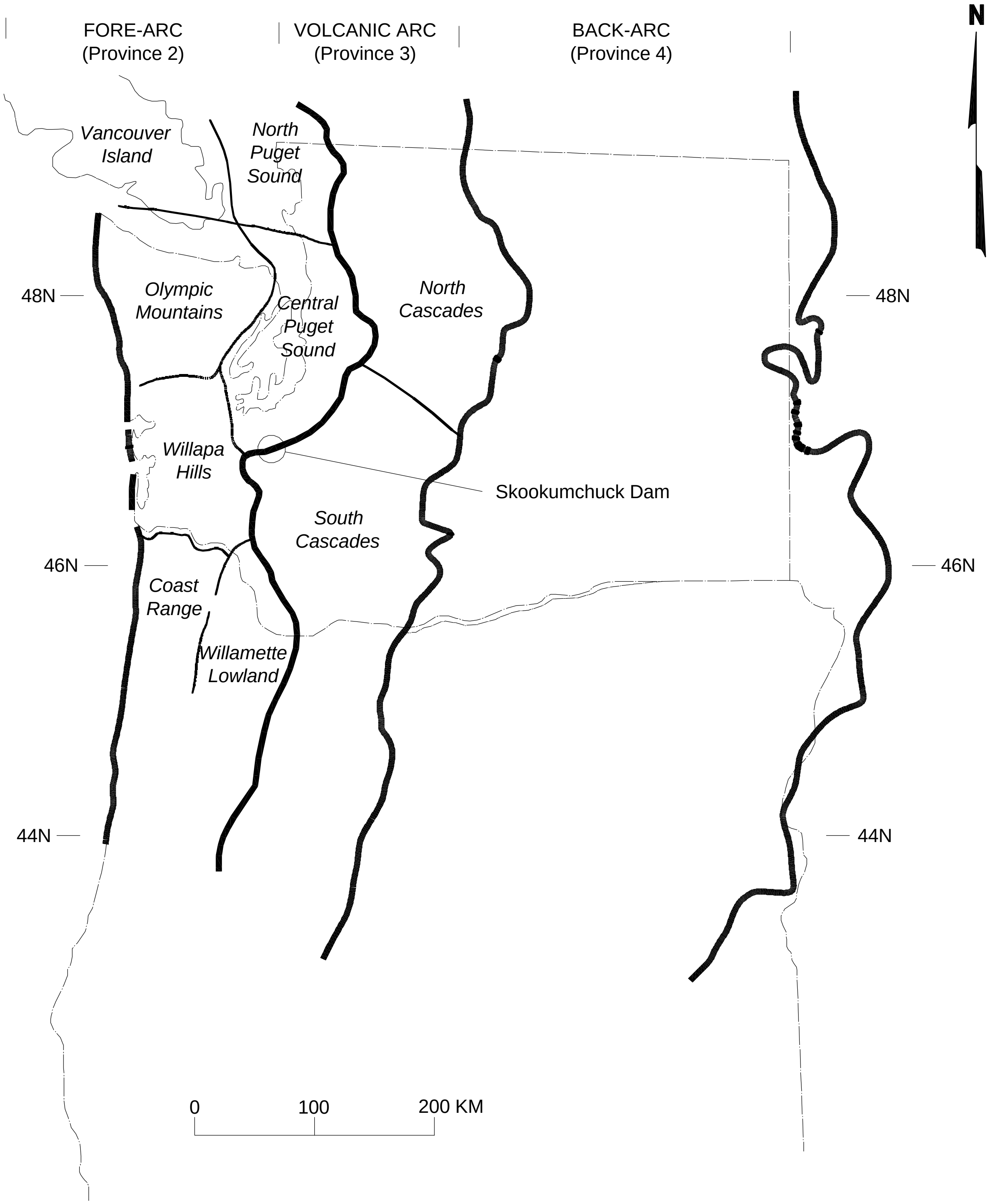

NOTE

Figure adapted from McCrumb et al., 1989.

Seismic Ground Motion Study
Skookumchuck Dam
Lewis County, Washington

NORTH AMERICAN PLATE TECTONIC PROVINCES IN WESTERN WASHINGTON

July 2000 21-1-08920-001

SHANNON & WILSON, INC.
Geotechnical and Environmental Consultants

FIG. 3-1

File: I:\Drafting\211\08920-001\21-1-08920-001 Fig 3-1.dwg Date: 03-05-2001 Author: LR

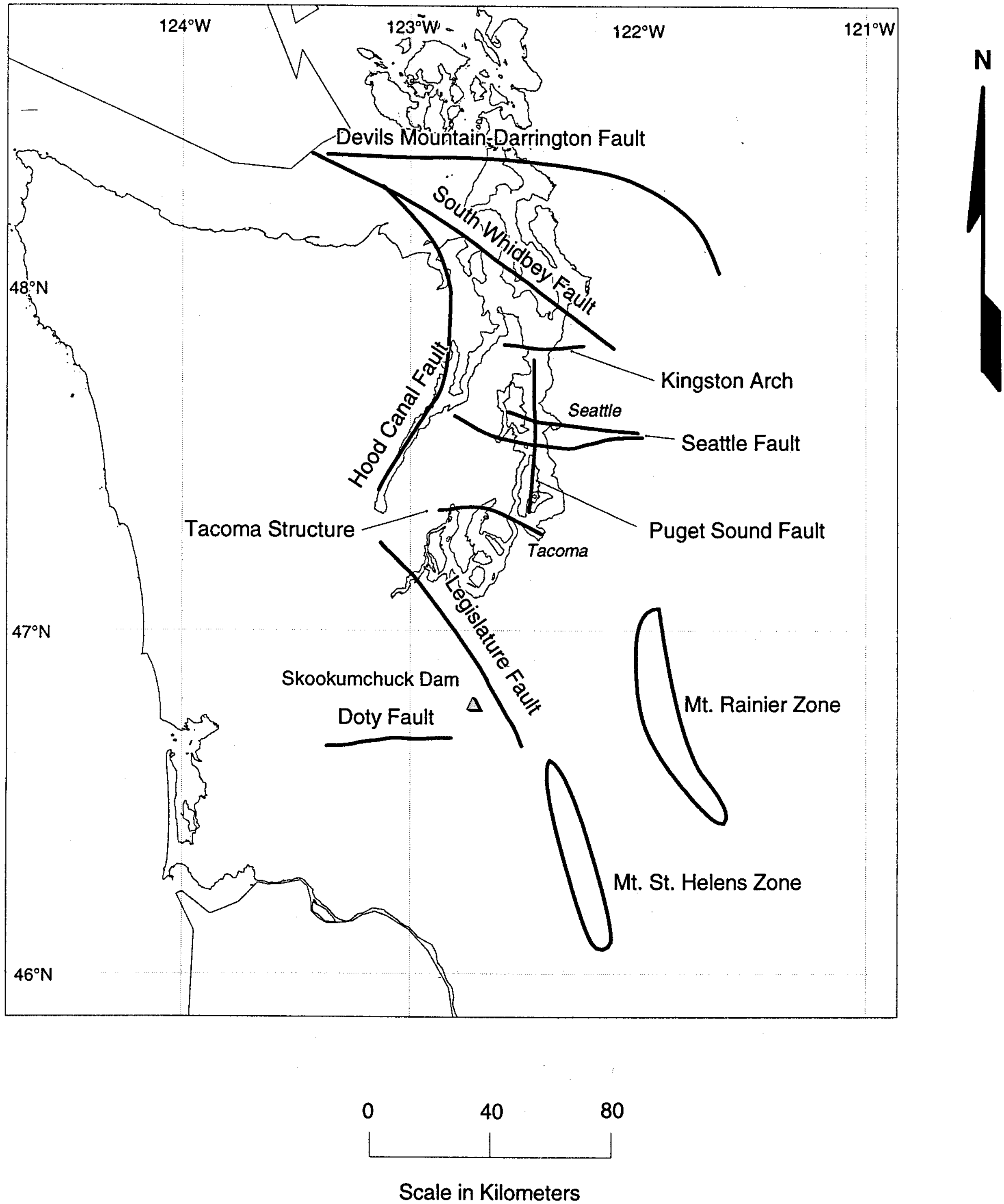

NOTE

Structural Features after Gower et al., (1985), Johnson et al., (1996), Rogers et. al., (1996), Pratt et al., 1997, Johnson et al., (1999).

Seismic Ground Motion Study
Skookumchuck Dam
Lewis County, Washington

CRUSTAL STRUCTURAL FEATURES IN WESTERN WASHINGTON

July 2000 21-1-0890-001

SHANNON & WILSON, INC.
Geotechnical and Environmental Consultants

FIG. 3-2

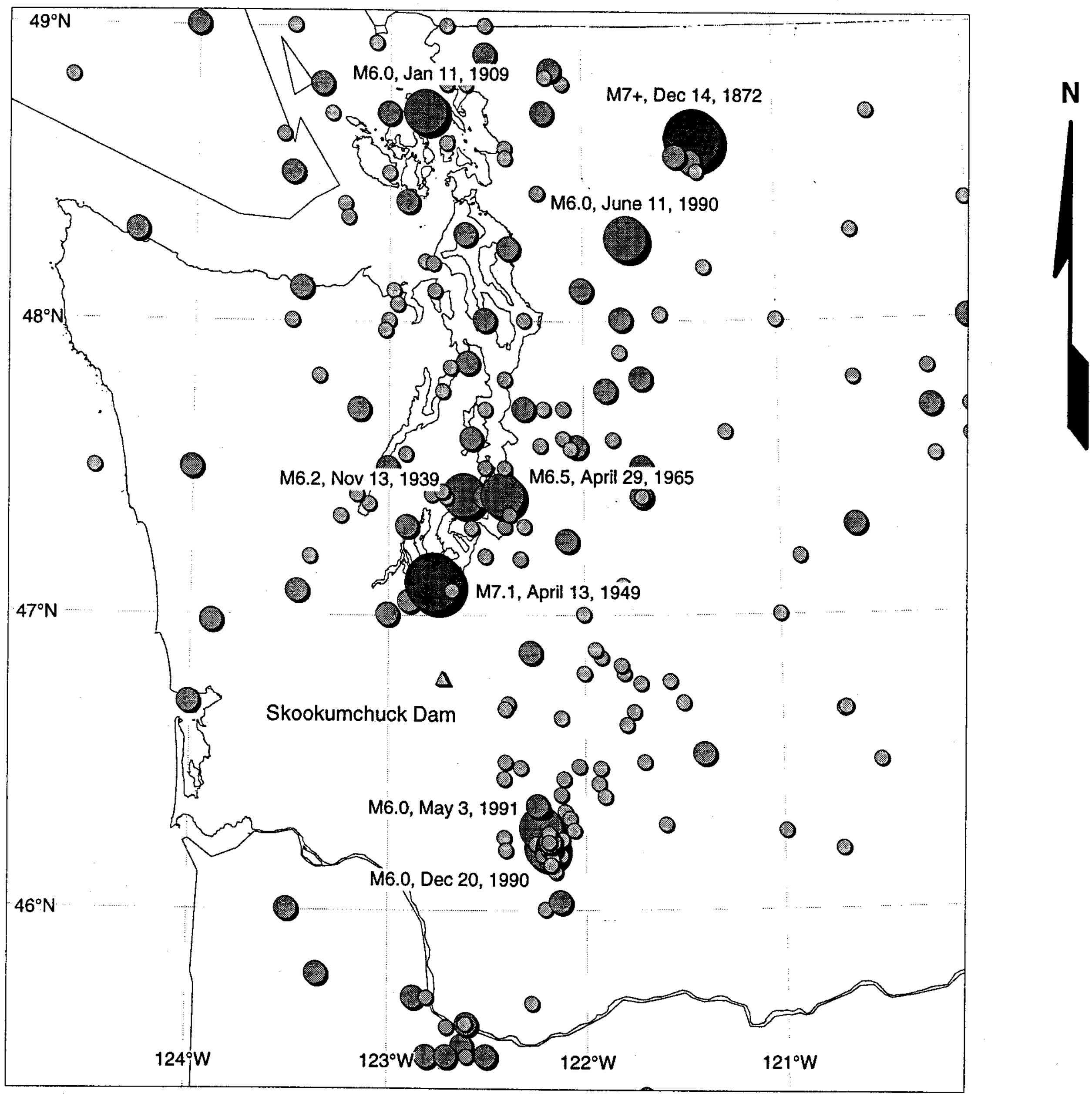

LEGEND

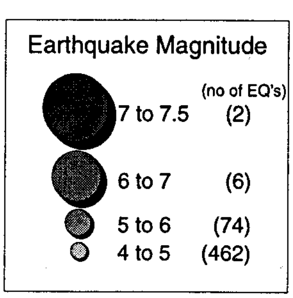

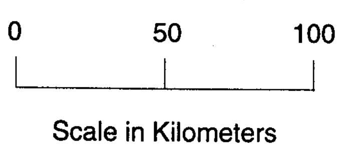

NOTE

Historic Earthquakes shown on this figure are tabulated on table 3-2.

Seismic Ground Motion Study Skookumchuck Dam Lewis County, Washington	
HISTORIC EARTHQUAKES IN OR NEAR WESTERN WASHINGTON	
July 2000	21-1-0890-001
SHANNON & WILSON, INC. Geotechnical and Environmental Consultants	**FIG. 3-3**

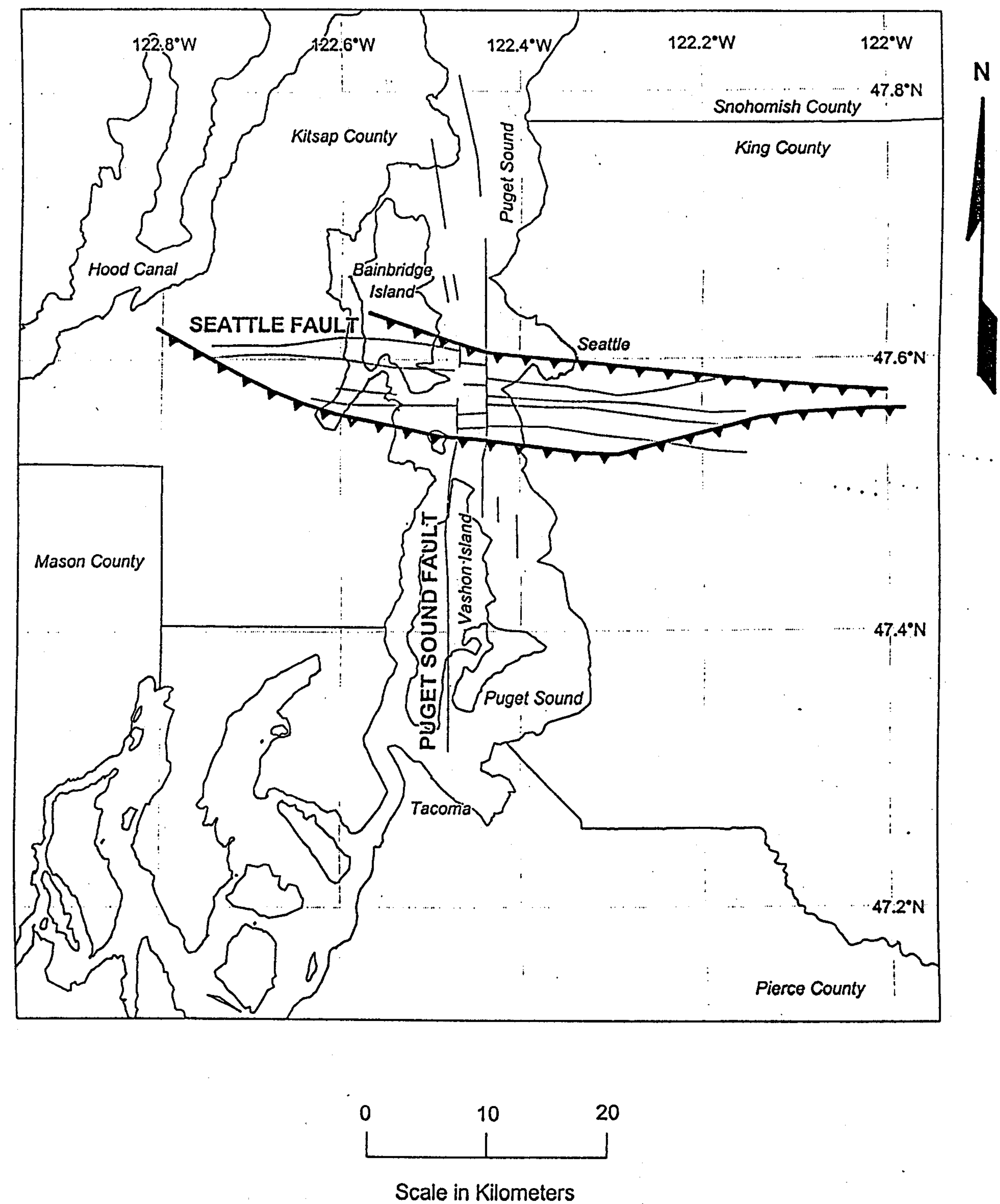

LEGEND

Seattle Fault Strands from Gower et al., 1985 (teeth on up-thrown side)

Seattle and Puget Sound Fault Strands from Johnson et al., 1999

Seismic Ground Motion Study Skookumchuck Dam Lewis County, Washington	
SEATTLE AND PUGET SOUND FAULTS	
July 2000	21-1-08920-001
SHANNON & WILSON, INC. Geotechnical and Environmental Consultants	FIG. 3-4

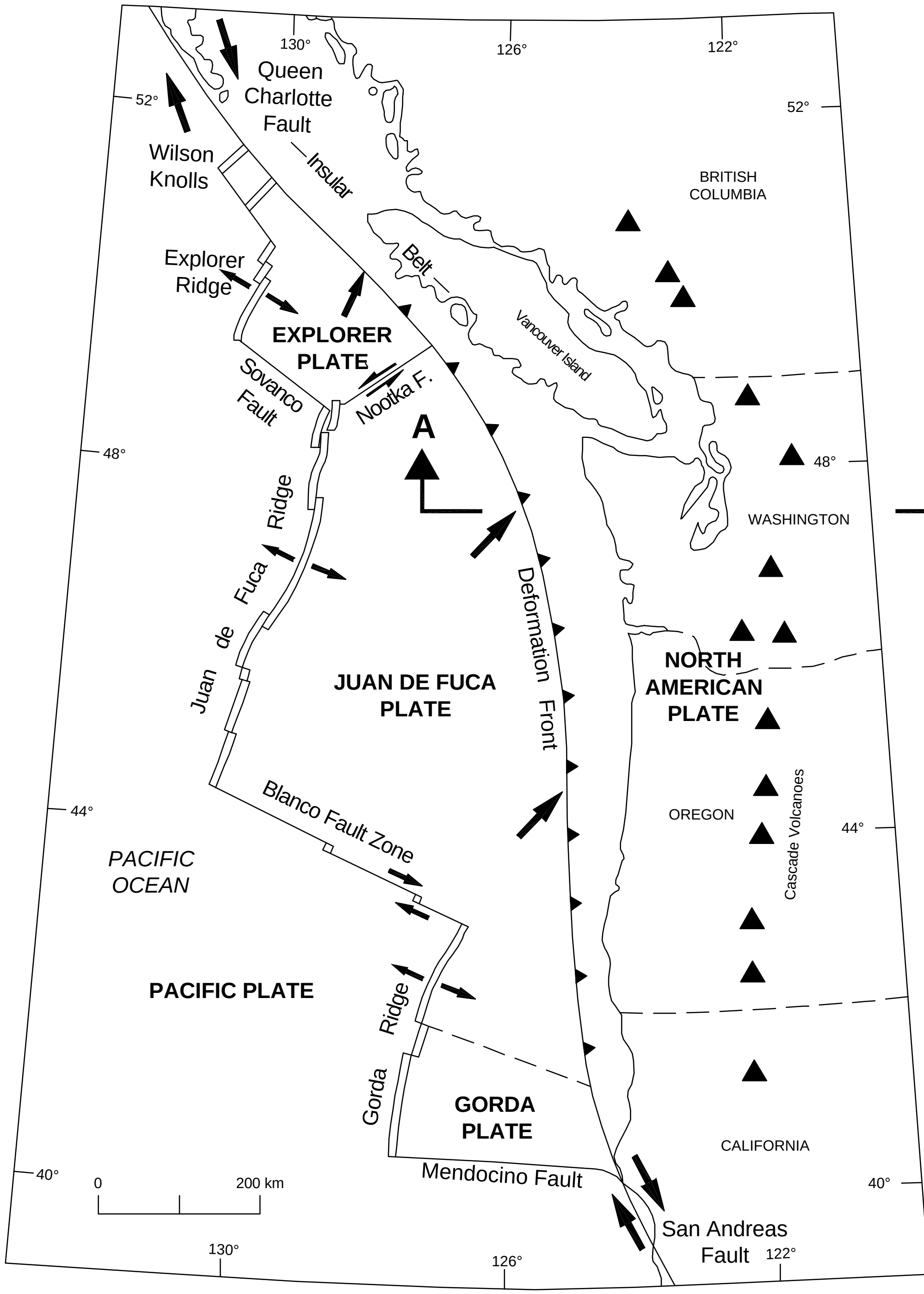

NOTE

Map based on Hyndman and Wang (1993), Peterson et al. (1993), and Geomatrix (1995)

Seismic Ground Motion Study
Skookumchuck Dam
Lewis County, Washington

REGIONAL MAP OF THE CASCADIA SUBDUCTION ZONE

July 2000 21-1-08920-001

SHANNON & WILSON, INC.
Geotechnical and Environmental Consultants

FIG. 4-1

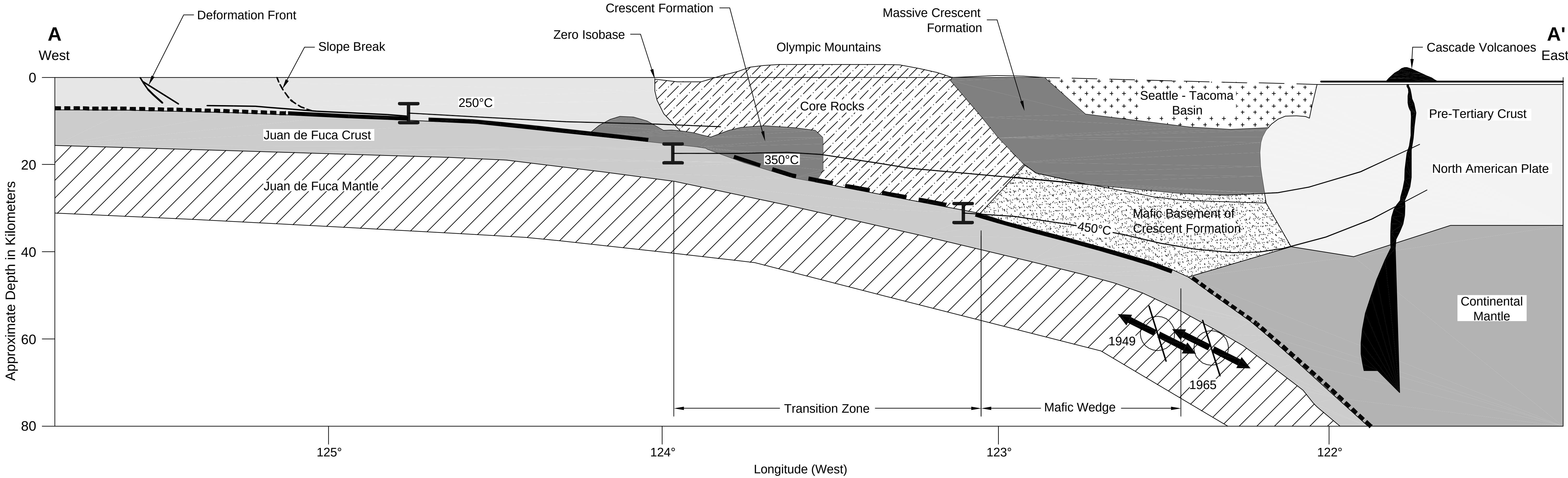

0 50 100

Approximate Scale in kilometers

FRICTIONAL STATES ON THRUST

- Free Slip
- Locked (stick-slip)
- Transitional
- Locations of 1949 and 1965 Earthquakes (Tensional)
- Isotherm Contours

NOTE

Figure Based on Stanley, et al, (1999) & Hyndman and Wang (1995).

Seismic Ground Motion Study
Skookumchuck Dam
Lewis County, Washington

GEOLOGIC INTERPRETATION CENTRAL PUGET SOUND SECTION A-A'

July 2000 21-1-08920-001

SHANNON & WILSON, INC.
Geotechnical and Environmental Consultants

FIG. 4-2

File: I:\Drafting\211\08920-001\21-1-08920-001 Fig 4-2.dwg Date: 03-05-2001 Author: LR

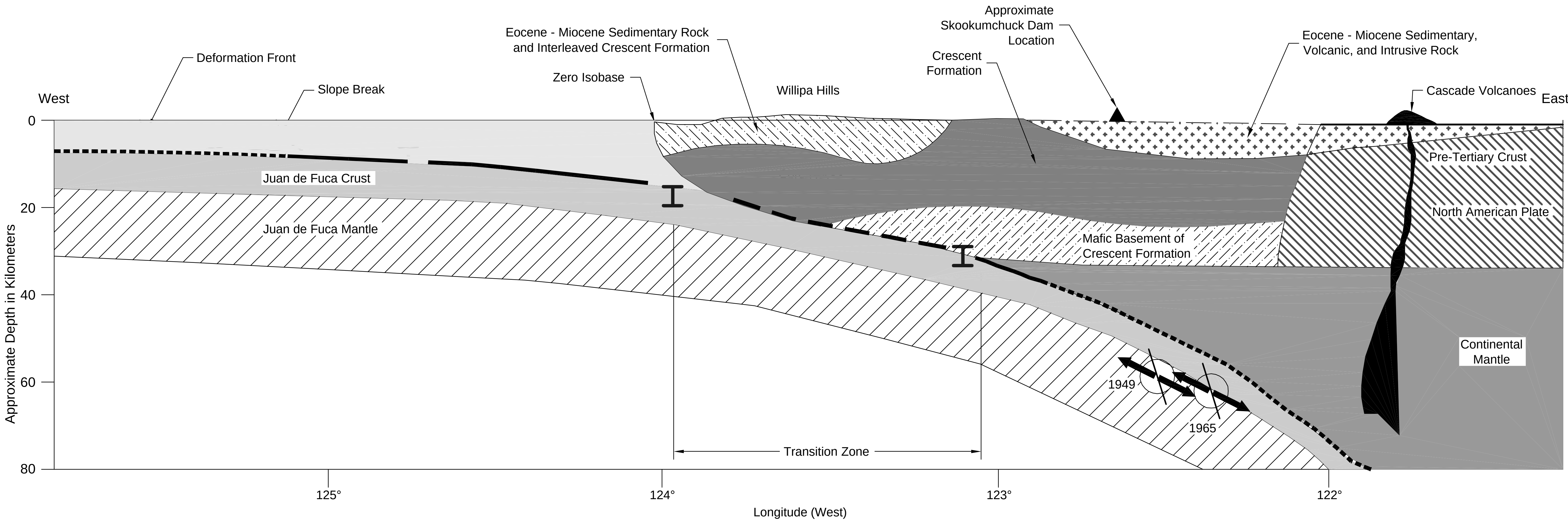

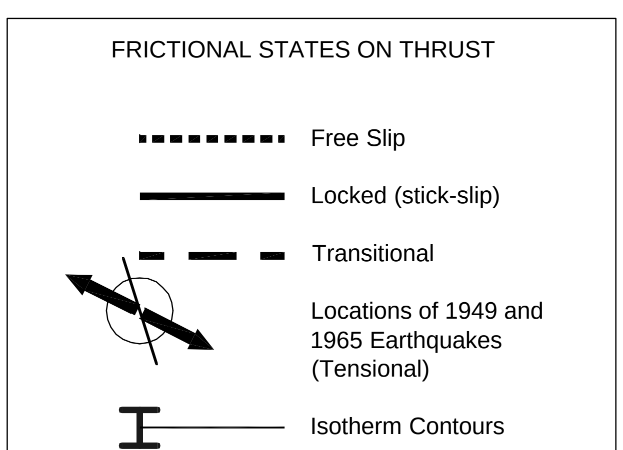

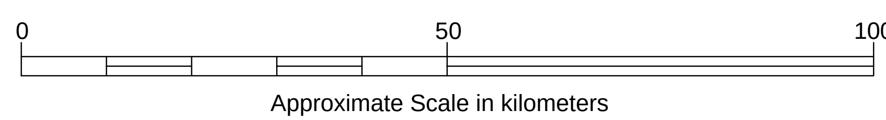

NOTE

Figure Based on Stanley, et al, (1999) & Hyndman and Wang (1995).

Seismic Ground Motion Study
Skookumchuck Dam
Lewis County, Washington

GEOLOGIC INTERPRETATION LATITUDE OF SKOOKUMCHUCK DAM

July 2000 21-1-08920-001

SHANNON & WILSON, INC.
Geotechnical and Environmental Consultants

FIG. 4-3

File: I:\Drafting\211\08920-001\21-1-08920-001 Fig 4-2.dwg Date: 03-05-2001 Author: LR

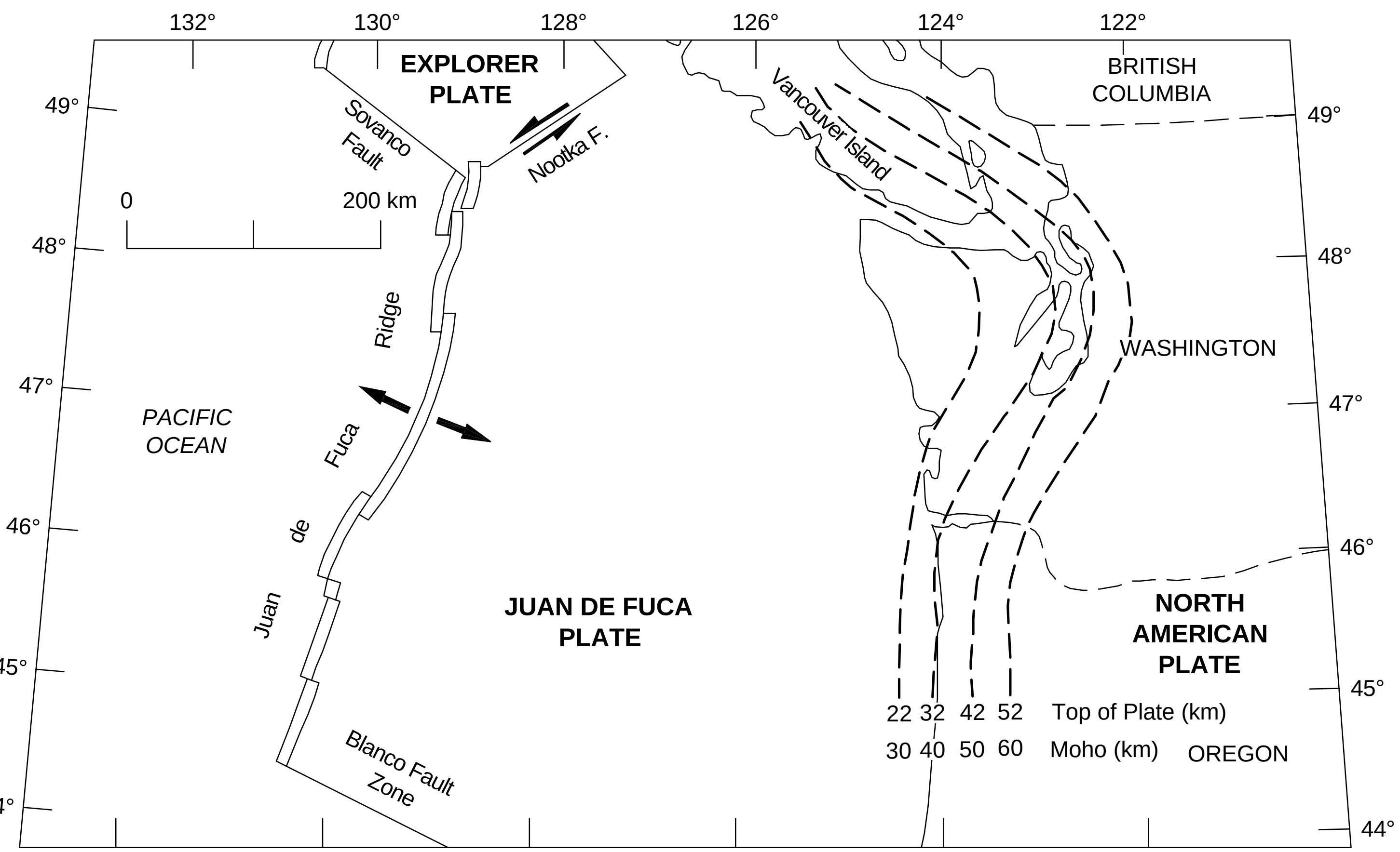

(a) Crosson & Owens (1987)

(b) Stanley et al. (1999)

Seismic Ground Motion Study
Skookumchuck Dam
Lewis County, Washington

DEPTH OF JUAN de FUCA PLATE

July 2000 21-1-08920-001

SHANNON & WILSON, INC.
Geotechnical and Environmental Consultants

FIG. 4-4

File: I:\Drafting\211\08920-001\21-1-08920-001 Figs 4- etc.dwg Date: 03-05-2001 Author: LR

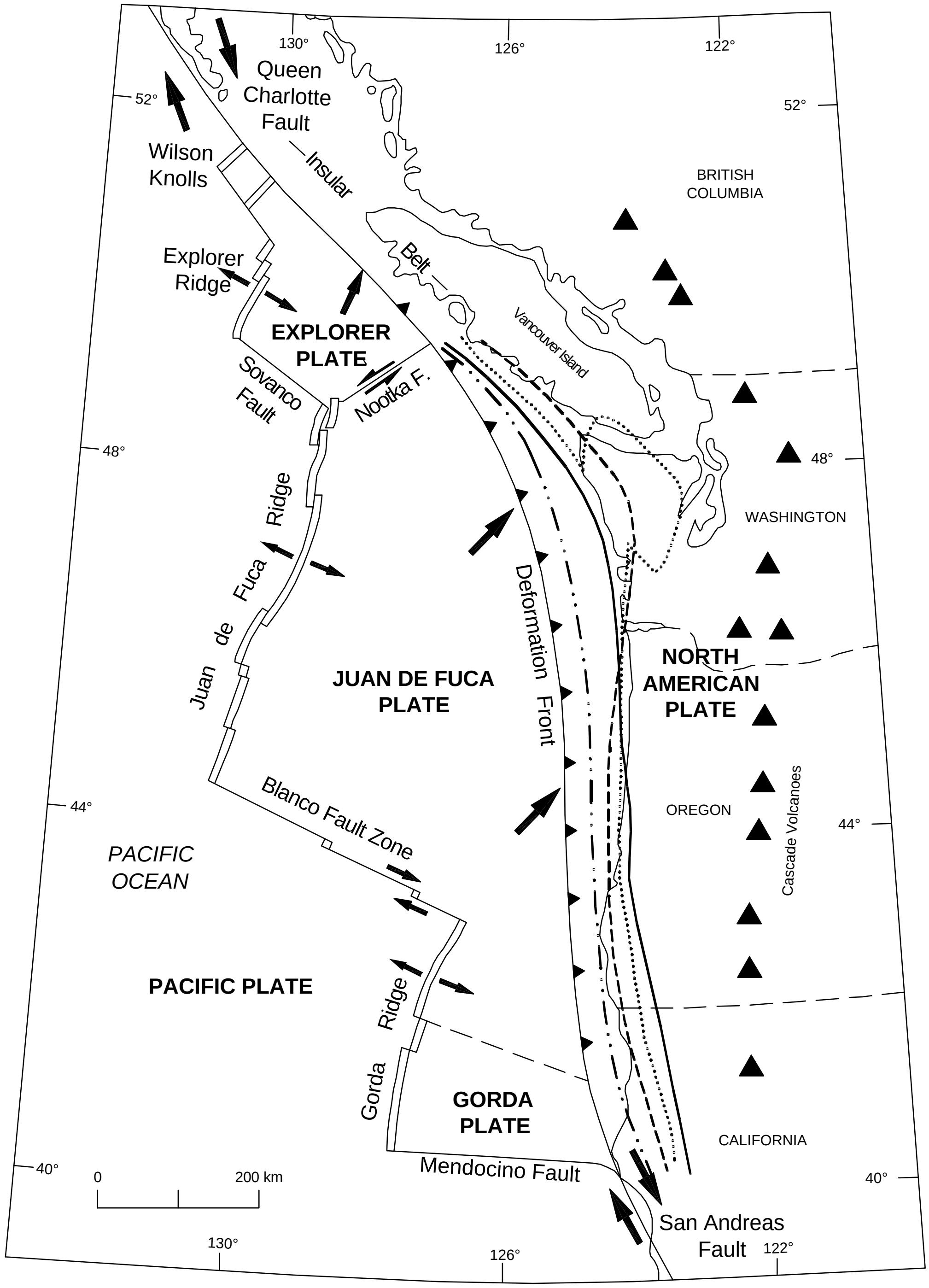

LEGEND

- Assumed location of Slope Break (updip)
- Landward extent of Zero Isobase (downdip)
- Midpoint of Transition Zone (downdip)
- Assumed Landward Extent of Mafic Zone, (downdip)

Map based on Hyndman and Wang (1993), Peterson et al. (1993), and Geomatrix (1995), Stanley et. al, (1999).

Seismic Ground Motion Study
Skookumchuck Dam
Lewis County, Washington

INFERRED UPDIP AND DOWNDIP EXTENTS OF THE CASCADIA SUBDUCTION ZONE

July 2000 | 21-1-08920-001

SHANNON & WILSON, INC.
Geotechnical and Environmental Consultants

FIG. 4-5

File: I:\Drafting\211\08920-001\21-1-08920-001 Figs 4- etc.dwg Date: 03-05-2001 Author: LR

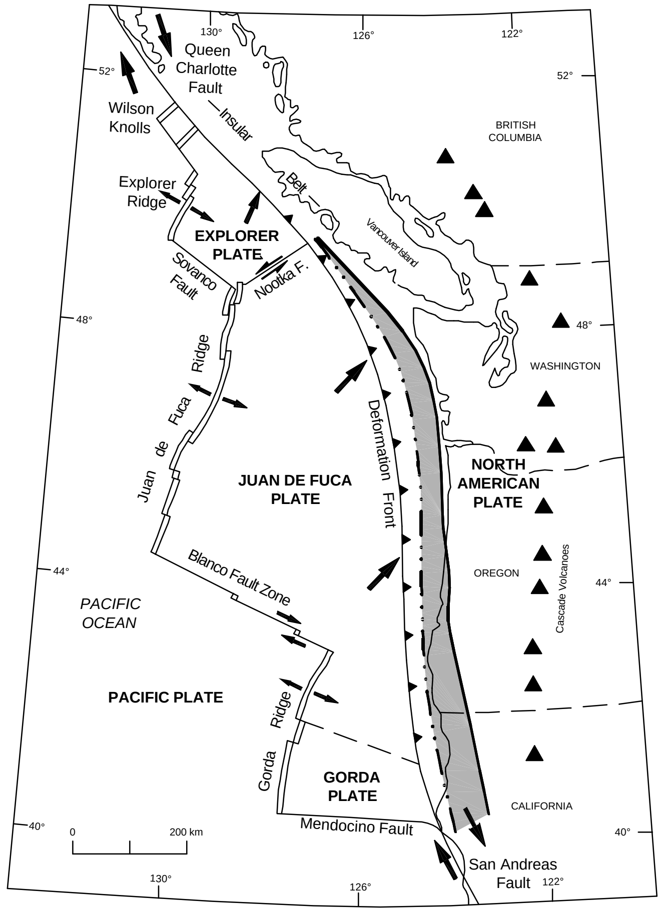

(a) Updip Extent: Slope break
Downdip Extent: Zero isobase

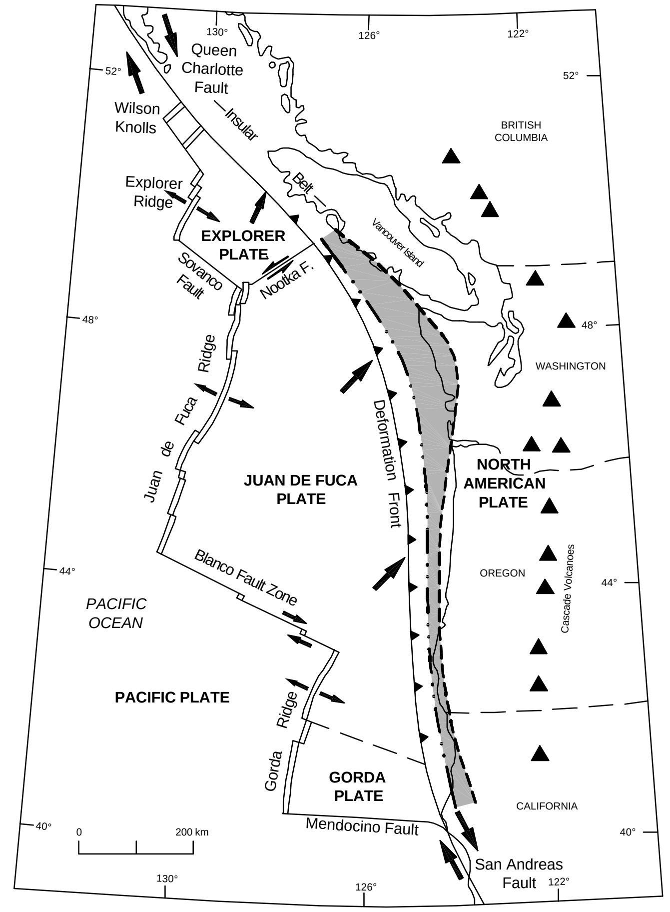

(b) Updip Extent: Slope break
Downdip Extent: Midpoint of Transition Zone

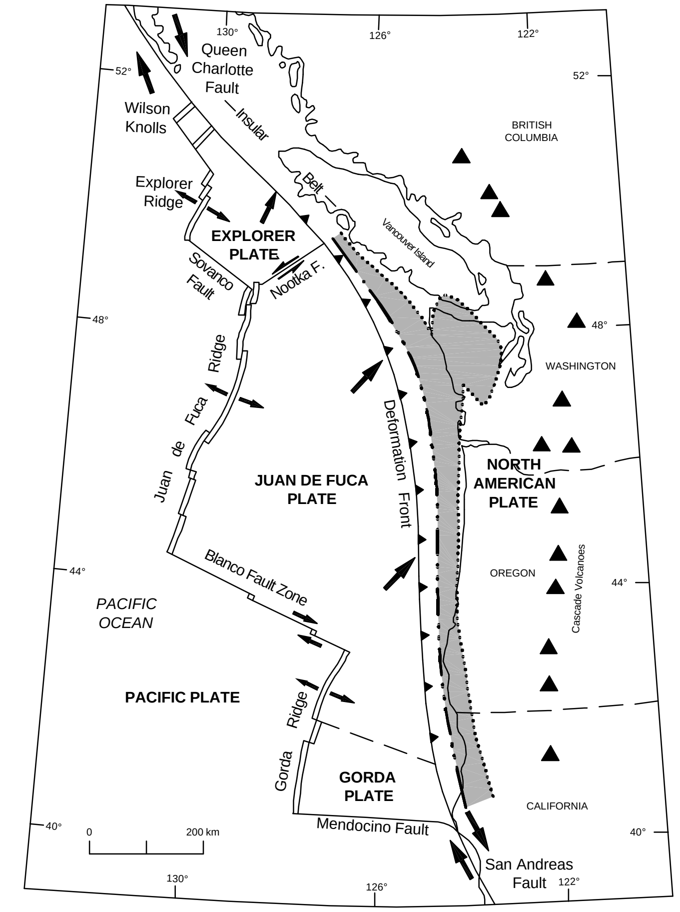

(c) Updip Extent: Slope break
Downdip Extent: Mafic Zone

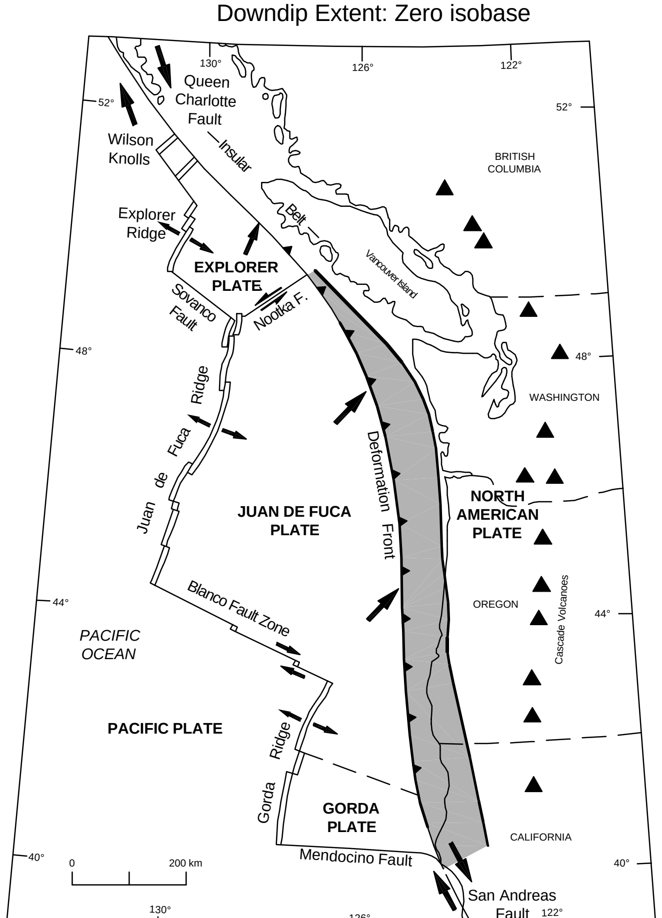

(d) Updip Extent: Deformation Front
Downdip Extent: Zero isobase

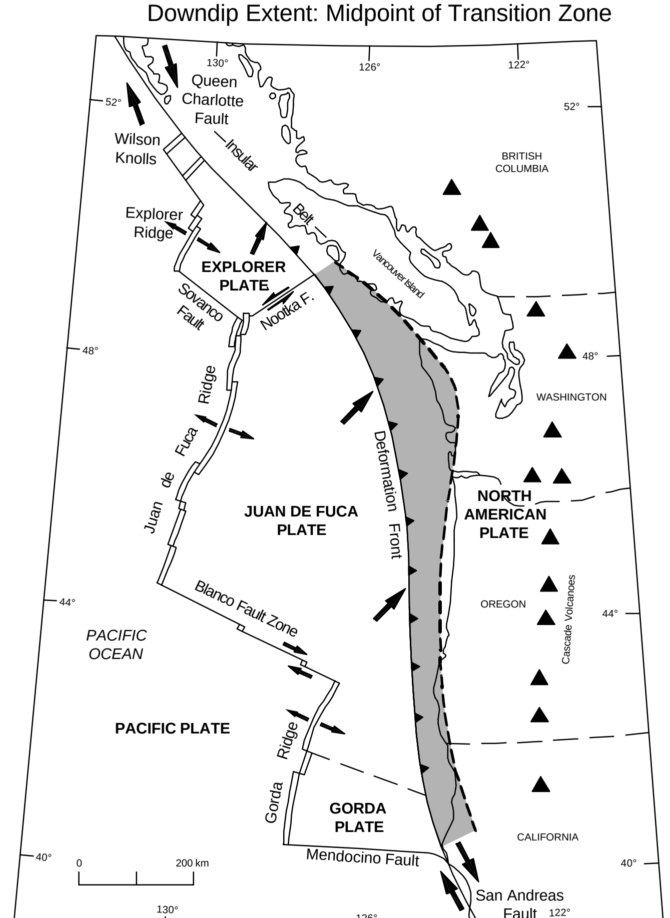

(e) Updip Extent: Deformation Front
Downdip Extent: Midpoint of Transition Zone

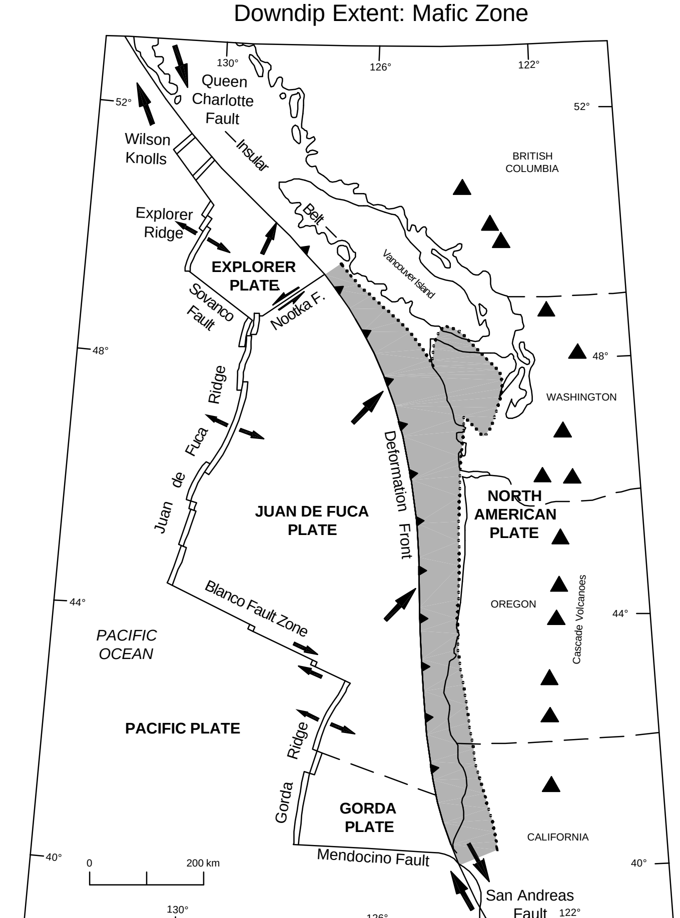

(f) Updip Extent: Deformation Front
Downdip Extent: Mafic Zone

Seismic Ground Motion Study
Skookumchuck Dam
Lewis County, Washington

SEISMOGENIC PLATE INTERFACE ALTERNATIVES

July 2000 21-1-08920-001

SHANNON & WILSON, INC.
Geotechnical and Environmental Consultants

FIG. 4-6

File: I:\Drafting\211\08920-001\21-1-08920-001 Figs 4- etc.dwg Date: 03-05-2001 Author: LR

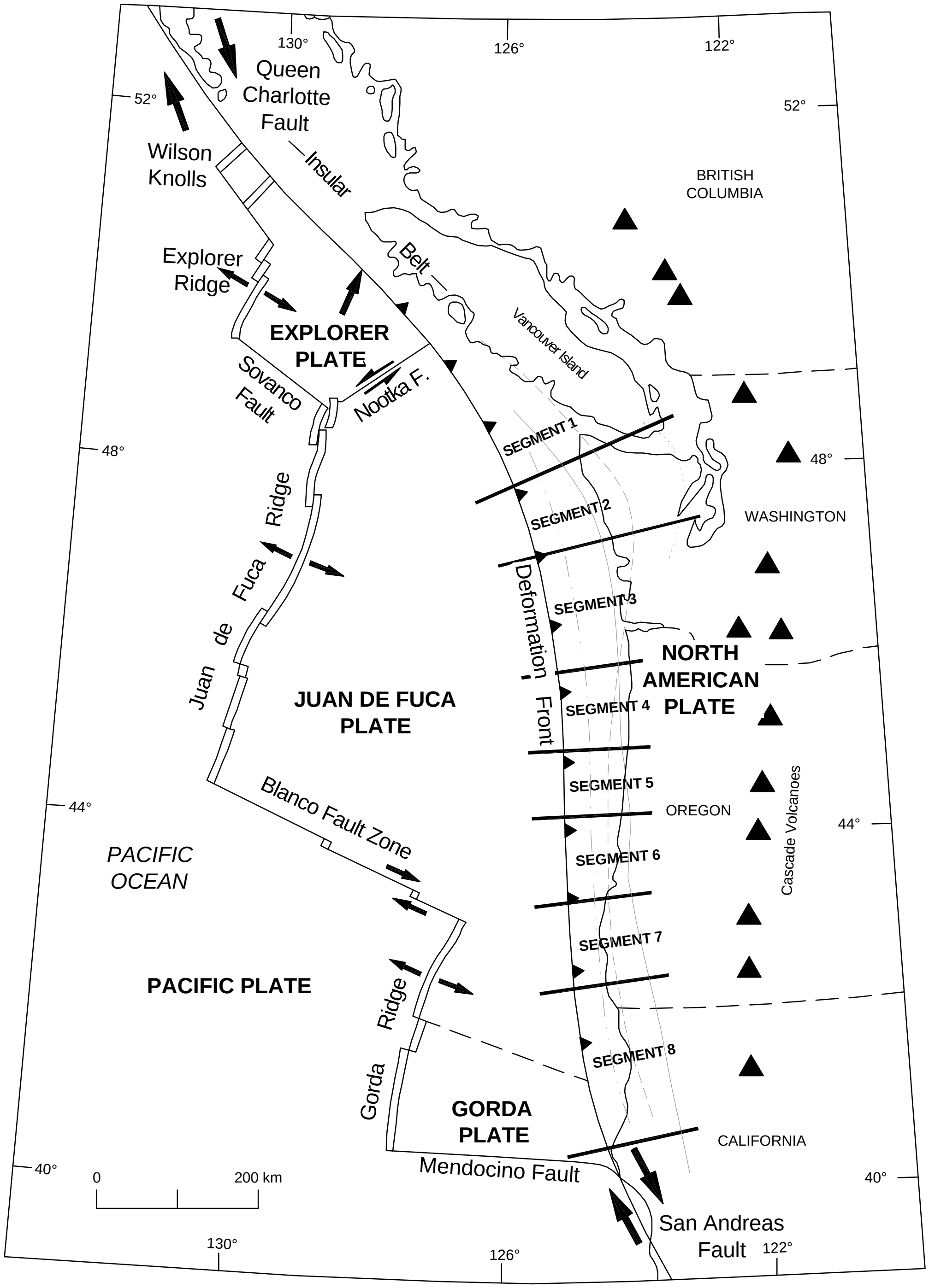

Map based on Hyndman and Wang (1993), Peterson et al. (1993), and Geomatrix (1995)

Seismic Ground Motion Study
Skookumchuck Dam
Lewis County, Washington

SEGMENTATION OF THE CASCADIA SUBDUCTION ZONE

July 2000 21-1-08920-001

SHANNON & WILSON, INC.
Geotechnical and Environmental Consultants

FIG. 4-7

File: I:\Drafting\211\08920-001\21-1-08920-001 Figs 4- etc.dwg Date: 03-05-2001 Author: LR

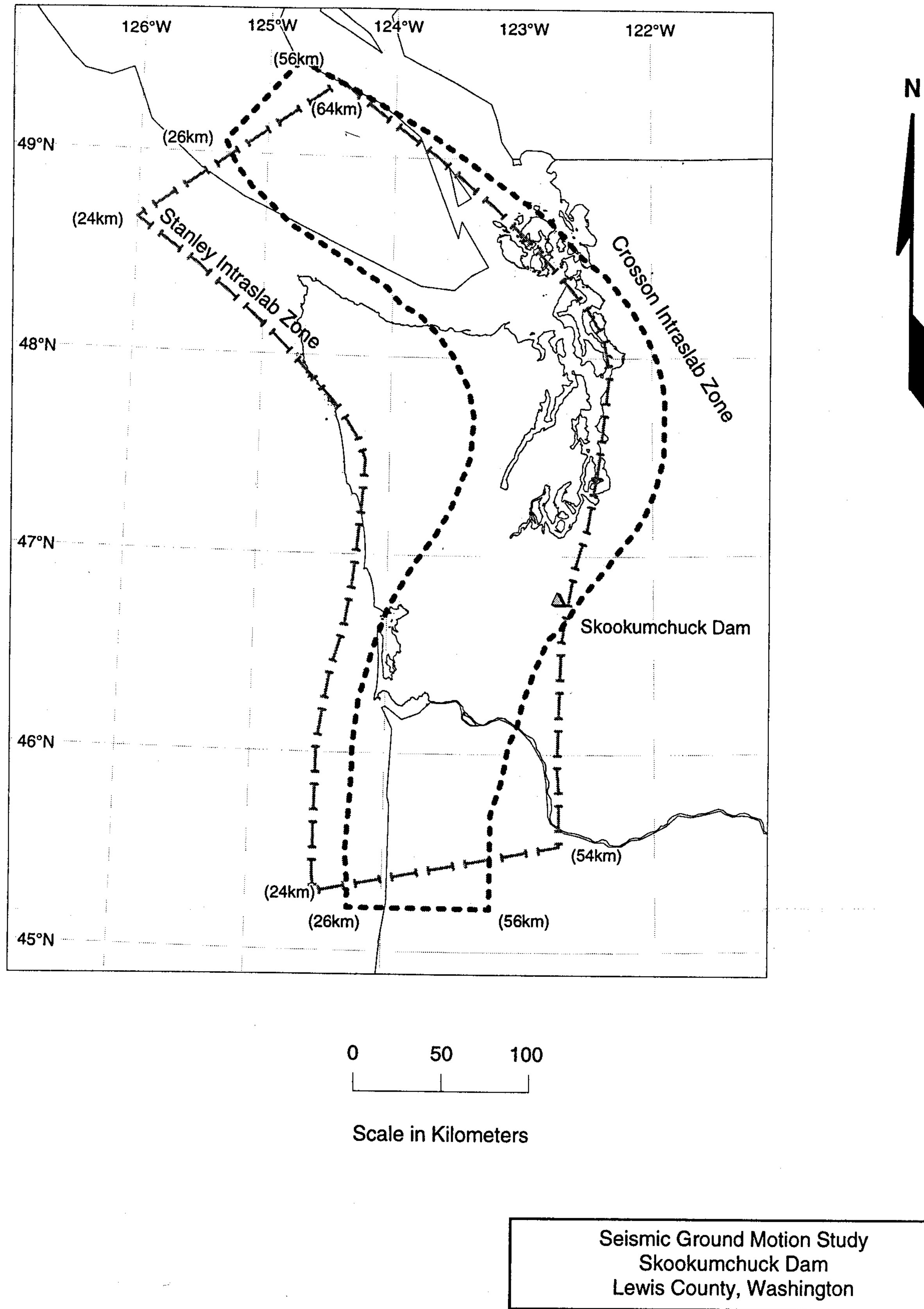

NOTE

Depth of corner of modeled zone is indicated in parenthesis.

Seismic Ground Motion Study Skookumchuck Dam Lewis County, Washington	
MODELED INTRASLAB SOURCE ZONES July 2000 21-1-0890-001	
SHANNON & WILSON, INC. Geotechnical and Environmental Consultants	**FIG. 4-8**

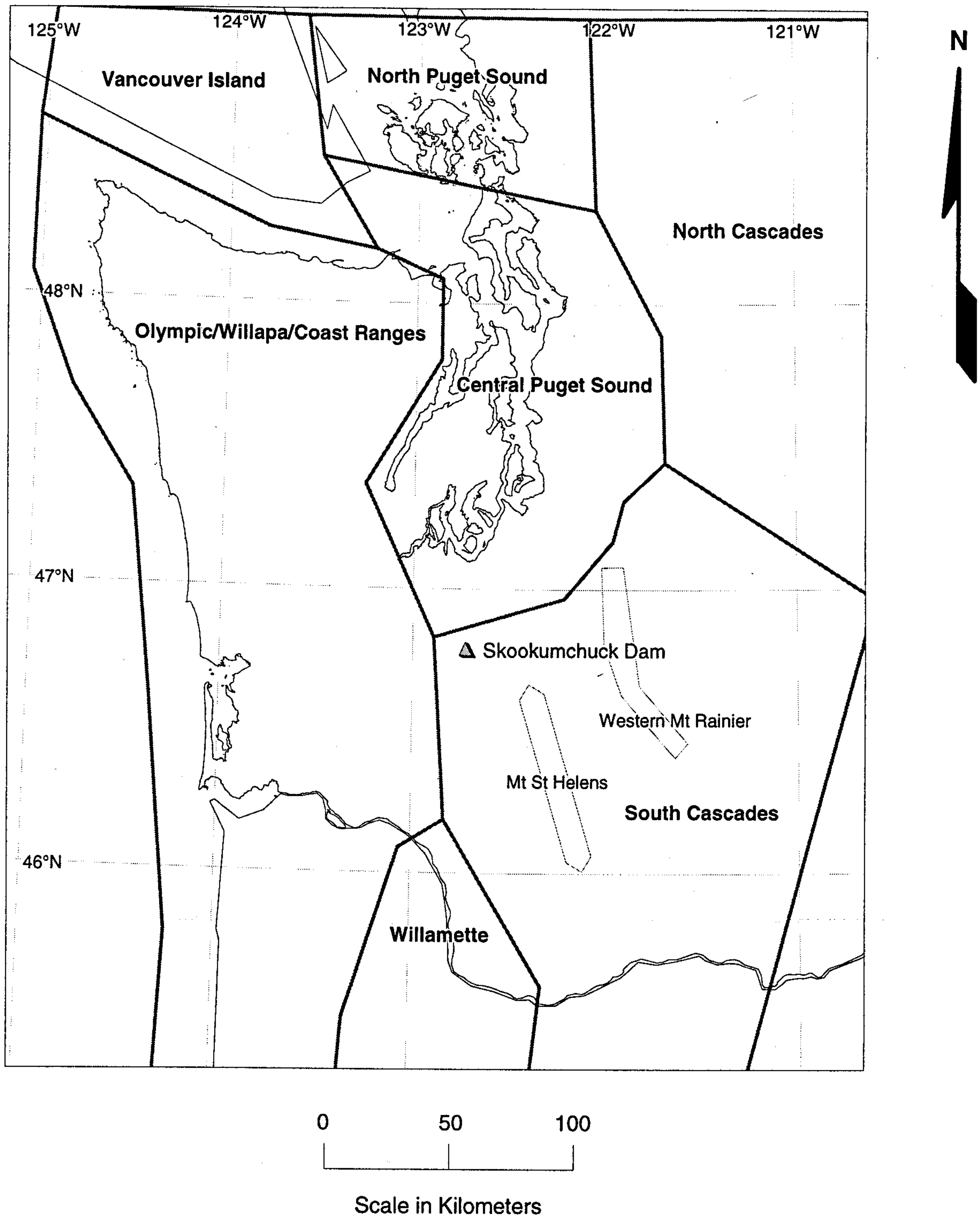

Seismic Ground Motion Study
Skookumchuck Dam
Lewis County, Washington

MODELED CRUSTAL SOURCE ZONES

July 2000 21-1-0890-001

SHANNON & WILSON, INC.
Geotechnical and Environmental Consultants

FIG. 4-9

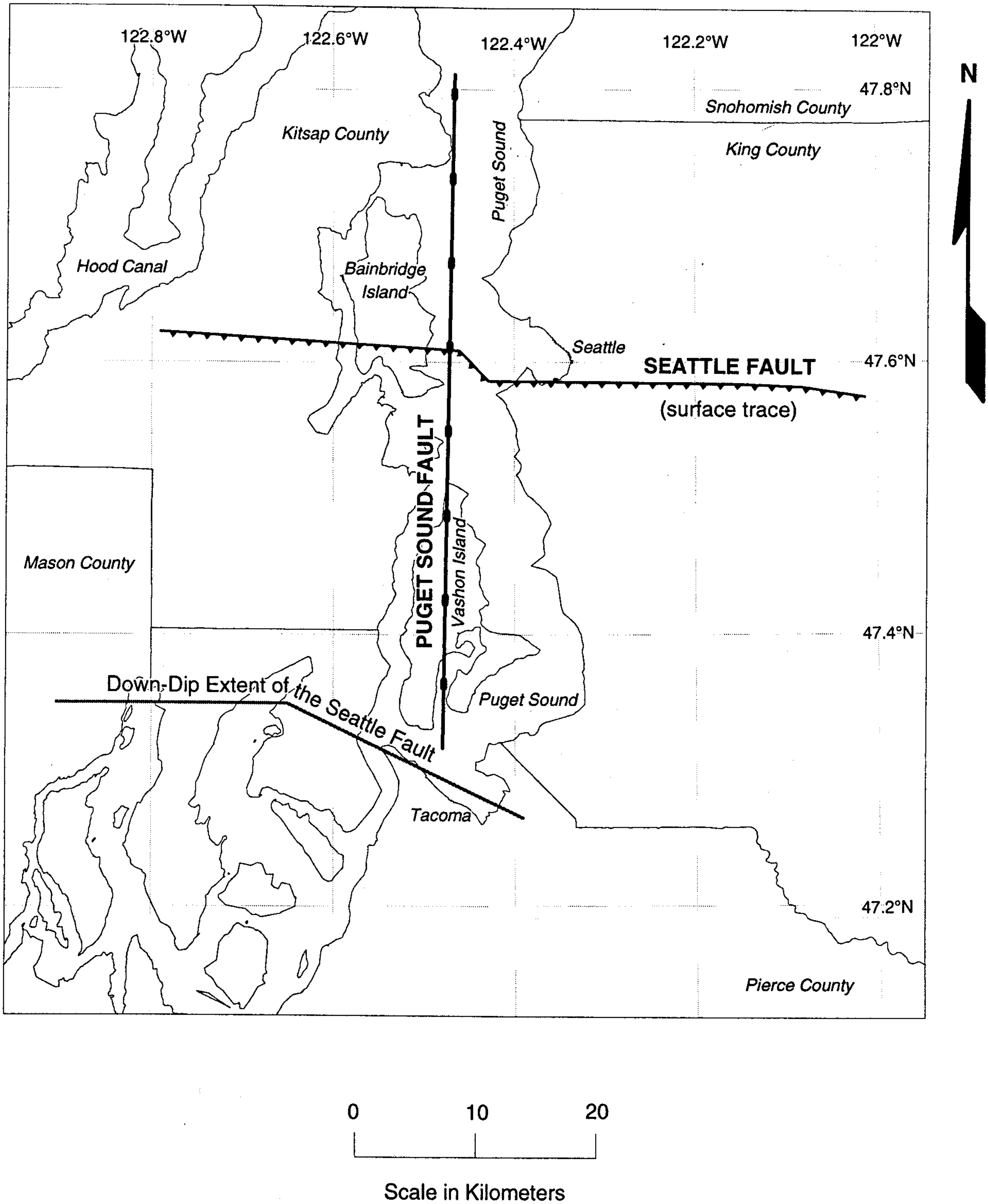

Seismic Ground Motion Study
Skookumchuck Dam
Lewis County, Washington

MODELED SEATTLE AND PUGET SOUND FAULTS

Julyl 2000 | 21-1-0890-001

SHANNON & WILSON, INC.
Geotechnical and Environmental Consultants

FIG. 4-10

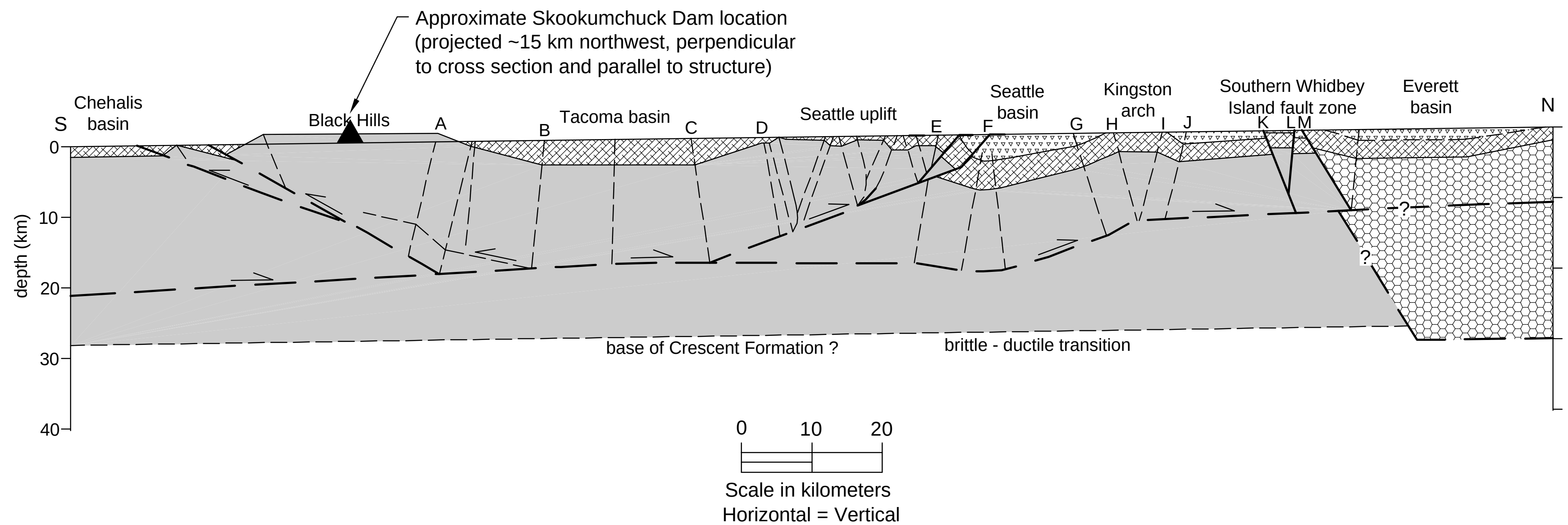

LEGEND

Mesozoic rocks

Crescent Fm

Eocene and Oligocene

Miocene, Pliocene

NOTE

Figure from Pratt et al., 1997.

Seismic Ground Motion Study
Skookumchuck Dam
Lewis County, Washington

PUGET LOWLAND CRUSTAL CROSS SECTION

July 2000 | 21-1-08920-001

SHANNON & WILSON, INC.
Geotechnical and Environmental Consultants

FIG. 4-11

File: I:\Drafting\211\08920-001\21-1-08920-001 Fig 4-11.dwg Date: 03-05-2001 Author: LR

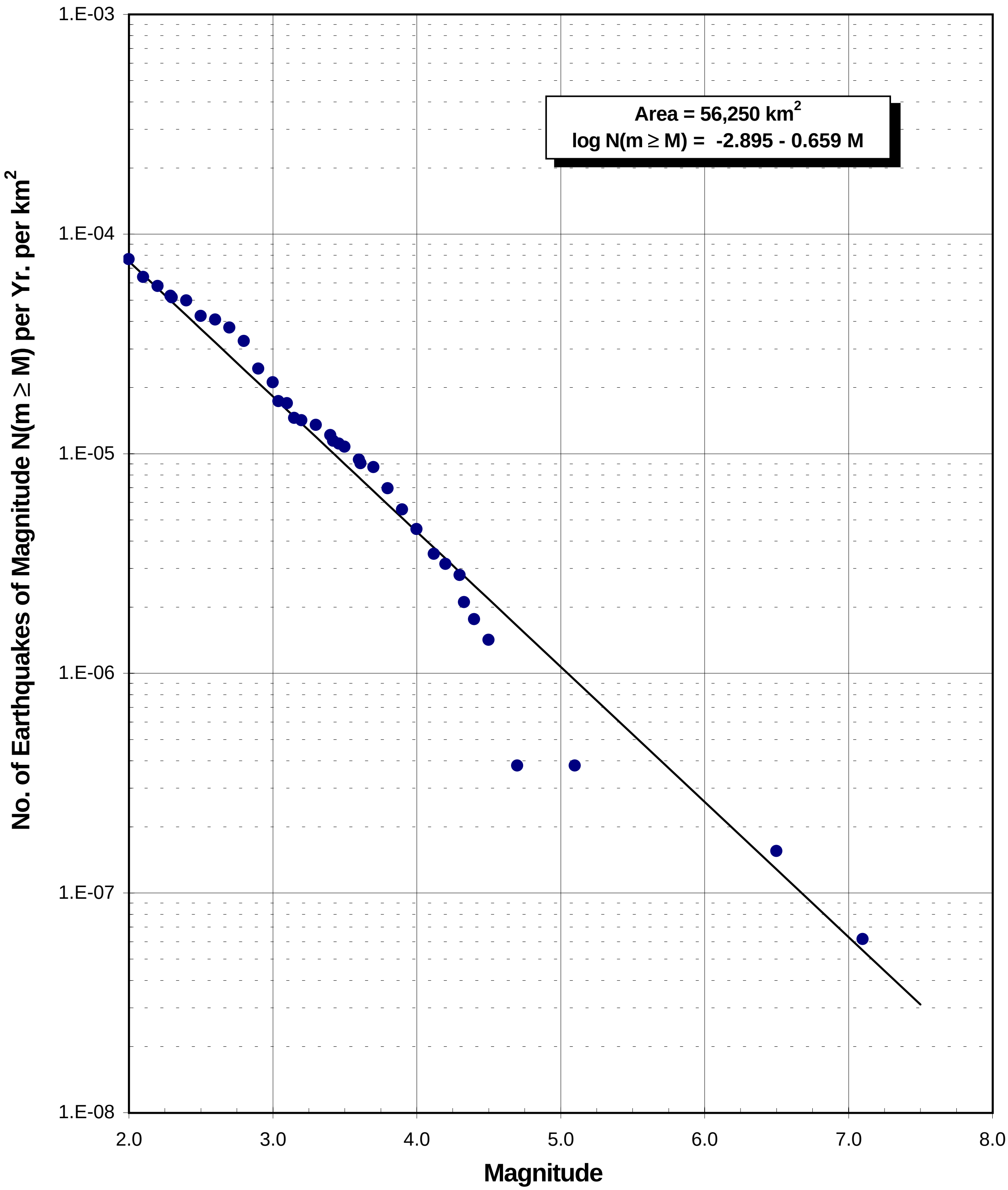

Seismic Ground Motion Study
Skookumchuck Dam
Lewis County, Washington

RECURRENCE CURVE FOR INTRASLAB ZONE

July 2000 | 21-1-08920-001

SHANNON & WILSON, INC.
Geotechnical and Environmental Consultants

FIG. 5-1

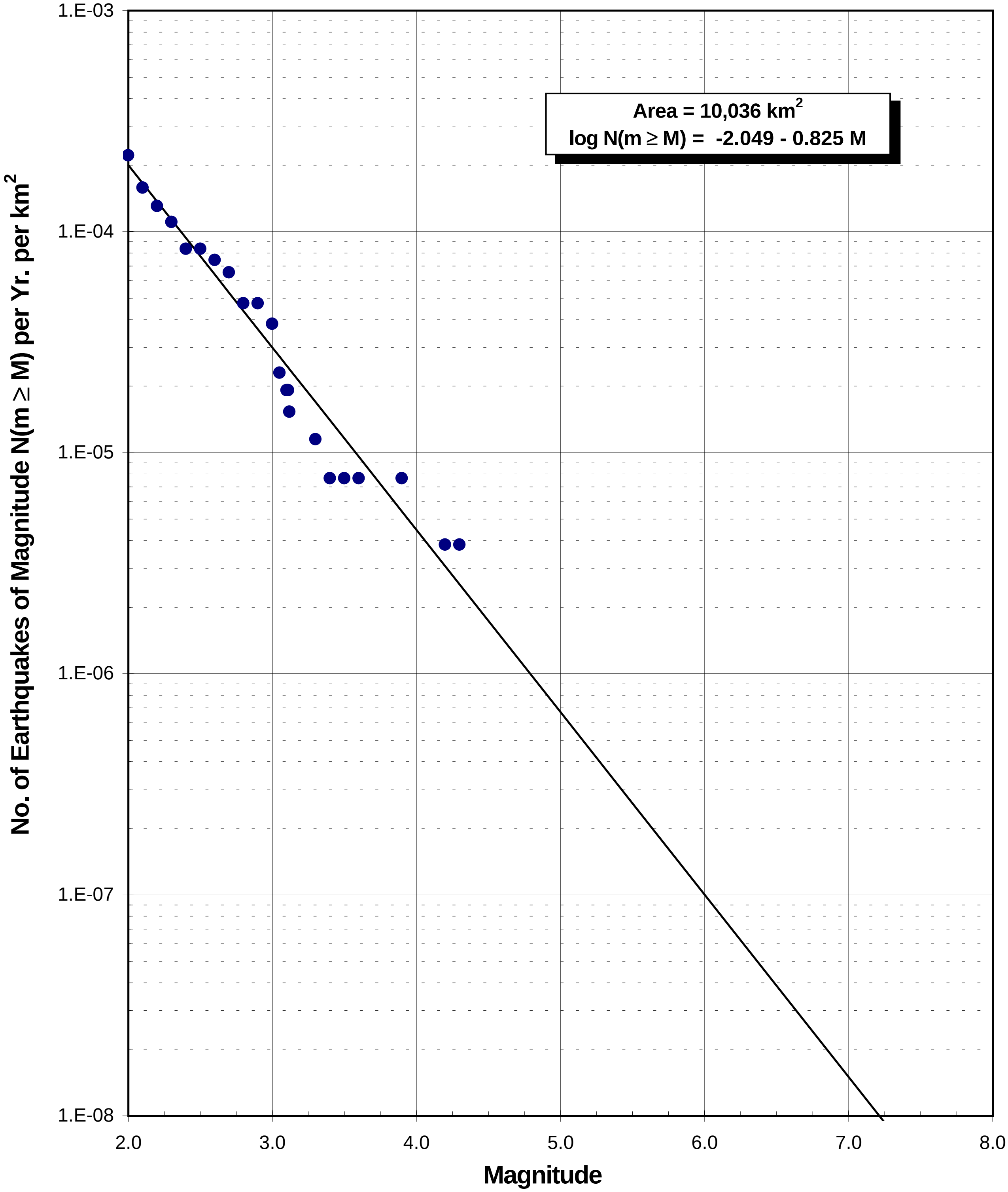

Seismic Ground Motion Study
Skookumchuck Dam
Lewis County, Washington

RECURRENCE CURVE FOR VANCOUVER ISLAND ZONE

July 2000 | 21-1-08920-001

SHANNON & WILSON, INC.
Geotechnical and Environmental Consultants

FIG. 5-2

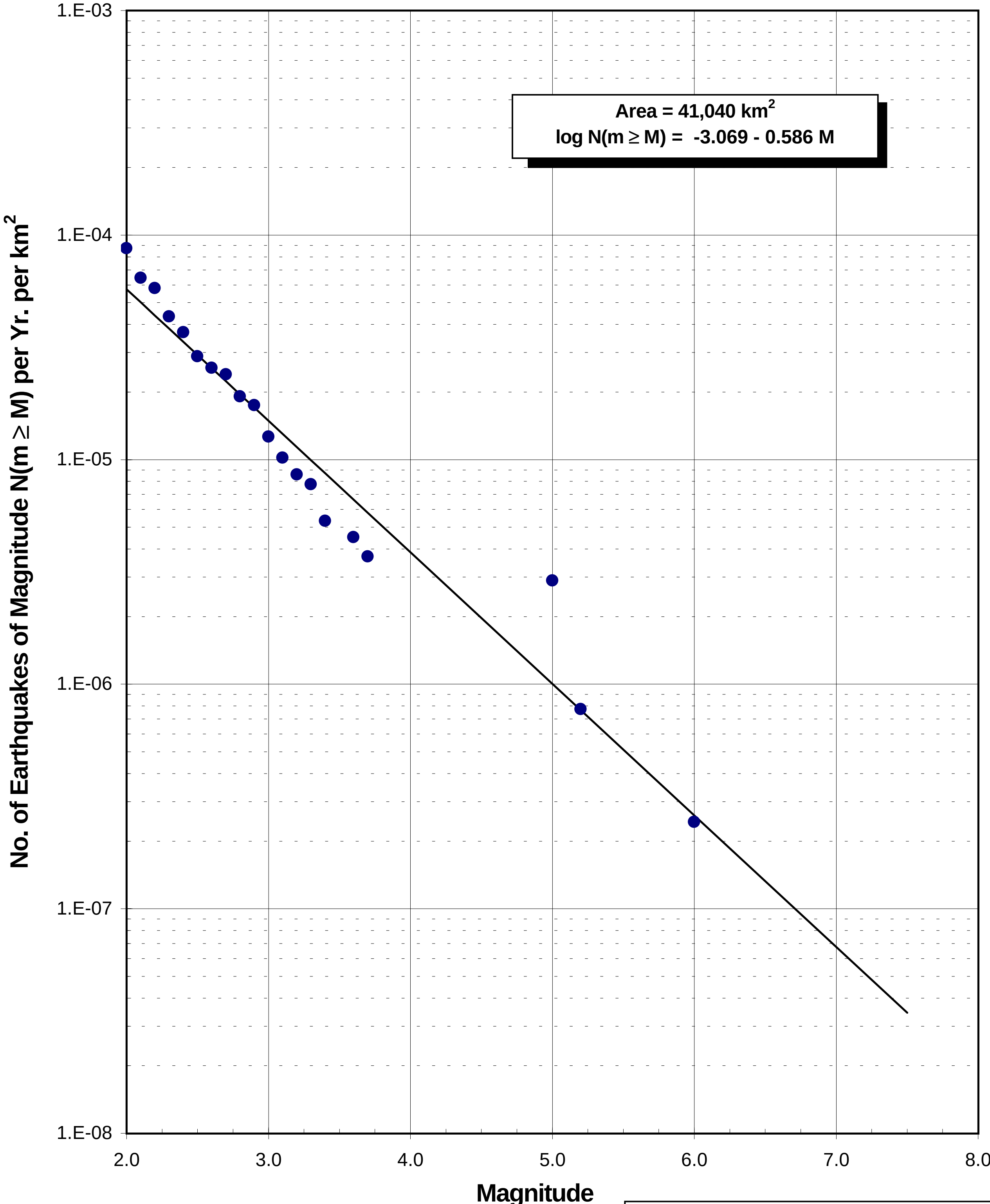

Seismic Ground Motion Study
Skookumchuck Dam
Lewis County, Washington

RECURRENCE CURVE FOR OLYMPIC MOUNTAINS., WILLAPA HILLS, & COAST RANGE ZONES

July 2000 | 21-1-08920-001

SHANNON & WILSON, INC.
Geotechnical and Environmental Consultants

FIG. 5-3

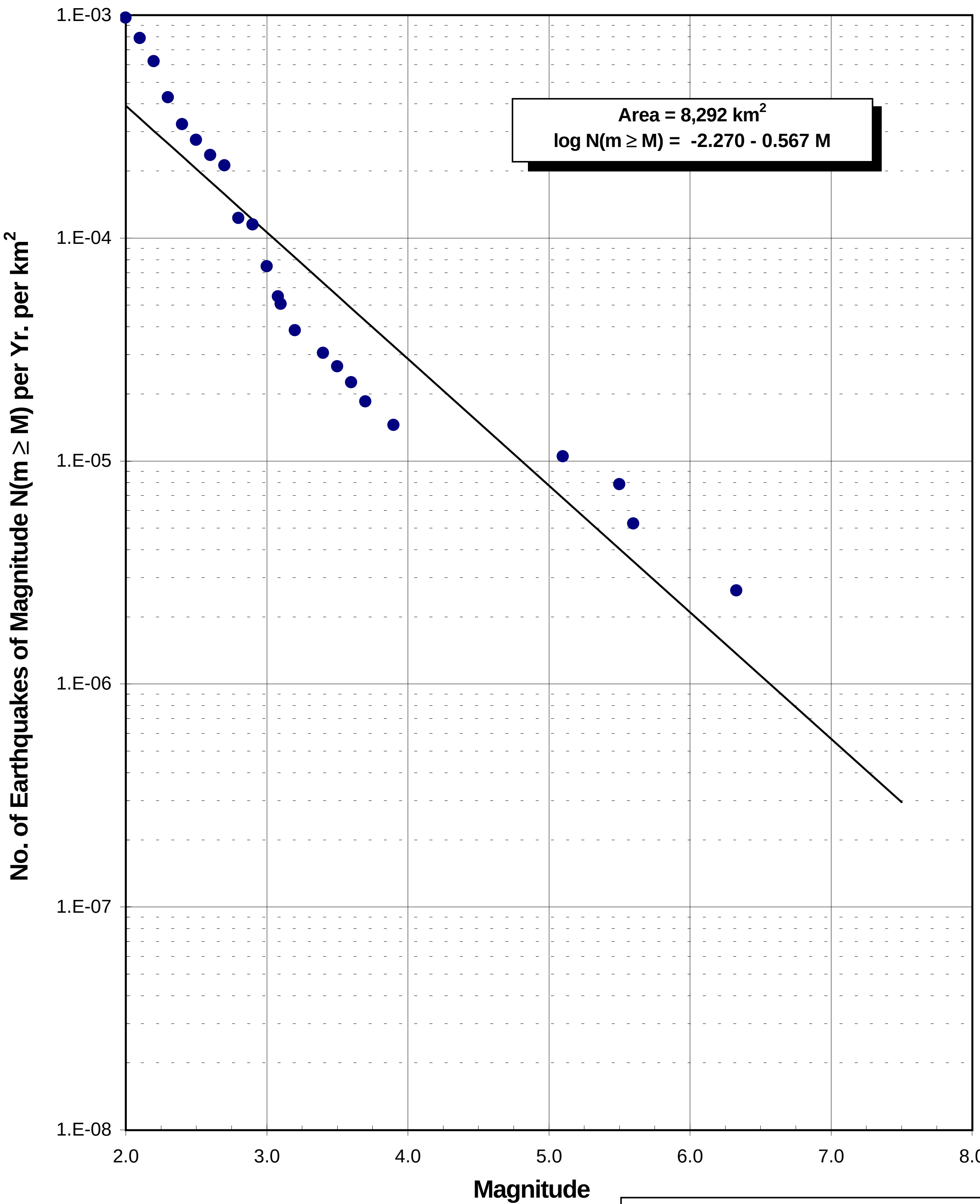

Seismic Ground Motion Study
Skookumchuck Dam
Lewis County, Washington

RECURRENCE CURVE FOR WILAMETTE LOWLAND ZONE

July 2000 | 21-1-08920-001

SHANNON & WILSON, INC.
Geotechnical and Environmental Consultants

FIG. 5-4

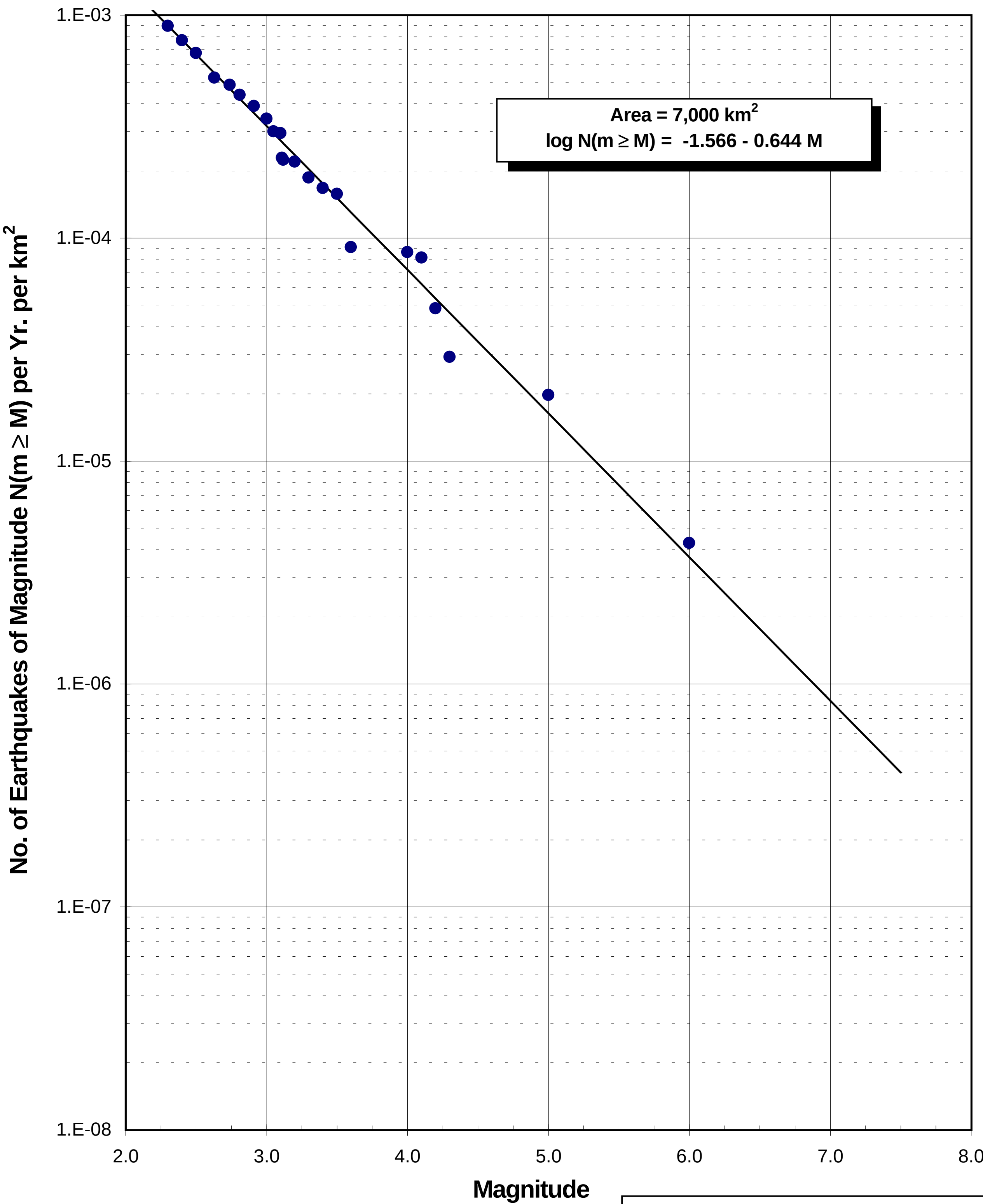

Seismic Ground Motion Study
Skookumchuck Dam
Lewis County, Washington

RECURRENCE CURVE FOR NORTH PUGET SOUND ZONE

July 2000 | 21-1-08920-001

SHANNON & WILSON, INC.
Geotechnical and Environmental Consultants

FIG. 5-5

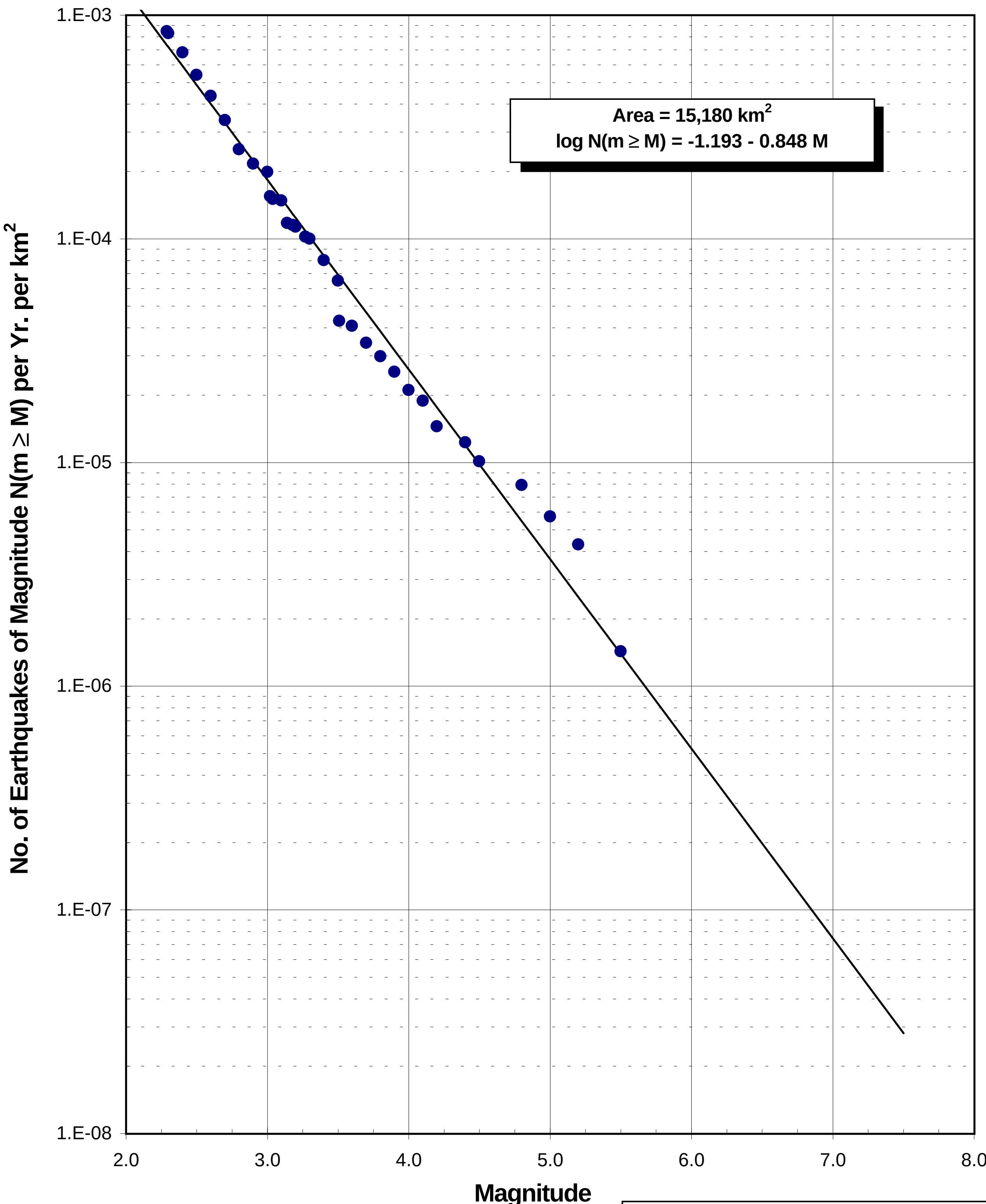

Seismic Ground Motion Study
Skookumchuck Dam
Lewis County, Washington

RECURRENCE CURVE FOR CENTRAL PUGET SOUND ZONE

July 2000 21-1-08920-001

SHANNON & WILSON, INC.
Geotechnical and Environmental Consultants

FIG. 5-6

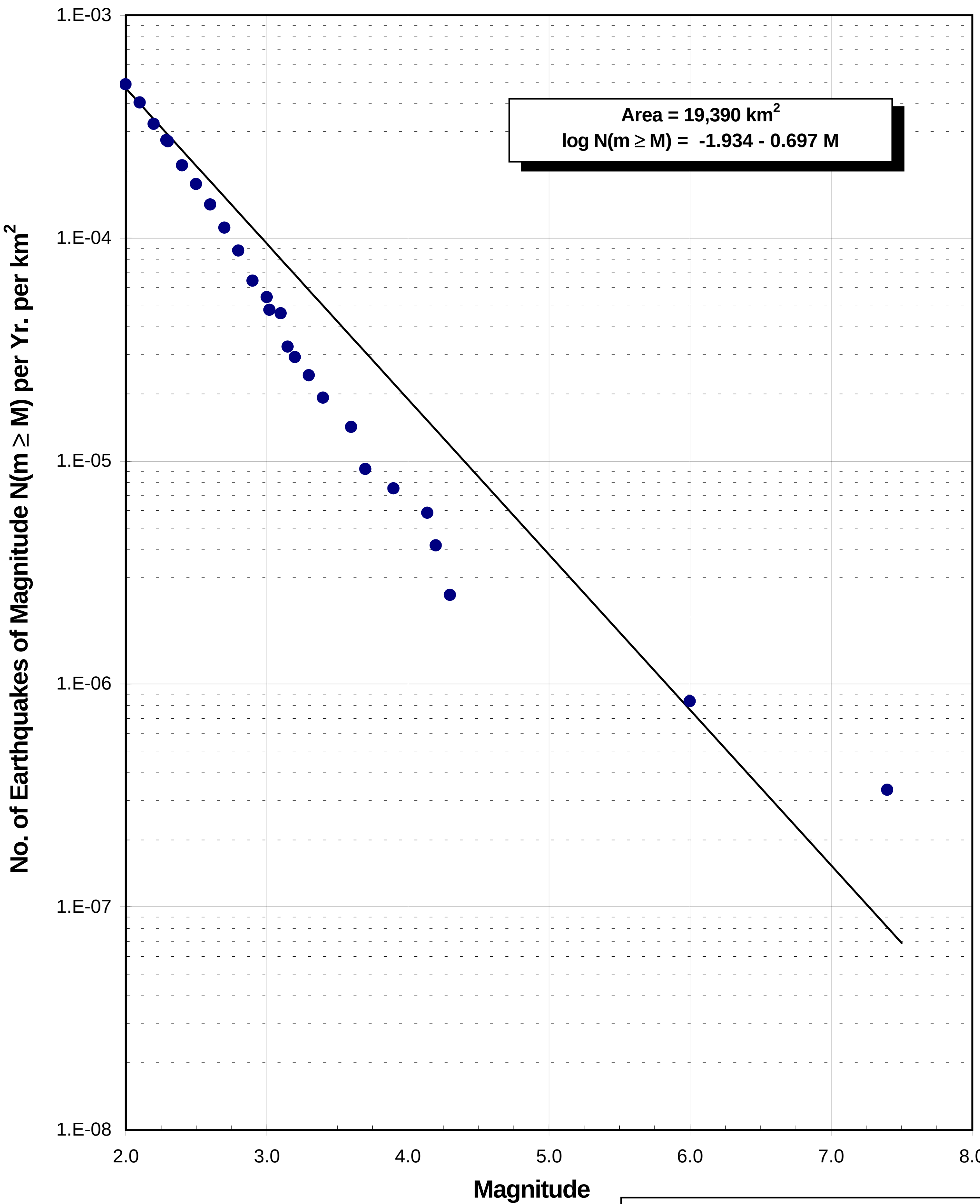

Seismic Ground Motion Study Skookumchuck Dam Lewis County, Washington	
RECURRENCE CURVE FOR NORTH CASCADES ZONE	
July 2000	21-1-08920-001
SHANNON & WILSON, INC. Geotechnical and Environmental Consultants	**FIG. 5-7**

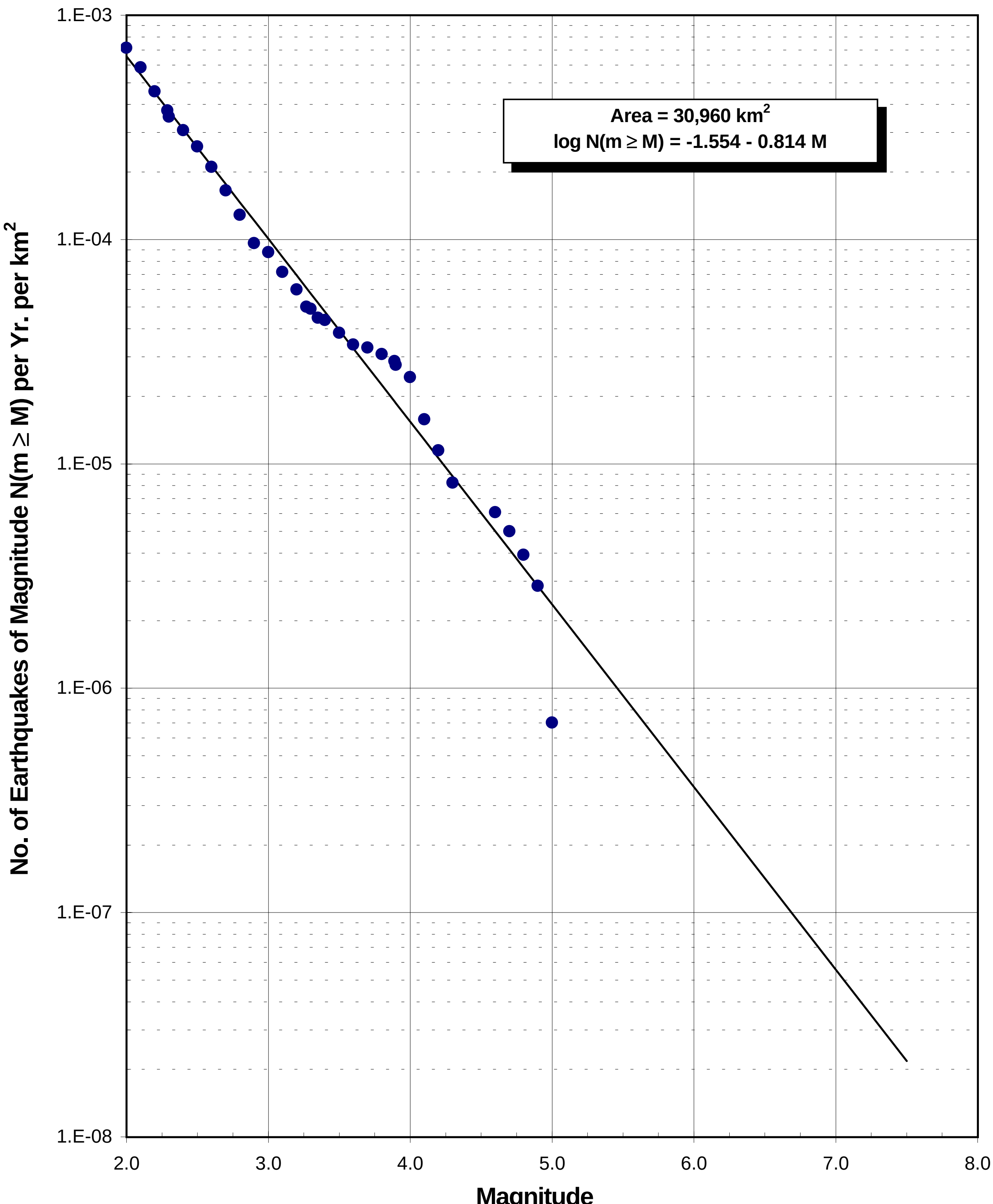

Seismic Ground Motion Study
Skookumchuck Dam
Lewis County, Washington

RECURRENCE CURVE FOR SOUTH CASCADES ZONE

July 2000 21-1-08920-001

SHANNON & WILSON, INC.
Geotechnical and Environmental Consultants

FIG. 5-8

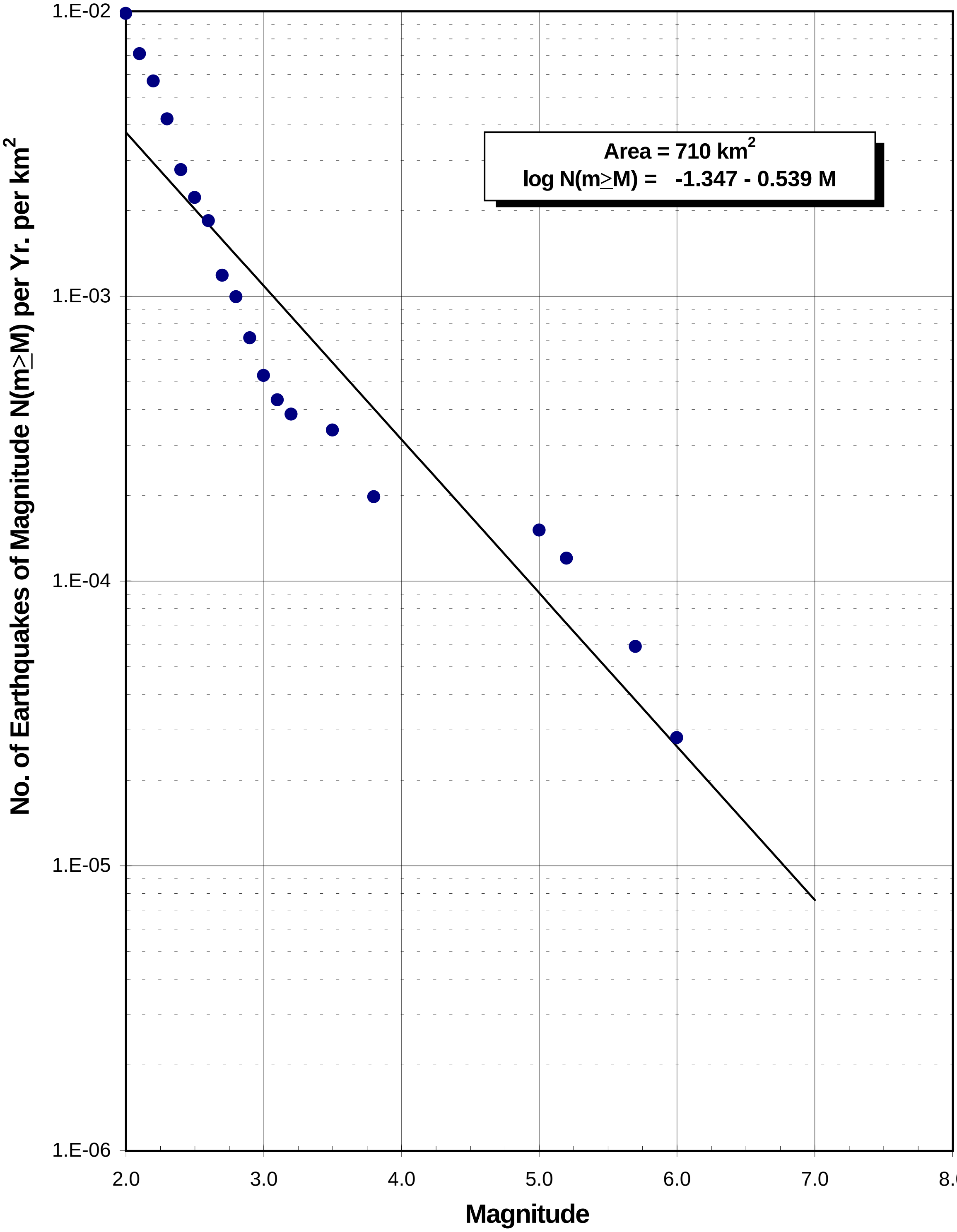

Seismic Ground Motion Study Skookumchuck Dam Lewis County, Washington
RECURRENCE CURVE FOR MT. ST. HELENS ZONE
July 2000 21-1-08920-
SHANNON & WILSON, INC. Geotechnical and Environmental Consultants — **FIG. 5-9**

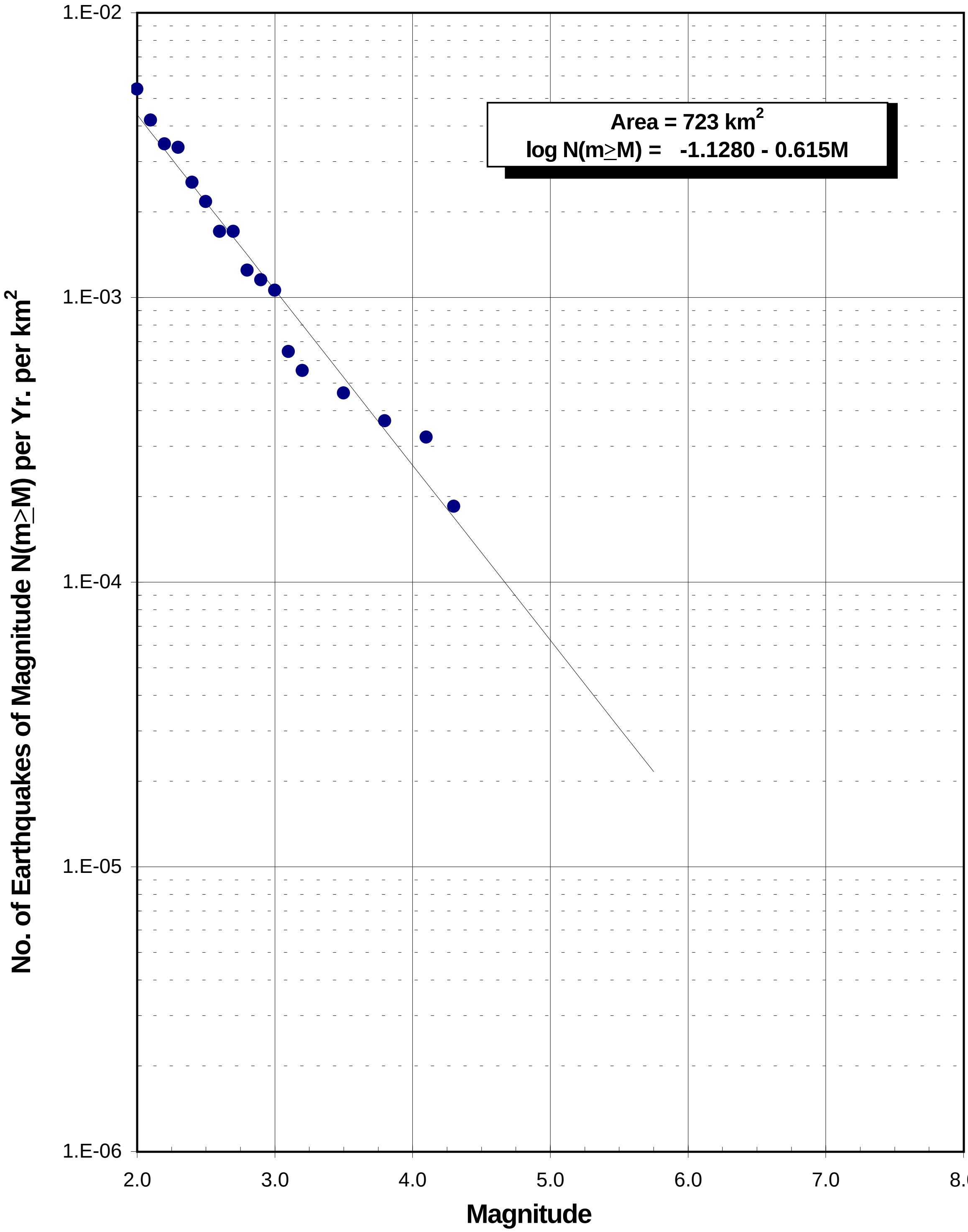

Seismic Ground Motion Study
Skookumchuck Dam
Lewis County, Washington

RECURRENCE CURVE FOR WESTERN MT. RAINIER ZONE

July 2000 | 21-1-08920-001

SHANNON & WILSON, INC.
Geotechnical and Environmental Consultants

FIG. 5-10

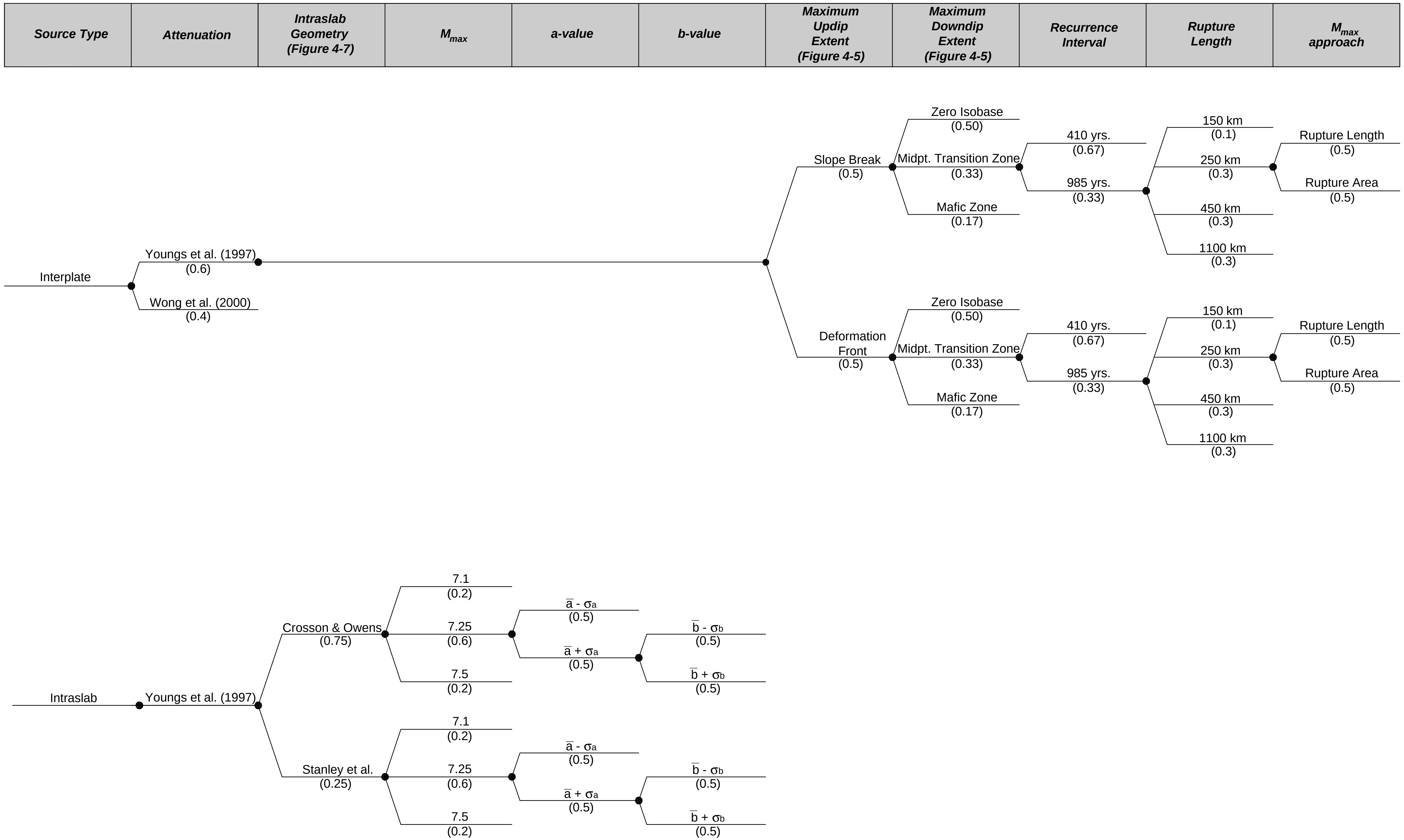

NOTE

Assumed weights for the various logic tree branches are indicated in parenthesis.

Seismic Ground Motion Study
Skookumchuck Dam
Lewis County, Washington

SEISMIC SOURCE LOGIC TREE

July 2000 21-1-08920-001

SHANNON & WILSON, INC.
Geotechnical and Environmental Consultants

FIG. 5-11
Sheet 1 of 2

File: I:\Drafting\211\08920-001\21-1-08920-001 Fig 5-11.dwg Date: 03-05-2001 Author: LR

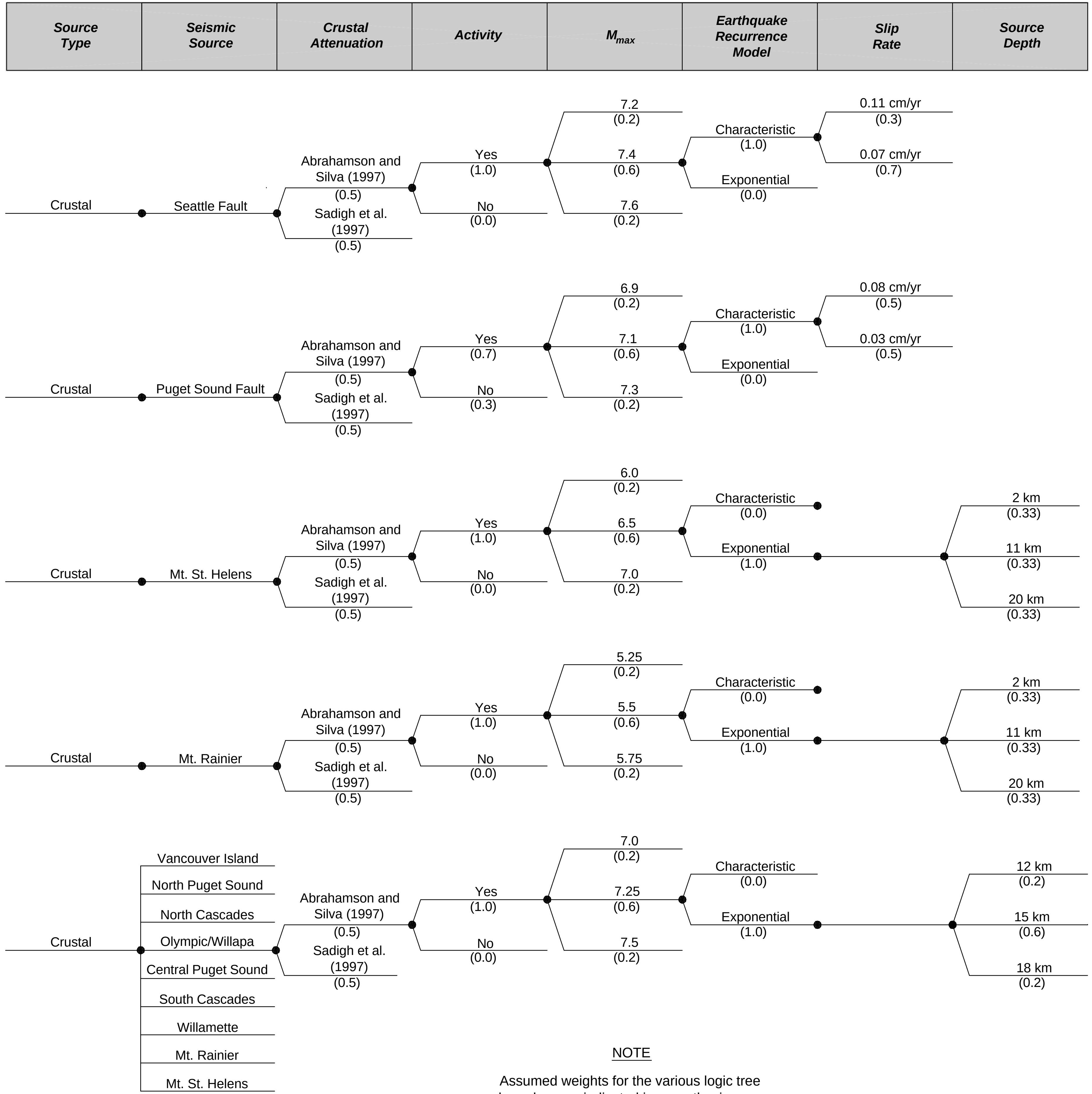

NOTE

Assumed weights for the various logic tree branches are indicated in parenthesis.

Seismic Ground Motion Study
Skookumchuck Dam
Lewis County, Washington

SEISMIC SOURCE LOGIC TREE

July 2000 | 21-1-08920-001

SHANNON & WILSON, INC.
Geotechnical and Environmental Consultants

FIG. 5-11
Sheet 2 of 2

File: I:\Drafting\211\08920-001\21-1-08920-001 Fig 5-11.dwg Date: 03-05-2001 Author: LR

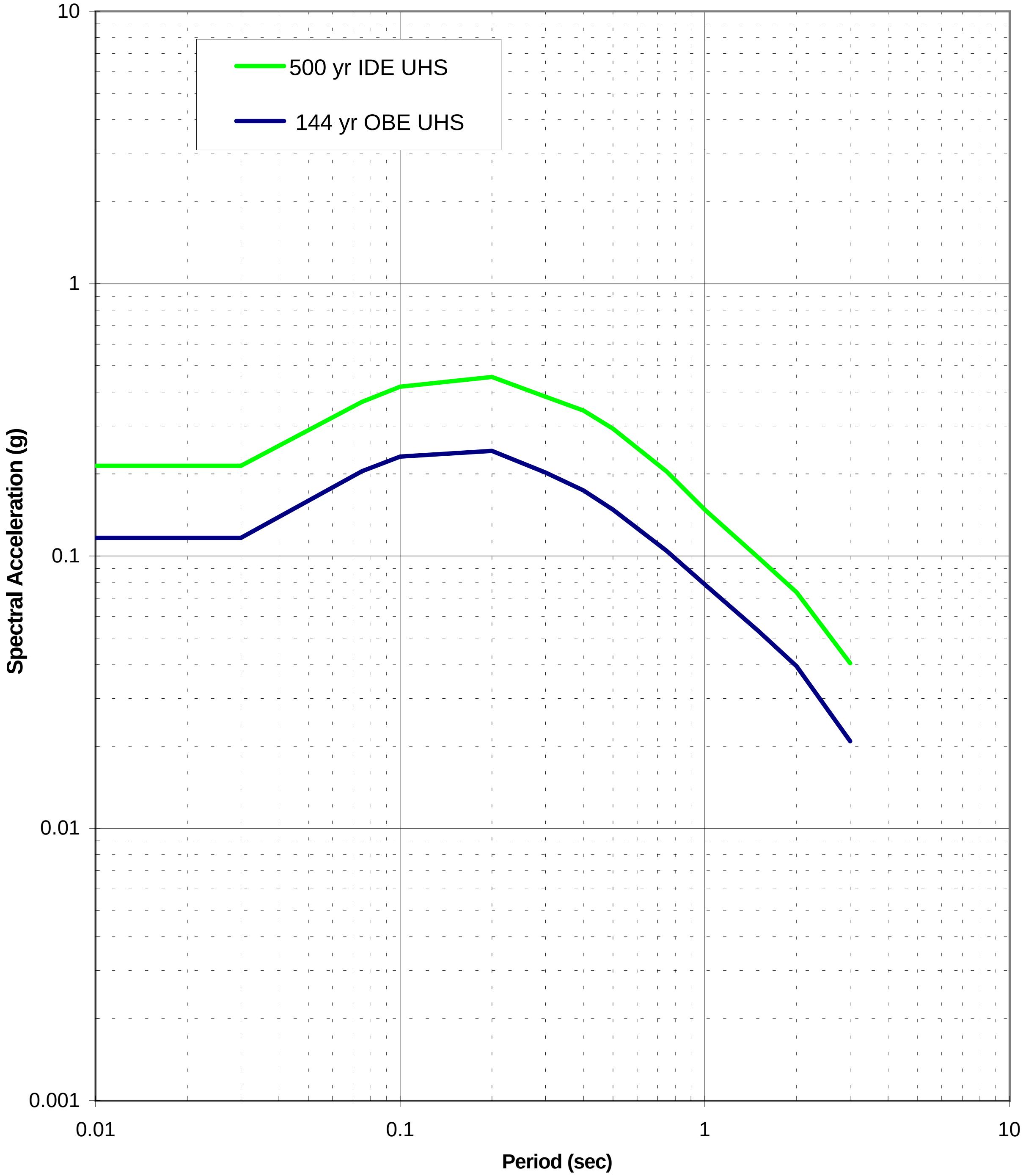

Seismic Ground Motion Study
Skookumchuck Dam
Lewis County, Washington

SOFT ROCK UNIFORM HAZARD ACCELERATION SPECTRA 144-YR (OBE) AND 500-YR (IDE)

March 2001 | 21-1-08920-001

SHANNON & WILSON, INC.
Geotechnical and Environmental Consultants

FIG. 5-12

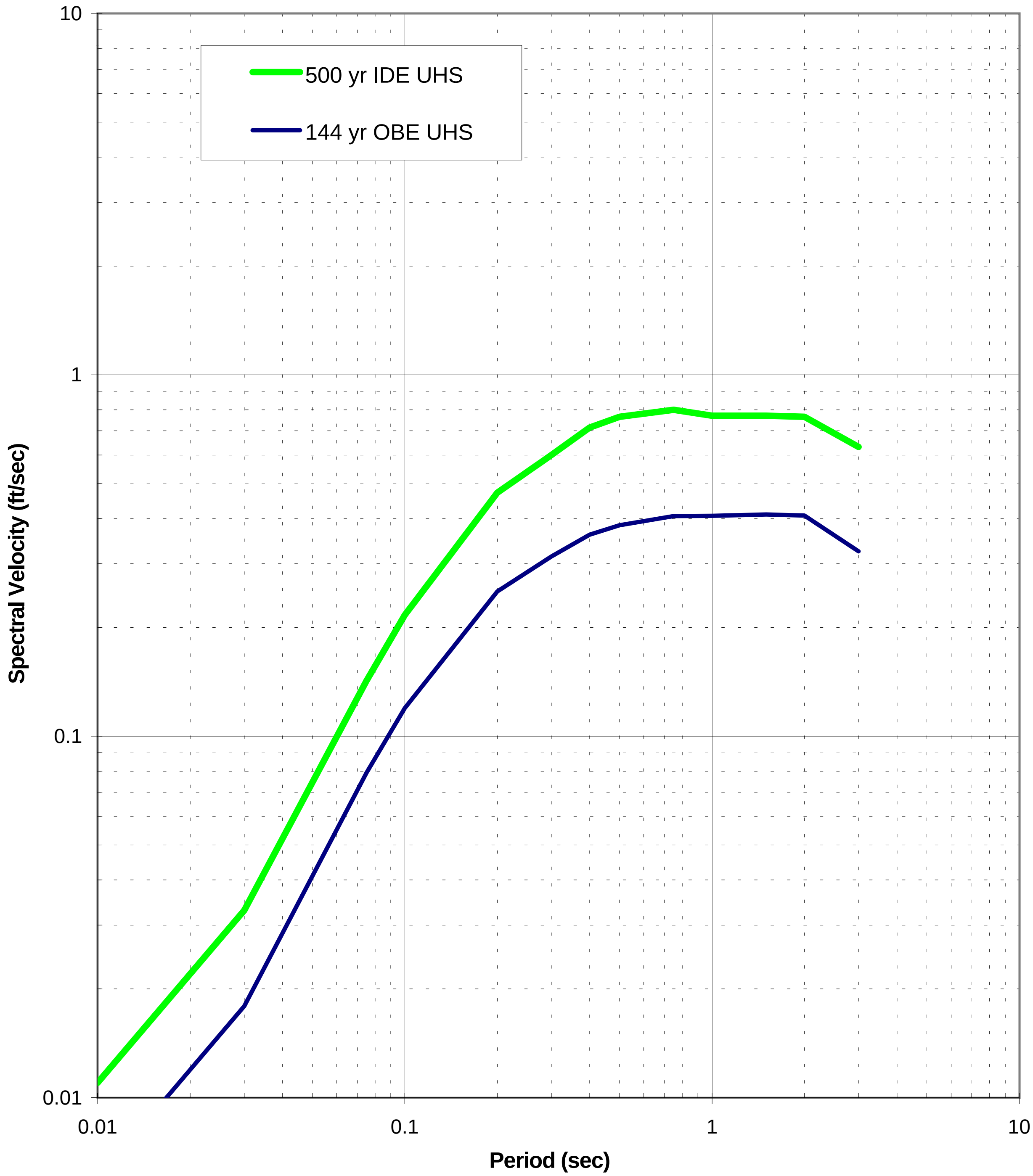

Seismic Ground Motion Study
Skookumchuck Dam
Lewis County, Washington

SOFT ROCK UNIFORM HAZARD VELOCITY SPECTRA 144-YR (OBE) AND 500-YR (IDE) RETURN PERIODS

March 2001 21-1-08920-001

SHANNON & WILSON, INC.
Geotechnical and Environmental Consultants

FIG. 5-13

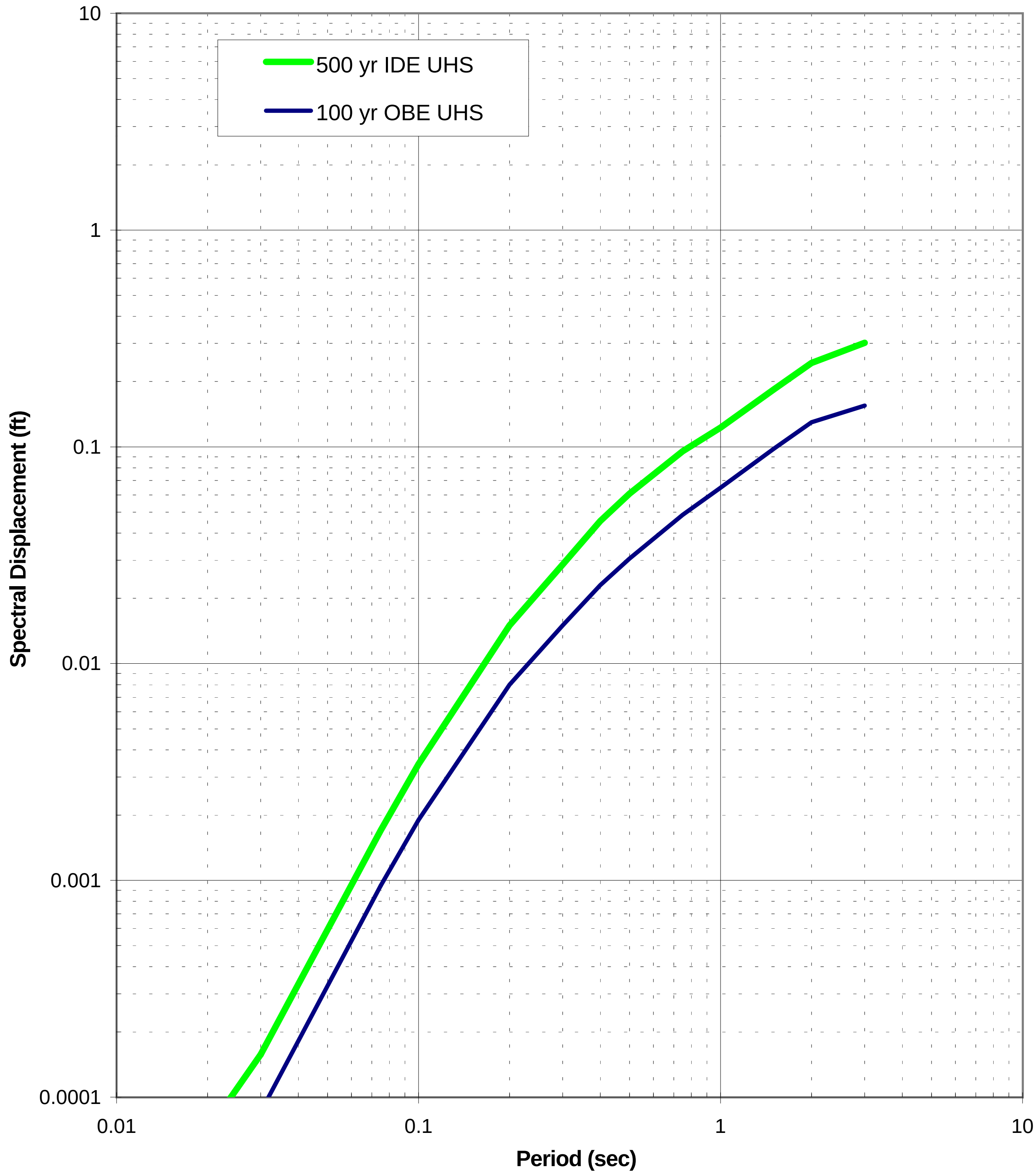

Seismic Ground Motion Study
Skookumchuck Dam
Lewis County, Washington

SOFT ROCK UNIFORM HAZARD DISPLACEMENT SPECTRA 144-YR (OBE) AND 500-YR (IDE)

March 2001 21-1-08920-001

SHANNON & WILSON, INC.
Geotechnical and Environmental Consultants

FIG. 5-14

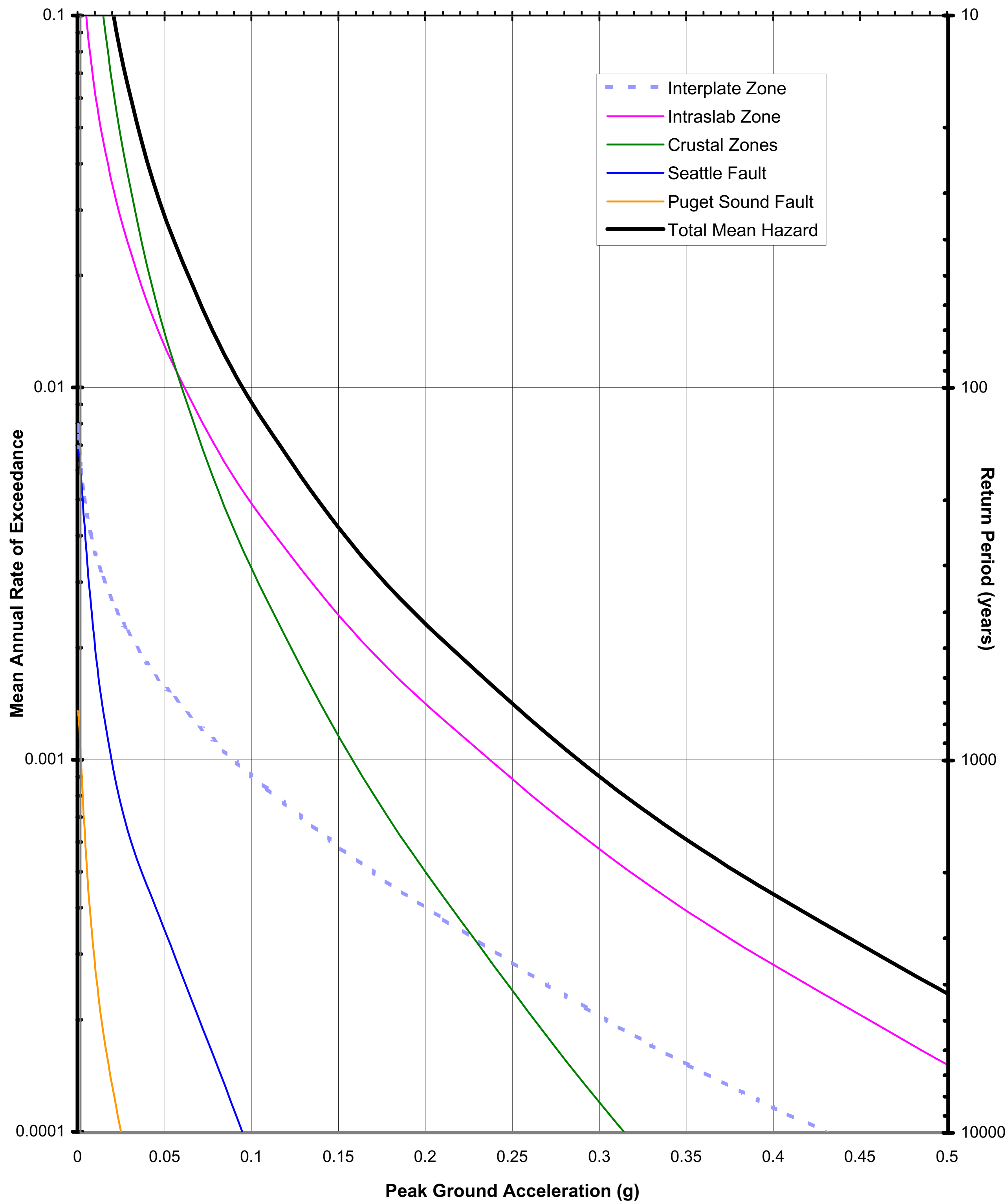

Seismic Ground Motion Study
Skookumchuck Dam
Lewis County, Washington

SEISMIC SOURCE CONTRIBUTIONS TO PEAK GROUND ACCELERATION

March 2001 21-1-08920-001

SHANNON & WILSON, INC.
Geotechnical and Environmental Consultants

FIG. 5-15

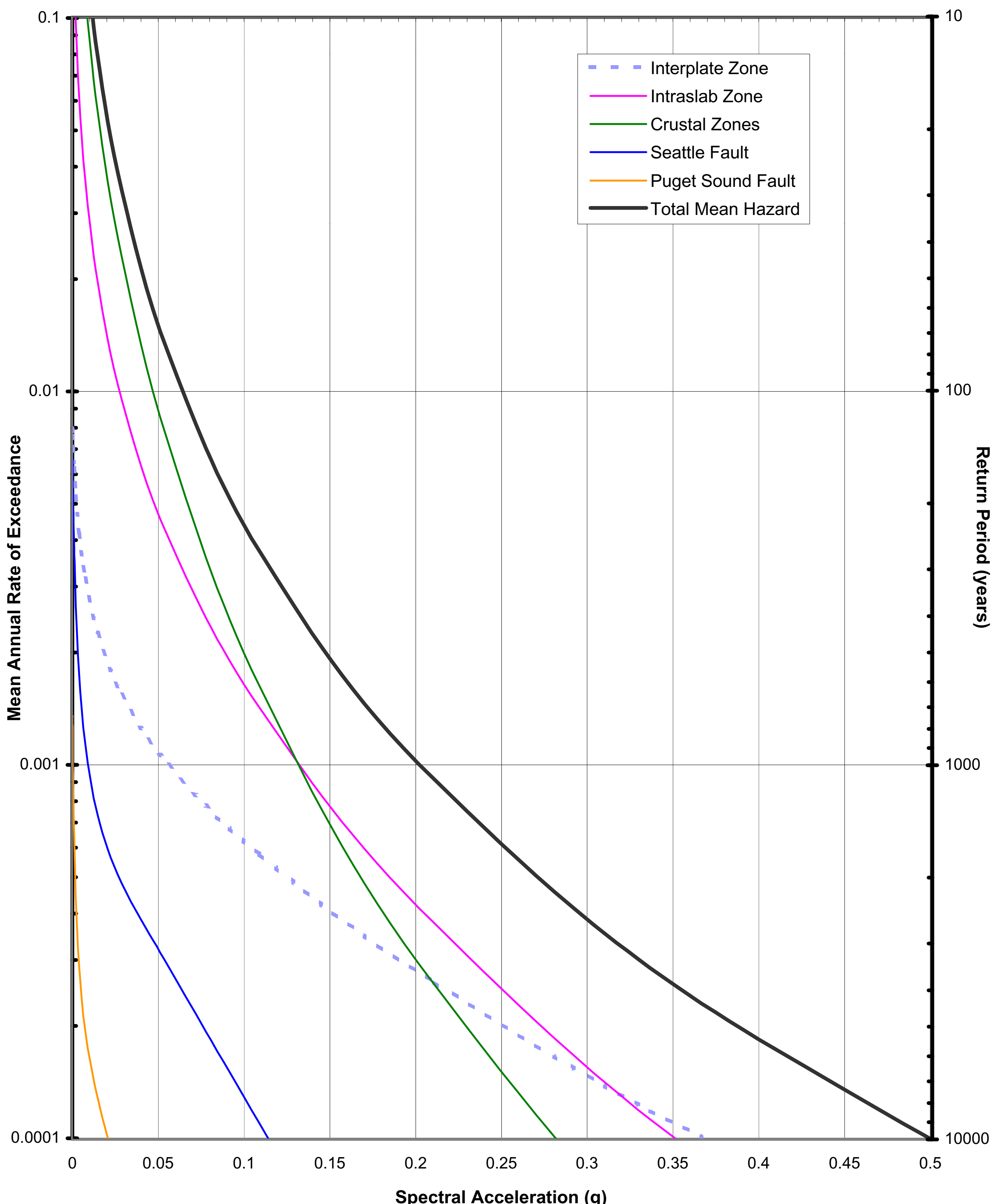

Seismic Ground Motion Study
Skookumchuck Dam
Lewis County, Washington

SEISMIC SOURCE CONTRIBUTIONS TO 1 SECOND HORIZONTAL SPECTRAL ACCELERATION

March 2001 21-1-08920-001

SHANNON & WILSON, INC.
Geotechnical and Environmental Consultants

FIG. 5-16

Hazard_final_epson1.xls-3/7/01-man

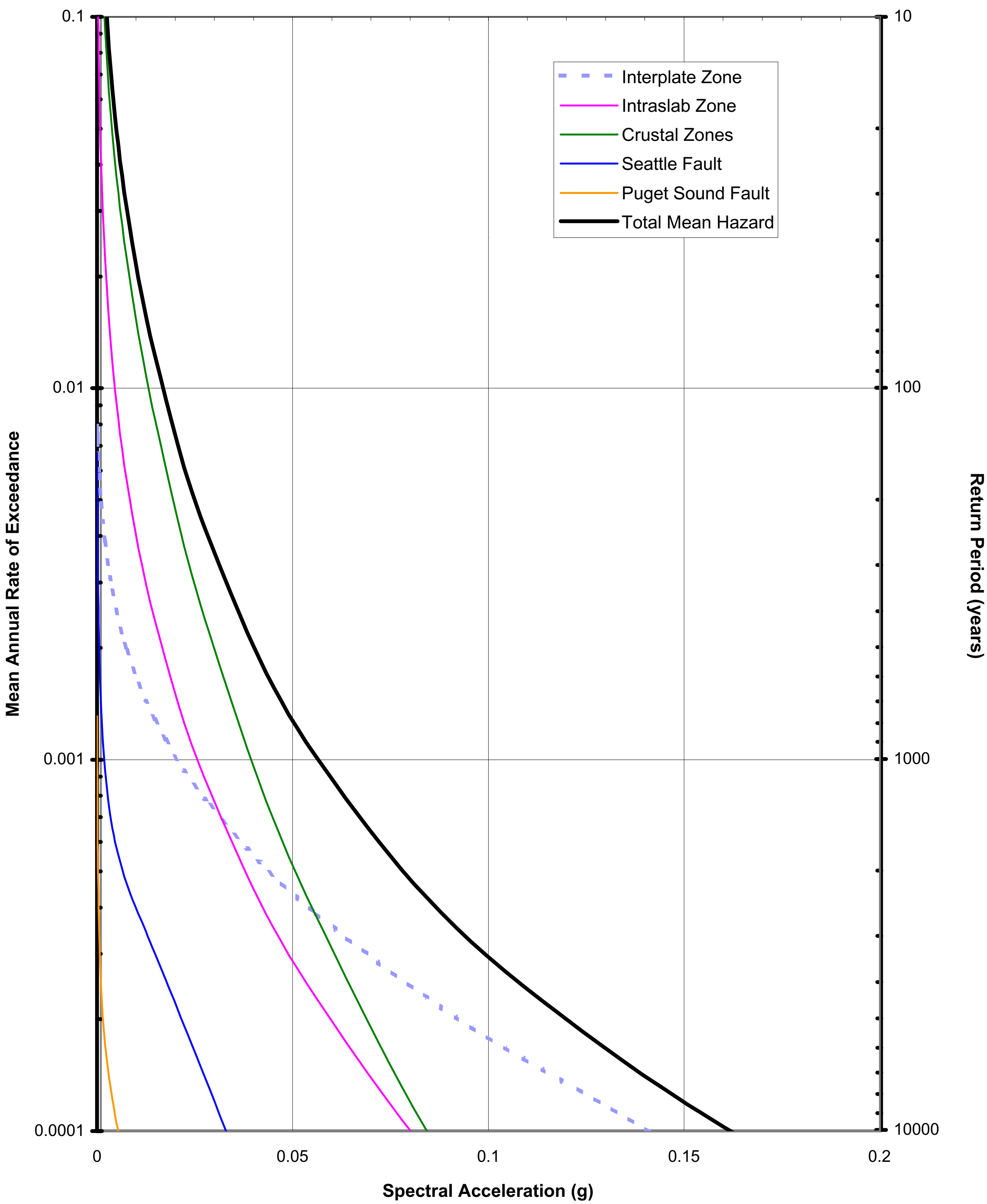

Seismic Ground Motion Study
Skookumchuck Dam
Lewis County, Washington

SEISMIC SOURCE CONTRIBUTIONS TO 3 SECOND HORIZONTAL SPECTRAL ACCELERATION

March 2001 21-1-08920-001

SHANNON & WILSON, INC.
Geotechnical and Environmental Consultants

FIG. 5-17

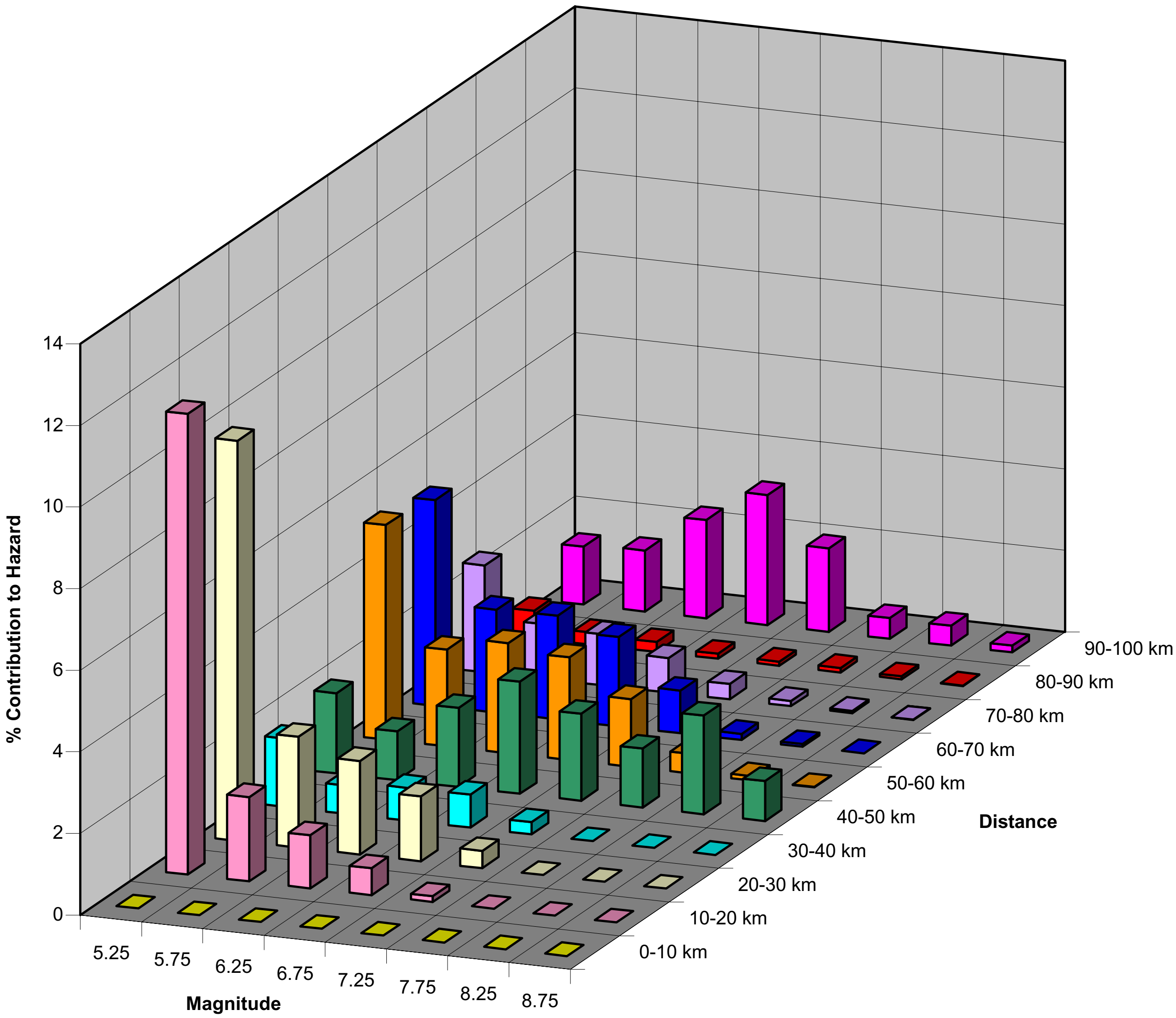

Magnitude	Distance Range (kilometers)									
	0-10	10-20	20-30	30-40	40-50	50-60	60-70	70-80	80-90	90-100
5.25	0.00	11.29	9.81	1.68	1.96	5.26	5.04	2.62	0.67	1.42
5.75	0.00	2.07	2.71	0.69	1.19	2.37	2.52	1.33	0.30	1.49
6.25	0.00	1.30	2.29	0.80	1.94	2.70	2.54	1.25	0.25	2.41
6.75	0.00	0.66	1.59	0.81	2.75	2.52	2.19	0.85	0.12	3.19
7.25	0.00	0.14	0.42	0.30	2.13	1.66	1.04	0.38	0.10	2.05
7.75	0.00	0.00	0.00	0.00	1.44	0.48	0.15	0.13	0.11	0.51
8.25	0.00	0.00	0.00	0.00	2.42	0.10	0.07	0.05	0.07	0.48
8.75	0.00	0.00	0.00	0.00	0.98	0.01	0.01	0.00	0.01	0.16

Seismic Ground Motion Study
Skookumchuck Dam
Lewis County, Washington

MAGNITUDE & DISTANCE CONTRIBUTION
PEAK GROUND ACCELERATION
144-YEAR EARTHQUAKE (OBE)

March 2001 | 21-1-08920-001

SHANNON & WILSON, INC.
Geotechnical and Environmental Consultants

FIG. 5-18

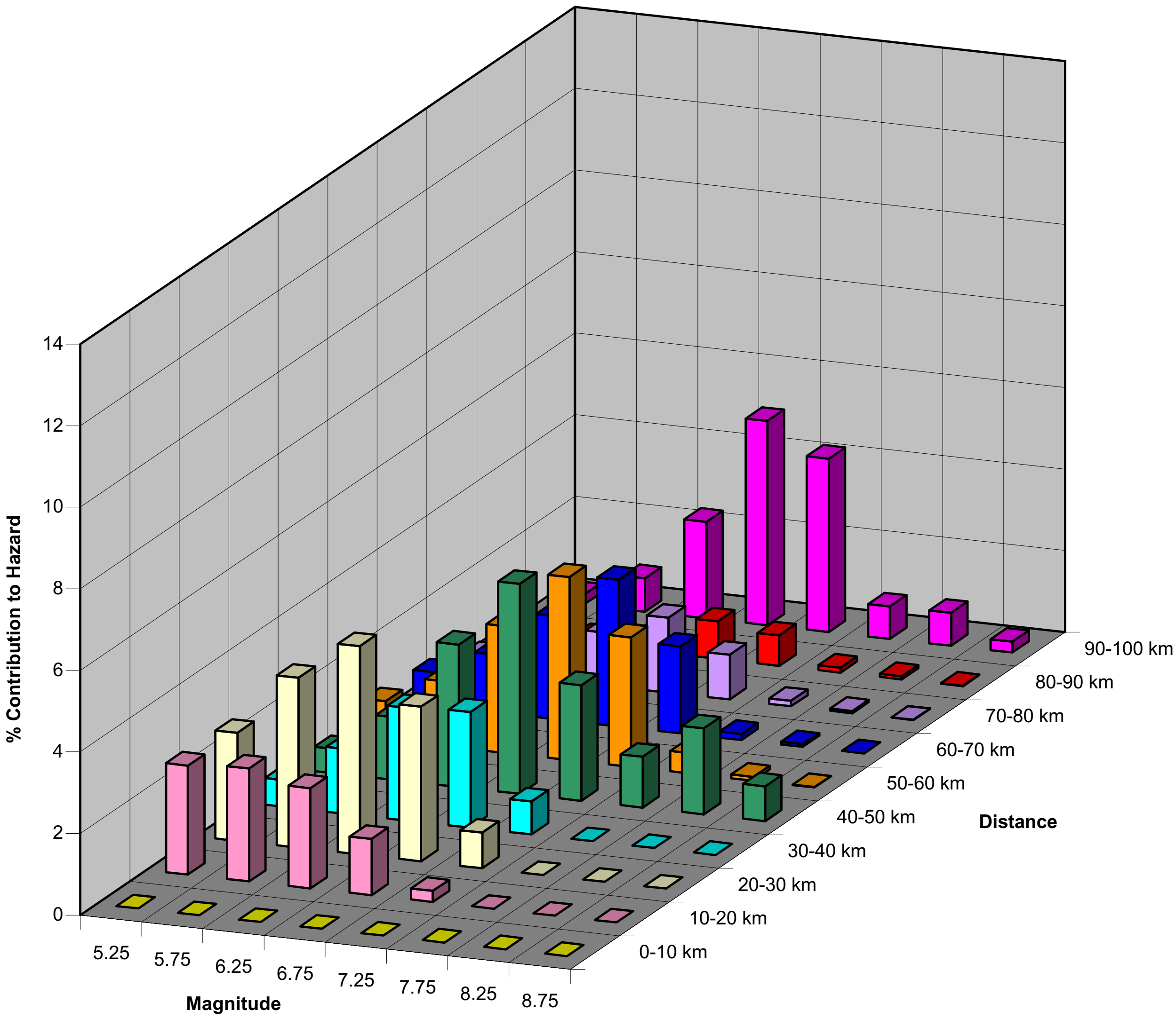

Magnitude	Distance Range (kilometers)									
	0-10	10-20	20-30	30-40	40-50	50-60	60-70	70-80	80-90	90-100
5.25	0.00	2.68	2.65	0.65	0.60	0.94	0.83	0.42	0.11	0.24
5.75	0.00	2.77	4.17	1.58	1.54	1.59	1.42	0.74	0.20	0.82
6.25	0.00	2.45	5.11	2.77	3.49	3.11	2.53	1.30	0.43	2.37
6.75	0.00	1.38	3.79	2.83	5.15	4.49	3.59	1.84	0.92	5.01
7.25	0.00	0.27	0.87	0.81	2.83	3.18	2.13	1.10	0.75	4.25
7.75	0.00	0.00	0.00	0.00	1.25	0.50	0.15	0.13	0.12	0.80
8.25	0.00	0.00	0.00	0.00	2.11	0.09	0.06	0.05	0.08	0.81
8.75	0.00	0.00	0.00	0.00	0.85	0.01	0.01	0.00	0.01	0.27

Seismic Ground Motion Study
Skookumchuck Dam
Lewis County, Washington

MAGNITUDE & DISTANCE CONTRIBUTION
PERIOD = 1 SECOND
144-YEAR EARTHQUAKE (OBE)

March 2001 21-1-08920-001

SHANNON & WILSON, INC.
Geotechnical and Environmental Consultants

FIG. 5-19

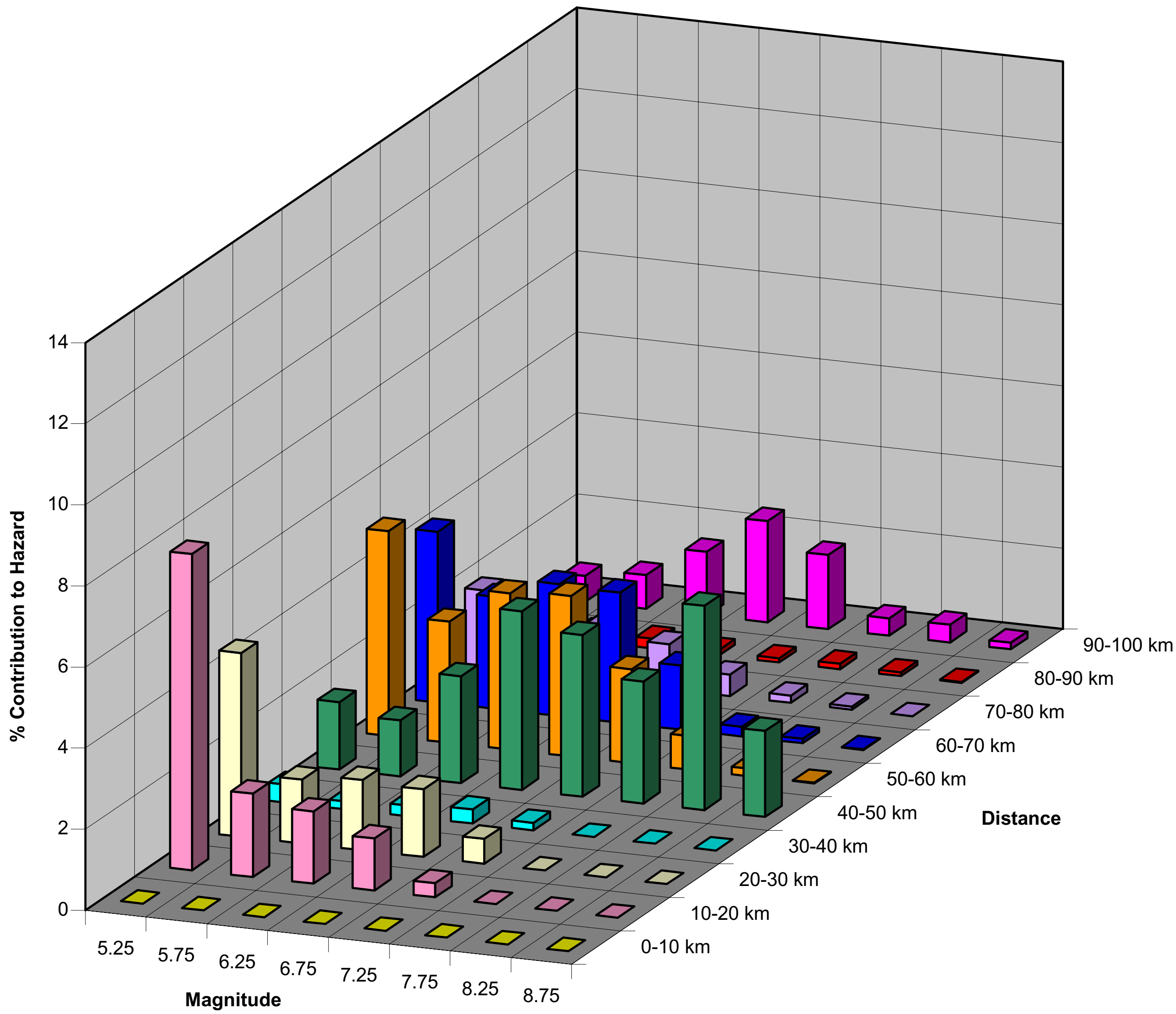

Magnitude	Distance Range (kilometers)									
	0-10	10-20	20-30	30-40	40-50	50-60	60-70	70-80	80-90	90-100
5.25	0.00	7.80	4.53	0.44	1.66	5.05	4.21	1.93	0.44	0.64
5.75	0.00	2.05	1.57	0.19	1.38	2.99	2.77	1.29	0.26	0.83
6.25	0.00	1.78	1.73	0.27	2.63	3.86	3.25	1.41	0.24	1.57
6.75	0.00	1.28	1.67	0.35	4.40	3.96	3.21	1.11	0.13	2.49
7.25	0.00	0.35	0.62	0.18	3.99	2.32	1.58	0.53	0.11	1.83
7.75	0.00	0.00	0.00	0.00	3.01	0.83	0.24	0.18	0.14	0.43
8.25	0.00	0.00	0.00	0.00	5.04	0.19	0.11	0.08	0.09	0.44
8.75	0.00	0.00	0.00	0.00	2.13	0.02	0.02	0.00	0.02	0.17

Seismic Ground Motion Study
Skookumchuck Dam
Lewis County, Washington

MAGNITUDE & DISTANCE CONTRIBUTION
PEAK GROUND ACCELERATION
500-YEAR EARTHQUAKE (IDE)

March 2001 21-1-08920-001

SHANNON & WILSON, INC.
Geotechnical and Environmental Consultants

FIG. 5-20

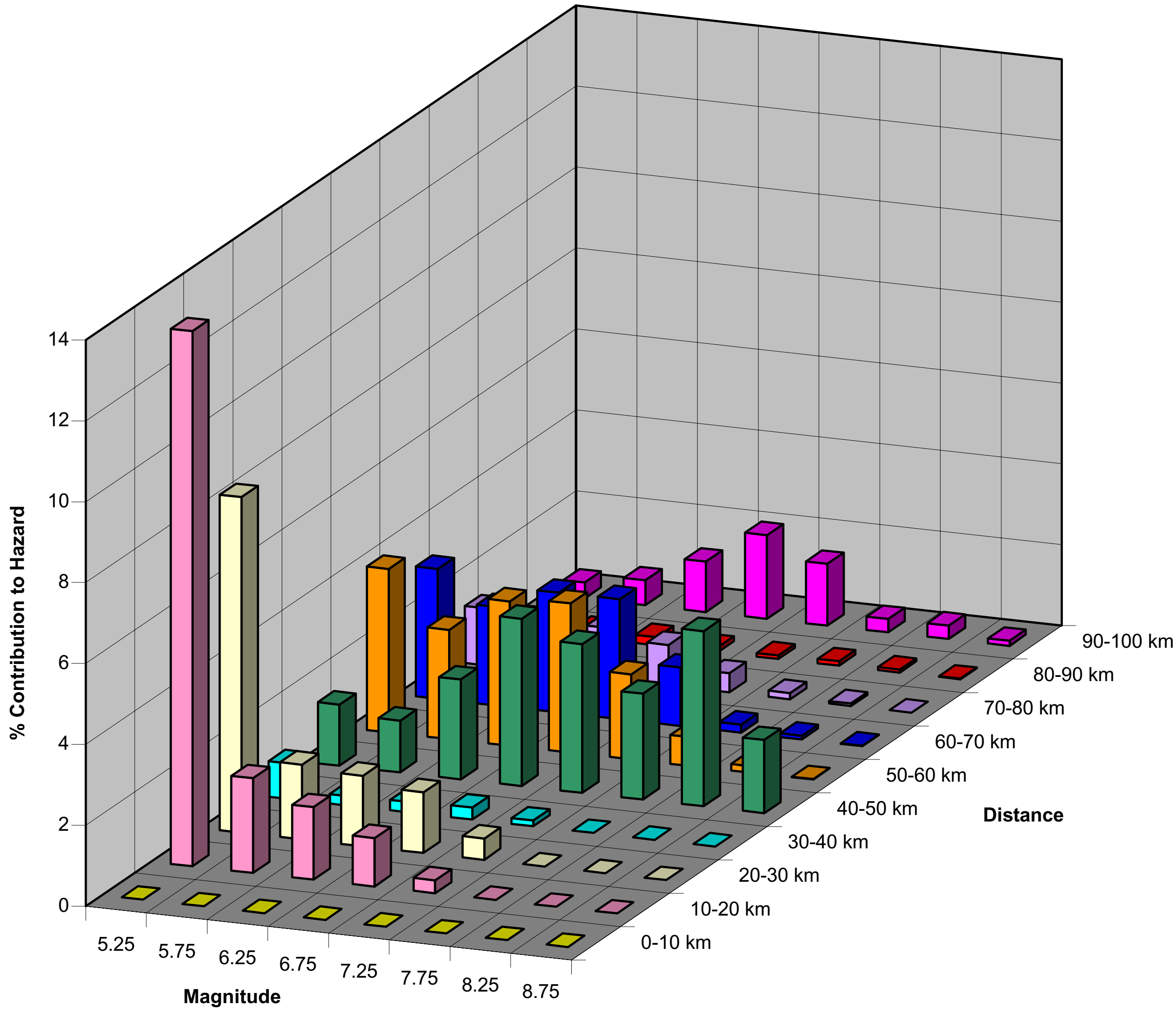

Magnitude	Distance Range (kilometers)									
	0-10	10-20	20-30	30-40	40-50	50-60	60-70	70-80	80-90	90-100
5.25	0.00	13.23	8.29	0.89	1.51	4.04	3.21	1.41	0.31	0.40
5.75	0.00	2.34	1.85	0.23	1.28	2.70	2.43	1.10	0.22	0.62
6.25	0.00	1.80	1.74	0.26	2.47	3.57	2.96	1.26	0.21	1.25
6.75	0.00	1.20	1.50	0.29	4.13	3.69	2.96	1.01	0.12	2.07
7.25	0.00	0.32	0.53	0.14	3.68	2.10	1.44	0.47	0.09	1.53
7.75	0.00	0.00	0.00	0.00	2.62	0.71	0.20	0.15	0.11	0.33
8.25	0.00	0.00	0.00	0.00	4.33	0.16	0.09	0.06	0.08	0.33
8.75	0.00	0.00	0.00	0.00	1.81	0.01	0.01	0.00	0.02	0.12

Seismic Ground Motion Study
Skookumchuck Dam
Lewis County, Washington

MAGNITUDE & DISTANCE CONTRIBUTION
PERIOD = 0.1 SECOND
500-YEAR EARTHQUAKE (IDE)

March 2001 21-1-08920-001

SHANNON & WILSON, INC.
Geotechnical and Environmental Consultants

FIG. 5-21

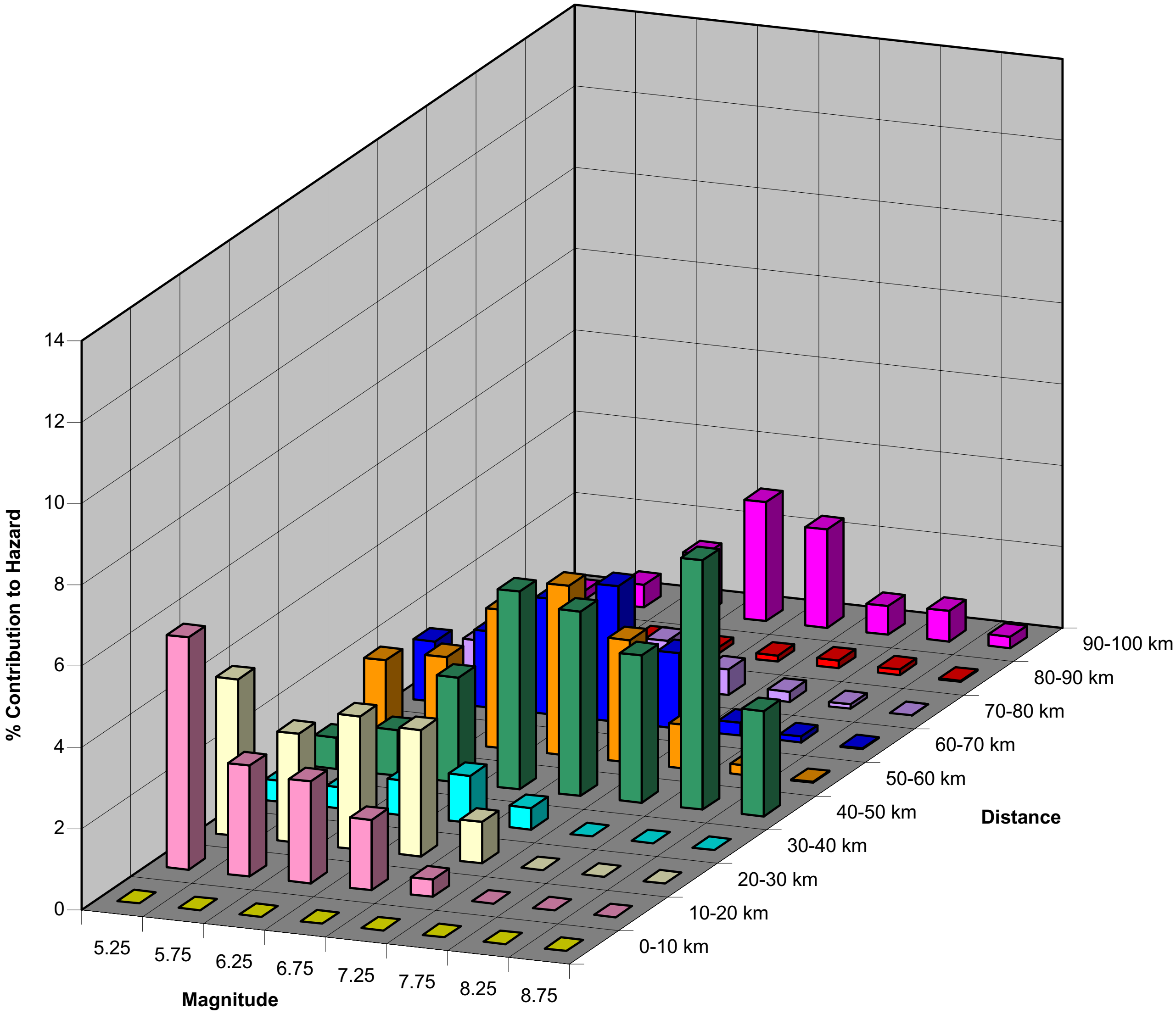

Magnitude	Distance Range (kilometers)									
	0-10	10-20	20-30	30-40	40-50	50-60	60-70	70-80	80-90	90-100
5.25	0.00	5.71	3.86	0.51	0.77	1.84	1.48	0.66	0.15	0.22
5.75	0.00	2.73	2.68	0.52	1.12	2.09	1.88	0.87	0.17	0.56
6.25	0.00	2.51	3.28	0.86	2.58	3.40	2.84	1.24	0.21	1.47
6.75	0.00	1.73	3.11	1.15	4.86	4.18	3.34	1.17	0.15	2.93
7.25	0.00	0.43	1.02	0.53	4.54	3.00	1.86	0.63	0.15	2.42
7.75	0.00	0.00	0.00	0.00	3.63	1.07	0.31	0.25	0.19	0.71
8.25	0.00	0.00	0.00	0.00	6.13	0.24	0.15	0.11	0.14	0.75
8.75	0.00	0.00	0.00	0.00	2.59	0.02	0.02	0.01	0.03	0.28

Seismic Ground Motion Study
Skookumchuck Dam
Lewis County, Washington

MAGNITUDE & DISTANCE CONTRIBUTION
PERIOD = 0.3 SECOND
500-YEAR EARTHQUAKE (IDE)

March 2001 21-1-08920-001

SHANNON & WILSON, INC.
Geotechnical and Environmental Consultants

FIG. 5-22

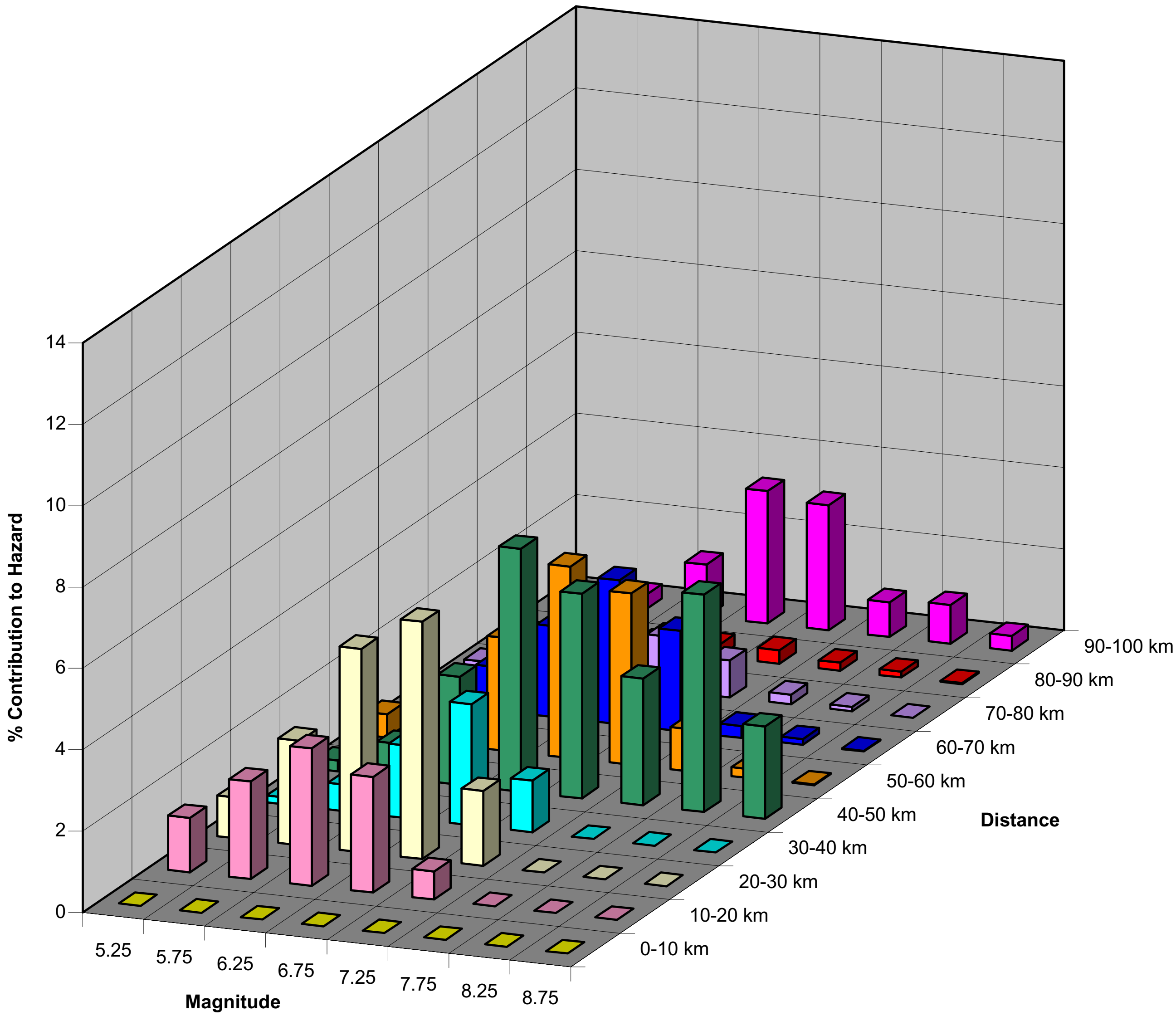

Magnitude	Distance Range (kilometers)									
	0-10	10-20	20-30	30-40	40-50	50-60	60-70	70-80	80-90	90-100
5.25	0.00	1.34	1.00	0.17	0.27	0.58	0.46	0.21	0.05	0.08
5.75	0.00	2.40	2.57	0.65	0.84	1.23	1.07	0.49	0.10	0.35
6.25	0.00	3.38	5.00	1.78	2.66	2.77	2.23	0.98	0.19	1.28
6.75	0.00	2.84	5.83	2.97	5.97	4.70	3.54	1.33	0.28	3.25
7.25	0.00	0.69	1.84	1.27	5.03	4.21	2.47	0.91	0.34	3.07
7.75	0.00	0.00	0.00	0.00	3.11	1.04	0.30	0.24	0.20	0.85
8.25	0.00	0.00	0.00	0.00	5.34	0.22	0.14	0.11	0.14	0.95
8.75	0.00	0.00	0.00	0.00	2.27	0.02	0.02	0.01	0.03	0.36

Seismic Ground Motion Study
Skookumchuck Dam
Lewis County, Washington

MAGNITUDE & DISTANCE CONTRIBUTION
PERIOD = 1 SECOND
500-YEAR EARTHQUAKE (IDE)

March 2001 21-1-08920-001

SHANNON & WILSON, INC.
Geotechnical and Environmental Consultants

FIG. 5-23

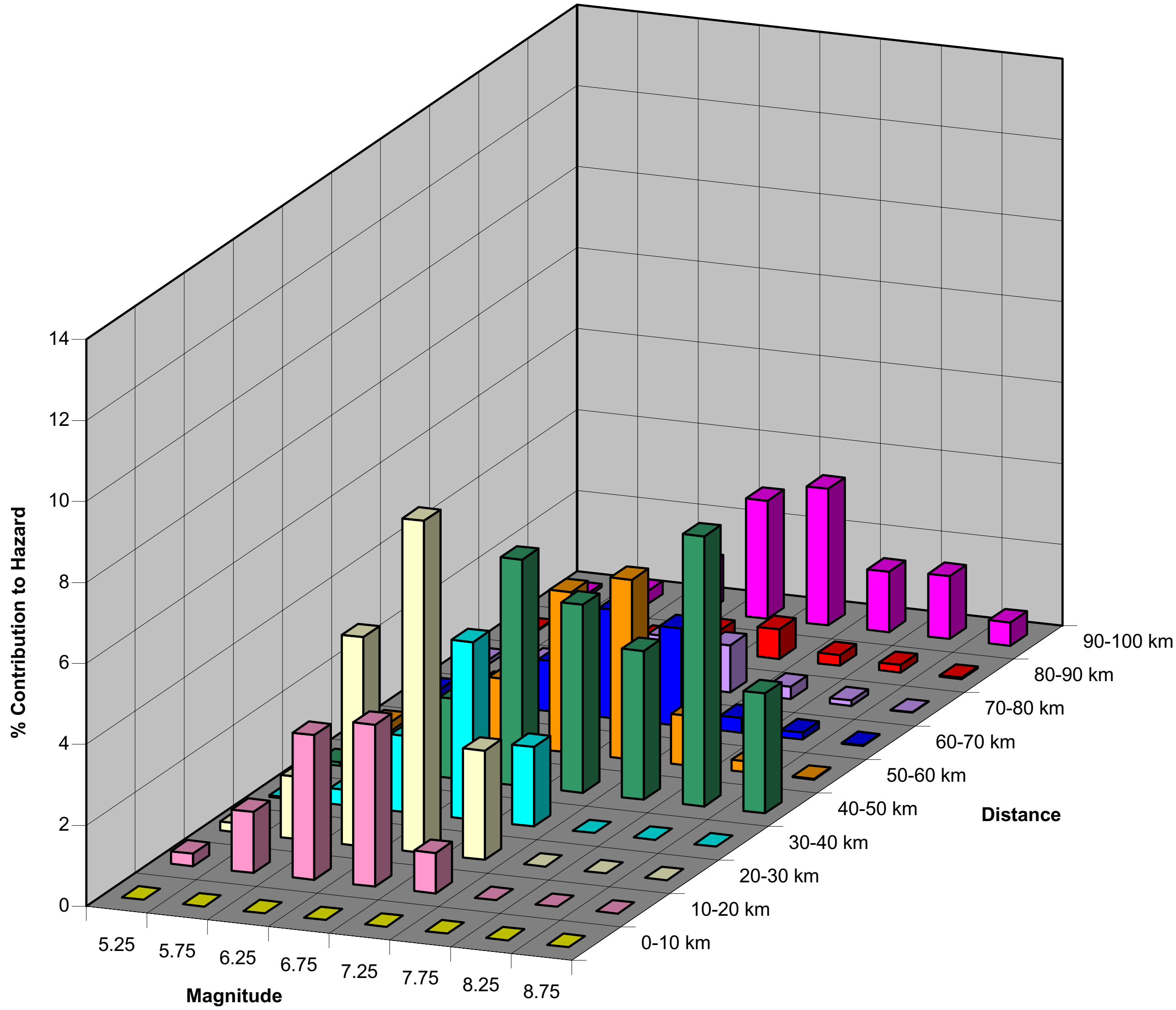

Magnitude	Distance Range (kilometers)									
	0-10	10-20	20-30	30-40	40-50	50-60	60-70	70-80	80-90	90-100
5.25	0.00	0.31	0.22	0.04	0.09	0.22	0.21	0.11	0.03	0.08
5.75	0.00	1.51	1.54	0.38	0.40	0.54	0.51	0.26	0.06	0.32
6.25	0.00	3.58	5.16	1.88	1.97	1.64	1.25	0.60	0.16	1.13
6.75	0.00	4.00	8.21	4.38	5.59	3.96	2.68	1.21	0.51	2.91
7.25	0.00	1.00	2.70	1.96	4.65	4.43	2.41	1.16	0.73	3.38
7.75	0.00	0.00	0.00	0.00	3.67	1.23	0.36	0.30	0.26	1.49
8.25	0.00	0.00	0.00	0.00	6.67	0.27	0.17	0.13	0.18	1.55
8.75	0.00	0.00	0.00	0.00	2.96	0.02	0.03	0.01	0.04	0.57

Seismic Ground Motion Study
Skookumchuck Dam
Lewis County, Washington

MAGNITUDE & DISTANCE CONTRIBUTION
PERIOD = 3 SECONDS
500-YEAR EARTHQUAKE (IDE)

March 2001

21-1-08920-001

SHANNON & WILSON, INC.
Geotechnical and Environmental Consultants

FIG. 5-24

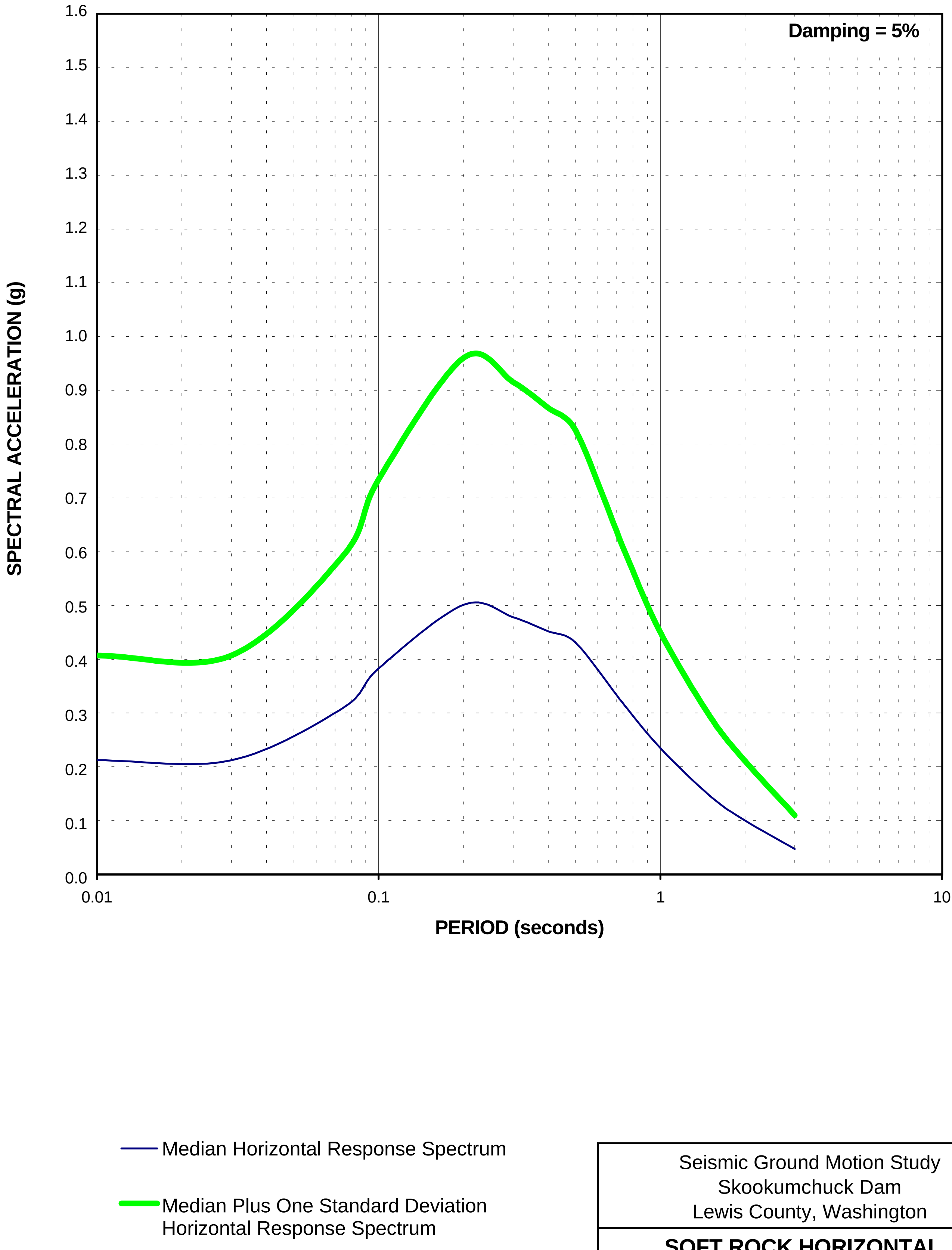

Seismic Ground Motion Study Skookumchuck Dam Lewis County, Washington	
SOFT ROCK HORIZONTAL RESPONSE SPECTRA CSZ MCE	
March 2001	21-1-08920-001
SHANNON & WILSON, INC. Geotechnical and Environmental Consultants	**FIG. 5-25**

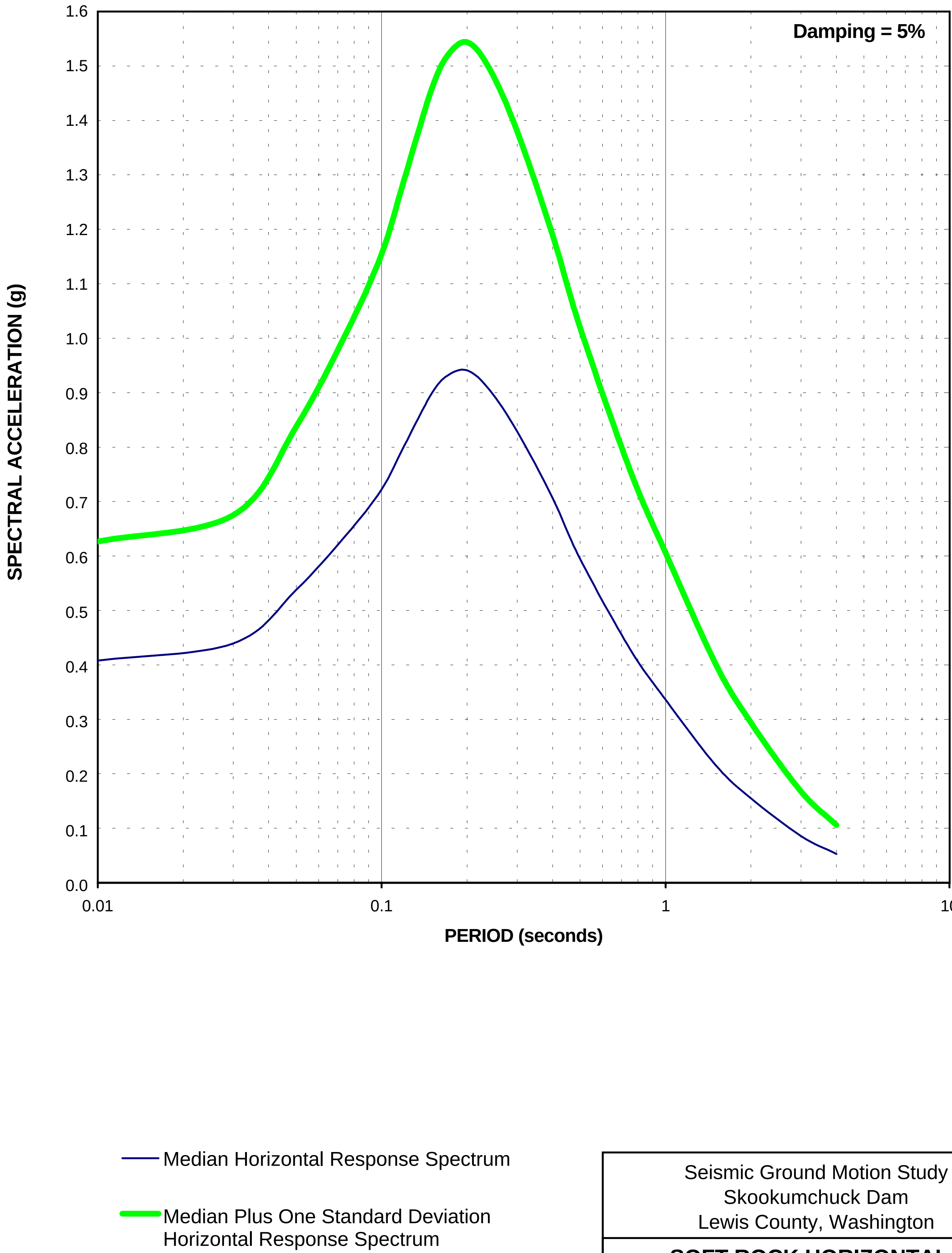

Seismic Ground Motion Study
Skookumchuck Dam
Lewis County, Washington

SOFT ROCK HORIZONTAL RESPONSE SPECTRA LF MCE

March 2001 | 21-1-08920-001

SHANNON & WILSON, INC.
Geotechnical and Environmental Consultants

FIG. 5-26

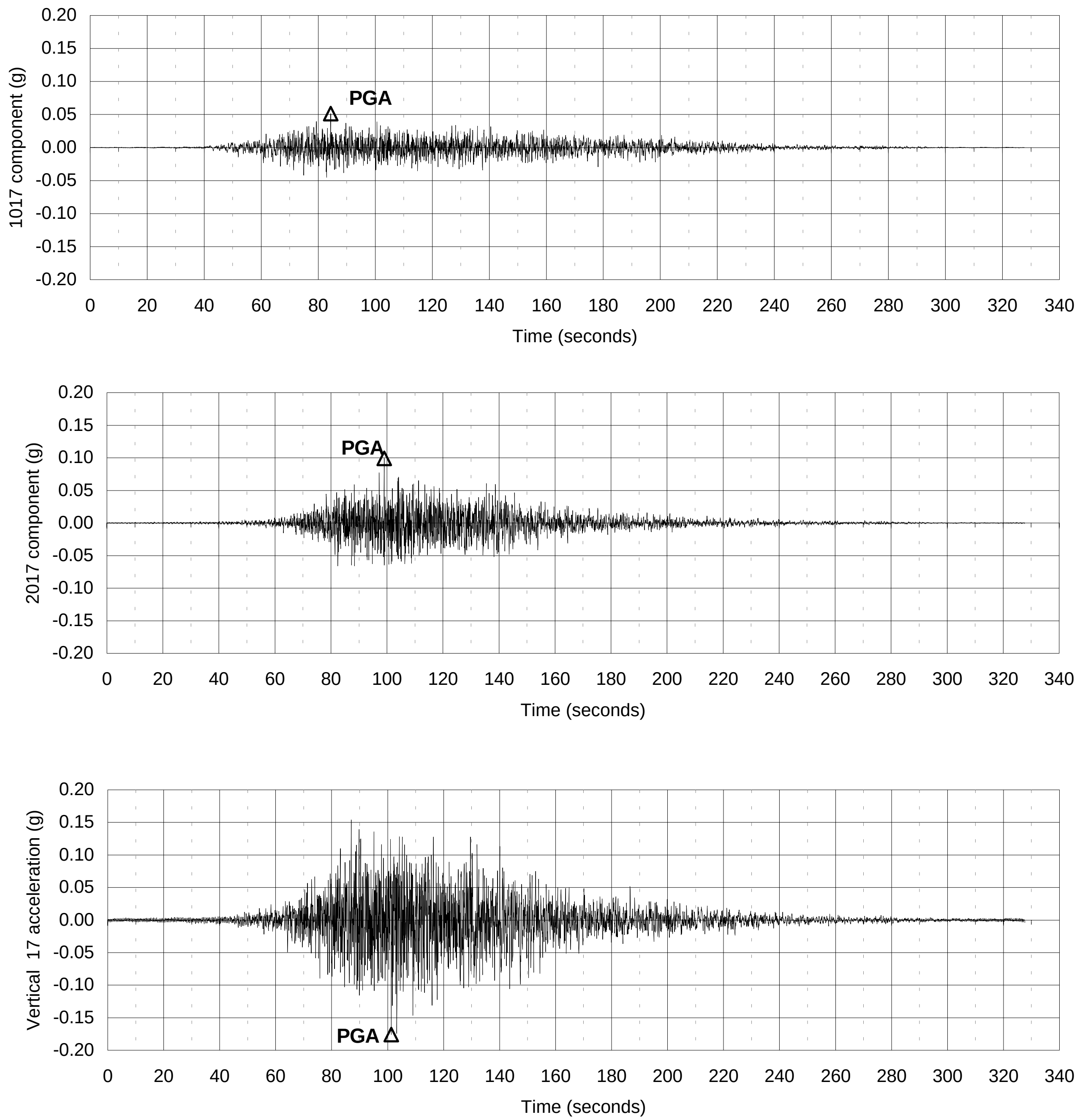

Peak Ground Motions

Acc 1017 comp	0.05 g
Acc 2017 comp	0.10 g
Acc Up17 comp	0.18 g

Seismic Ground Motion Study
Skookumchuck Dam
Lewis County, Washington

CSZ MCE SEED TIME HISTORIES
FINITE FAULT SIMULATION

March 2001 21-1-08920-001

SHANNON & WILSON, INC.
Geotechnical and Environmental Consultants

FIG. 5-27

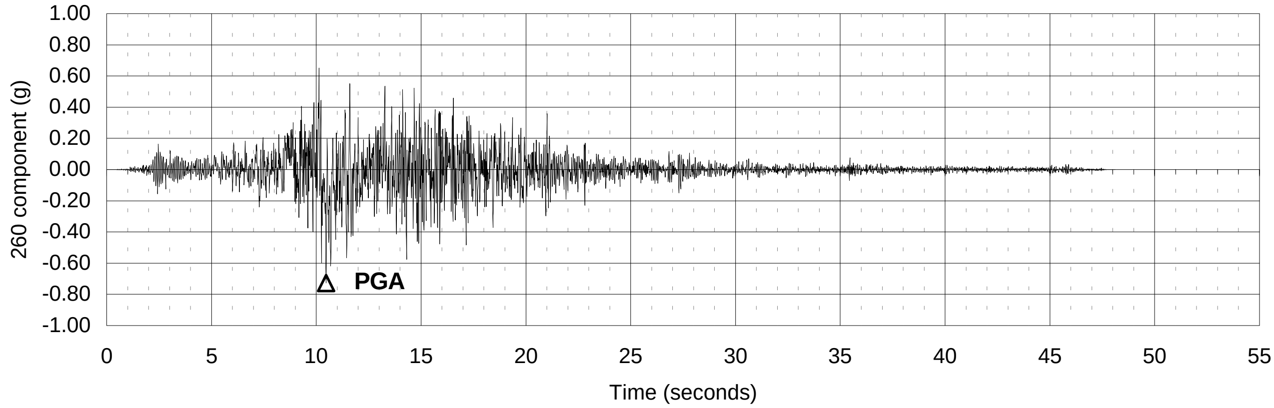

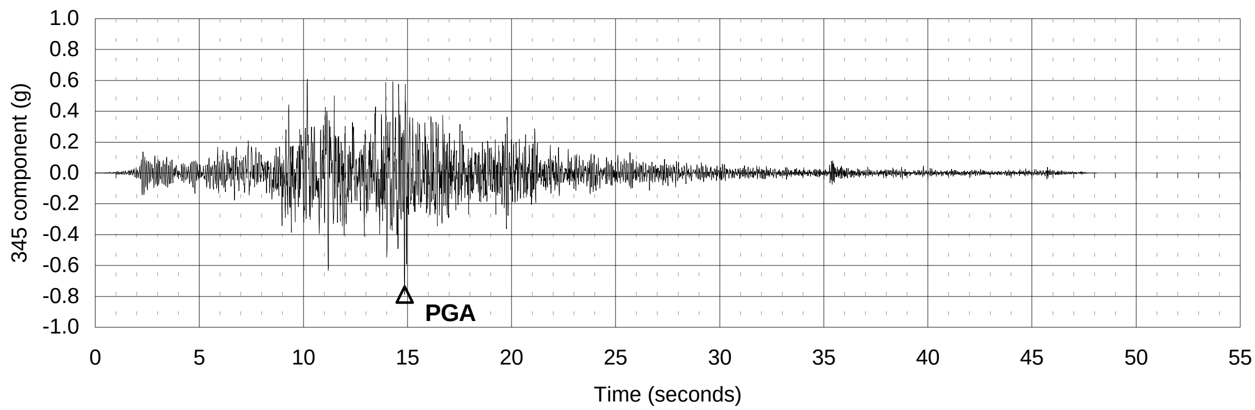

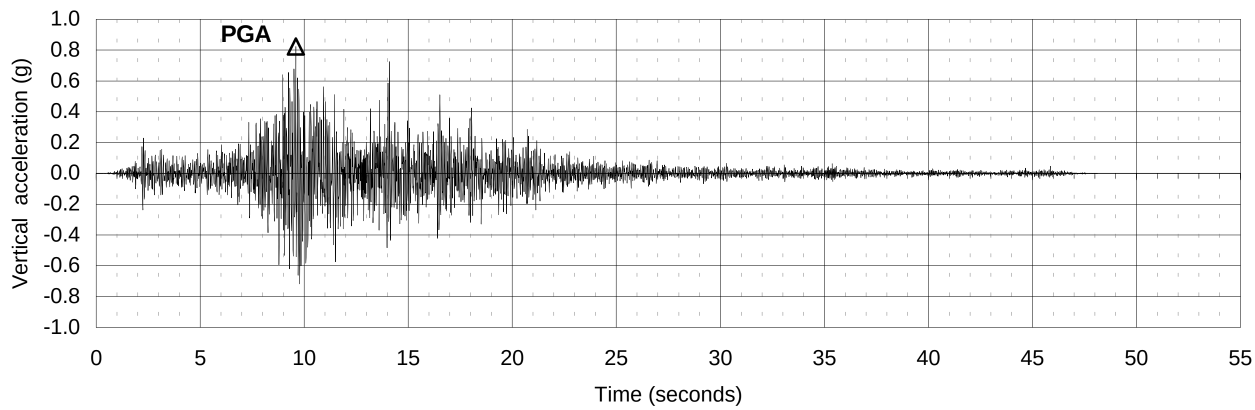

Peak Ground Motions

Acceleration345 comp	0.73 g
Acceleration260 comp	0.79 g
Acceleration Up comp	0.82 g

Seismic Ground Motion Study
Skookumchuck Dam
Lewis County, Washingtion

LF MCE SEED TIME HISTORIES
1992 LANDERS EARTHQUAKE
LUCERNE

March 2001 21-1-08920-001

SHANNON & WILSON, INC.
Geotechnical and Environmental Consultants

FIG. 5-28

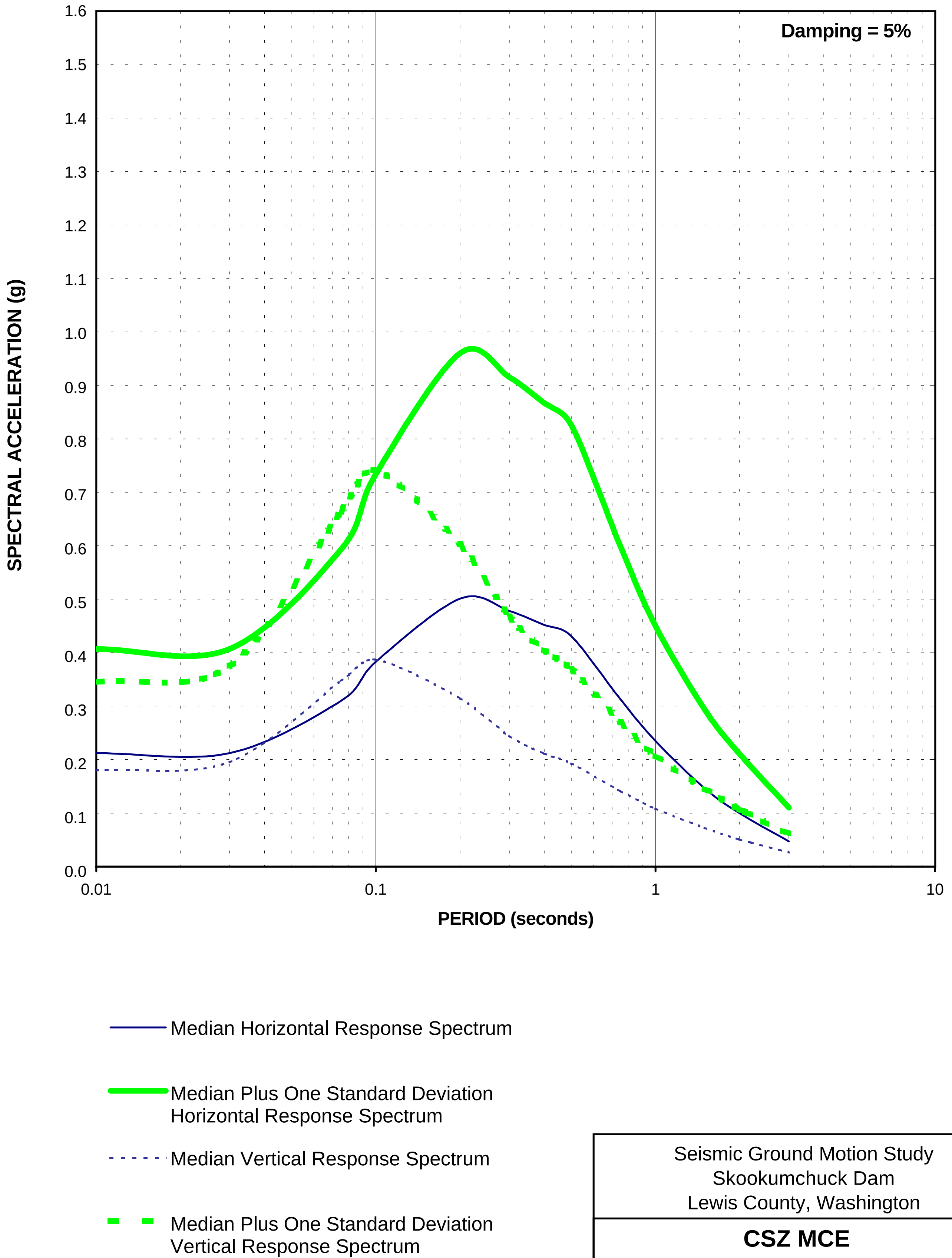

Seismic Ground Motion Study
Skookumchuck Dam
Lewis County, Washington

CSZ MCE
HORIZONTAL AND VERTICAL RESPONSE SPECTRA

March 2001 21-1-08920-001

SHANNON & WILSON, INC.
Geotechnical and Environmental Consultants

FIG. 6-1

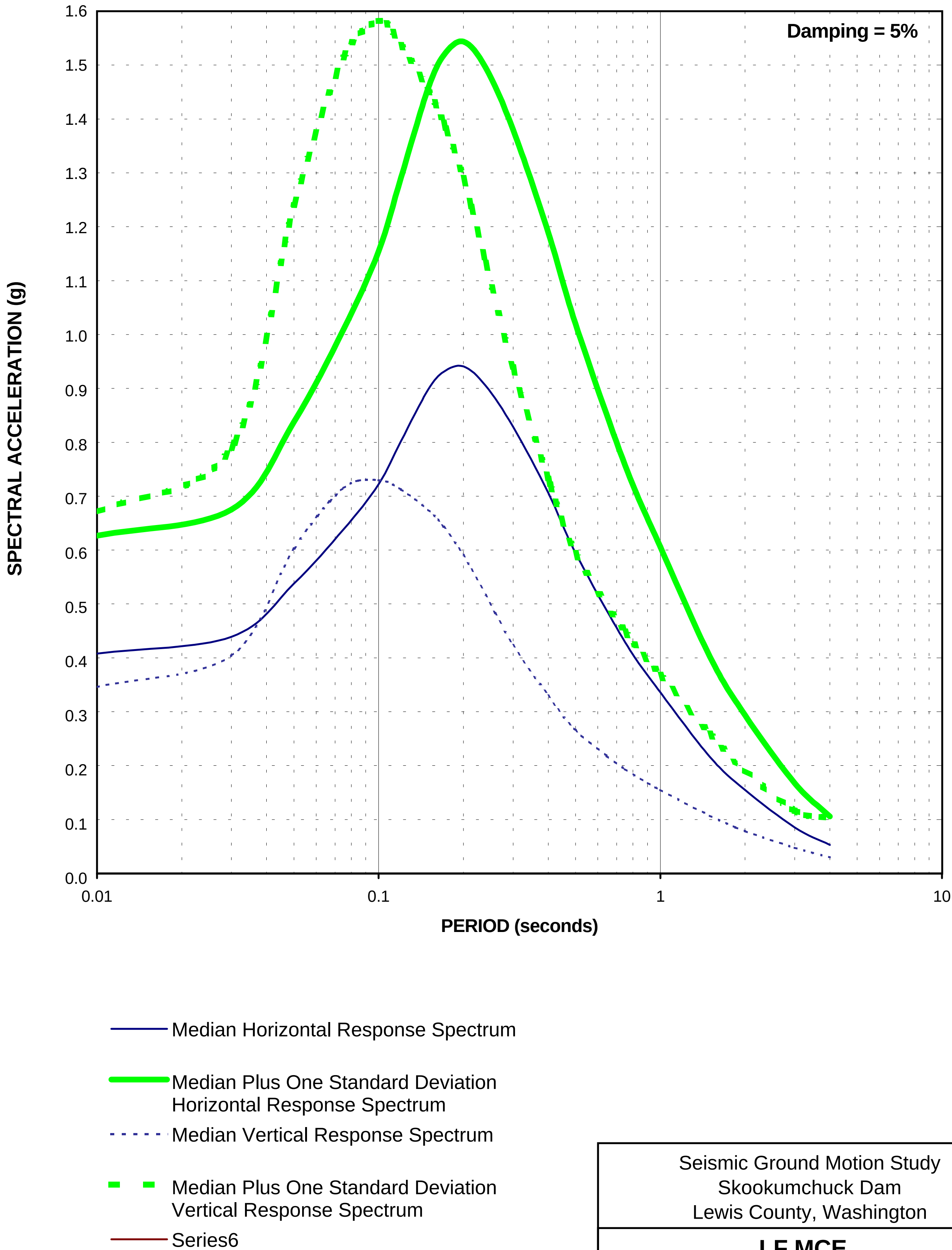

Seismic Ground Motion Study
Skookumchuck Dam
Lewis County, Washington

LF MCE
HORIZONTAL AND VERTICAL RESPONSE SPECTRA

March 2001 | 21-1-08920-001

SHANNON & WILSON, INC.
Geotechnical and Environmental Consultants

FIG. 6-2

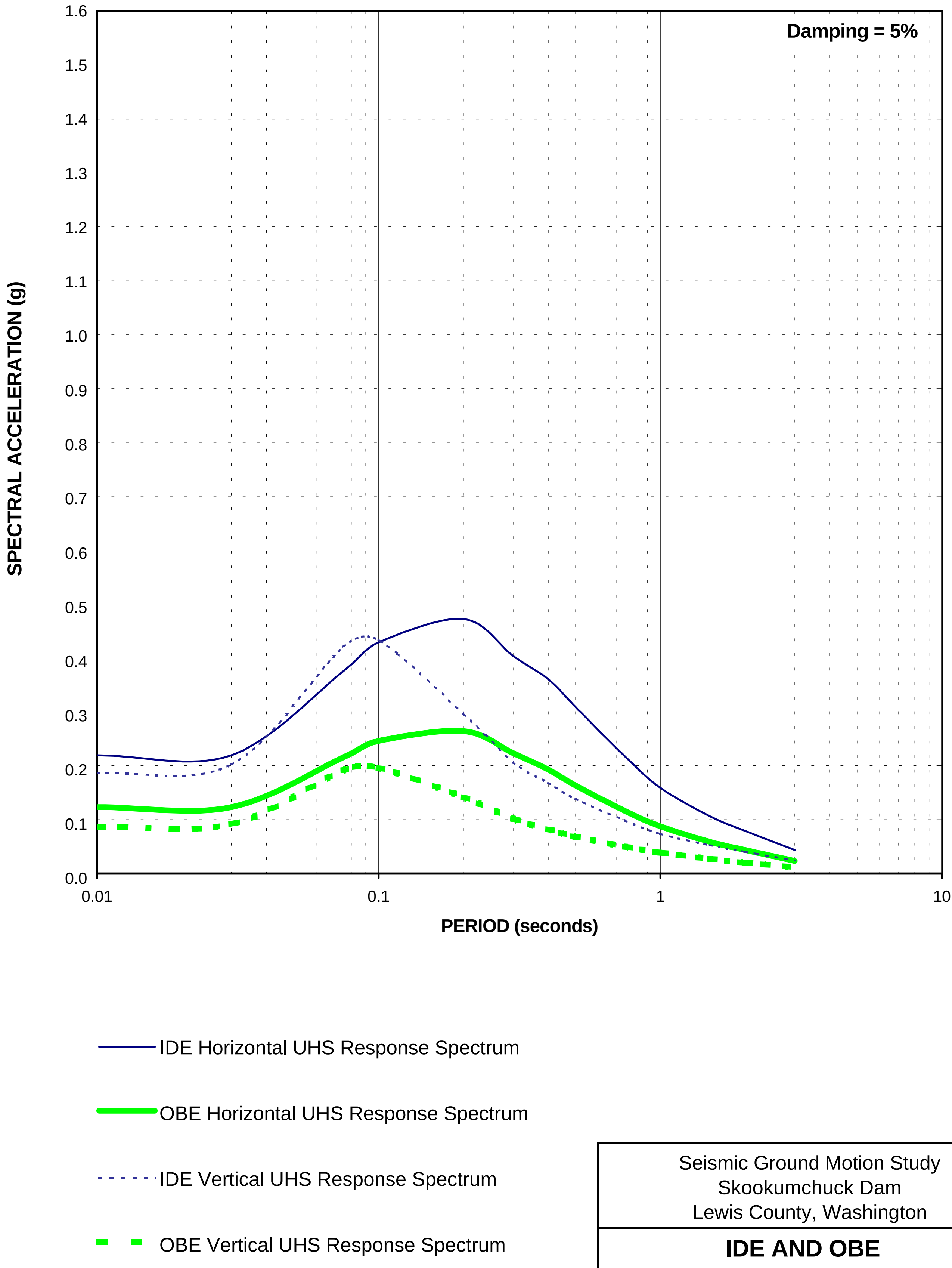

Seismic Ground Motion Study
Skookumchuck Dam
Lewis County, Washington

IDE AND OBE HORIZONTAL AND VERTICAL RESPONSE SPECTRA

March 2001 | 21-1-08920-001

SHANNON & WILSON, INC.
Geotechnical and Environmental Consultants

FIG. 6-3

APPENDIX A

STOCHASTIC GROUND MOTION MODEL DESCRIPTION

Prepared by:
Walter J. Silva and Sylvia Li
Pacific Engineering and Analysis
311 Pomona Avenue
El Cerrito, California 94530

APPENDIX A

STOCHASTIC GROUND MOTION MODEL DESCRIPTION

TABLE OF CONTENTS

Page

LIST OF TABLES

Table No.

APPENDIX A
STOCHASTIC GROUND MOTION MODEL DESCRIPTION

A.1 GENERAL

A.1.1 Finite Fault Simulations

For the simulations of the M 9.0 mega-thrust earthquake, the stochastic finite-fault methodology was used. To accommodate uncertainty in rupture geometry and corresponding rupture distance, three rupture scenarios were used: Mafic model with a length and width of 680 km x 148 km; transition zone model with a length and width of 800 km x 126 km; and the zero Isobase model with a length and width of 1,150 km x 87 km. For each rupture scenario, three site locations were sued: a best estimate assuming the northern terminus of the rupture occurs offshore near the Canadian border as well as translating the northern terminus 100 km north and 100 km south. For each rupture model and site location, thirty scenarios are simulated to accommodate uncertainty in nucleation point (rupture directivity), slip model, crustal damping, and the site shear-wave velocity as well as nonlinear material properties. Site conditions consisted of soft rock, typical of western United States, and consistent with the rock site conditions implied by the attenuation relations. In all 270 acceleration, velocity, and displacement time histories were generated and median and ±10 response spectra based on a log average of the 270 simulations. The time histories have durations appropriate for such large magnitude earthquakes and may be used for structural analyses.

A.2 BACKGROUND

In the context of strong ground motion, the term "stochastic" can be a fearful concept to some and may be interpreted to represent a fundamentally incorrect or inappropriate model (albeit the many examples demonstrating that it works well; Boore, 1983, 1986). To allay any initial misgivings, a brief discussion to explain the term stochastic in the stochastic ground motion model seems prudent.

The stochastic point-source model may be termed a spectral model in that it fundamentally describes the Fourier amplitude spectral density at the surface of a half-space (Hanks and McGuire, 1981). The model uses a Brune (1970, 1971) omega-square description of the earthquake source Fourier amplitude spectral density. This model is easily the most widely used and qualitatively validated source description available. Seismic sources ranging from **M** = -6 (hydrofracture) to **M** = 8 have been interpreted in terms of the Brune omega-square model in dozens of papers over the last 30 years. The general conclusion is that it provides a reasonable and consistent representation of crustal sources, particularly for tectonically active regions such as plate margins. A unique phase spectrum can be associated with the Brune source amplitude spectrum to produce a complex spectrum which can be propagated using either exact or approximate (1-2- or 3-D) wave propagation algorithms to produce single or multiple component time histories. In this context the model is not stochastic, it is decidedly deterministic and as exact and rigorous as one chooses. A two-dimensional array of such point-sources may be appropriately located on a fault surface (area) and fired with suitable delays to simulate rupture propagation on an extended rupture plane. As with the single point-source, any degree of rigor may be used in the wave propagation algorithm to produce multiple component or average horizontal component time histories. The result is a kinematic[1] finite-source model which has as its basis a source time history defined as a Brune pulse whose Fourier amplitude spectrum follows an omega-square model. This finite-fault model would be very similar to that used in published inversions for slip models if the 1-D propagation were treated using a reflectivity algorithm (Aki and Richards, 1980). This algorithm is a complete solution to the wave equation from static offsets (near-field terms) to an arbitrarily selected high frequency cutoff (generally 1-2 Hz).

Alternatively, to model the wave propagation more accurately, recordings of small earthquakes at the site of interest and with source locations distributed along the fault of interest may be used as empirical Green functions (Hartzell, 1978). To model the design earthquake, the empirical Green functions are delayed and summed in a manner to simulate rupture propagation (Hartzell, 1978). Provided a sufficient number of small earthquakes are recorded at the site of interest, the source locations adequately cover the expected rupture surface, and sufficient low frequency energy is present in the Green functions, this would be the most appropriate procedure to use if nonlinear site response is not an issue. With this approach the wave propagation is, in principle, exactly represented from each Green function source to the site. However, nonlinear site response is not treated unless Green function motions are recorded at a nearby rock outcrop with dynamic material properties similar to the rock underlying the soils at the site or recordings are made at depth within the site soil column. These motions may then be used as input to either

[1]Kinematic source model is one whose slip (displacement) is defined (imposed) while in a dynamic source model forces (stress) are defined (see Aki and Richards 1980 for a complete description).

total or effective stress site response codes to model nonlinear effects. Important issues associated with this approach include the availability of an appropriate nearby (1 to 2 km) rock outcrop and, for the downhole recordings, the necessity to remove all downgoing energy from the at-depth soil recordings. The downgoing energy must be removed from the downhole Green functions (recordings) prior to generating the control motions (summing) as only the upgoing wavefields are used as input to the nonlinear site response analyses. Removal of the downgoing energy from each recording requires multiple site response analyses which introduce uncertainty into the Green functions due to uncertainty in dynamic material properties and the numerical site response model used to separate the upgoing and downgoing wavefields.

To alleviate these difficulties one can use recordings well distributed in azimuth at close distances to a small earthquake and correct the recordings back to the source by removing wave propagation effects using a simple approximation (say 1/R plus a constant for crustal amplification and radiation pattern), to obtain an empirical source function. This source function can be used to replace the Brune pulse to introduce some natural (although source, path, and site specific) variation into the dislocation time history. If this is coupled to an approximate wave propagation algorithm (asymptotic ray theory) which includes the direct rays and those which have undergone a single reflection, the result is the empirical source function method (EPRI, 1993). Combining the reflectivity propagation (which is generally limited to frequencies # 1-2 Hz due to computational demands) with the empirical source function approach (appropriate for frequencies $ 1 Hz; EPRI, 1993) results in a broad band simulation procedure which is strictly deterministic at low frequencies (where an analytical source function is used) and incorporates some natural variation at high frequencies through the use of an empirical source function (Sommerville et al., 1995).

All of these techniques are fundamentally similar, well founded in seismic source and wave propagation physics, and importantly, they are <u>all</u> approximate. Simply put, all models are wrong (approximate) and the single essential element in selecting a model is to incorporate the appropriate degree of rigor, commensurate with uncertainties and variabilities in crustal structure and site effects, through extensive validation exercises. It is generally felt that more complicated models produce more accurate results, however, the implications of more sophisticated models with the increased number of parameters which must be specified is often overlooked. This is not too serious a consequence in modeling past earthquakes since a reasonable range in parameter space can be explored to give the "best" results. However for future predictions, this increased rigor may carry undesirable baggage in increased parametric variability (Roblee et al., 1996). The effects of lack of knowledge (epistemic uncertainty; EPRI, 1993) regarding parameter values for future occurrences results in uncertainty or variability in ground motion predictions. It may easily be the case that a very simple model, such as the point-source model can have comparable, or even smaller, total variability (modeling plus parametric) than a much more rigorous model with an increased number of parameters (EPRI, 1993). What is desired in a model is sufficient sophistication such that it captures the dominant and stable features of source, distance, and site dependencies observed in strong ground motions. It is these considerations which led to the development of the stochastic point- and finite-source models and, in part, leads to the stochastic element of the models.

The stochastic nature of the point- and finite-source RVT models is simply the assumption made about the character of ground motion time histories that permits stable estimates of peak parameters (e.g. acceleration, velocity, strain, stress, oscillator response) to be made without computing detailed time histories (Hanks and McGuire, 1981; Boore, 1983). This process uses random vibration theory to relate a time domain peak value to the time history root-mean-square (RMS) value (Boore, 1983). The assumption of the character of the time history for this process to strictly apply is that it be normally distributed random noise and stationary (its statistics do not change with time) over its duration. A visual examination of any time history quickly reveals that this is clearly not the case: time histories (acceleration, velocity, stress, strain, oscillator) start, build up, and then diminish with time. However poor the assumption of stationary Gaussian noise may appear, the net result is that the assumption is weak enough to permit the approach to work surprisingly well, as numerous comparisons with recorded motions and both qualitative and quantitative validations have shown (Hanks and McGuire, 1981; Boore, 1983, 1986; McGuire et al., 1984; Boore and Atkinson, 1987; Silva and Lee, 1987; Toro and McGuire, 1987; Silva et al., 1990; EPRI, 1993; Schneider et al., 1993; Silva and Darragh, 1995; Silva et al., 1997). Corrections to RVT are available to accommodate different distributions as well as non-stationarity and are usually applied to the estimation of peak oscillator response in the calculated response spectra (Boore and Joyner, 1984; Toro, 1985).

A.3 POINT-SOURCE MODEL

The conventional stochastic ground motion model uses an ? -square source model (Brune, 1970, 1971) with a single corner frequency and a constant stress drop (Boore, 1983; Atkinson, 1984). Random vibration theory is used to relate RMS (root-mean-square) values to peak values of acceleration (Boore, 1983), and oscillator response (Boore and Joyner, 1984; Toro, 1985; Silva and Lee, 1987) computed from the power spectra to expected peak time domain values (Boore, 1983).

The shape of the acceleration spectral density, a(f), is given by

$$a(f) = C \frac{f^2}{1+(\frac{f}{f_0})^2} \frac{MSUB0}{R} P(f) A(f) e^{-\frac{p f R}{b_0 Q(f)}} \quad \text{(A-1)}$$

where

C $= (\frac{1}{r_0 b_0^3}) \bullet (2) \bullet (0.55) \bullet (\frac{1}{\sqrt{2}}) \bullet p$.

M_0 = seismic moment,
R = hypocentral distance,
$ß_0$ = shear-wave velocity at the source,
$?_0$ = density at the source
Q(f) = frequency dependent quality factor (crustal damping),
A(f) = crustal amplification,
P(f) = high-frequency truncation filter,
f_0 = source corner frequency.

C is a constant which contains source region density ($?_0$) and shear-wave velocity terms and accounts for the free-surface effect (factor of 2), the source radiation pattern averaged over a sphere (0.55) (Boore, 1986), and the partition of energy into two horizontal components (1/*l* 2).

Source scaling is provided by specifying two independent parameters, the seismic moment (M_0) and the high-frequency stress parameter or stress drop (?s). The seismic moment is related to magnitude through the definition of moment magnitude **M** by the relation

log M_0 = 1.5 **M** + 16.05 (Hanks and Kanamori, 1979) (A-2).

The stress drop (?s) relates the corner frequency f_0 to M_0 through the relation

$f_0 = ß_0 (?s/8.44\ M_0)^{1/3}$ (Brune; 1970, 1971) (A-3).

The stress drop is sometimes referred to as the high frequency stress parameter (Boore, 1983) (or simply the stress parameter) since it directly scales the Fourier amplitude spectrum for frequencies above the corner frequency (Silva, 1991; Silva and Darragh 1995). High (> 1 Hz) frequency model predictions are then very sensitive to this parameter (Silva, 1991; EPRI, 1993) and the interpretation of it being a stress drop or simply a scaling parameter depends upon how well real earthquake sources (on average) obey the omega-square scaling (Equation A-3) and how well they are fit by the single-corner-frequency model. If earthquakes truly have single-corner-frequency omega-square sources, the stress drop in Equation A-3 is a physical parameter and its values have a physical interpretation of the forces (stresses) accelerating the relative slip across the rupture surface. High stress drop sources are due to a smaller source (fault) area (for the same **M**) than low stress drop sources (Brune, 1970). Otherwise, it simply a high frequency scaling or fitting parameter.

The spectral shape of the single-corner-frequency ? -square source model is then described by the two free parameters M_0 and ?s. The corner frequency increases with the shear-wave velocity and with increasing stress drop, both of which may be region dependent.

The crustal amplification accounts for the increase in wave amplitude as seismic energy travels through lower- velocity crustal materials from the source to the surface. The amplification depends on average crustal and near surface shear-wave velocity and density (Boore, 1986).

The P(f) filter is used in an attempt to model the observation that acceleration spectral density appears to fall off rapidly beyond some region- or site-dependent maximum frequency (Hanks, 1982; Silva and Darragh, 1995). This observed phenomenon truncates the high frequency portion of the spectrum and is responsible for the band-limited nature of the stochastic model. The band limits are the source corner frequency at low frequency and the high frequency spectral attenuation. This spectral fall-off at high frequency has been attributed to near-site attenuation (Hanks, 1982; Anderson and Hough, 1984) or to source processes (Papageorgiou and Aki, 1983) or perhaps to both effects. In the Anderson and Hough (1984) attenuation model, adopted here, the form of the P(f) filter is taken as

$$P(f, r) = e^{-p?(r)f} \qquad \text{(A-4).}$$

Kappa (r) (?(r) in Equation A-4) is a site and distance dependent parameter that represents the effect of intrinsic attenuation upon the wavefield as it propagates through the crust from source to receiver. Kappa (r) depends on epicentral distance (r) and on both the shear-wave velocity (ß) and quality factor (Q_S) averaged over a depth of H beneath the site (Hough et al., 1988). At zero epicentral distance kappa (?) is given by

$$k(0) = \frac{H}{\bar{b}\ \overline{QSUBS}} \qquad \text{(A-5)},$$

and is referred to as ?.

The bar in Equation A-5 represents an average of these quantities over a depth H. The value of kappa at zero epicentral distance is attributed to attenuation in the very shallow crust directly below the site (Hough and Anderson, 1988; Silva and Darragh, 1995). The intrinsic attenuation along this part of the path is not thought to be frequency dependent and is modeled as a frequency independent, but site and crustal region dependent, constant value of kappa (Hough et al., 1988; Rovelli et al., 1988). This zero epicentral distance kappa is the model implemented in this study.

The crustal path attenuation from the source to just below the site is modeled with the frequency-dependent quality factor Q(f). Thus the distance component of the original ?(r) (Equation A-4) is accommodated by Q(f) and R in the last term of Equation A-1:

$$k(r) = \frac{H}{\bar{b}\ \overline{QSUBS}} + \frac{R}{b_0 Q(f)} \qquad \text{(A-6)}.$$

The Fourier amplitude spectrum, a(f), given by Equation A-1 represents the stochastic ground motion model employing a Brune source spectrum that is characterized by a single corner frequency. It is a point source and models direct shear-waves in a homogeneous half-space (with effects of a velocity gradient captured by the A(f) filter, Equation A-1). For horizontal motions, vertically propagating shear-waves are assumed. Validations using incident inclined SH-waves accompanied with raytracing to find appropriate incidence angles leaving the source showed little reduction in uncertainty compared to results using vertically propagating shear-waves. For vertical motions, P/SV propagators are used coupled with raytracing to model incident inclined plane waves (EPRI, 1993). This approach has been validated with recordings from the 1989 **M** 6.9 Loma Prieta earthquake (EPRI, 1993).

Equation A-1 represents an elegant ground motion model that accommodates source and wave propagation physics as well as propagation path and site effects with an attractive simplicity. The model is appropriate for an engineering characterization of ground motion since it captures the general features of strong ground motion in terms of peak acceleration and spectral composition with a minimum of free parameters (Boore, 1983; McGuire et al., 1984; Boore, 1986; Silva and

Green, 1988; Silva et al., 1988; Schneider et al., 1993; Silva and Darragh, 1995). An additional important aspect of the stochastic model employing a simple source description is that the region-dependent parameters may be evaluated by observations of small local or regional earthquakes. Region-specific seismic hazard evaluations can then be made for areas with sparse strong motion data with relatively simple spectral analyses of weak motion (Silva, 1992).

In order to compute peak time-domain values, i.e. peak acceleration and oscillator response, RVT is used to relate RMS computations to peak value estimates. Boore (1983) and Boore and Joyner (1984) present an excellent development of the RVT methodology as applied to the stochastic ground motion model. The procedure involves computing the RMS value by integrating the power spectrum from zero frequency to the Nyquist frequency and applying Parsevall's relation. Extreme value theory is then used to estimate the expected ratio of the peak value to the RMS value of a specified duration of the stochastic time history. The duration is taken as the inverse of the source corner frequency (Boore, 1983).

Factors that affect strong ground motions such as surface topography, finite and propagating seismic sources, laterally varying near-surface velocity and Q gradients, and random inhomogeneities along the propagation path are not included in the model. While some or all of these factors are generally present in any observation of ground motion and may exert controlling influences in some cases, the simple stochastic point-source model appears to be robust in predicting median or average properties of ground motion (Boore 1983, 1986; Schneider et al., 1993; Silva and Stark, 1993). For this reason it represents a powerful predictive and interpretative tool for engineering characterization of strong ground motion.

A.4 FINITE-SOURCE MODEL GROUND MOTION MODEL

In the near-source region of large earthquakes, aspects of a finite-source including rupture propagation, directivity, and source-receiver geometry can be significant and may be incorporated into strong ground motion predictions. To accommodate these effects, a methodology that combines the aspects of finite-earthquake-source modeling techniques (Hartzell, 1978; Irikura 1983) with the stochastic point-source ground motion model has been developed to produce response spectra as well as time histories appropriate for engineering design (Silva et al., 1990; Silva and Stark, 1993; Schneider et al., 1993). The approach is very similar to the empirical Green function methodology introduced by Hartzell (1978) and Irikura (1983). In this case however, the stochastic point-source is substituted for the empirical Green function and peak amplitudes; PGA, PGV, and response spectra (when time histories are not produced) are estimated using random process theory.

Use of the stochastic point-source as a Green function is motivated by its demonstrated success in modeling ground motions in general and strong ground motions in particular (Boore, 1983, 1986; Silva and Stark, 1993; Schneider et al., 1993; Silva and Darragh, 1995) and the desire to have a model that is truly site- and region-specific. The model can accommodate a region specific Q(f), Green function sources of arbitrary moment or stress drop, and site specific kappa values. The necessity for having available regional and site specific recordings or modifying possibly inappropriate empirical Green functions is eliminated.

For the finite-source characterization, a rectangular fault is discretized into NS subfaults of moment M_0^S. The empirical relationship

$$\log (A) = \mathbf{M} - 4.0, \quad A \text{ in } km^2 \qquad (A\text{-}7).$$

is used to assign areas to both the target earthquake (if its rupture surface is not fixed) as well as to the subfaults. This relation results from regressing log area on **M** using the data of Wells and Coppersmith (1994). In the regression, the coefficient on **M** is set to unity which implies a constant static stress drop of about 30 bars (Equation A-9). This is consistent with the general observation of a constant static stress drop for earthquakes based on aftershock locations (Wells and Coppersmith 1994). The static stress drop, defined by Equation A-10, is related to the average slip over the rupture surface as well as rupture area. It is theoretically identical to the stress drop in Equation A-3 which defines the omega-square source corner frequency assuming the rupture surface is a circular crack model (Brune, 1970; 1971). The stress drop determined by the source corner frequency (or source duration) is usually estimated through the Fourier amplitude spectral density while the static stress drop uses the moment magnitude and an estimate of the rupture area. The two estimates for the same earthquake seldom yield the same values with the static generally being the smaller. In a recent study (Silva et al., 1997), the average stress drop based on Fourier amplitude spectra determined from an empirical attenuation relation (Abrahamson and Silva, 1997) is about 70 bars while the average static stress drop for the crustal earthquakes studied by Wells and Coppersmith (1994) is about 30 bars. These results reflect a general factor of about 2 on average between the two values. These large differences may simply be the result of using an inappropriate estimate of rupture area as the zone of actual slip is difficult to determine unambiguously. In general however, even for individual earthquakes, the two stress drops scale similarly with high static stress drops (> 30 bars) resulting in large high frequency (> 1 Hz for $\mathbf{M} \geq 5$) ground motions which translates to high corner frequencies (Equation A-3).

The subevent magnitude M_S is generally taken in the range of 5.0-6.5 depending upon the size of the target event. M_S 5.0 is used for crustal earthquakes with **M** in the range of 5.5 to 8.0 and M_S 6.4 is used for large subduction earthquakes with **M** > 7.5. The value of NS is determined as the ratio of the target event area to the subfault area. To constrain the proper moment, the total number of events summed (N) is given by the ratio of the target event moment to the subevent moment. The subevent and target event rise times (duration of slip at a point) are determined by the equation

$$\log t = 0.33 \log M_0 - 8.54 \tag{A-8}$$

which results from a fit to the rise times used in the finite-fault modeling exercises, (Silva et al., 1997). Slip on each subfault is assumed to continue for a time t. The ratio of target-to-subevent rise times is given by

$$\frac{t}{t^{s}} = 10^{0.5\,(\mathrm{M} - \mathrm{MSUPs})} \tag{A-9}$$

and determines the number of subevents to sum in each subfault. This approach is generally referred to as the constant-rise-time model and results in variable slip velocity for nonuniform slip distributions. Alternatively, one can assume a constant slip velocity resulting in a variable-rise-time model for heterogeneous slip distributions.

Recent modeling of the Landers (Wald and Heaton, 1994), Kobe (Wald, 1996) and Northridge (Hartzell et al. 1996) earthquakes suggests that a mixture of both constant rise time and constant slip velocity may be present. Longer rise times seem to be associated with areas of larger slip with the ratio of slip-to-rise time (slip velocity) being depth dependent. Lower slip velocities (longer rise times) are associated with shallow slip resulting in relatively less short period seismic radiation. This result may explain the general observation that shallow slip is largely aseismic. The significant contributions to strong ground motions appear to originate at depths exceeding about 4 km (Campbell, 1993; Boore et al., 1994) as the fictitious depth term in empirical attenuation relation (Abrahamson and Silva, 1997; Boore et al., 1997). Finite-fault models generally predict unrealistically large strong ground motions for large shallow (near surface) slip using rise times or slip velocities associated with deeper (> 4 km) zones of slip. This is an important and unresolved issue in finite-fault modeling and the general approach is constrain the slip to relatively small values in the top 2 to 4 km. A more thorough analysis is necessary, ideally using several well validated models, before this issue can be satisfactorily resolved.

To introduce heterogeneity of the earthquake source process into the stochastic finite-fault model, the location of the sub-events within each subfault (Hartzell, 1978) are randomized as well as the subevent rise time. The stress drop of the stochastic point-source Green function is taken as 30 bars, consistent with the static value based on the **M** 5.0 subevent area using the equation

$$\Delta s = \frac{7}{16}\left(\frac{M_e}{R_e^3}\right) \qquad \text{(Brune, 1970, 1971)} \qquad \text{(A-10)}$$

where R_e is the equivalent circular radius of the rectangular sub-event.

Different values of slip are assigned to each subfault as relative weights so that asperities or non-uniform slip can be incorporated into the methodology. For validation exercises, slip models are taken from the literature and are based on inversions of strong motion as well as regional or teleseismic recordings. To produce slip distributions for future earthquakes, random slip models are generated based on a statistical asperity model with parameters calibrated to the published slip distributions. This approach has been validated by comparing the modeling uncertainty and bias estimates for the Loma Prieta and Whittier Narrows earthquakes using motion at each site averaged over several (30) random slip models to the bias and uncertainty estimates using the published slip model. The results show nearly identical bias and uncertainty estimates suggesting that averaging the motions over random slip models produces as accurate a prediction at a site as a single motion computed using the “true” slip model which is determined from inverting actual recordings.

The rupture velocity is taken as depth independent at a value of 0.8 times the shear-wave velocity, generally at the depth of the dominant slip. This value is based on a number of studies of source rupture processes which also suggest that rupture velocity is non-uniform. To capture the effects of non-uniform rupture velocity, a random component (20%) is added. The radiation pattern is computed for each subfault, a random component added, and the RMS applied to the motions computed at the site.

The ground-motion time history at the receiver is computed by summing the contributions from each subfault associated with the closest Green function, transforming to the frequency domain, and convolving with the Green function spectrum (Equation A-1). The locations of the Green functions are generally taken at center of each subfault for small subfaults or at a maximum separation of about 5 to 10 km for large subfaults. As a final step, the individual contributions associated with each Green function are summed in the frequency domain, multiplied by the RMS radiation pattern, and the resultant power spectrum at the site is computed. The appropriate duration used in the RVT computations for PGA, PGV, PGD, and oscillator response is computed by transforming the summed Fourier spectrum into the time domain and computing the 5 to 75% Arias intensity (Ou and Herrmann, 1990).

As with the point-source model, crustal response effects are accommodated through the amplification factor (A(f)) or by using vertically propagating shear waves through a vertically heterogeneous crustal structure. Propagation path damping, through the Q(f) model, is incorporated from each fault element to the site. Near-surface crustal damping is incorporated through the kappa operator (Equation A-1). To model crustal propagation path effects, the raytracing method of Ou and Herrmann (1990) is applied from each subfault to the site.

Time histories may be computed in the process as well by simply adding a phase spectrum appropriate to the subevent earthquake. The phase spectrum can be extracted from a recording made at close distance to an earthquake of a size comparable to that of the subevent (generally **M** 5.0 to 6.5). Interestingly, the phase spectrum need not be from a recording in the region of interest (Silva et al., 1989). A recording in WNA (Western North America) can effectively be used to simulate motions appropriate to ENA (Eastern North America). Transforming the Fourier spectrum computed at the site into the time domain results in a computed time history which then includes all of the aspects of rupture propagation and source finiteness, as well as region specific propagation path and site effects.

For fixed fault size, mechanism, and moment, the specific source parameters for the finite-fault are slip distribution, location of nucleation point, and site azimuth. The propagation path and site parameters remain identical for both the point- and finite-source models.

A.5 INCORPORATION OF SITE EFFECTS

To accommodate the effects of shallow potentially nonlinear materials on the simulated motions, a random vibration theory (RVT) equivalent-linear computational scheme has been incorporated into the point-and finite-source codes. For cases where control motions have been specified, such as a rock site uniform hazard spectrum, spectral matching is done to generate a power spectral density (PSD) whose RVT response spectrum matches the specified target spectrum. The resulting PSD is then used as an outcrop control motion for the soil profile.

A.5.1 Horizontal Motions and Equivalent-Linear Computational Scheme

The computational scheme which has been most widely employed to evaluate one-dimensional site response assumes vertically-propagating plane shear waves. Departures of soil response from a linear constitutive relation are treated in an approximate manner through the use of the equivalent-linear approach.

The equivalent-linear approach, in its present form, was introduced by Seed and Idriss (1970). This scheme is a particular application of the general equivalent-linear theory introduced by Iwan (1967). Basically, the approach is to approximate a second order nonlinear equation, over a limited range of its variables, by a linear equation. Formally this is done in such a way that an average of the difference between the two systems is minimized. This was done in an ad-hoc manner for ground response modeling by defining an effective strain which is assumed to exist for the duration of the excitation. This value is usually taken as 65% of the peak time-domain strain calculated at the midpoint of each layer, using a linear analysis. Modulus and damping curves are then used to define new parameters for each layer based on the effective strain computations. The linear response calculation is repeated, new effective strains evaluated, and iterations performed until the changes in parameters are below some tolerance level. Generally a few iterations are sufficient to achieve a strain-compatible linear solution.

This stepwise analysis procedure was formalized into a one-dimensional, vertically propagating shear-wave code called SHAKE (Schnabel et al., 1972). Subsequently, this code has easily become the most widely used analysis package for one-dimensional site response calculations.

The advantages of the equivalent-linear approach are that parameterization of complex nonlinear soil models is avoided and the mathematical simplicity of linear analysis is preserved.

A truly nonlinear approach requires the specification of the shapes of hysteresis curves and their cyclic dependencies. In the equivalent-linear methodology the soil data are utilized directly and, because at each iteration the problem is linear and the material properties are frequency independent, the damping is rate independent and hysteresis loops close.

While the assumptions of vertically propagating shear waves and equivalent-linear soil response certainly represent approximations to actual conditions, their combination has achieved demonstrated success in modeling observations of site effects (Schnabel et al., 1972; Silva et al., 1988; Schneider et al., 1993; EPRI, 1993, Silva et al., 1997).

A.5.2 RVT Based Computational Scheme

The computational scheme employed to compute the site response uses the stochastic model to generate the power spectral density and spectral acceleration of the rock or control motion. This motion or power spectrum is then propagated through the one-dimensional soil profile using the plane-wave propagators of Silva (1976). In this formulation only SH waves are considered. Arbitrary angles of incidence may be specified but normal incidence is used throughout the present analyses.

In order to treat possible material nonlinearities, an RVT (Random Vibration Theory) based equivalent-linear formulation is employed. Random process theory is used to predict peak time domain values of shear strain based upon the shear strain power spectrum. In this sense the procedure is analogous to the program SHAKE except that peak shear strains in SHAKE are measured in the time domain. The purely frequency domain approach obviates a time domain control motion and, perhaps just as significant, eliminates the need for a suite of analyses based on different input motions. This arises because each time domain analysis may be viewed as one realization of a random process. In this case, several realizations of the random process must be sampled to have a statistically stable estimate of site response. The realizations are usually performed by employing different control motions with approximately the same level of peak acceleration and response spectrum.

In the case of the frequency domain approach, the estimates of peak shear strain as well as oscillator response are, as a result of the random process theory, fundamentally probabilistic in nature. Stable estimates of site response can then be computed by forming the ratio of spectral acceleration predicted at the surface of a soil profile to the spectral acceleration predicted for the control motion.

The procedure of generating the point or finite-source stochastic power spectrum, computing the equivalent-linear layered-soil response, and estimating peak time domain values has been incorporated into a single code termed RASCALS (RASCALFS for finite-fault simulations).

A.5.3 Computational Scheme for Vertical Motions

To model vertical motions, inclined P-SV waves from the stochastic point-source ground motion model (EPRI, 1993) are assumed and the P-SV propagators of Silva (1976) are used to model the crust and soil response to inclined P-SV wavefields. The angle of incidence at the top of the source layer is computed by two-point ray tracing through the crust and soil column (if present) assuming incident inclined compression or SV shear-waves.

To model soil response, a soil column is placed on top of the crustal structure and the incident inclined P-SV wavefield is propagated to the surface where the vertical (or radial) motions are computed.

A.5.4 Treatment of Soil Response for Vertical Motions

Commonly, equivalent-linear site response analyses for vertical motions have used strain iterated shear moduli from a horizontal motion analysis to adjust the compression-wave velocities assuming either a strain independent Poisson's ratio or bulk modulus. Some fraction (generally 30% to 100%) of the strain iterated shear-wave damping is used to model the compression-wave damping and a linear analyses is performed for vertically propagating compression waves using the horizontal control motions scaled by some factor near 2/3.

The equivalent-linear approach implicity assumes some coupling between horizontal and vertical motions. This is necessitated by the lack of well determined M/M_{max} and damping curves for the constrained modulus. Ideally, the strain dependency of the constrained modulus should be determined independently of the shear modulus. Also, the conventional approach assumes vertically-propagating compression waves and not inclined P-SV waves. Additionally, the use of some fraction of the horizontal control motion is an approximation and does not reflect the generally greater high-frequency content of vertical component motions at rock sites due to lower kappa values (EPRI, 1993).

Alternatively, fully nonlinear analyses can be made using two- or three-component control motions (Costantino, 1967; 1969; Li et al., 1992; EPRI, 1993). These nonlinear analyses require two- or three-dimensional soil models which describe plastic flow and yielding and the accompanying volume changes as well as coupling between vertical and horizontal motions through Poisson's effect. While these analyses are important to examine expected dependencies of computed motions on material properties and may have applications to the study of soil compaction, deformation, slope stability, and component coupling, the models are very sophisticated and require specification of many parameters, at least some of which are poorly understood.

In the current implementation of the RVT equivalent-linear approach to estimate vertical and horizontal motions, the horizontal component analyses are performed for vertically propagating shear-waves using the equivalent-linear (RVT) methodology. To compute the vertical motions, a linear analysis is performed for incident inclined P-SV waves using low-strain, compression- and shear-wave velocities derived from the shear- and compression-wave velocity profiles. Compression-wave damping is assumed to be equal to the low strain shear-wave damping (Johnson and Silva, 1981). The horizontal component and vertical component analyses are assumed to be independent.

These approximations, linear analysis for the vertical component and uncoupled vertical and horizontal components, have been checked by comparing results of fully nonlinear analyses at soil sites Gilroy 2 and Treasure Island to recorded vertical and horizontal motions from the 1989 Loma Prieta earthquake (EPRI, 1993). The nonlinear analyses indicate that little coupling exists between the vertical and horizontal motions for the ranges in control motions analyzed (maximum about 0.5g). These assumptions are expected to result in conservative estimates of vertical motions since a higher degree of coupling implies degradation of constrained modulus and an accompanying increase in compression-wave damping.

A.5.5 Incorporation of Site Parameter Variability

To incorporate profile variability (uncertainty and randomness) in terms of velocities, layer thickness, and depth to very stiff materials, motions are computed for 30 to 50 random variations of these parameters.

The profile randomization scheme, which varies both layer velocity and thickness, is based on a correlation model developed from an analysis of variance on about 500 measured shear-wave velocity profiles (EPRI, 1993; Silva et al., 1997). For applications to vertical motions, Poisson's ratio is fixed using the base case compression- and shear-wave velocities. Random compression-wave velocities are then computed from the random suite of shear-wave velocities are the initial Poisson's ratios. The parametric variation which is reflected in fractiles in the computed spectra includes profile velocity and layer thickness variation in addition to variability in the G/Gmax and hysteretic damping curves.

To accommodate variability in the modulus reduction and damping curves on a generic basis, the curves are independently randomized about the base case values. A log normal distribution is assumed with a σ_{ln} of 0.35 at a cyclic shear strain of 3 x 10^{-2}% with upper and lower bounds of 2σ. The distribution is based on an analysis of variance of measured G/G_{max} and hysteretic damping curves and is considered appropriate for applications to generic (material type specific) nonlinear properties. The truncation is necessary to prevent modulus reduction or damping models that are not physically possible. The random curves are generated by sampling the transformed normal distribution with a σ_{ln} of 0.35, computing the change in normalized modulus reduction or percent damping at 3 x 10^{-2}% shear strain, and applying this factor at all strains. The random perturbation factor is reduced or tapered near the ends of the strain range to preserve the general shape of the median curves (Silva, 1992).

A.6 PARTITION AND ASSESSMENT OF GROUND MOTION VARIABILITY

An essential requirement of any numerical modeling approach, particularly one which is implemented in the process of defining design ground motions, is a quantitative assessment of prediction accuracy. A desirable approach to achieving this goal is in a manner which lends itself to characterizing the variability associated with model predictions. For a ground motion model, prediction variability is comprised of two components: modeling variability and parametric variability. Modeling variability is a measure of how well the model works (how accurately it predicts ground motions) when specific parameter values are known. Modeling variability is measured by misfits of model predictions to recorded motions through validation exercises and is due to unaccounted for components in the source, path, and site models (i.e. a point-source cannot model the effects of directivity and linear site response cannot accommodate nonlinear effects). Results from a viable range of values for model parameters (i.e., slip distribution, soil profile, G/G_{max} and hysteretic damping curves, etc). Parametric variability is the sensitivity of a model to a viable range of values for model parameters. The total variability, modeling plus parametric, represents the variance associated with the ground motion prediction and, because it is a necessary component in estimating fractile levels, may be regarded as important as median predictions.

Both the modeling and parametric variabilities may have components of randomness and uncertainty. Table A.1 summarizes the four components of total variability in the context of ground motion predictions. Uncertainty is that portion of both modeling and parametric variability which, in principle, can be reduced as additional information becomes available, whereas randomness represents the intrinsic or irreducible component of variability for a given model or parameter. Randomness is that component of variability which is intrinsic or irreducible <u>for a given model.</u> The uncertainty component reflects a lack of knowledge and may be reduced as more data are analyzed. For example, in the point-source model, stress drop is generally taken to be independent of source mechanism as well as tectonic region and is found to have a standard error of about 0.7 (natural log) for the CEUS (EPRI, 1993). This variation or uncertainty plus randomness in ?s results in a variability in ground motion predictions for future earthquakes. If, for example, it is found that normal faulting earthquakes have generally lower stress drops than strike-slip which are, in turn, lower than reverse mechanism earthquakes, perhaps much of the variability in ?s may be reduced. In extensional regimes, where normal faulting earthquakes are most likely to occur, this new information may provide a reduction in variability (uncertainty component) for stress drop, say to 0.3 or 0.4 resulting in less ground motion variation due to a lack of knowledge of the mean or median stress drop. There is, however, a component of this stress drop variability which can <u>never</u> be reduced in the context of the Brune model. This is simply due to the heterogeneity of the earthquake dynamics which is not accounted for in the model and results in the randomness component of parametric variability in stress drop. A more sophisticated model may be able to accommodate or model more accurately source dynamics but, perhaps, at the expense of a larger number of parameters and increased parametric uncertainty (i.e. the finite-fault with slip model and nucleation point as unknown parameters for future earthquakes). That is, more complex models typically seek to reduce modeling randomness by more closely modeling physical phenomena. However, such models often require more comprehensive sets of observed data to constrain additional model parameters, which generally leads to increased parametric variability. If the increased parametric variability is primarily in the form of uncertainty, it is possible to reduce total variability, but only at the additional expense of constraining the additional parameters. Therefore, existing knowledge and/or available resources may limit the ability of more complex models to reduce total variability.

The distinction of randomness and uncertainty is model driven and somewhat arbitrary. The allocation is only important in the context of probabilistic seismic hazard analyses as uncertainty is treated as alternative hypotheses in logic trees while randomness is integrated over in the hazard calculation (Cornell, 1968). For example, the uncertainty component in stress drop may be treated by using an N-point approximation to the stress drop distribution and assigning a branch in a logic tree for each stress drop and associated weight. A reasonable three point approximation to a normal distribution is given by weights of 0.2, 0.6, 0.2 for expected 5%, mean, and 95% values of stress drop respectively. If the distribution of uncertainty in stress drop was such that the 5%, mean, and 95% values were 50, 100, and 200 bars respectively, the stress drop branch on a logic tree would have 50, and 200 bars with weights of 0.2 and 100 bars with a weight of 0.6. The randomness component in stress drop variability would then be formally integrated over in the hazard calculation.

A.6.1 Assessment of Modeling Variability

Modeling variability (uncertainty plus randomness) is usually evaluated by comparing response spectra computed from recordings to predicted spectra and is a direct assessment of model accuracy. The modeling variability is defined as the standard error of the residuals of the log of the average horizontal component (or vertical component) response spectra. The residual is defined as the difference of the logarithms of the observed average 5% damped acceleration response spectra and the predicted response spectra. At each period, the residuals are squared, and summed over the total number of sites for one or all earthquakes modeled. Dividing the resultant sum by the number of sites results in an estimate of the model variance. Any model bias (average offset) that exists may be estimated in the process (Abrahamson et al., 1990; EPRI, 1993) and used to correct (lower) the variance (and to adjust the median as well). In this approach, the modeling variability can be separated into randomness and uncertainty where the bias corrected variability represents randomness and the total variability represents randomness plus uncertainty. The uncertainty is captured in the model bias as this may be reduced in the future by refining the model. The remaining variability (randomness) remains irreducible for this model. In computing the variance and bias estimates only the frequency range between processing filters at each site (minimum of the 2 components) should be used.

A.6.2 Assessment of Parametric Variability

Parametric variability, or the variation in ground motion predictions due to uncertainty and randomness in model parameters is difficult to assess. Formally, it is straight-forward in that a Monte Carlo approach may be used with each parameter randomly sampled about its mean (median) value either individually for sensitivity analyses (Silva, 1992; Roblee et al., 1996) or in combination to estimate the total parametric variability (Silva, 1992; EPRI, 1993). In reality, however, there are two complicating factors.

The first factor involves the specific parameters kept fixed with all earthquakes, paths, and sites when computing the modeling variability. These parameters are then implicitly included in modeling variability provided the data sample a sufficiently wide range in source, path, and site conditions. The parameters which are varied during the assessment of modeling variation should have a degree of uncertainty and randomness associated with them for the next earthquake. Any ground motion prediction should then have a variation reflecting this lack of knowledge and randomness in the free parameters.

An important adjunct to fixed and free parameters is the issue of parameters which may vary but by fixed rules. For example, source rise time (Equation A-8) is magnitude dependent and in the stochastic finite-source model is specified by an empirical relation. In evaluating the modeling variability with different magnitude earthquakes, rise time is varied, but because it follows a strict rule, any variability associated with rise time variation is counted in modeling variability. This is strictly true only if the sample of earthquakes has adequately spanned the space of magnitude, source mechanism, and other factors which may affect rise time. Also, the earthquake to be modeled must be within that validation space. As a result, the validation or assessment of model variation should be done on as large a number of earthquakes of varying sizes and mechanisms as possible.

The second, more obvious factor in assessing parametric variability is a knowledge of the appropriate distributions for the parameters (assuming correct values for median or mean estimates are known). In general, for the stochastic models, median parameter values and uncertainties are based, to the extent possible, on evaluating the parameters derived from previous earthquakes (Silva, 1992; EPRI, 1993).

The parametric variability is site, path, and source dependent and must be evaluated for each modeling application (Roblee et al., 1996). For example, at large source-to-site distances, crustal path damping may control short-period motions. At close distances to a large fault, both the site and finite-source (asperity location and nucleation point) may dominate, and, depending upon site characteristics, the source or site may control different frequency ranges (Silva, 1992;

Roblee et al., 1996). Additionally, level of control motion may affect the relative importance of G/G_{max} and hysteretic damping curves.

In combining modeling and parametric variations, independence is assumed (covariance is zero) and the variances are simply added to give the total variability.

$$_{ln}s^{2}_{?} = {}_{ln}s^{2}_{?} + {}_{ln}s^{2}_{P} \quad \text{(A-11),}$$

where

$_{ln}s^{2}_{?}$ = modeling variation,

$_{ln}s^{2}_{P}$ = parametric variation.

A.7 VALIDATION OF THE POINT- AND FINITE-SOURCE MODELS

In a recent Department of Energy sponsored project (Silva et al., 1997), both the point- and finite-source stochastic models were validated in a systematic and comprehensive manner. In this project, 16 well recorded earthquakes were modeled at about 500 sites. Magnitudes ranged from **M** 5.3 to **M** 7.4 with fault distances from about 1 km out to 218 km for WUS earthquakes and 460 km for CEUS earthquakes. This range in magnitude and distance as well as number of earthquakes and sites results in the most comprehensively validated model currently available to simulate strong ground motions.

A unique aspect of this validation is that rock and soil sites were modeled using generic rock and soil profiles and equivalent-linear site response. Validations done with other simulation procedures typically neglect site conditions as well as nonlinearity resulting in ambiguity in interpretation of the simulated motions.

A.7.1 Point-Source Model

Final model bias and variability estimates for the point-source model are shown in Figure A1. Over all the sites (Figure A1) the bias is slightly positive for frequencies greater than about 10 Hz and is near zero from about 10 Hz to 1 Hz. Below 1 Hz, a stable point-source overprediction is reflected in the negative bias. The analyses are considered reliable down to about 0.3 Hz (3.3 sec) where the point-source shows about a 40% overprediction.

The model variability is low, about 0.5 above about 3 to 4 Hz and increases with decreasing frequency to near 1 at 0.3 Hz. Above 1 Hz, there is little difference between the total variability (uncertainty plus randomness) and randomness (bias corrected variability) reflecting the near zero bias estimates. Below 1 Hz there is considerable uncertainty contributing to the total variability suggesting that the model can be measurably improved as its predictions tend to be consistently high at very low frequencies (# 1 Hz). This stable misfit may be interpreted as the presence of a second corner frequency for WNA sources (Atkinson and Silva, 1997).

A.7.2 Finite-Source Model

For the finite-fault, Figure A2 shows the corresponding bias and variability estimates. For all the sites, the finite-source model provides slightly smaller bias estimates and, surprisingly, slightly higher variability for frequencies exceeding about 5 Hz. The low frequency (# 1 Hz) point-source overprediction is not present in the finite-source results, indicating that it is giving more accurate predictions than the point-source model over a broad frequency range, from about 0.3 Hz (the lowest frequency of reliable analyses) to the highest frequency of the analyses.

In general, for frequencies of about 1 Hz and above the point-source and finite-source give comparable results: the bias estimates are small (near zero) and the variabilities range from about 0.5 to 0.6. These estimates are low considering the analyses are based on a data set comprised of earthquakes with **M** less than **M** 6.5 (288 of 513 sites) and high frequency ground motion variance decreases with increasing magnitude, particularly above **M** 6.5 (Youngs et al., 1995) Additionally, for the vast majority of sites, generic site conditions were used (inversion kappa values were used for only the Saguenay and Nahanni earthquake analyses, 25 rock sites). As a result, the model variability (mean = 0) contains the total uncertainty and randomness contribution for the site. The parametric variability due to uncertainty and randomness in site parameters: shear-wave velocity, profile depth, G/G_{max} and hysteretic damping curves need not be added to the model variability estimates. It is useful to perform parametric variations to assess site parameter sensitivities on the ground motions, but only source and path damping Q(f) parametric variabilities require assessment on a site specific basis and added to the model variability. The source uncertainty and randomness components include point-source stress drop and finite-source slip model and nucleation point variations (Silva, 1992).

A.7.3 Empirical Attenuation Model

As an additional assessment of the stochastic models, bias and variability estimates were made over the same earthquakes (except Saguenay since it was not used in the regressions) and sites using a recently develop empirical attenuation relation (Abrahamson and Silva, 1997). For all the sites, the estimates are shown in Figure A3. Interestingly, the point-source overprediction below about 1 Hz is present in the empirical relation perhaps suggesting that this suite of earthquakes possess lower than expected motions in this frequency range as the empirical model does not show this bias over all earthquakes (. 50) used in its development. Comparing these results to the point- and finite-source results (Figures A1 and A2) show comparable bias and variability estimates. For future predictions, source and path damping parametric variability must be added to the numerical simulations which will contribute a s_{ln} of about 0.2 to 0.4, depending upon frequency, source and path conditions, and site location. This will raise the modeling variability from about 0.50 to the range of 0.54 to 0.64, about 10 to 30%. These values are still comparable to the variability of the empirical relation indicating that the point- and finite-source numerical models perform about as well as a recently developed empirical attenuation relation for the validation earthquakes and sites.

These results are very encouraging and provide an additional qualitative validation of the point- and finite-source models. Parenthetically this approach provides a rational basis for evaluating empirical attenuation models.

A.8 REFERENCES

Abrahamson, N.A. and W.J. Silva (1997). "Empirical response spectral attenuation relations for shallow crustal earthquakes." *Seismological Research Let.*, 68(1), 94-127.

Abrahamson, N.A., P.G. Somerville, and C.A. Cornell (1990). "Uncertainty in numerical strong motion predictions" *Proc. Fourth U.S. Nat. Conf. Earth. Engin.*, Palm Springs, CA., 1, 407-416.

Aki, K. and P.G. Richards. (1980). *"Quantitative siesmology."* W. H. Freeman and Co., San Francisco, California.

Atkinson, G.M and W.J. Silva (1997). "An empirical study of earthquake source spectra for California earthquakes." *Bull. Seism. Soc. Am.* 87(1), 97-113.

Anderson, J.G. and S.E. Hough (1984). "A Model for the Shape of the Fourier Amplitude Spectrum of Acceleration at High Frequencies." *Bulletin of the Seismological Society of America*, 74(5), 1969-1993.

Atkinson, G.M. (1984). "Attenuation of strong ground motion in Canada from a random vibrations approach." *Bull. Seism. Soc. Am.*, 74(5), 2629-2653.

Boore, D.M., W.B. Joyner, and T.E. Fumal (1997). "Equations for estimating horizontal response spectra and peak acceleration from Western North American earthquakes: A summary of recent work." *Seism. Res. Lett.* 68(1), 128-153.

Boore, D.M., W.B. Joyner, and T.E. Fumal (1994). "Estimation of response spectra and peak accelerations from western North American earthquakes: and interim report. Part 2. *U.S. Geological Survey Open-File Rept.* 94-127.

Boore, D.M., and G.M. Atkinson (1987). "Stochastic prediction of ground motion and spectral response parameters at hard-rock sites in eastern North America." *Bull. Seism. Soc. Am.*, 77(2), 440-467.

Boore, D.M. (1986). "Short-period P- and S-wave radiation from large earthquakes: implications for spectral scaling relations." *Bull. Seism. Soc. Am.*, 76(1) 43-64.

Boore, D.M. and W.B. Joyner (1984). "A note on the use of random vibration theory to predict peak amplitudes of transient signals." *Bull. Seism. Soc. Am.*, 74, 2035-2039.

Boore, D.M. (1983). "Stochastic simulation of high-frequency ground motions based on seismological models of the radiated spectra." *Bull. Seism. Soc. Am.*, 73(6), 1865-1894.

Brune, J.N. (1971). "Correction." *J. Geophys. Res.* 76, 5002.

Brune, J.N. (1970). "Tectonic stress and the spectra of seismic shear waves from earthquakes." *J. Geophys. Res.* 75, 4997-5009.

Campbell, K.W. (1993) "Empirical prediction of near-source ground motion from large earthquakes." in V.K. Gaur, ed., Proceedings, Intern'l Workshop on Earthquake Hazard and Large Dams in the Himalya. INTACH, New Delhi, p. 93-103.

Cornell, C.A. (1968). "Engineering seismic risk analysis." *Bull. Seism. Soc. Am.*, 58, 1583-1606.

Costantino, C.J. (1969). "Two dimensional wave propagation through nonlinear media." J. Compt. Physics, vol. 4.

Costantino, C.J. (1967). "Finite element approach to wave propagation problems." J. Engin. Mechanics Div., vol. 93.

Electric Power Research Institute (1993). "Guidelines for determining design basis ground motions." Palo Alto, Calif: Electric Power Research Institute, vol. 1-5, EPRI TR-102293.
vol. 1: Methodology and guidelines for estimating earthquake ground motion in eastern North America.
vol. 2: Appendices for ground motion estimation.
vol. 3: Appendices for field investigations.
vol. 4: Appendices for laboratory investigations.
vol. 5: Quantification of seismic source effects.

Hanks, T.C. (1982). "f_{max}." *Bull. Seism. Soc. Am.,* 72, 1867-1879.

Hanks, T.C. and R.K. McGuire (1981). "The character of high-frequency strong ground motion." *Bull. Seism. Soc. Am.*, 71(6), 2071-2095.

Hanks, T.C. and H. Kanamori (1979). "A moment magnitude scale." *J. Geophys. Res.,*84, 2348-2350.

Hartzell, S., A. Leeds, A. Frankel, and J. Michael (1996). "Site response for urban Los Angeles using aftershocks of the Northridge earthquake." *Bull. Seism. Soc. Am.,* 86(1B), S168-S192.

Hartzell, S.H. (1978). "Earthquake aftershocks as Green's functions." *Geophys. Res. Letters,* 5, 1-4.

Hough, S.E., J.G. Anderson, J. Brune, F. Vernon III, J. Berger, J. Fletcher, L. Haar, T. Hanks, and L. Baker (1988). "Attenuation near Anza, California." *Bull. Seism. Soc. Am.*, 78(2), 672-691.

Hough, S.E. and J.G. Anderson (1988). "High-Frequency Spectra Observed at Anza, California: Implications for Q Structure." *Bull. Seism. Soc. Am.*, 78(2), 692-707.

Irikura, K. (1983). “Semi-empirical estimation of strong ground motions during large earthquakes.” *Bull. Disaster Prevention* R*es. Inst*., Kyoto Univ., 33, 63-104.

Iwan, W.D. (1967). “On a class of models for the yielding behavior of continuous and composite systems.” *J. Appl. Mech.,* 34, 612-617.

Johnson, L.R., and Silva, W. (1981). “The effects of unconsolidated sediments upon the ground motion during local earthquakes.” *Bull. Seism. Soc. Am.*, 71, 127-142.

Li, X.S., Z.L. Wang, C.K. Shen (1992). ASUMDES: A nonlinear procedure for response analysis of horizontally-layered sites subjected to multi-directional earthquake loading.@ Dept. of Civil Engi. Univ. of Calif., Davis.

McGuire, R. K., A.M. Becker, and N.C. Donovan (1984). “Spectral Estimates of Seismic Shear Waves.” *Bull. Seism. Soc. Am.*, 74(4), 1427-1440.

Ou, G.B. and R.B. Herrmann (1990). “Estimation theory for strong ground motion.” *Seism.*Res. Letters. 61.

Papageorgiou, A.S. and K. Aki (1983). “A specific barrier model for the quantitative description of inhomogeneous faulting and the prediction of strong ground motion, part I, Description of the model.” *Bull. Seism. Soc. Am.*, 73(4), 693-722.

Roblee, C.J., W.J. Silva, G.R. Toro and N. Abrahamson (1996). “Variability in site-specific seismic ground-motion design predictions.” in press.

Rovelli, A., O. Bonamassa, M. Cocco, M. Di Bona, and S. Mazza (1988). “Scaling laws and spectral parameters of the ground motion in active extensional areas in Italy.” *Bull. Seism. Soc. Am.*, 78(2), 530-560.

Schnabel, P.B., Lysmer, J., and Seed, H.B. (1972). *SHAKE: a Computer Program for Earthquake Response Analysis of Horizontally Layered Sites.* Earthq. Engin. Res. Center, Univ. of Calif. at Berkeley, EERC 72-12.

Schneider, J.F., W.J. Silva, and C.L. Stark (1993). “Ground motion model for the 1989 **M** 6.9 Loma Prieta earthquake including effects of source, path and site.” *Earthquake Spectra,* 9(2), 251-287.

Seed, H.B. and I.M. Idriss (1970). “Soil moduli and damping factors for dynamic response *analyses.”* Earthq. Eng. Res. Center, Univ. of Calif. at Berkeley, Report No. UCB/EERC-70/10.

Silva, W.J., N. Abrahamson, G. Toro, and C. Costantino (1997). “Description and validation of the stochastic ground motion model.” Submitted to Brookhaven National Laboratory, Associated Universities, Inc. Upton, New York.

Silva, W.J. and R. Darragh (1995). "Engineering characterization of earthquake strong ground motion recorded at rock sites." Palo Alto, Calif:Electric Power Research Institute, TR-102261.

Silva, W.J. and C.L. Stark (1993) "Source, path, and site ground motion model for the 1989 **M** 6.9 Loma Prieta earthquake." CDMG draft final report.

Silva, W.J. (1992). "Factors controlling strong ground motions and their associated uncertainties." Dynamic Analysis and Design Considerations for High Level Nuclear Waste Repositories, ASCE 132-161.

Silva, W.J. (1991). "Global characteristics and site geometry." Chapter 6 in *Proceedings:* NSF/EPRI Workshop on Dynamic Soil Properties and Site Characterization. Palo Alto, Calif.: Electric Power Research Institute, NP-7337.

Silva, W. J., R. Darragh, C. Stark, I. Wong, J. C. Stepp, J. Schneider, and S-J. Chiou (1990). "A Methodology to Estimate Design Response Spectra in the Near-Source Region of Large Earthquakes Using the Band-Limited-White-Noise Ground Motion Model". *Procee. of the Fourth U.S. Conf. on Earthquake Engineering,* Palm Springs, California. 1, 487-494.

Silva, W.J., R.B. Darragh, R.K. Green and F.T. Turcotte (1989). *Estimated Ground Motions for a new madrid Event.* U.S. Army Engineer Waterways Experiment Station, Wash., DC, Misc. Paper GL-89-17.

Silva, W. J. and R. K. Green (1988). "Magnitude and Distance Scaling of Response Spectral Shapes for Rock Sites with Applications to North American Environments." In *Proceedings: Workshop on Estimation of Ground Motion in the Eastern United States*, EPRI NP-5875, Electric Power Research Institute.

Silva, W. J., T. Turcotte, and Y. Moriwaki (1988). "Soil Response to Earthquake Ground Motion," Electric Power Research Institute, Walnut Creek, California, Report No. NP-5747.

Silva, W.J. and K. Lee (1987). *"WES RASCAL code for synthesizing earthquake ground motions.*" State-of-the-Art for Assessing Earthquake Hazards in the United States, Report 24, U.S. Army Engineers Waterways Experiment Station, Miscellaneous Paper S-73-1.

Silva, W.J. (1976). "Body Waves in a Layered Anelastic solid." *Bull. Seis. Soc. Am.*, vol. 66(5), 1539-1554.

Somerville, P.G., R. Graves and C. Saikia (1995). "TECHNICAL REPORT: Characterization of ground motions during the Northridge earthquake of January 17, 1994." *Structural Engineers Association of California (SEAOC).* Report No. SAC-95-03.

Toro, G. R. and R. K. McGuire (1987). "An Investigation into Earthquake Ground Motion Characteristics in Eastern North America." *Bull. Seism. Soc. Am.*, 77(2), 468-489.

Toro, G. R. (1985). “Stochastic Model Estimates of Strong Ground Motion.” In *Seismic Hazard Methodology for Nuclear Facilities in the Eastern United States*, Appendix B, R. K. McGuire, ed., Electric Power Research Institute, Project P101-29.

Wald, D.J. (1996). “Slip history of the 1995 Kobe, Japan, earthquake determined from strong motion, teleseismic, and geodetic data.” *J. of Physics of the Earth*, in press.

Wald, D.J. and T.H. Heaton (1994). “Spatial and temporal distribution of slip for the 1992 Landers, California, earthquake.” *Bull. Seism. Soc. Amer.*, 84(3), 668-691.

Wells, D.L. and K.J. Coppersmith (1994). “New empirical relationships among magnitude, rupture length, rupture width, rupture area, and surface displacement.” *Bull. Seism. Soc. Am.* 84(4), 974-1002.

Youngs, R.R., N.A. Abrahamson, F. Makdisi, and K. Sadigh (1995). “Magnitude dependent dispersion in peak ground acceleration.” *Bull. Seism. Soc. Amer.*, 85(1), 161-1, 176.

TABLE A.1
CONTRIBUTIONS TO TOTAL VARIABILITY
IN GROUND MOTION MODELS

	Modeling Variability	Parametric Variability
Uncertainty *(also Epistemic Uncertainty)*	Modeling Uncertainty: Variability in predicted motions resulting from particular model assumptions, simplifications and/or fixed parameter values. *Can be reduced by adjusting or "calibrating" model to better fit observed earthquake response.*	Parametric Uncertainty: Variability in predicted motions resulting from incomplete data needed to characterize parameters. *Can be reduced by collection of additional information which better constrains parameters*
Randomness *(also Aleatory Uncertainty)*	Modeling Randomness: Variability in predicted motions resulting from discrepancies between model and actual complex physical processes. *Cannot be reduced for a given model form.*	Parametric Randomness: Variability in predicted motions resulting from inherent randomness of parameter values. *Cannot be reduced a priori*[**] *by collection of additional information.*

[**]Some parameters (e.g. source characteristics) may be well defined after an earthquakes.

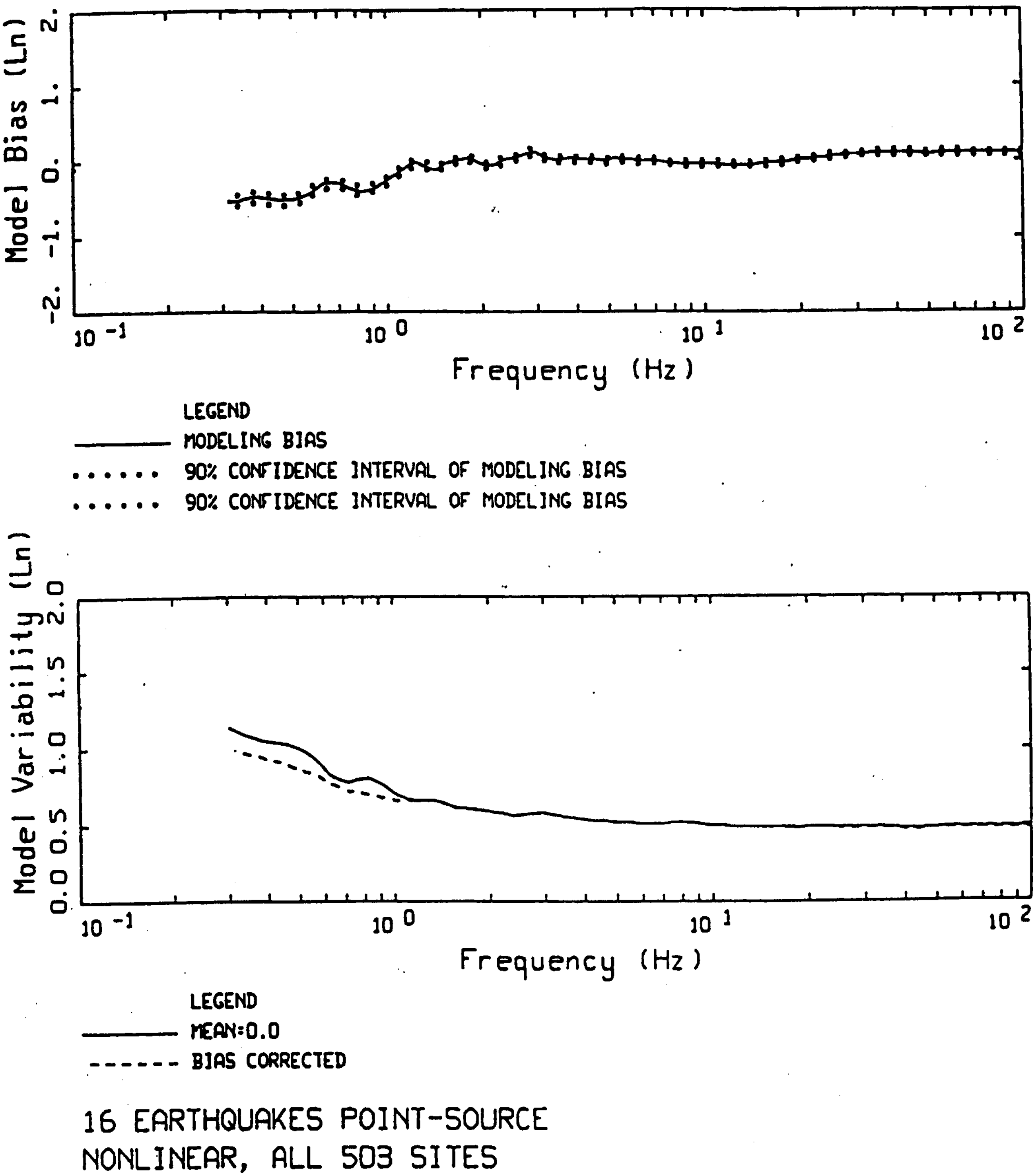

Figure A1. Model bias and variability estimates for all earthquakes computed over all 503 sites for the point-source model.

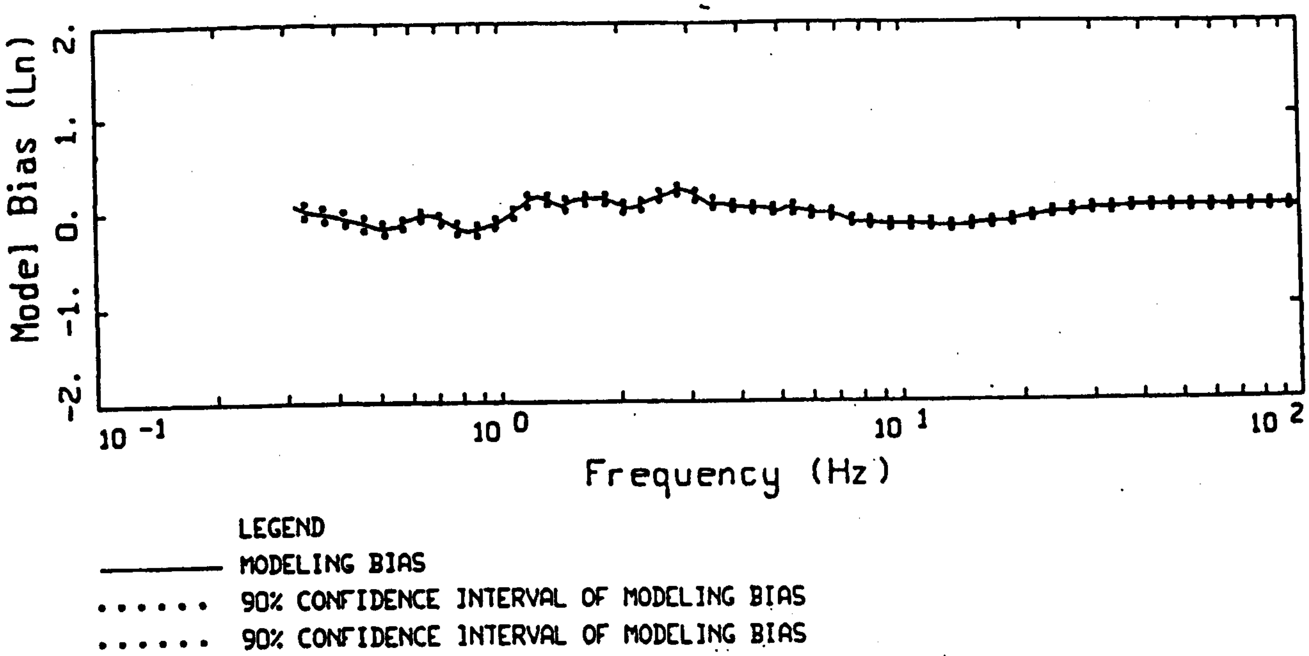

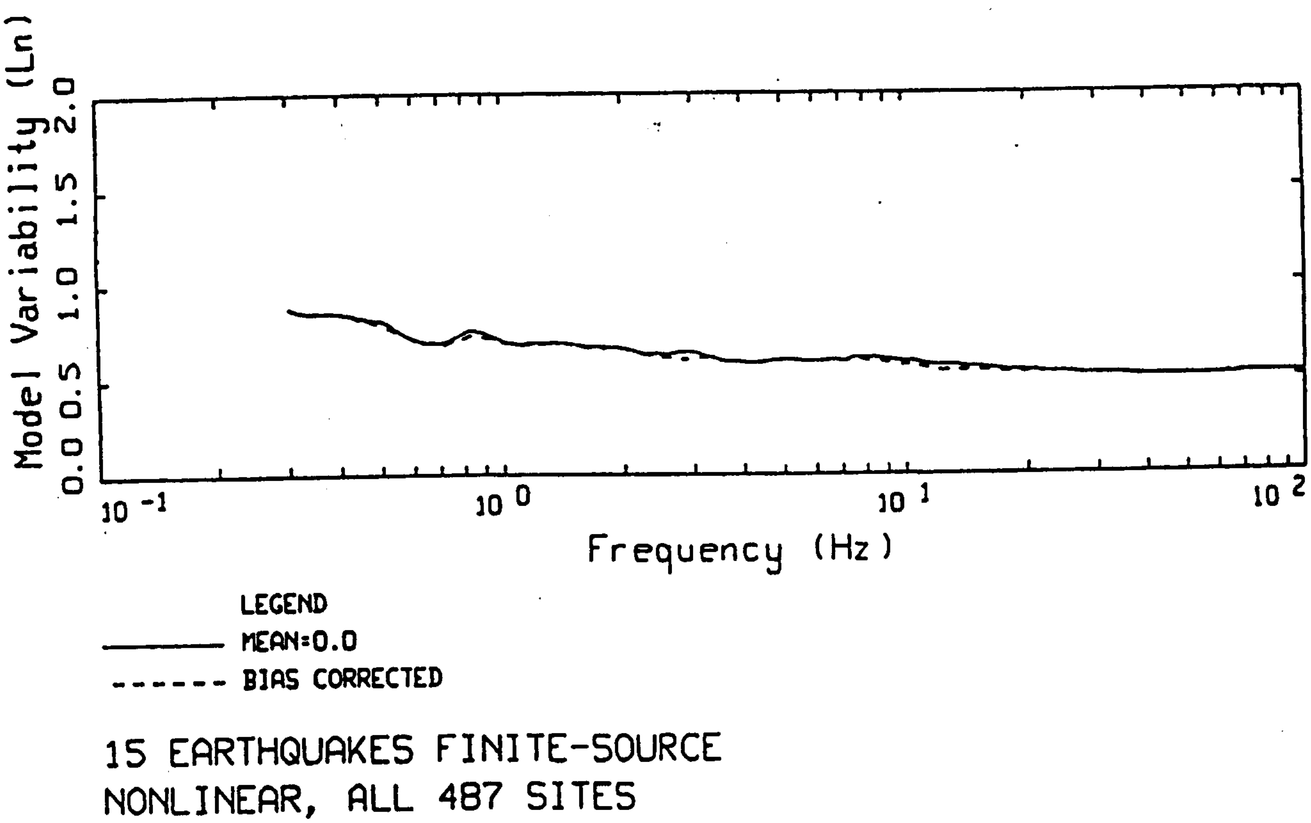

Figure A2. Model bias and variability estimates for all earthquakes computed over all 487 sites for the finite-source model.

APPENDIX B

GROUND MOTION TIME HISTORIES AND SPECTRA

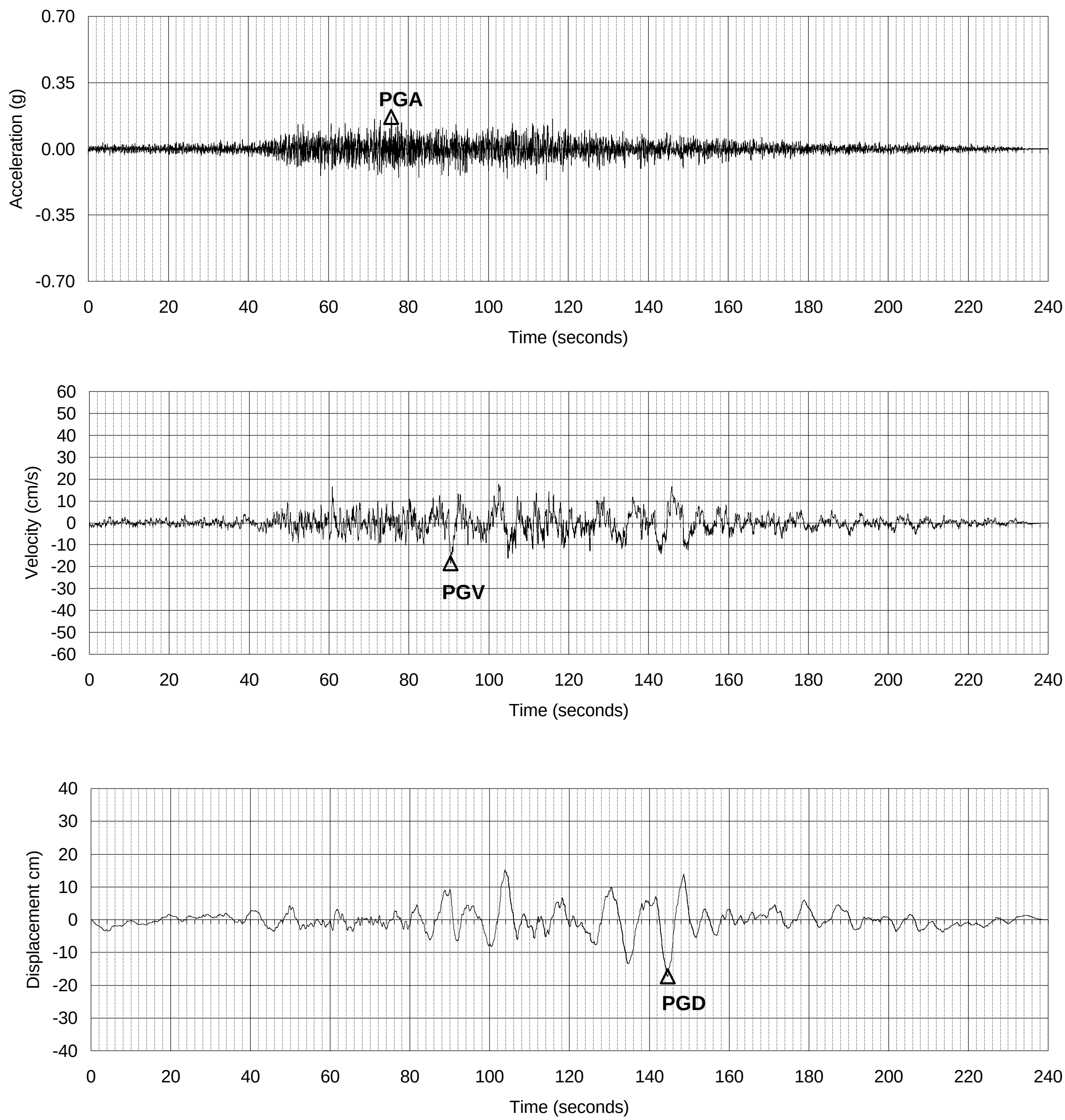

Peak Ground Motions

Acceleration	0.17 g
Velocity	18.56 cm/s
Displacement	17.32 cm

Seismic Ground Motion Study
Skookumchuck Dam
Lewis County, Washingtion

CSZ MEDIAN MCE
SYNTHETIC TIME HISTORY
HORIZONTAL 1

March 2001 21-1-08920-001

SHANNON & WILSON, INC.
Geotechnical and Environmental Consultants

FIG. B-1

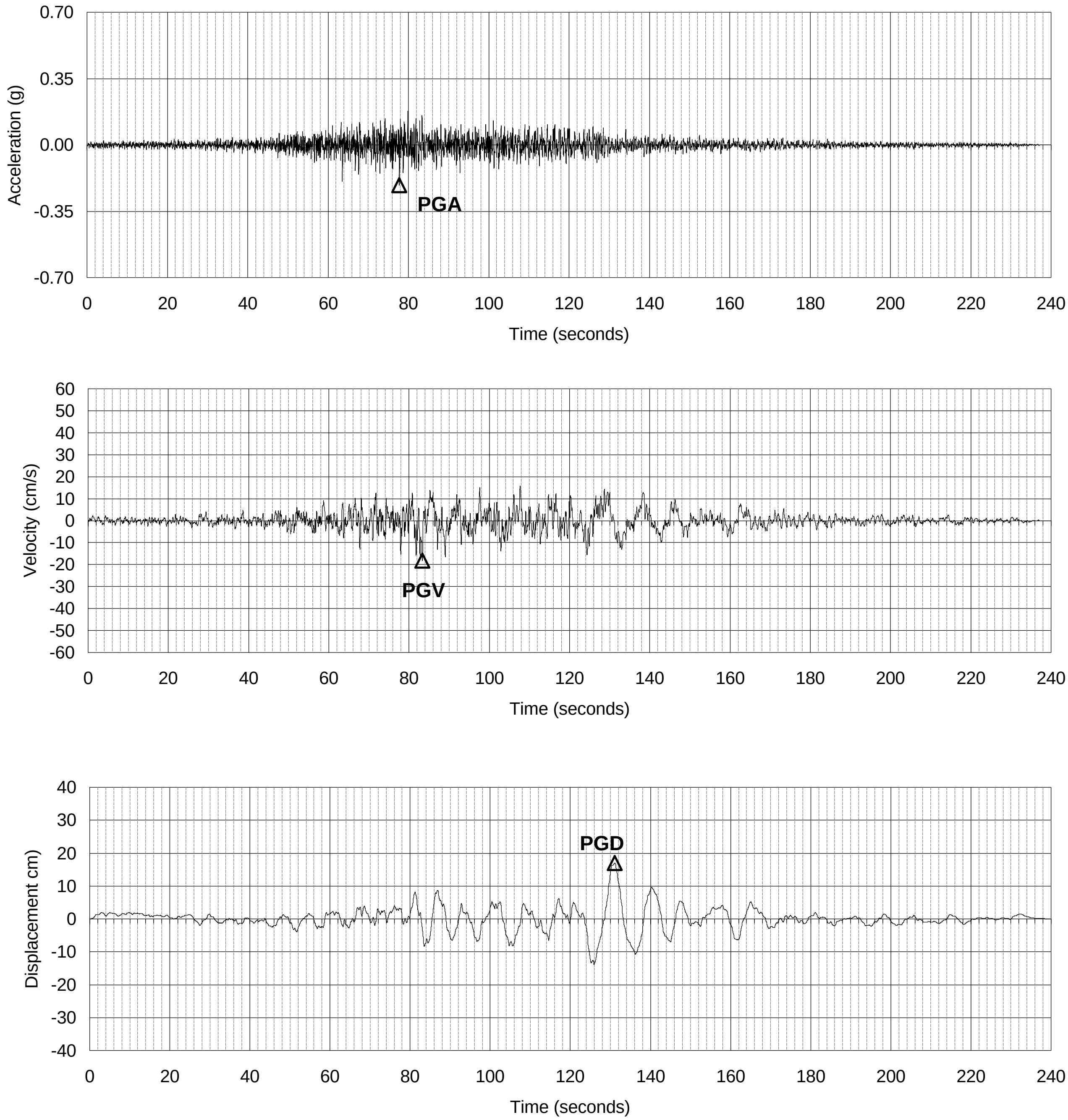

Peak Ground Motions

Acceleration	0.21 g
Velocity	18.13 cm/s
Displacement	16.95 cm

Seismic Ground Motion Study
Skookumchuck Dam
Lewis County, Washingtion

CSZ MEDIAN MCE
SYNTHETIC TIME HISTORY
HORIZONTAL 2

March 2001 21-1-08920-001

SHANNON & WILSON, INC.
Geotechnical and Environmental Consultants

FIG. B-2

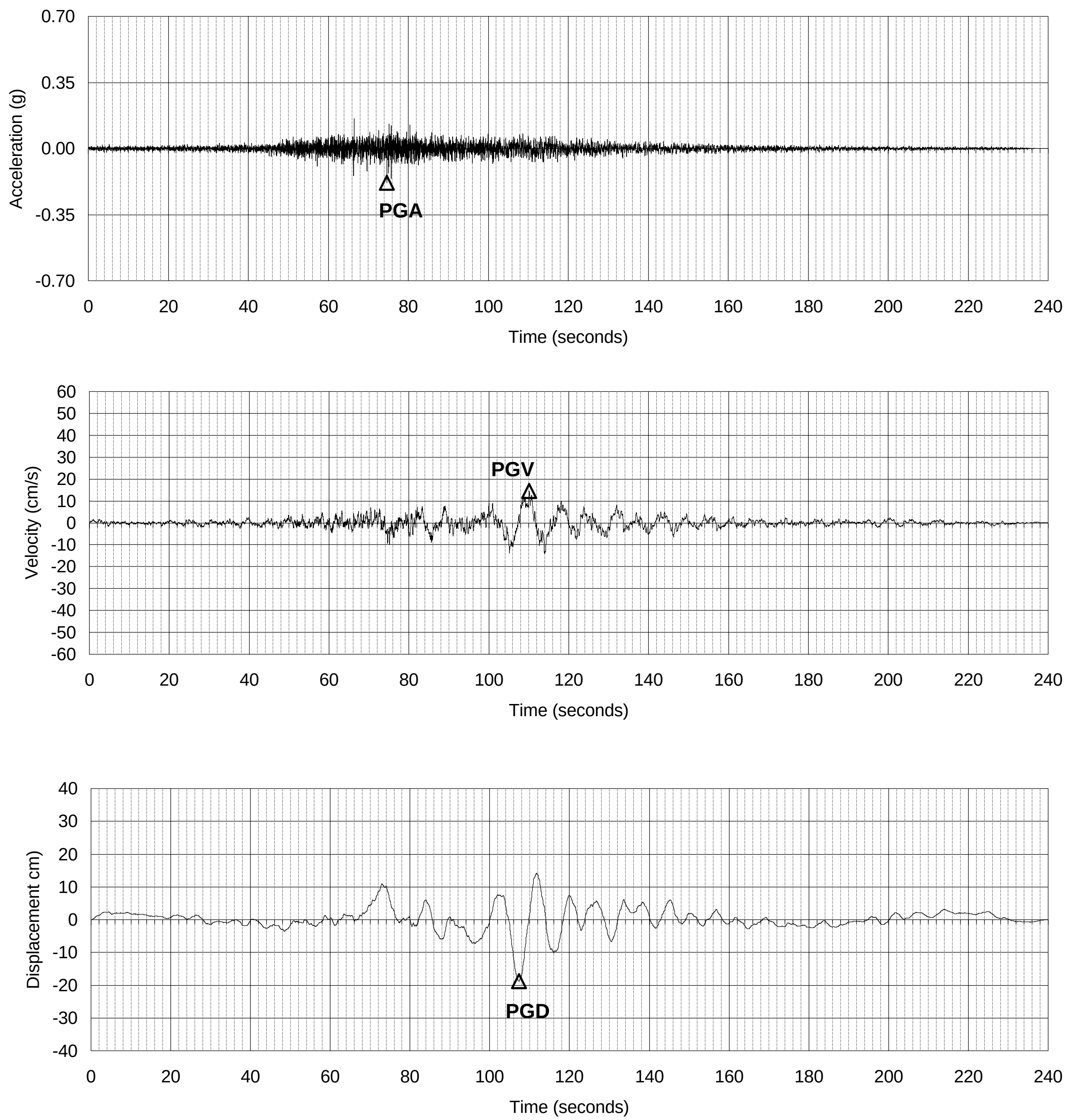

Peak Ground Motions

Acceleration	0.18 g
Velocity	14.59 cm/s
Displacement	18.78 cm

Seismic Ground Motion Study
Skookumchuck Dam
Lewis County, Washingtion

CSZ MEDIAN MCE
SYNTHETIC TIME HISTORY
VERTICAL

March 2001 21-1-08920-001

SHANNON & WILSON, INC.
Geotechnical and Environmental Consultants

FIG. B-3

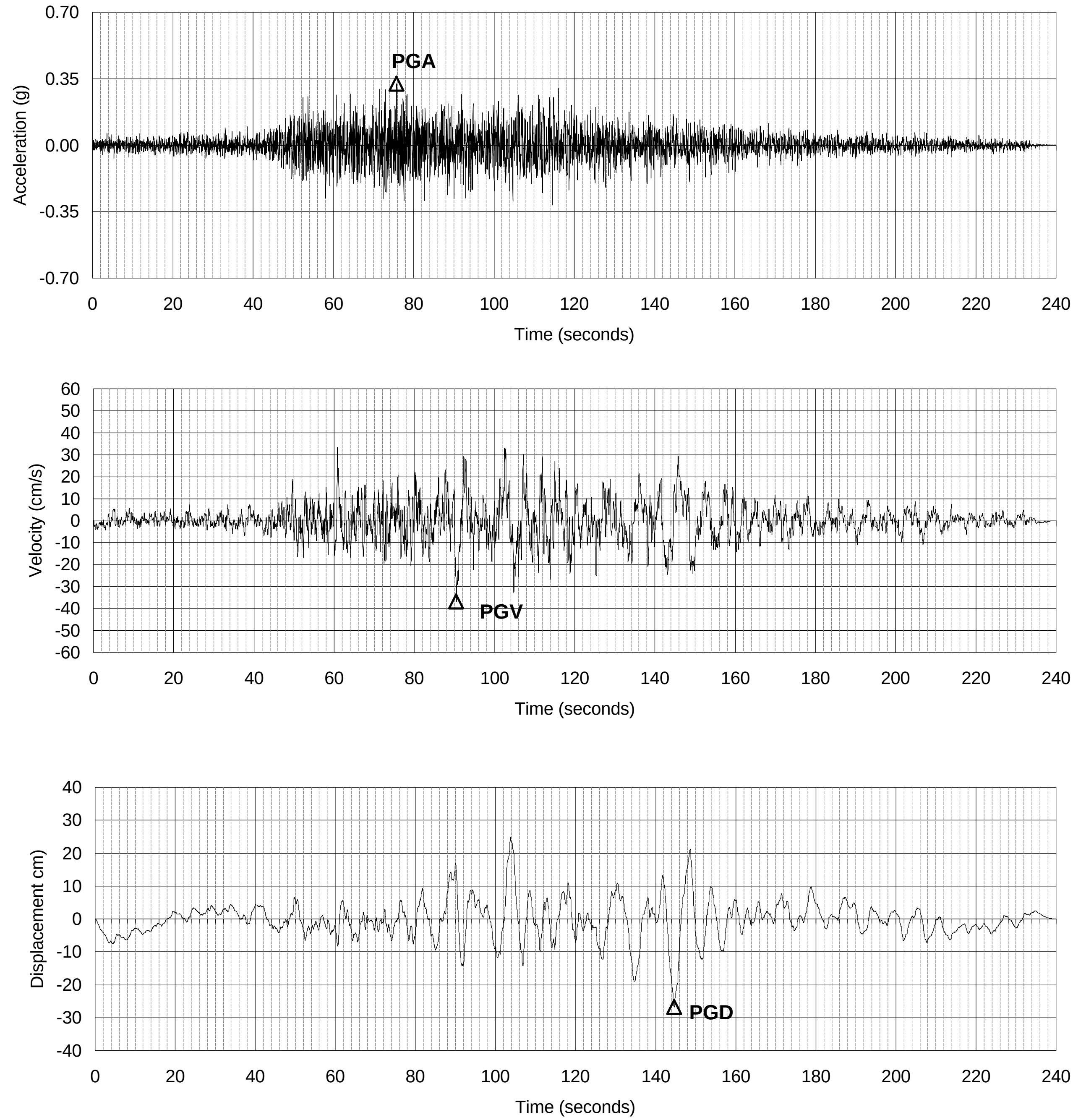

Peak Ground Motions

Acceleration	0.32 g
Velocity	36.80 cm/s
Displacement	26.85 cm

Seismic Ground Motion Study
Skookumchuck Dam
Lewis County, Washingtion

CSZ MEDIAN + 1s MCE
SYNTHETIC TIME HISTORY
HORIZONTAL 1

March 2001 21-1-08920-001

SHANNON & WILSON, INC.
Geotechnical and Environmental Consultants

FIG. B-4

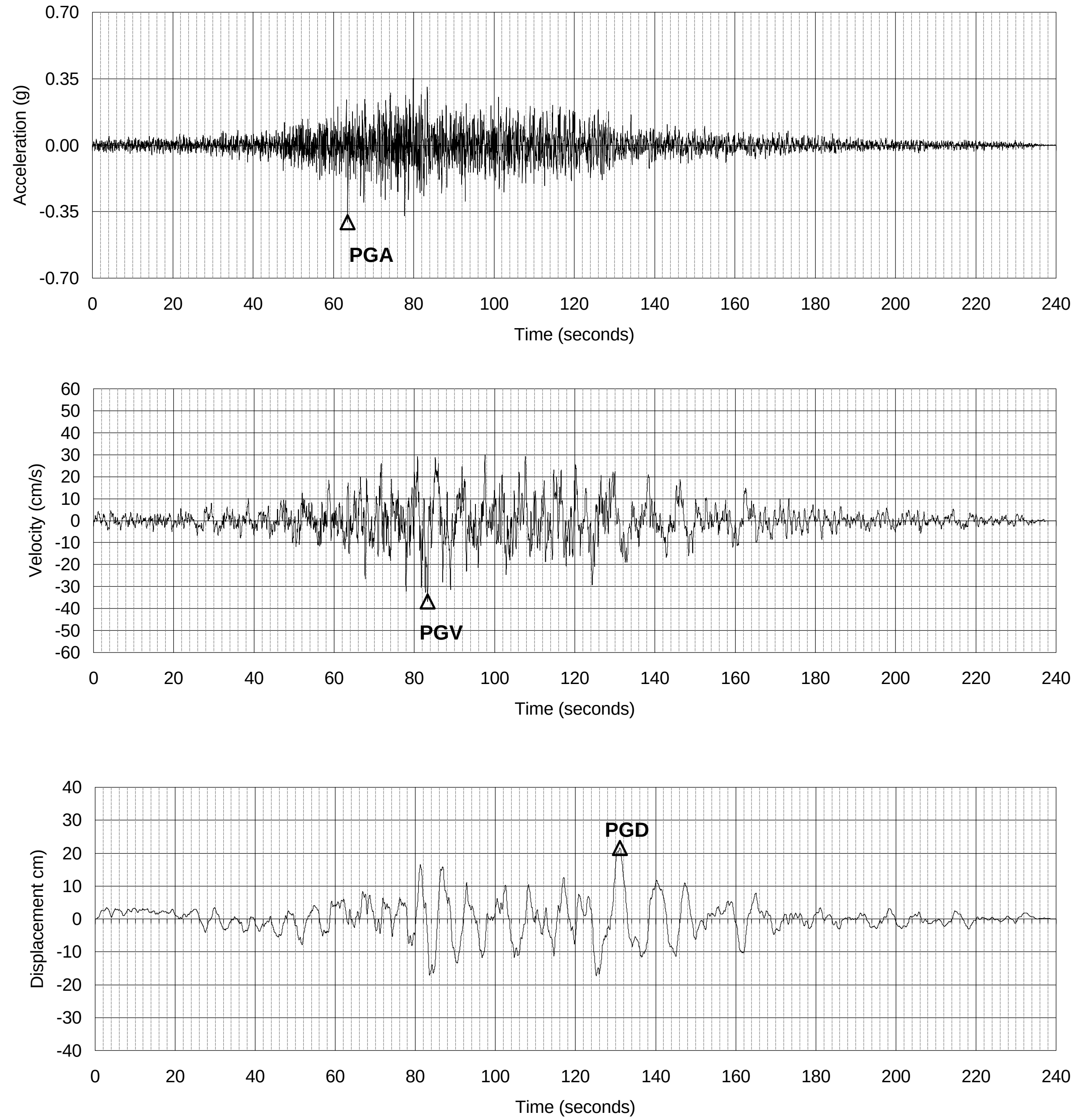

Peak Ground Motions

Acceleration	0.41 g
Velocity	36.90 cm/s
Displacement	21.50 cm

Seismic Ground Motion Study
Skookumchuck Dam
Lewis County, Washingtion

CSZ MEDIAN + 1s MCE
SYNTHETIC TIME HISTORY
HORIZONTAL 2

March 2001 21-1-08920-001

SHANNON & WILSON, INC.
Geotechnical and Environmental Consultants

FIG. B-5

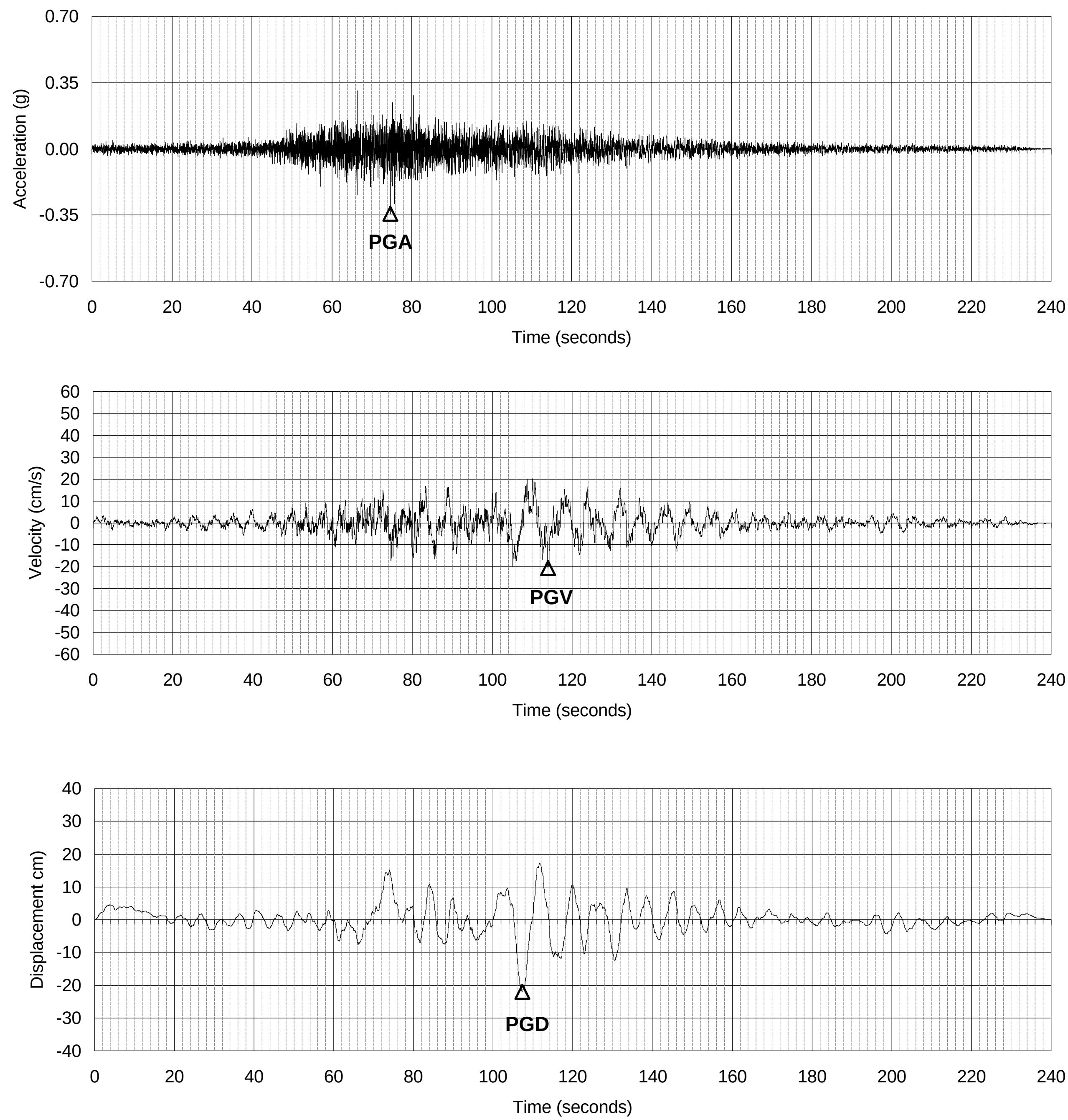

Peak Ground Motions

Acceleration	0.35 g
Velocity	20.71 cm/s
Displacement	22.11 cm

Seismic Ground Motion Study
Skookumchuck Dam
Lewis County, Washingtion

CSZ MEDIAN + 1s MCE
SYNTHETIC TIME HISTORY
VERTICAL

March 2001 21-1-08920-001

SHANNON & WILSON, INC.
Geotechnical and Environmental Consultants

FIG. B-6

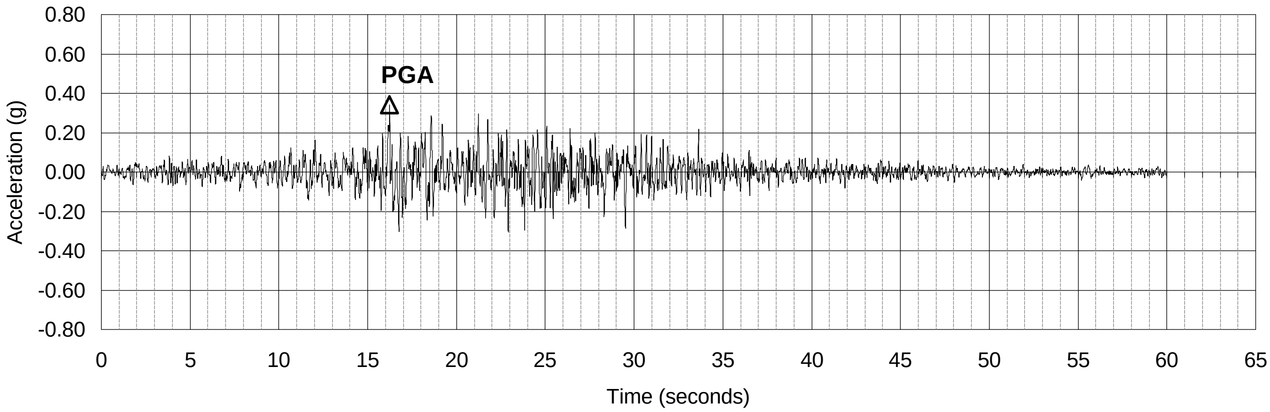

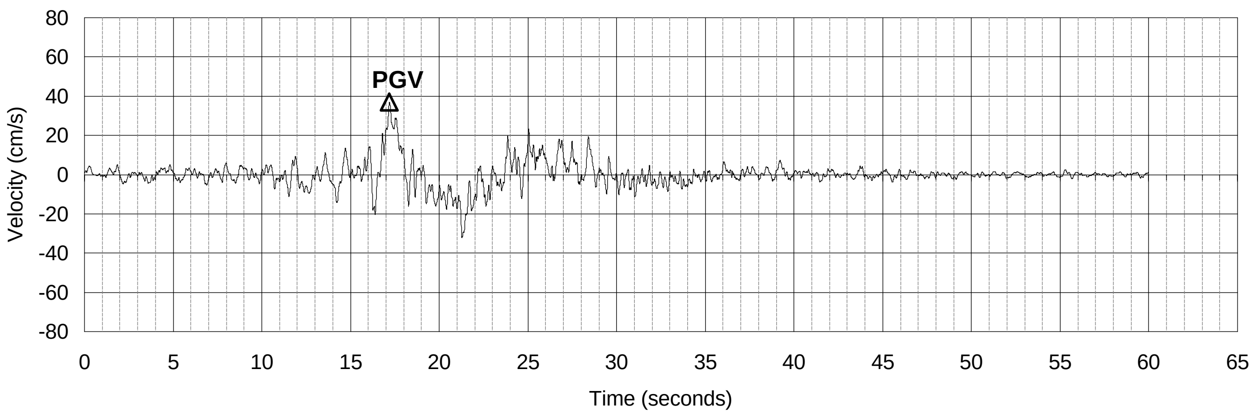

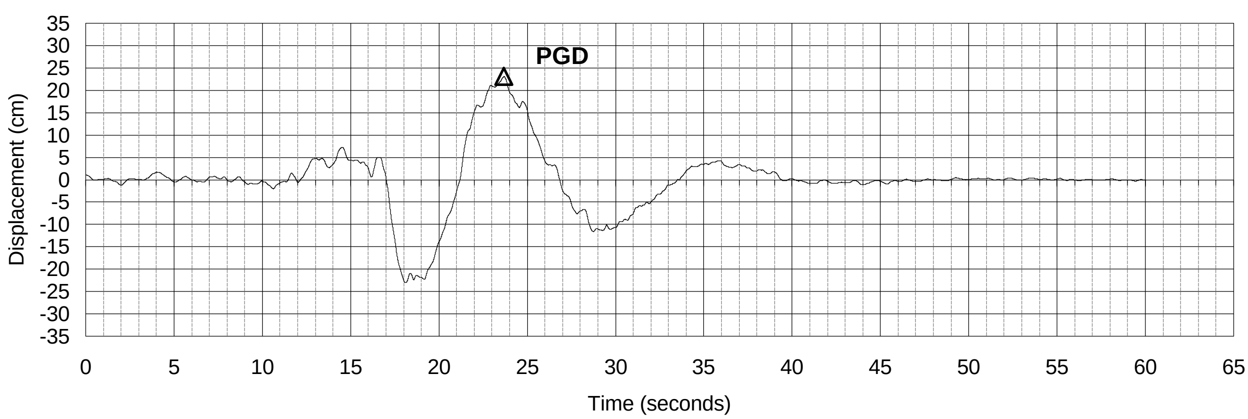

Peak Ground Motions

Acceleration	0.34 g
Velocity	36.86 cm/s
Displacement	23.07 cm

Seismic Ground Motion Study
Skookumchuck Dam
Lewis County, Washington

LF MEDIAN MCE
SYNTHETIC TIME HISTORY
HORIZONTAL 1

March 2001 21-1-08920-001

SHANNON & WILSON, INC.
Geotechnical and Environmental Consultants

FIG. B-7

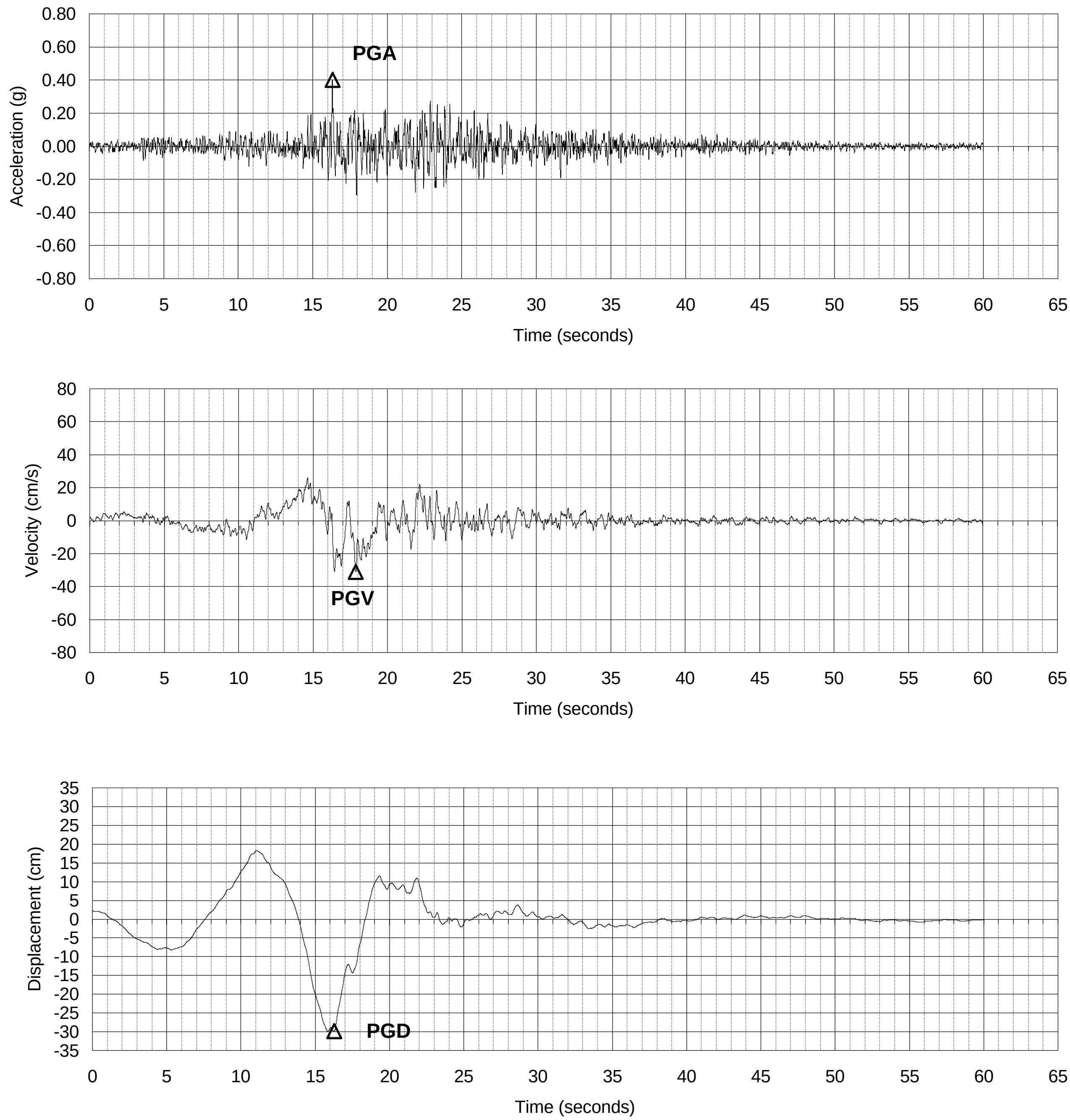

Peak Ground Motions

Acceleration	0.40 g
Velocity	31.14 cm/s
Displacement	29.89 cm

Seismic Ground Motion Study
Skookumchuck Dam
Lewis County, Washington

LF MEDIAN MCE
SYNTHETIC TIME HISTORY
HORIZONTAL 2

March 2001 21-1-08920-001

SHANNON & WILSON, INC.
Geotechnical and Environmental Consultants

FIG. B-8

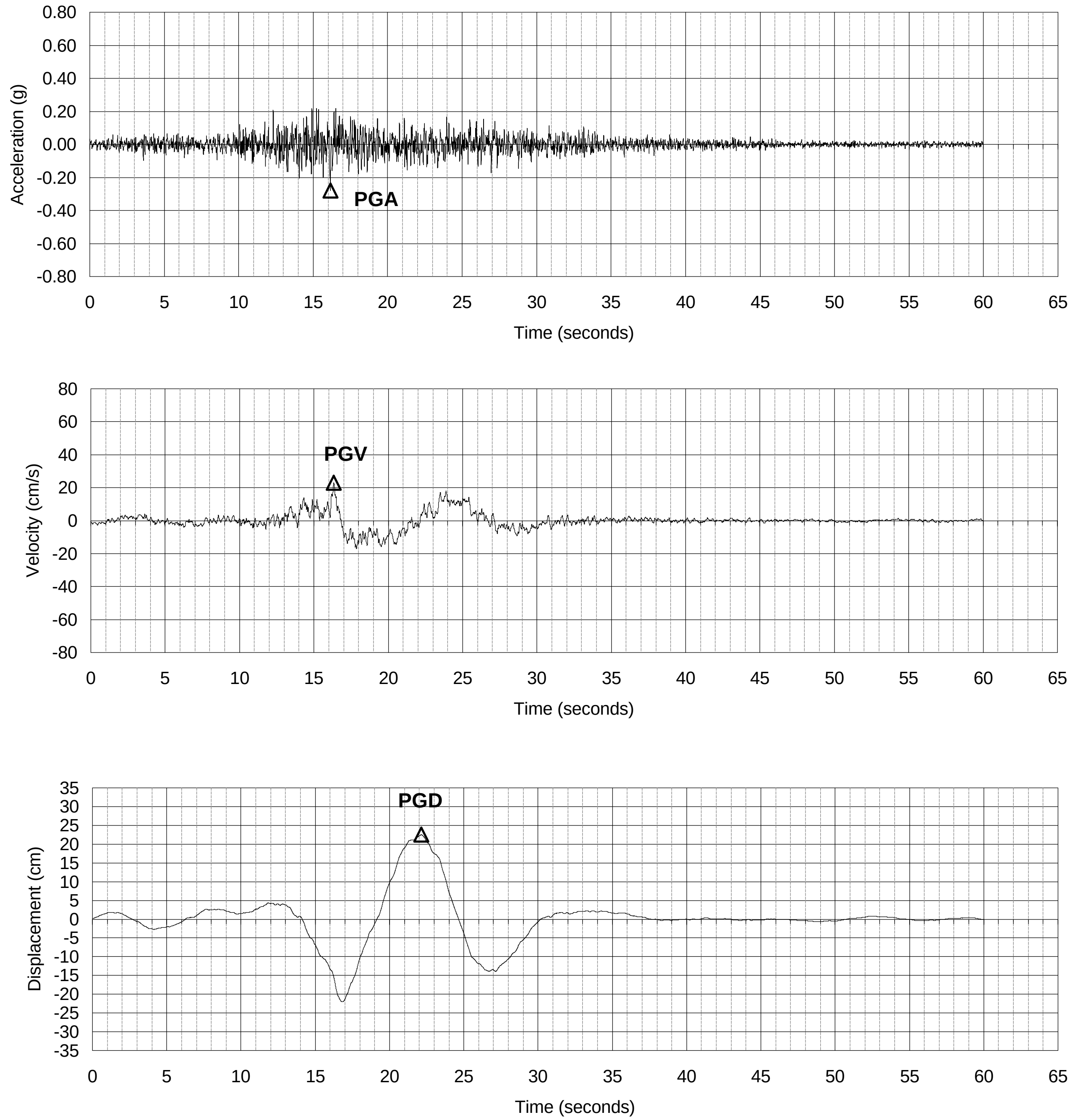

Peak Ground Motions

Acceleration	0.28 g
Velocity	22.83 cm/s
Displacement	22.52 cm

Seismic Ground Motion Study
Skookumchuck Dam
Lewis County, Washington

LF MEDIAN MCE
SYNTHETIC TIME HISTORY
VERTICAL

March 2001 21-1-08920-001

SHANNON & WILSON, INC.
Geotechnical and Environmental Consultants

FIG. B-9

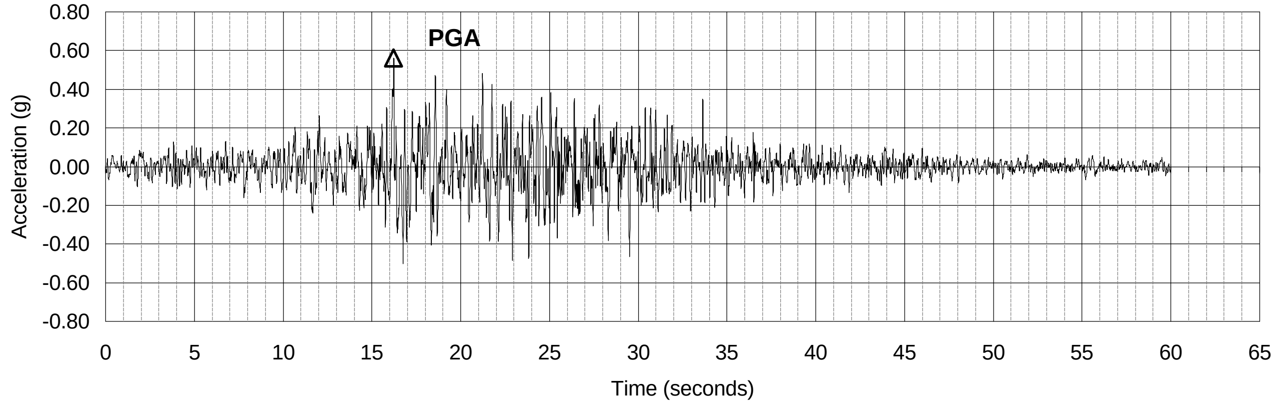

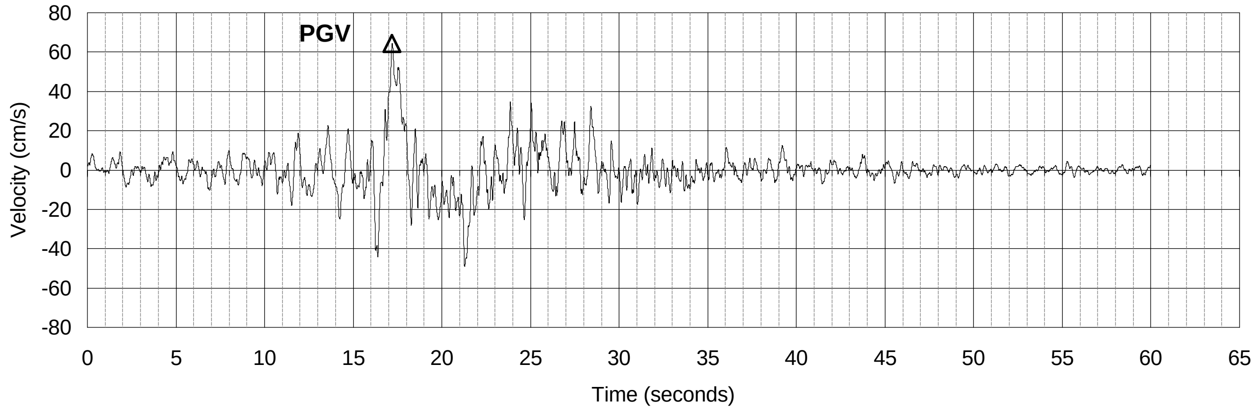

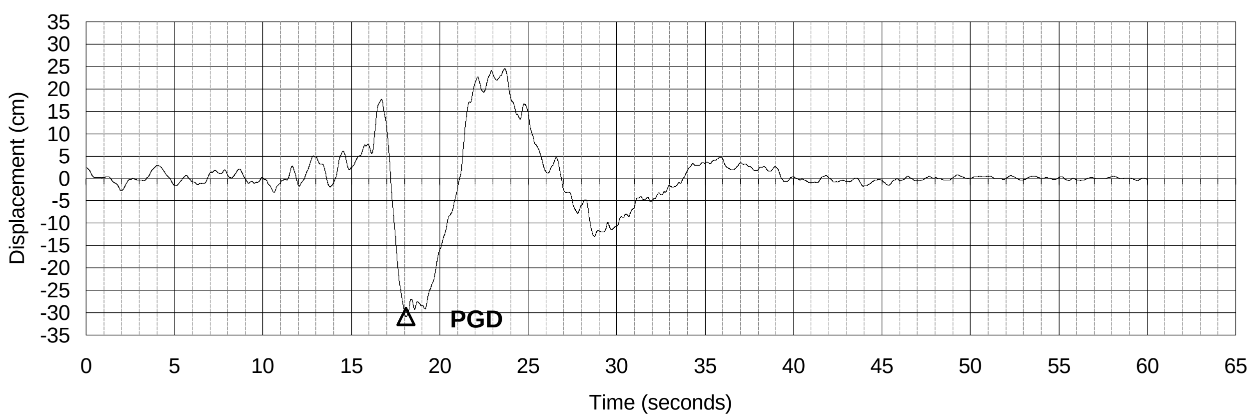

Peak Ground Motions

Acceleration	0.56 g
Velocity	64.43 cm/s
Displacement	30.86 cm

Seismic Ground Motion Study
Skookumchuck Dam
Lewis County, Washington

LF MEDIAN + 1s MCE
SYNTHETIC TIME HISTORY
HORIZONTAL 1

March 2001 21-1-08920-001

SHANNON & WILSON, INC.
Geotechnical and Environmental Consultants

FIG. B-10

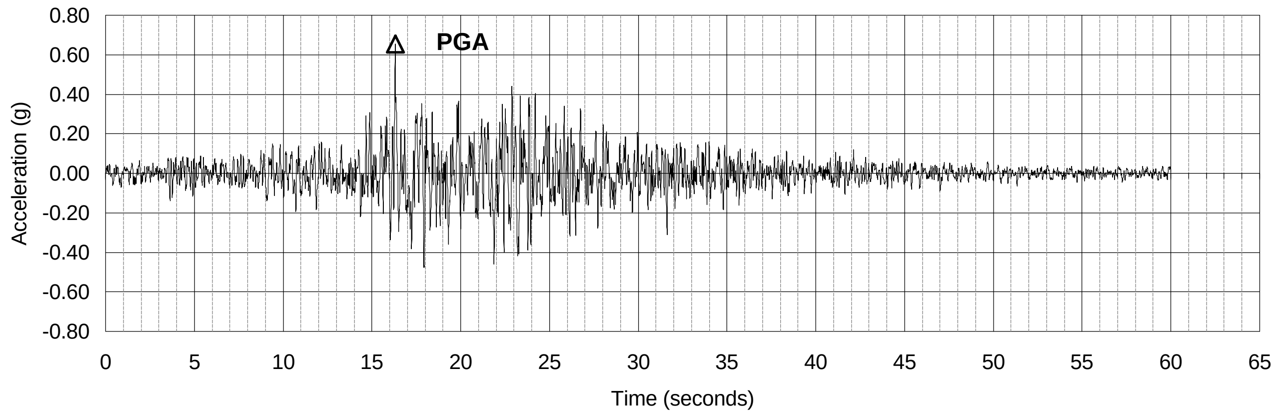

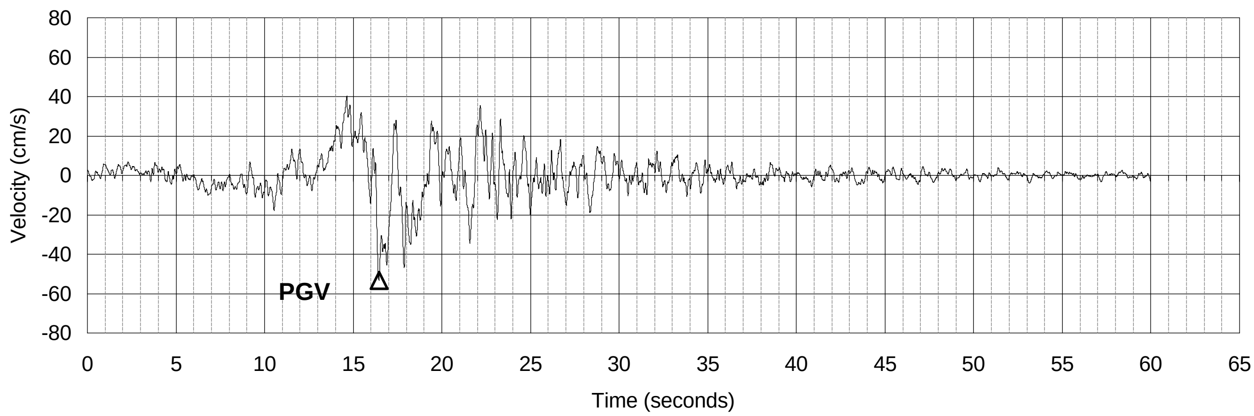

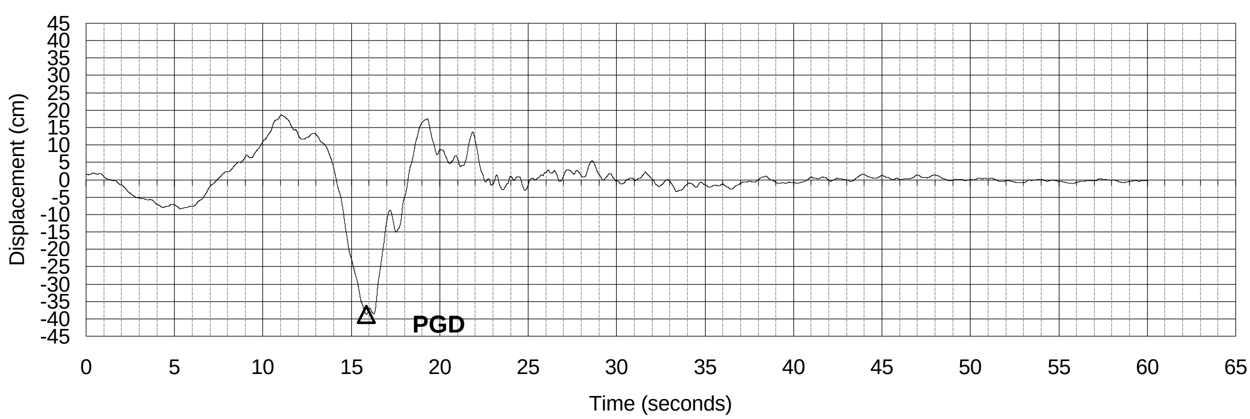

Peak Ground Motions

Acceleration	0.65 g
Velocity	53.18 cm/s
Displacement	38.71 cm

Seismic Ground Motion Study
Skookumchuck Dam
Lewis County, Washington

LF MEDIAN + 1s MCE
SYNTHETIC TIME HISTORY
HORIZONTAL 2

March 2001 21-1-08920-001

SHANNON & WILSON, INC.
Geotechnical and Environmental Consultants

FIG. B-11

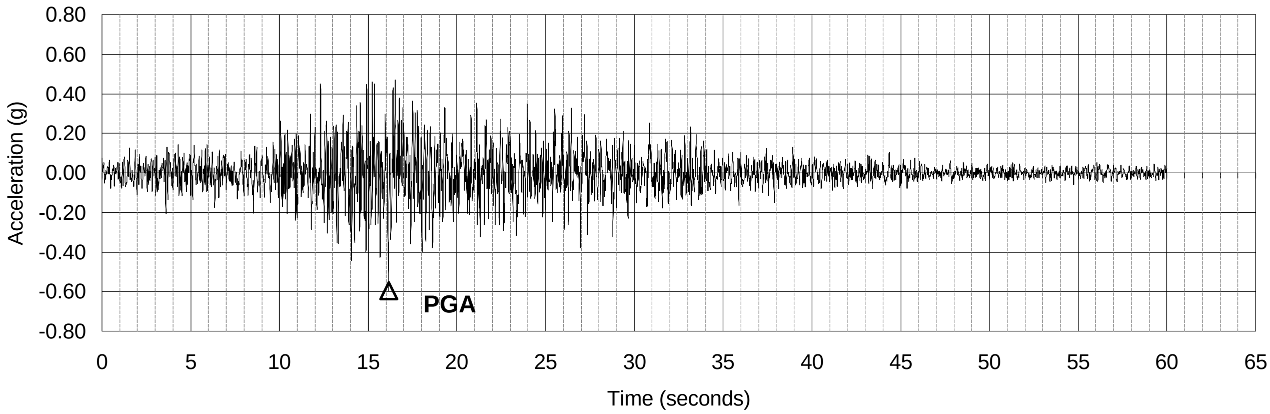

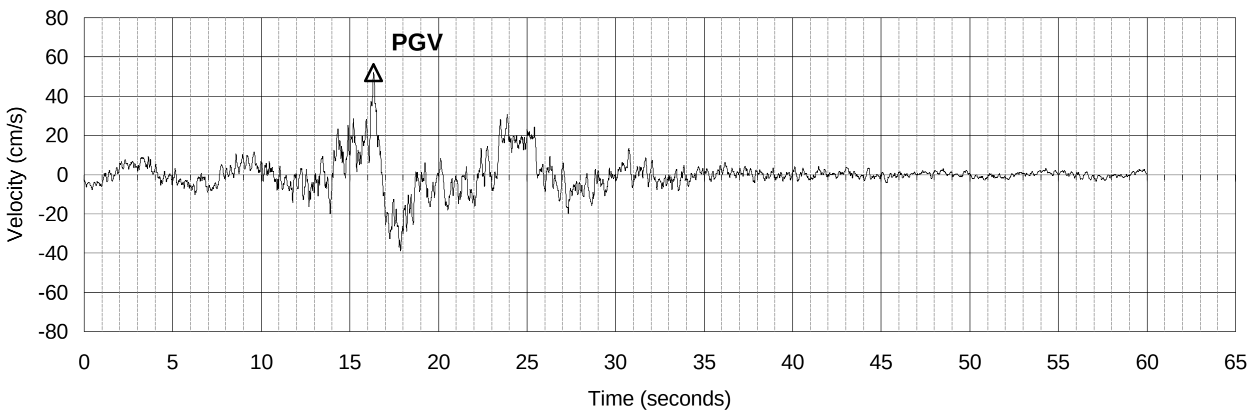

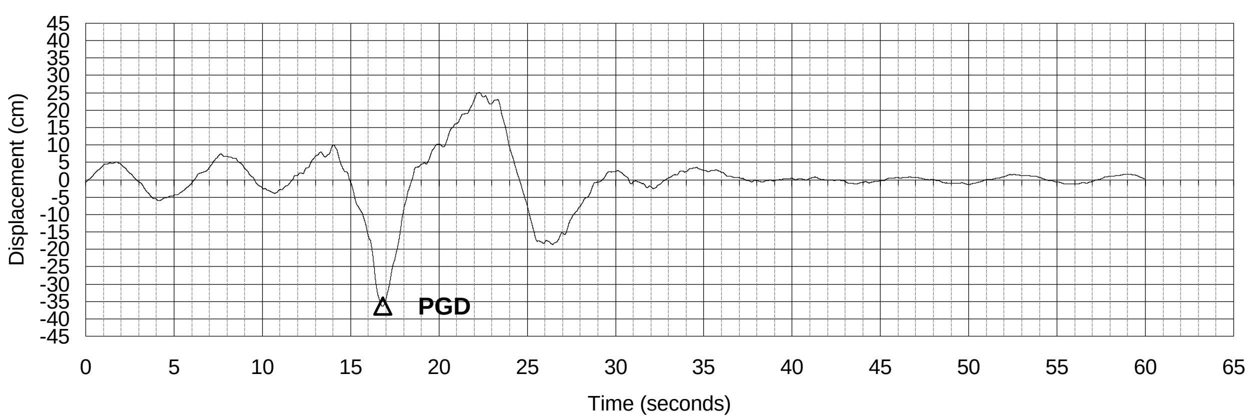

Peak Ground Motions

Acceleration	0.60 g
Velocity	52.06 cm/s
Displacement	36.34 cm

Seismic Ground Motion Study
Skookumchuck Dam
Lewis County, Washington

LF MEDIAN + 1s MCE
SYNTHETIC TIME HISTORY
VERTICAL

March 2001 21-1-08920-001

SHANNON & WILSON, INC.
Geotechnical and Environmental Consultants

FIG. B-12

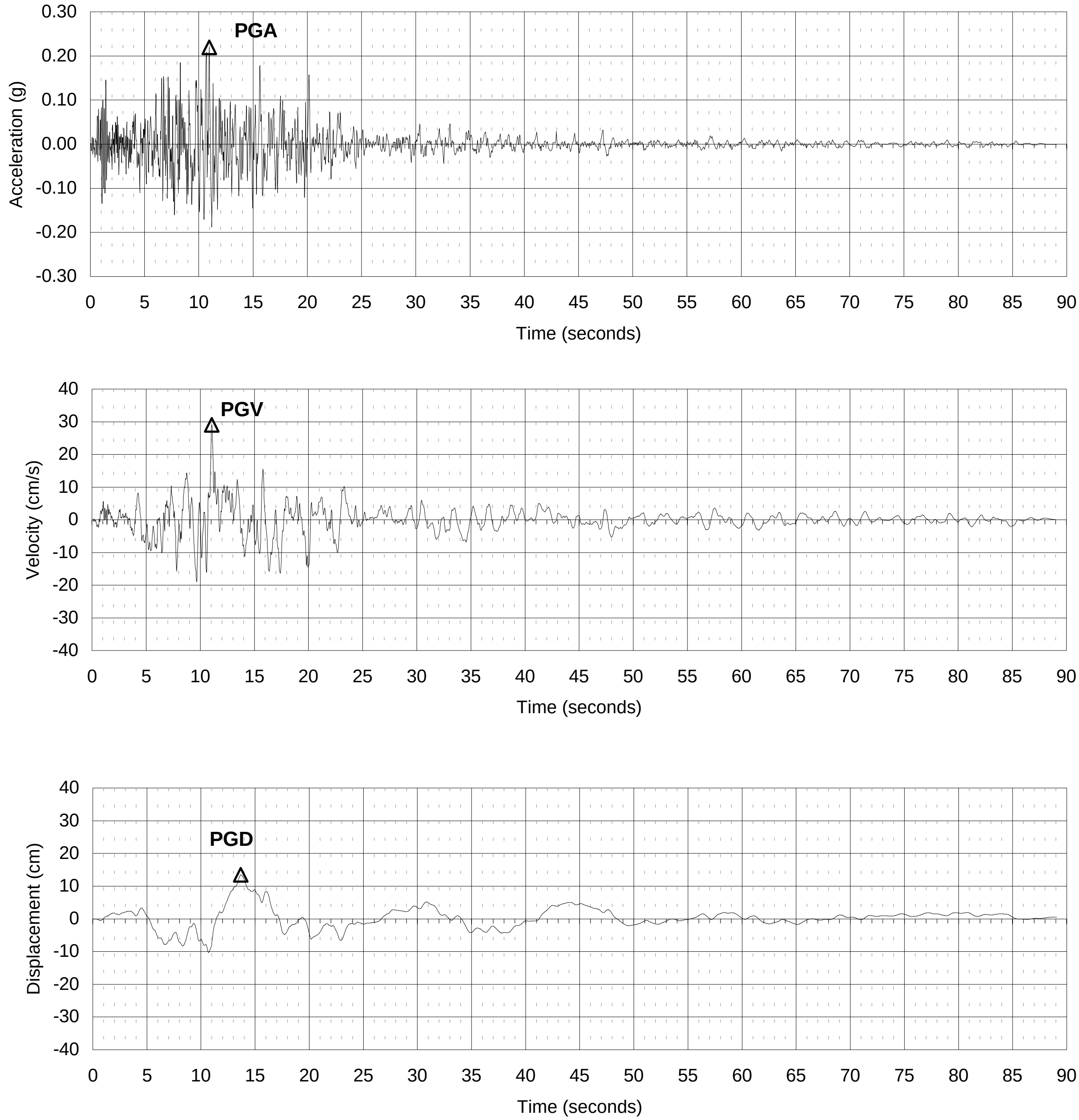

Peak Ground Motions

Acceleration	0.22 g
Velocity	29.08 cm/s
Displacement	13.47 cm

Seismic Ground Motion Study
Skookumchuck Dam
Lewis County, Washingtion

IDE
SCALED TIME HISTORY
1949 OLYMPIA 04 COMP

March 2001 21-1-08920-001

SHANNON & WILSON, INC.
Geotechnical and Environmental Consultants

FIG. B-13

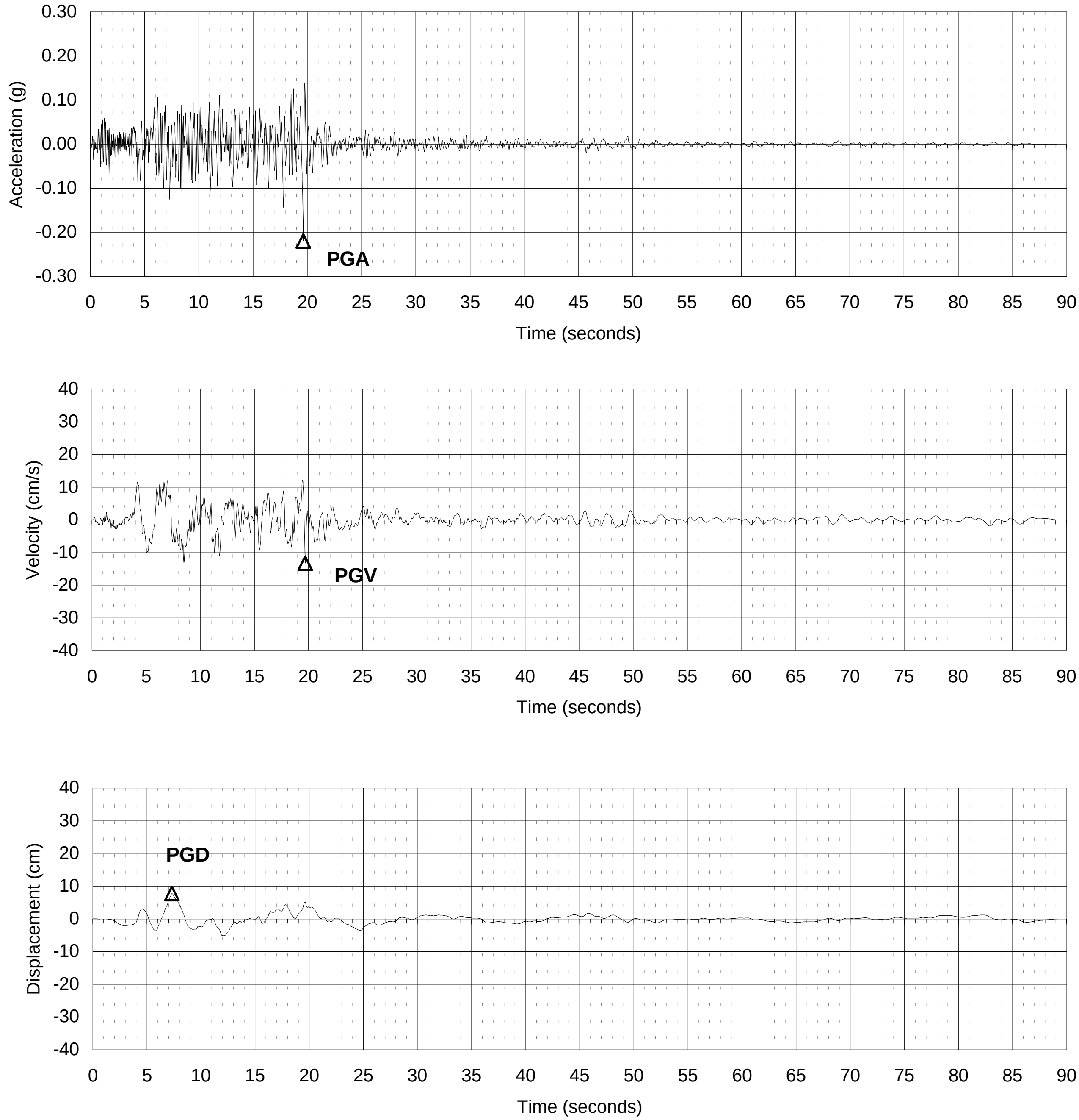

Peak Ground Motions

Acceleration	0.22 g
Velocity	13.28 cm/s
Displacement	7.73 cm

Seismic Ground Motion Study
Skookumchuck Dam
Lewis County, Washingtion

IDE
SCALED TIME HISTORY
1949 OLYMPIA 86 COMP

March 2001 21-1-08920-001

SHANNON & WILSON, INC.
Geotechnical and Environmental Consultants

FIG. B-14

3/7/01: olyvide.xls

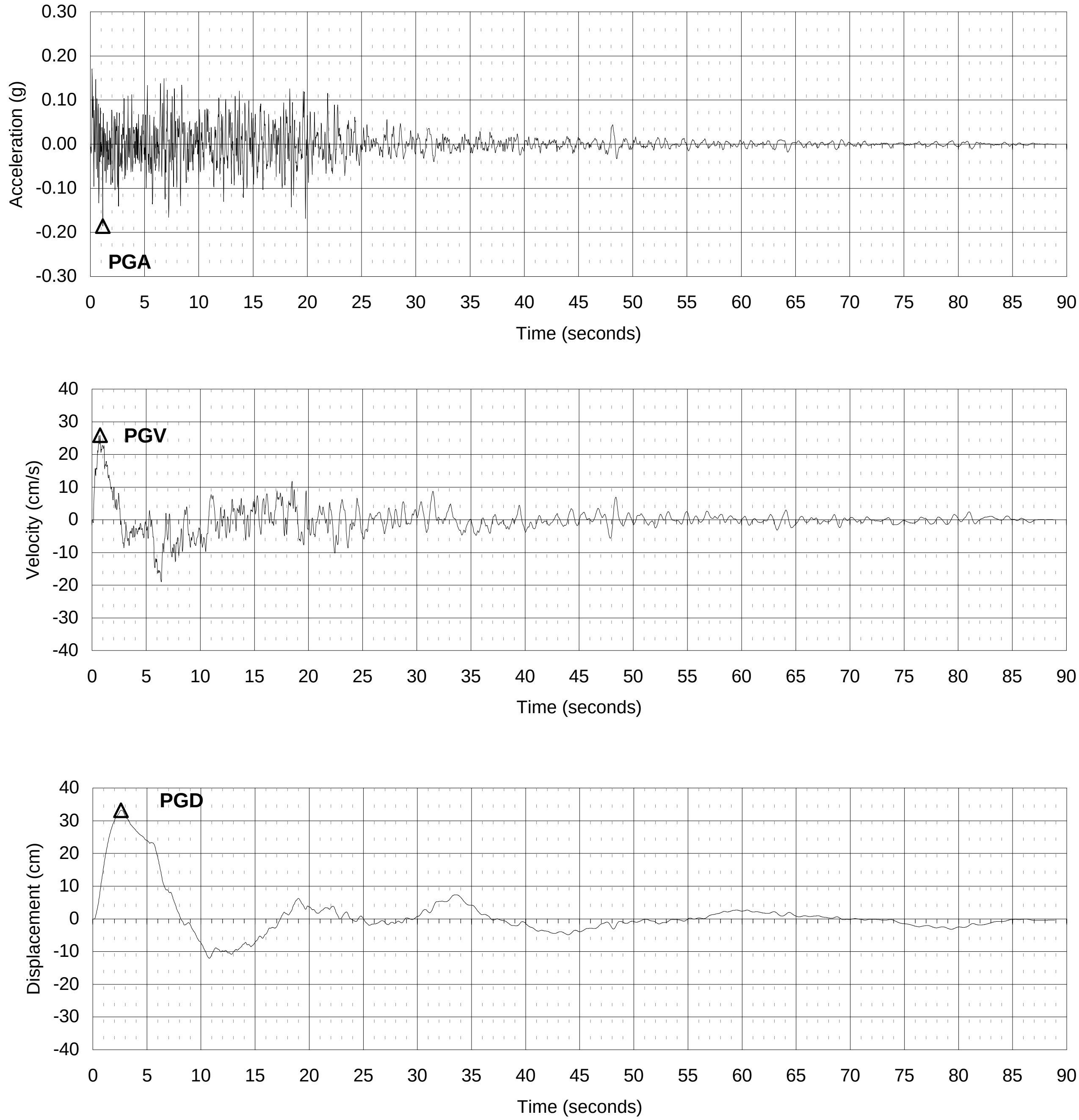

Peak Ground Motions

Acceleration	0.19 g
Velocity	25.93 cm/s
Displacement	33.22 cm

Seismic Ground Motion Study
Skookumchuck Dam
Lewis County, Washingtion

IDE
SCALED TIME HISTORY
1949 OLYMPIA VERTICAL COMP

March 2001 21-1-08920-001

SHANNON & WILSON, INC.
Geotechnical and Environmental Consultants

FIG. B-15

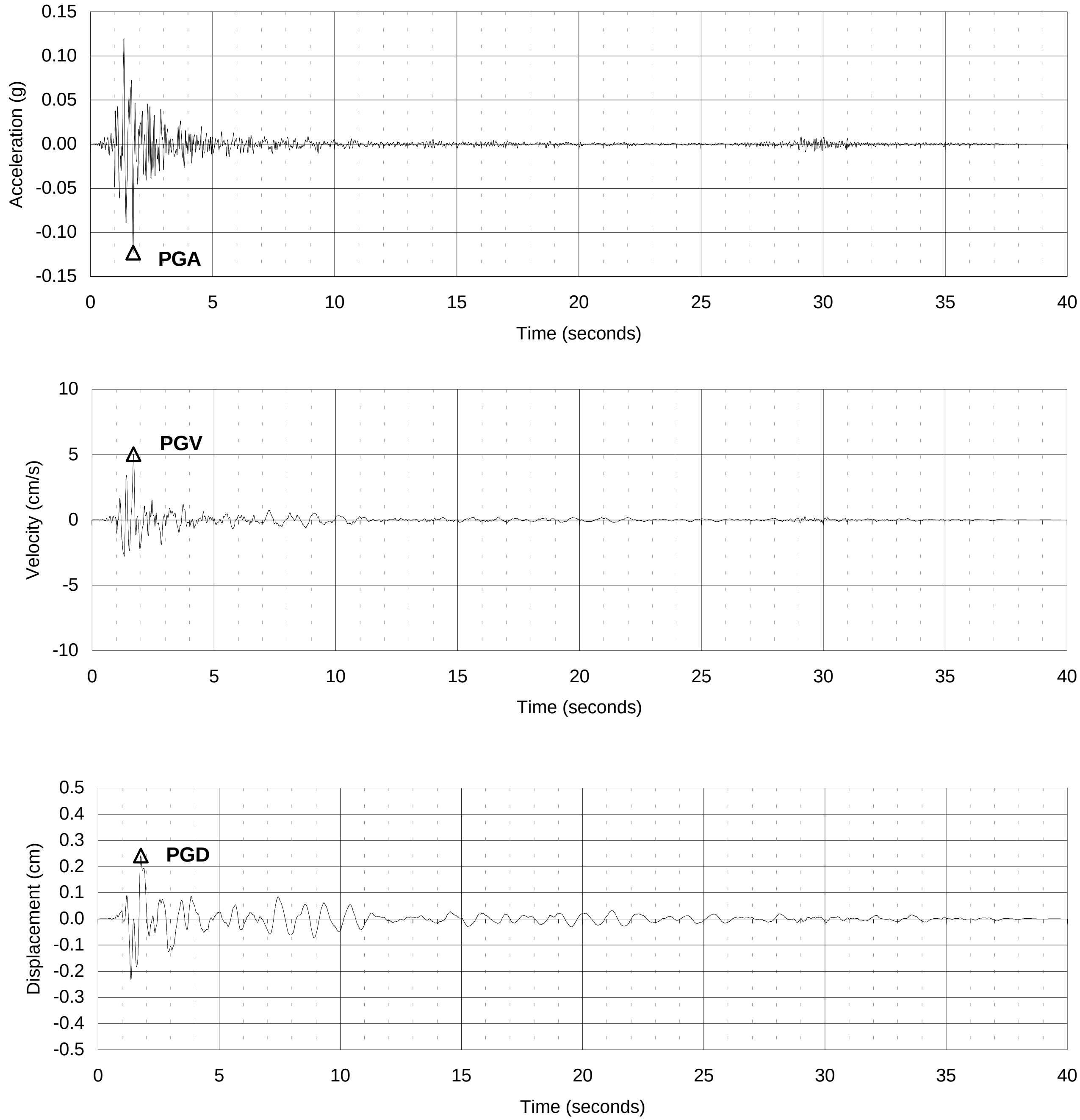

Peak Ground Motions

Acceleration	0.12 g
Velocity	5.04 cm/s
Displacement	0.24 cm

Seismic Ground Motion Study
Skookumchuck Dam
Lewis County, Washingtion

OBE
SCALED TIME HISTORY
GOLDEN GATE PARK 10 COMP

March 2001 21-1-08920-001

SHANNON & WILSON, INC.
Geotechnical and Environmental Consultants

FIG. B-16

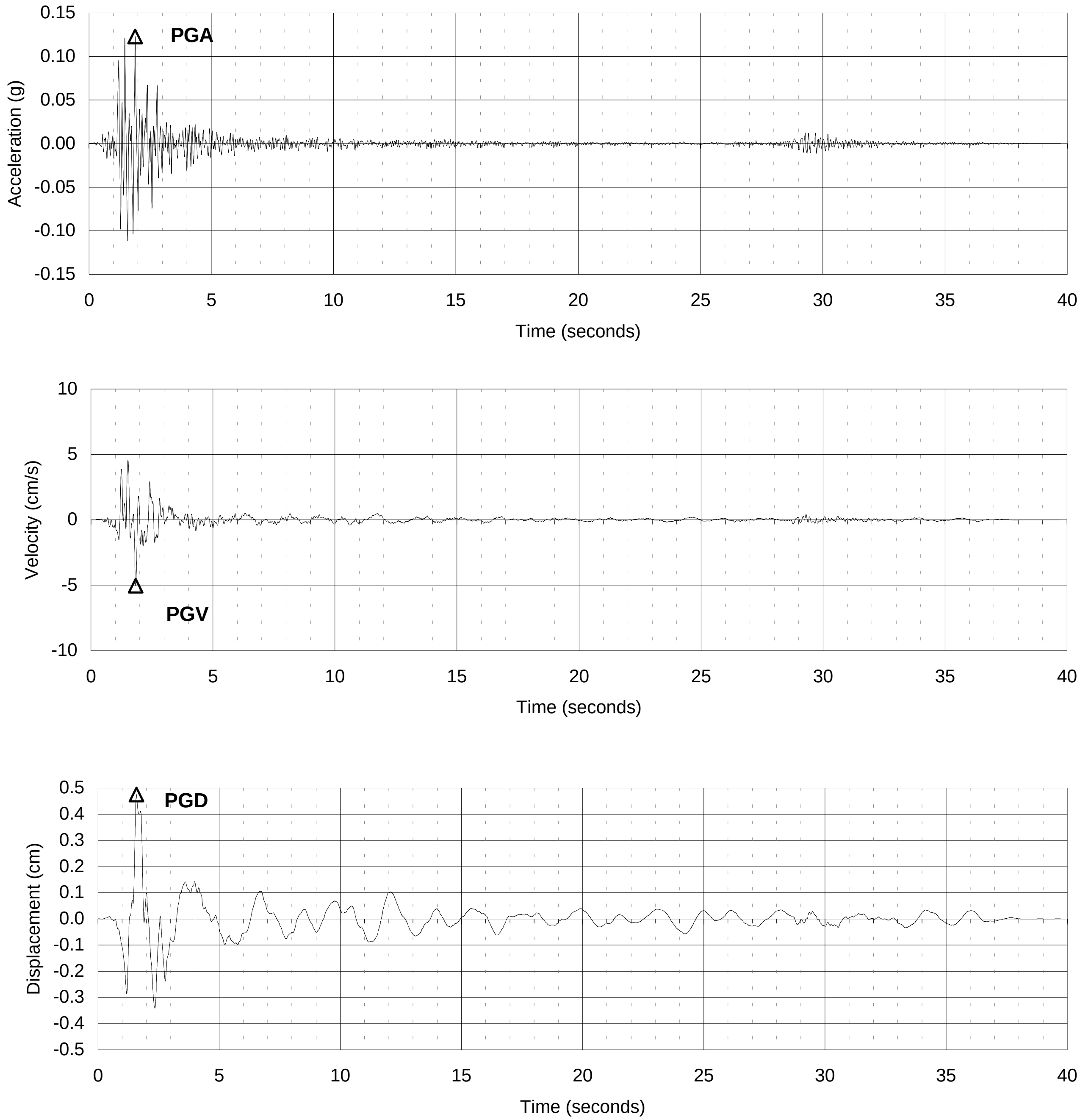

Peak Ground Motions

Acceleration	0.12 g
Velocity	5.04 cm/s
Displacement	0.47 cm

Seismic Ground Motion Study
Skookumchuck Dam
Lewis County, Washingtion

OBE
SCALED TIME HISTORY
GOLDEN GATE PARK 100 COMP

March 2001 21-1-08920-001

SHANNON & WILSON, INC.
Geotechnical and Environmental Consultants

FIG. B-17

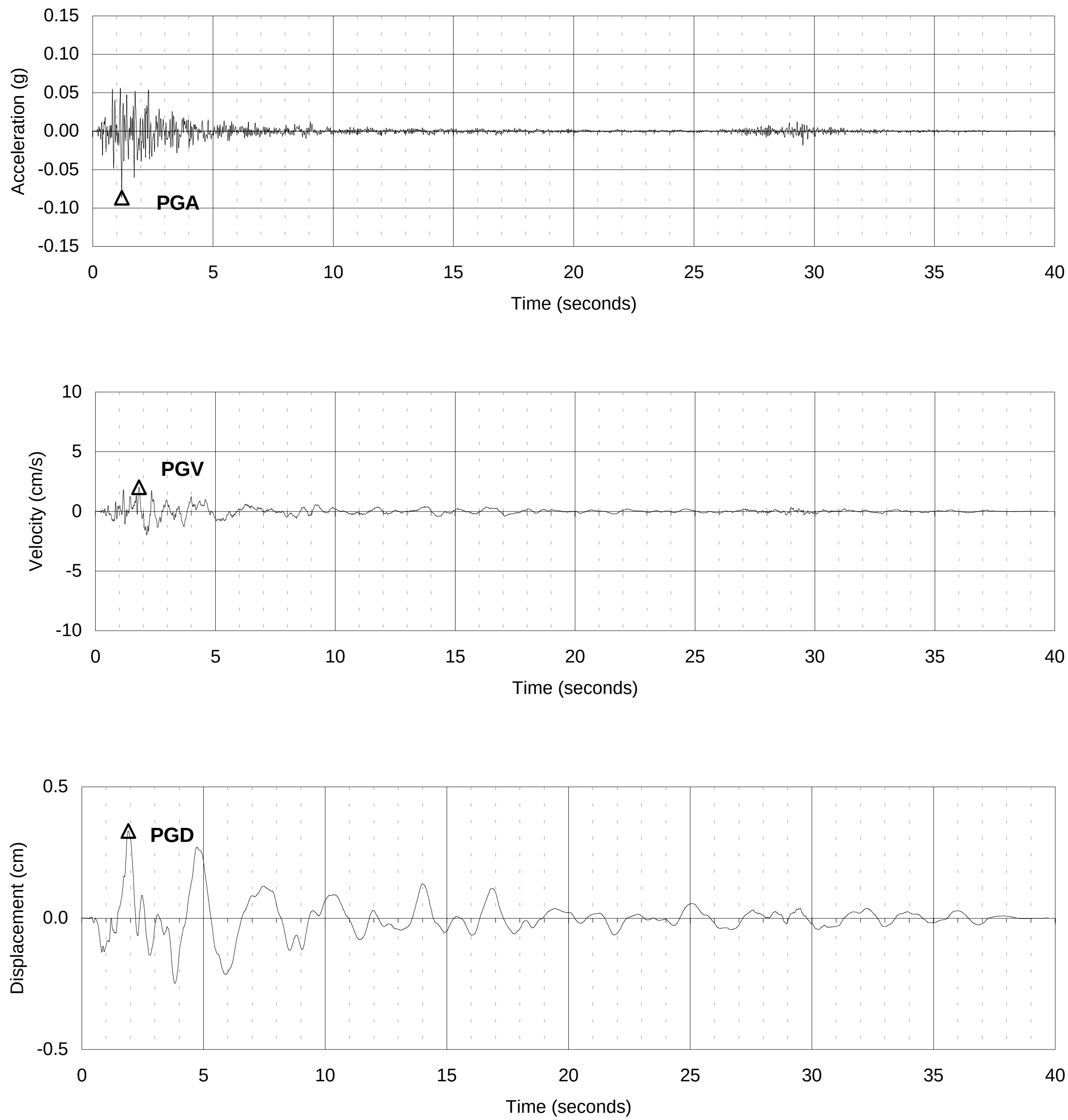

Peak Ground Motions

Acceleration	0.09 g's
Velocity	2.01 cm/s
Displacement	0.33 cm

Seismic Ground Motion Study
Skookumchuck Dam
Lewis County, Washingtion

OBE SCALED TIME HISTORY
GOLDEN GATE PARK
VERTICAL COMP

March 2001 21-1-08920-001

SHANNON & WILSON, INC.
Geotechnical and Environmental Consultants

FIG. B-18

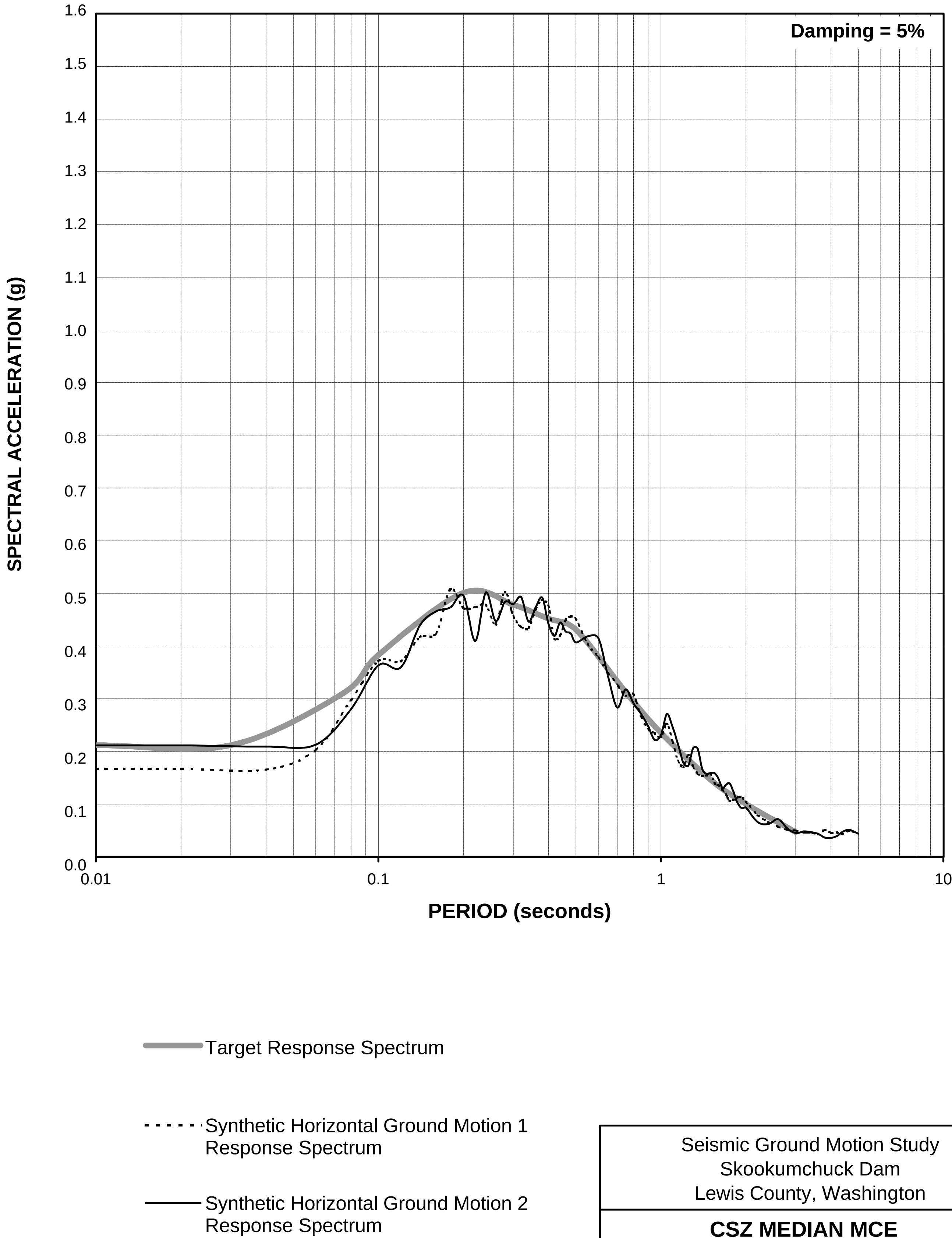

Seismic Ground Motion Study
Skookumchuck Dam
Lewis County, Washington

CSZ MEDIAN MCE HORIZONTAL RESPONSE SPECTRA

March 2001 21-1-08920-001

SHANNON & WILSON, INC.
Geotechnical and Environmental Consultants

FIG. B-19

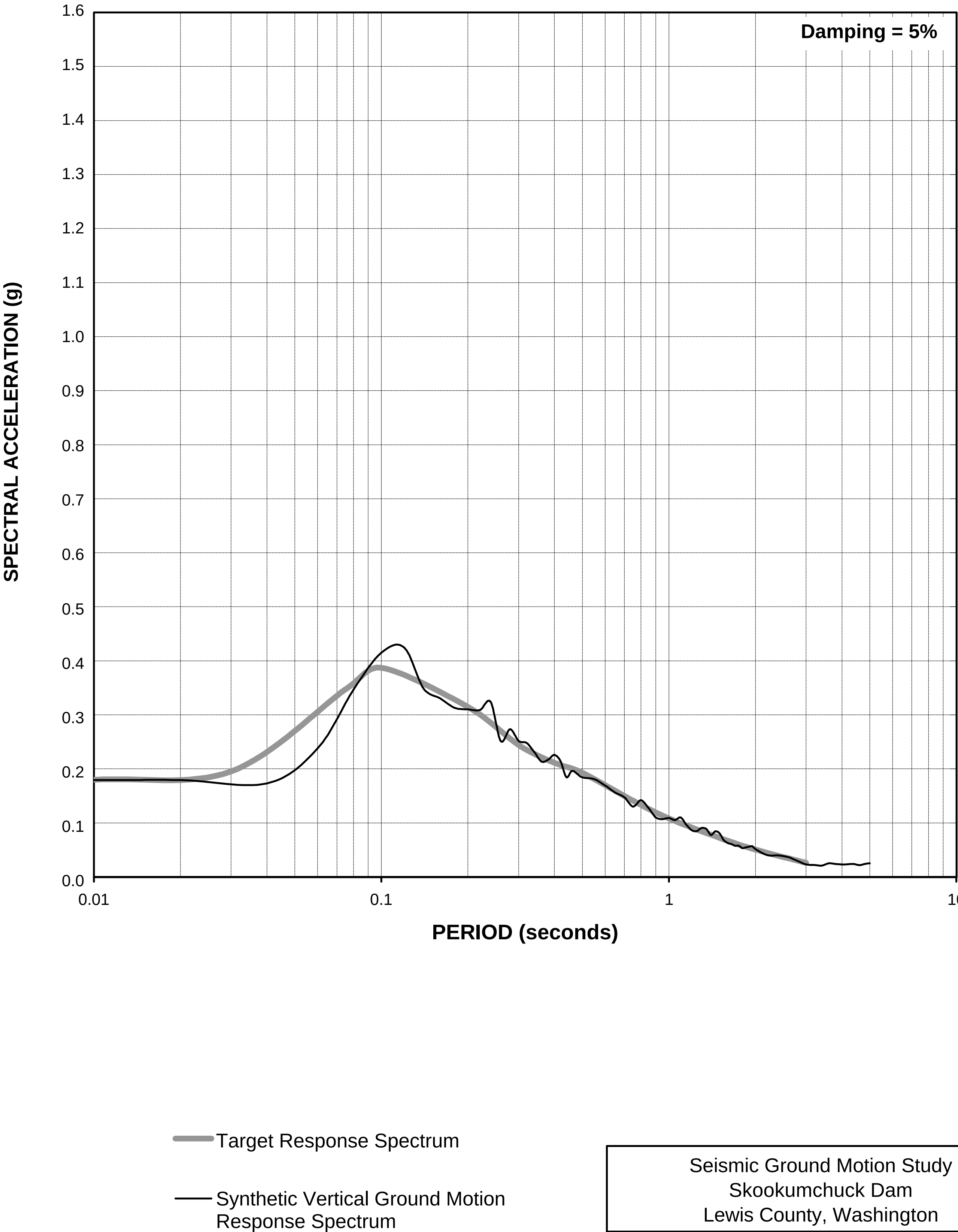

Seismic Ground Motion Study
Skookumchuck Dam
Lewis County, Washington

CSZ MEDIAN MCE VERTICAL RESPONSE SPECTRUM

March 2001 21-1-08920-001

SHANNON & WILSON, INC.
Geotechnical and Environmental Consultants

FIG. B-20

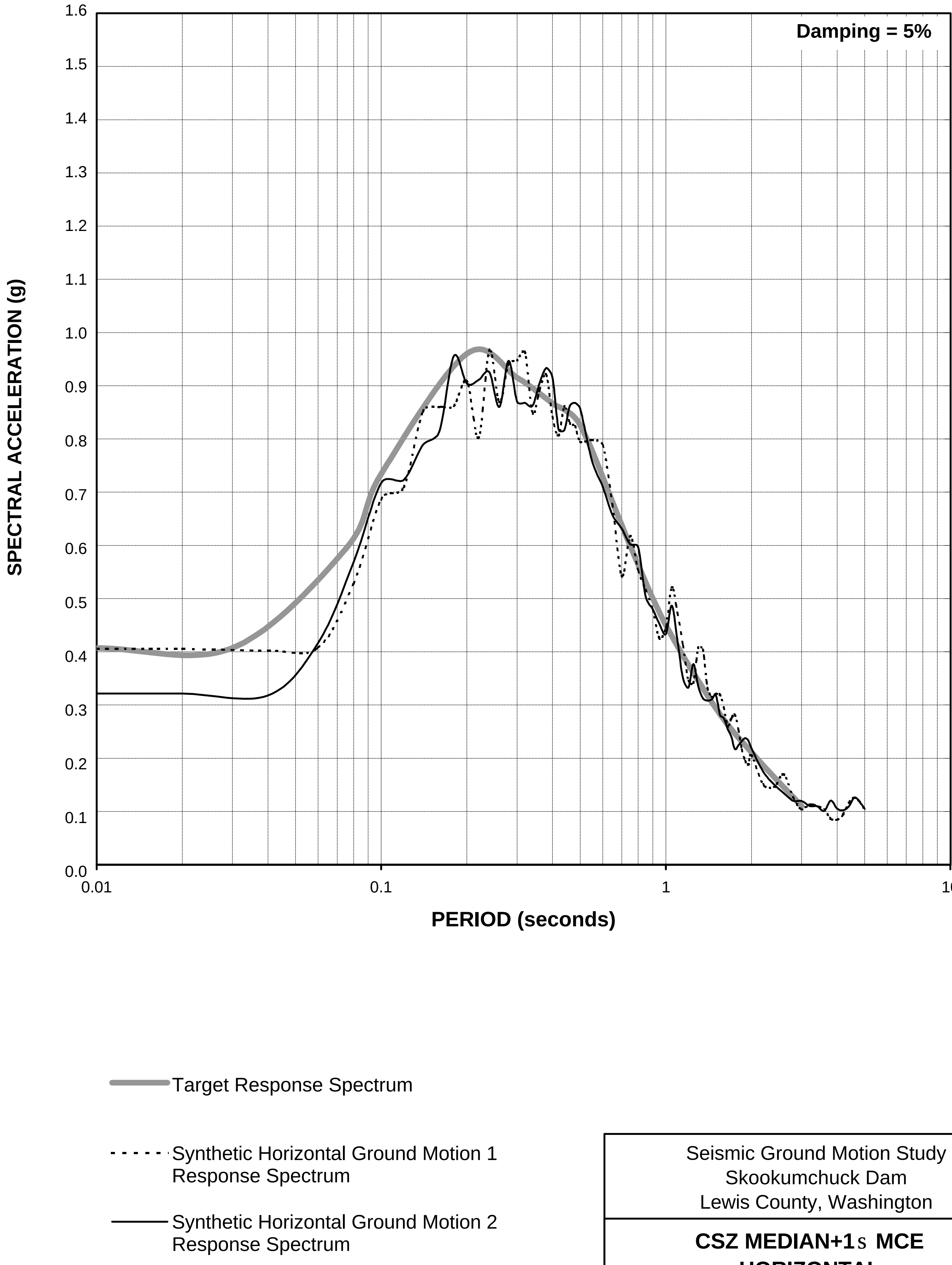

Seismic Ground Motion Study
Skookumchuck Dam
Lewis County, Washington

CSZ MEDIAN+1s MCE HORIZONTAL RESPONSE SPECTRA

March 2001 | 21-1-08920-001

SHANNON & WILSON, INC.
Geotechnical and Environmental Consultants

FIG. B-21

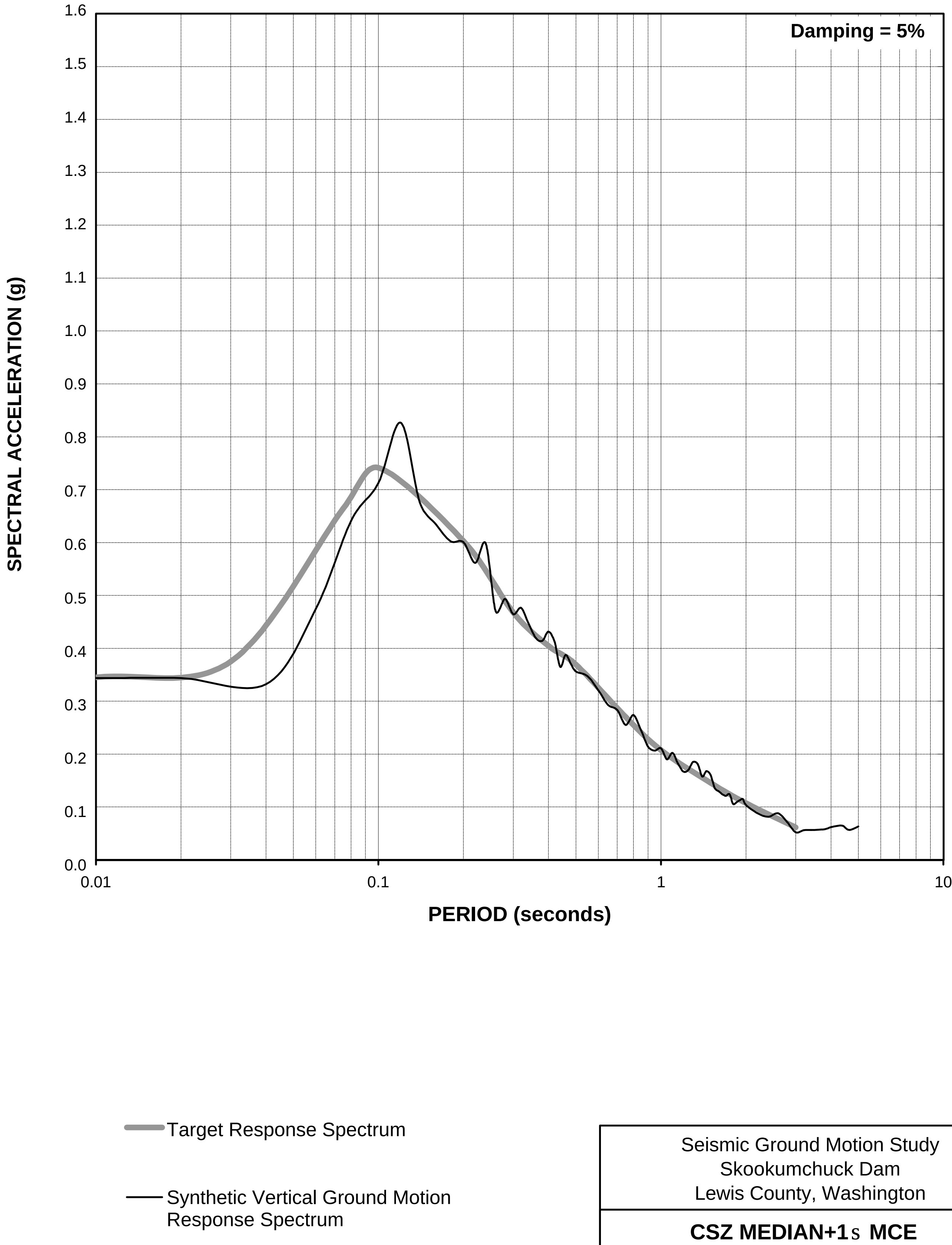

Seismic Ground Motion Study Skookumchuck Dam Lewis County, Washington	
CSZ MEDIAN+1s MCE VERTICAL RESPONSE SPECTRUM	
March 2001	21-1-08920-001
SHANNON & WILSON, INC. Geotechnical and Environmental Consultants	**FIG. B-22**

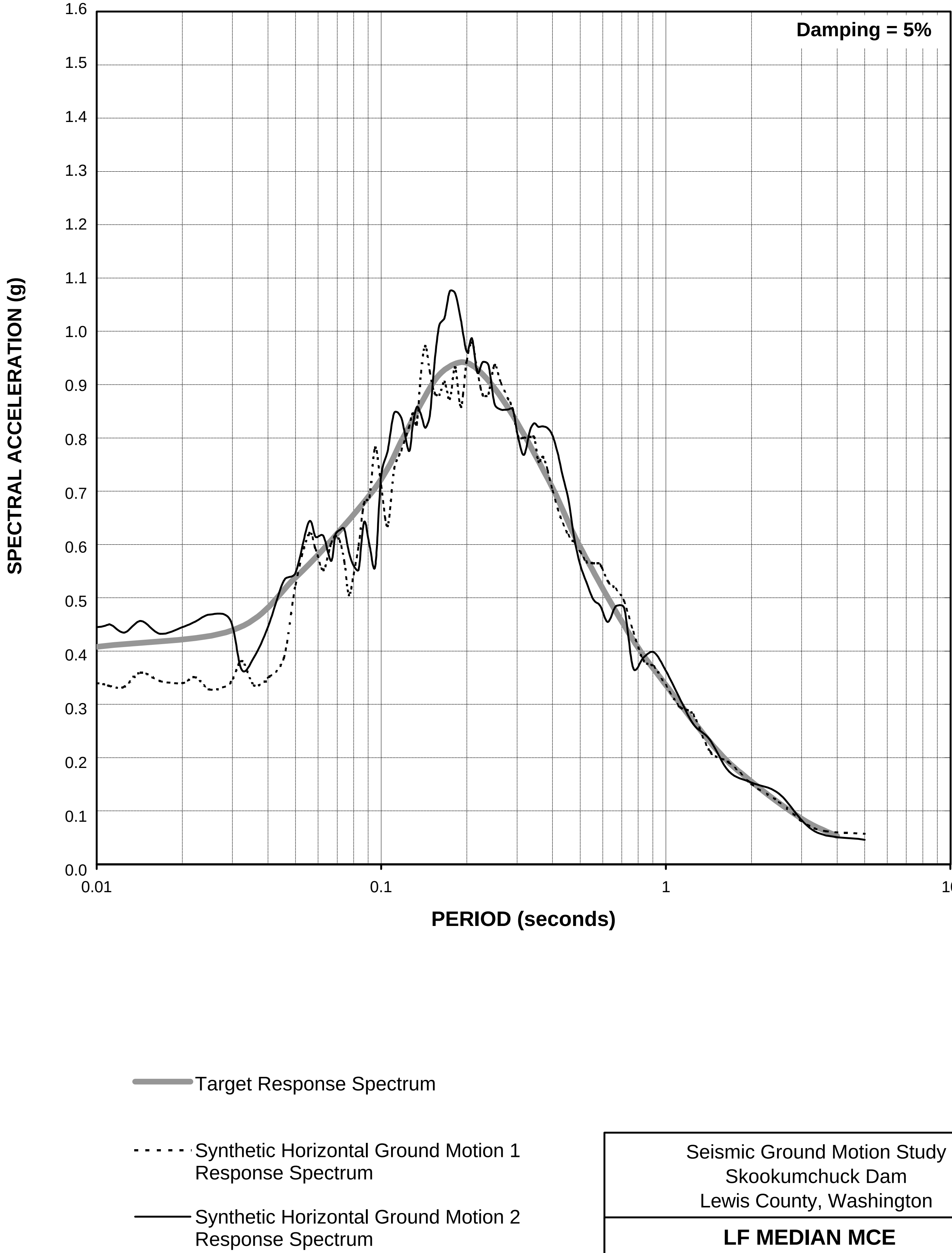

Seismic Ground Motion Study
Skookumchuck Dam
Lewis County, Washington

LF MEDIAN MCE HORIZONTAL RESPONSE SPECTRA

March 2001 | 21-1-08920-001

SHANNON & WILSON, INC.
Geotechnical and Environmental Consultants

FIG. B-23

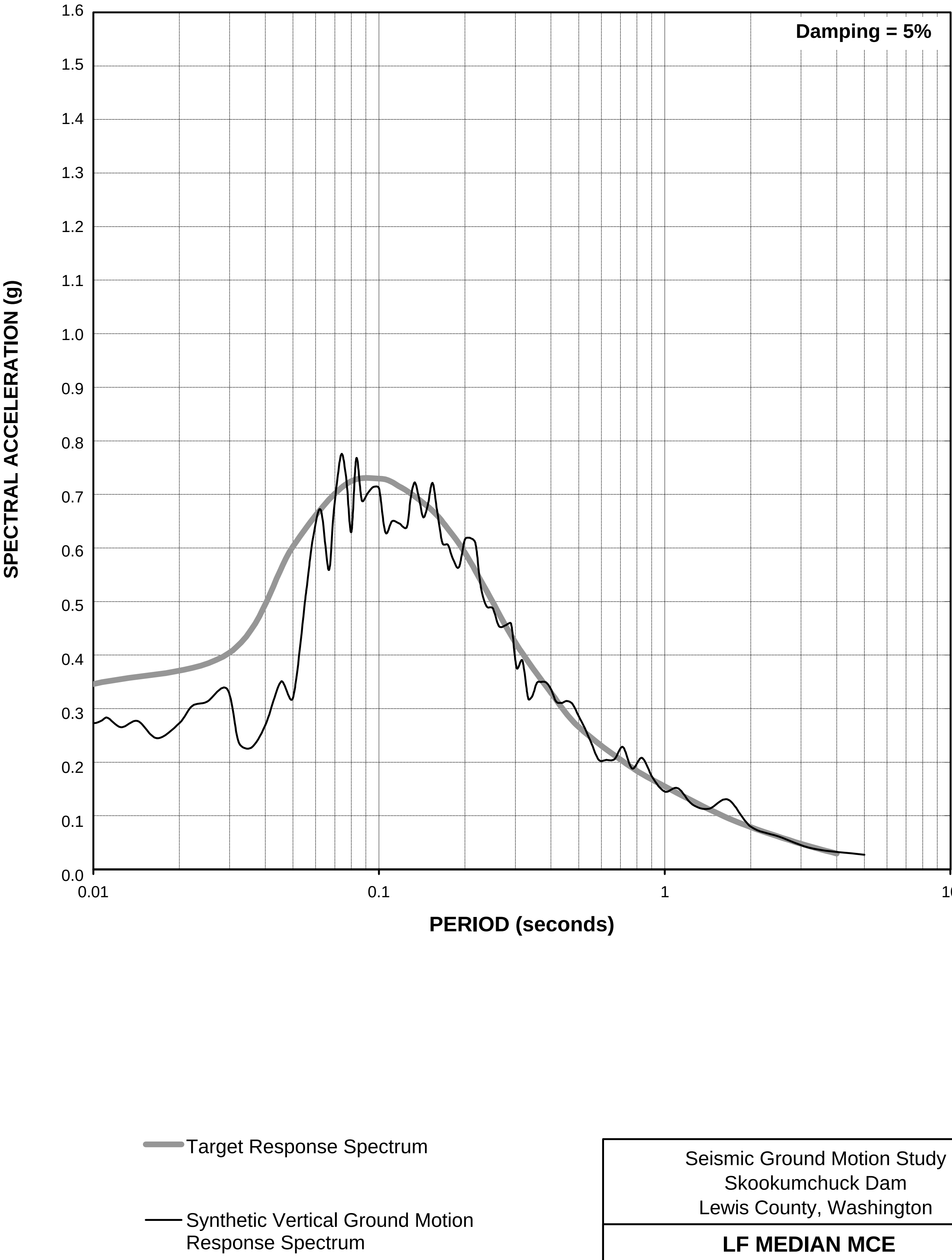

Seismic Ground Motion Study Skookumchuck Dam Lewis County, Washington	
LF MEDIAN MCE VERTICAL RESPONSE SPECTRUM	
March 2001	21-1-08920-001
SHANNON & WILSON, INC. Geotechnical and Environmental Consultants	**FIG. B-24**

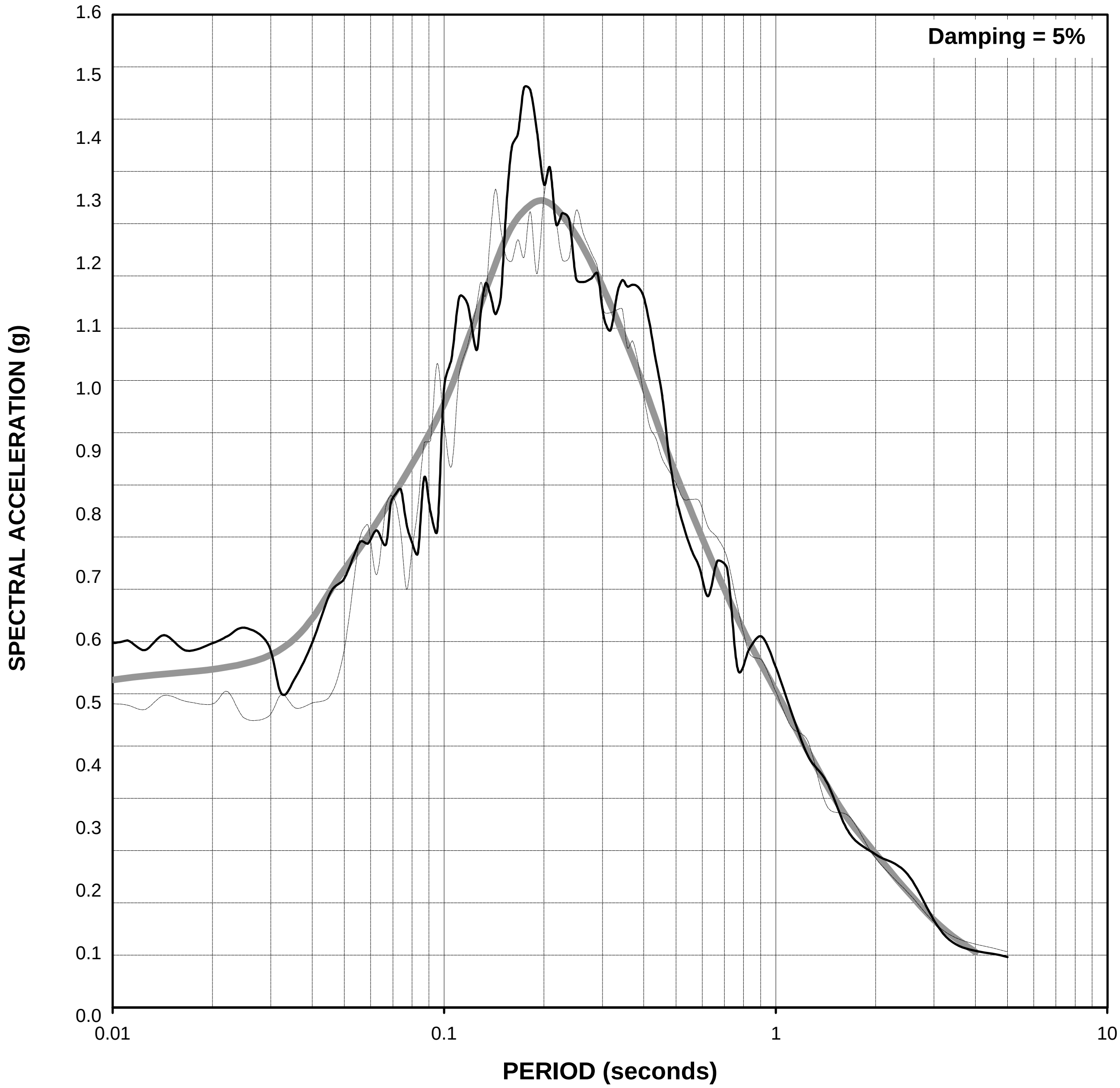

Target Response Spectrum

Synthetic Horizontal Ground Motion 1 Response Spectrum

Synthetic Horizontal Ground Motion 2 Response Spectrum

Seismic Ground Motion Study
Skookumchuck Dam
Lewis County, Washington

LF MEDIAN+1s MCE HORIZONTAL RESPONSE SPECTRA

March 2001 | 21-1-08920-001

SHANNON & WILSON, INC.
Geotechnical and Environmental Consultants

FIG. B-25

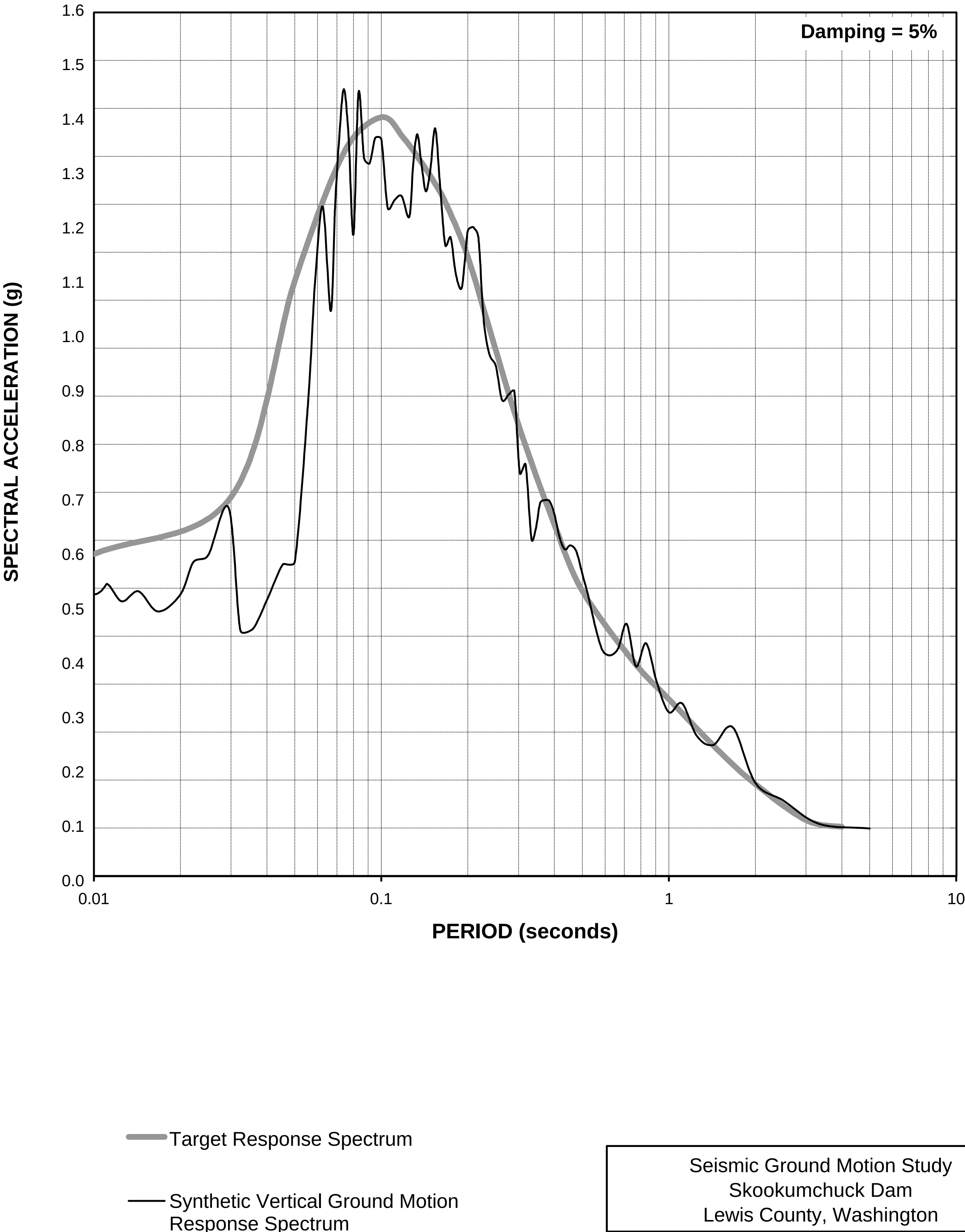

Seismic Ground Motion Study
Skookumchuck Dam
Lewis County, Washington

LF MEDIAN+1s MCE
VERTICAL
RESPONSE SPECTRUM

March 2001 21-1-08920-001

SHANNON & WILSON, INC.
Geotechnical and Environmental Consultants

FIG. B-26

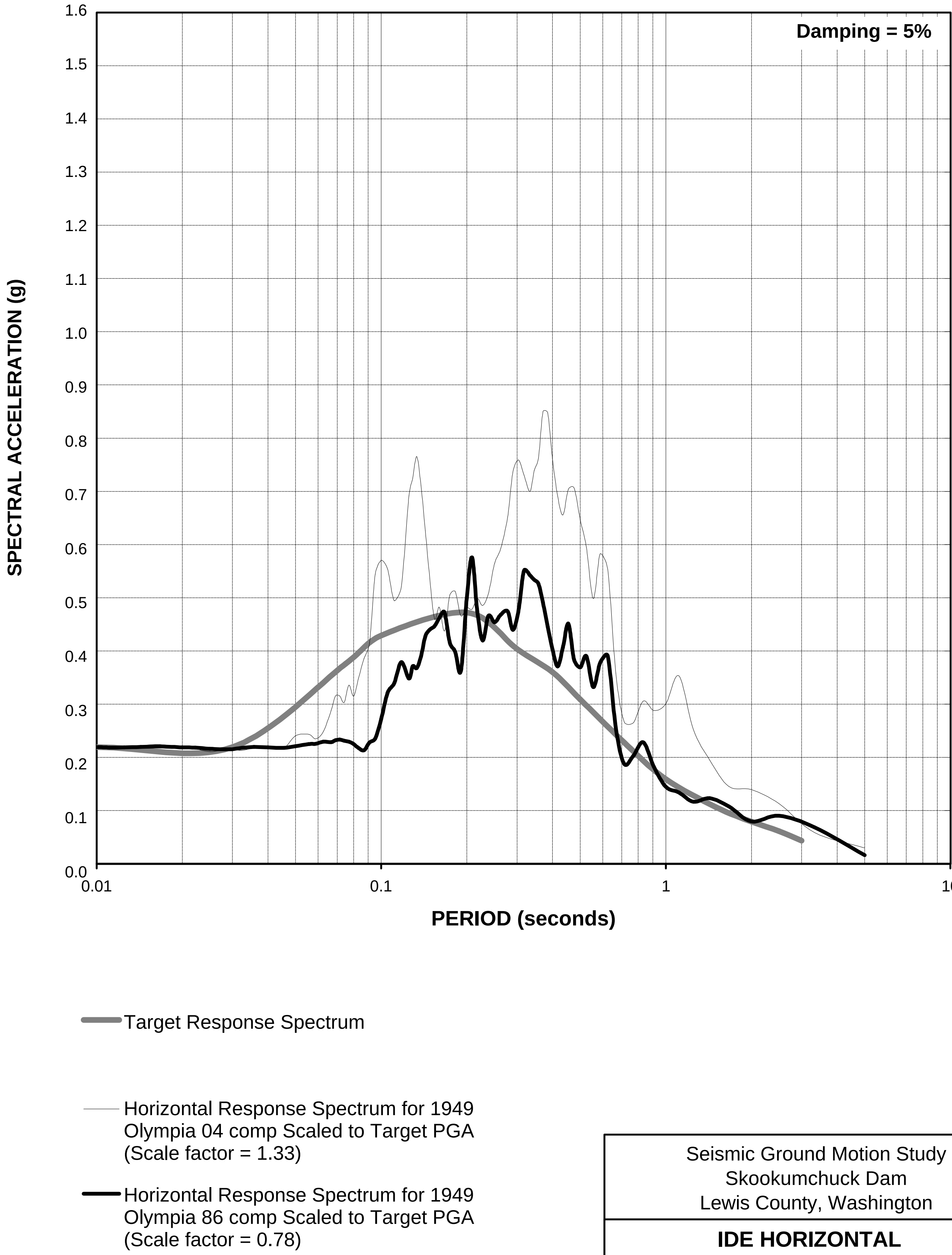

Seismic Ground Motion Study
Skookumchuck Dam
Lewis County, Washington

IDE HORIZONTAL RESPONSE SPECTRA SCALED TIME HISTORIES

March 2001 21-1-08920-001

SHANNON & WILSON, INC.
Geotechnical and Environmental Consultants

FIG. B-27

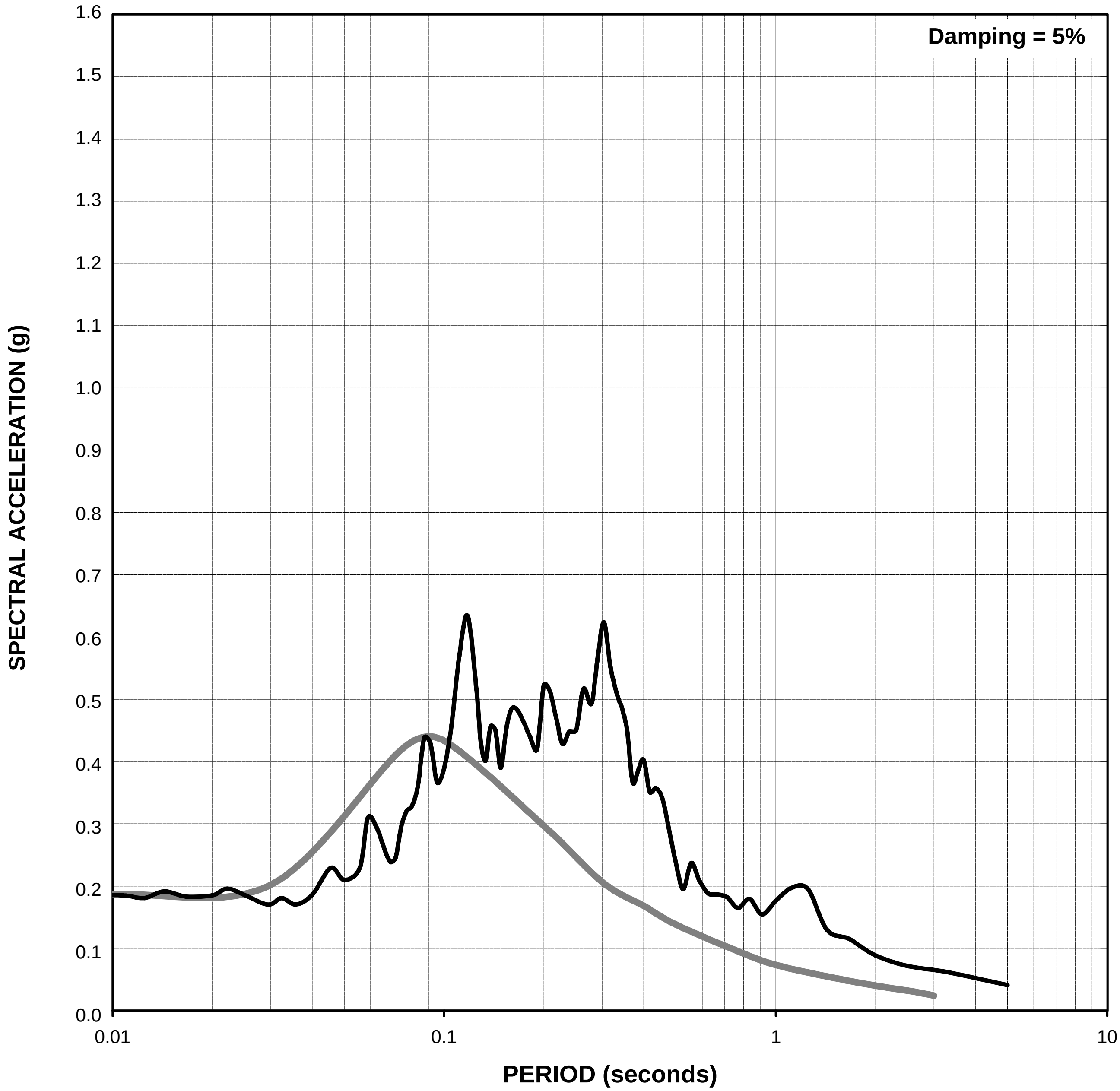

Target Vertical Response Spectrum

Vertical Response Spectrum for 1949 Olympia Vertical comp Scaled to Target PGA (Scale factor = 2.42)

Seismic Ground Motion Study
Skookumchuck Dam
Lewis County, Washington

IDE VERTICAL RESPONSE SPECTRUM SCALED TIME HISTORIES

March 2001 21-1-08920-001

SHANNON & WILSON, INC.
Geotechnical and Environmental Consultants

FIG. B-28

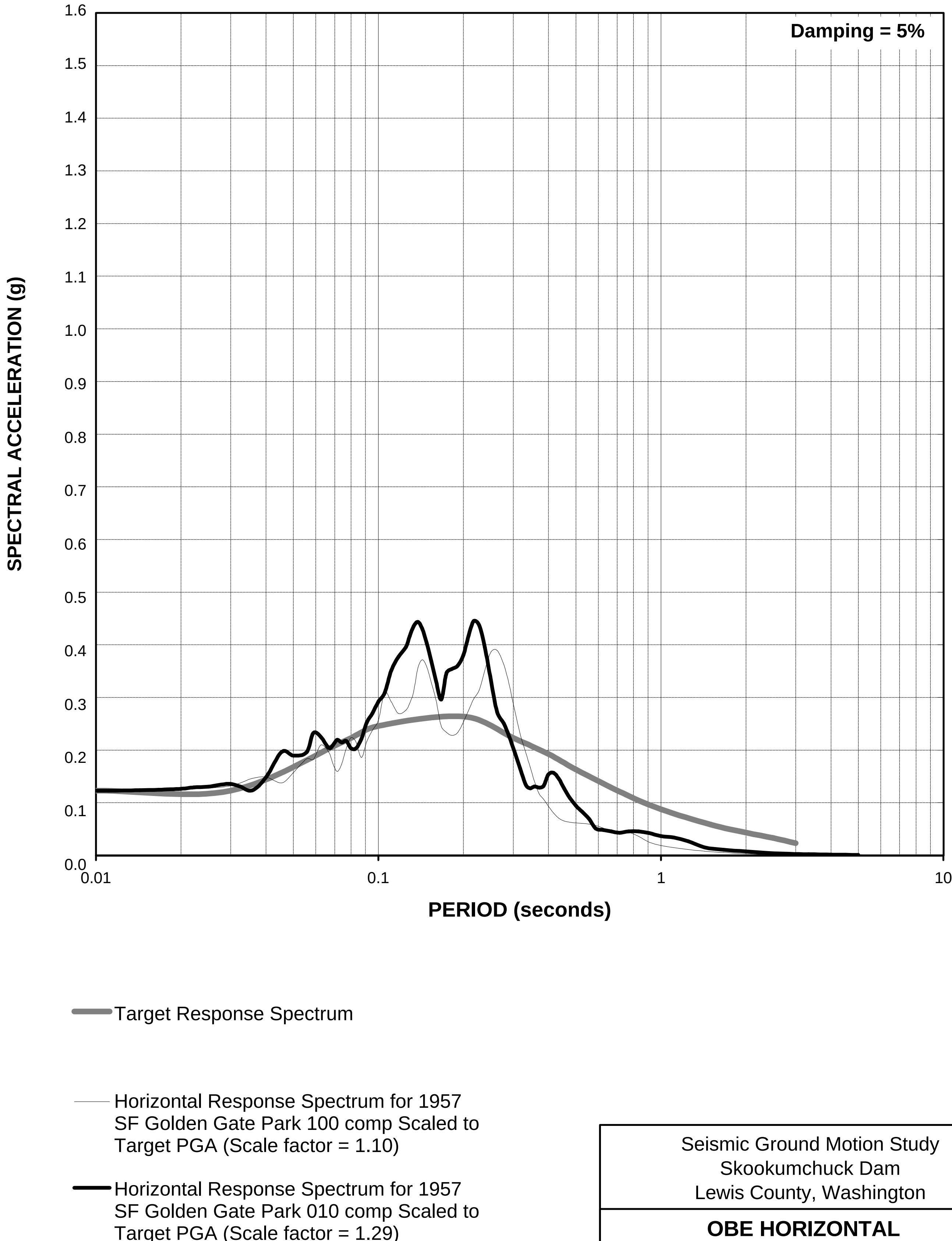

Seismic Ground Motion Study
Skookumchuck Dam
Lewis County, Washington

OBE HORIZONTAL RESPONSE SPECTRA SCALED TIME HISTORIES

March 2001 21-1-08920-001

SHANNON & WILSON, INC.
Geotechnical and Environmental Consultants

FIG. B-29

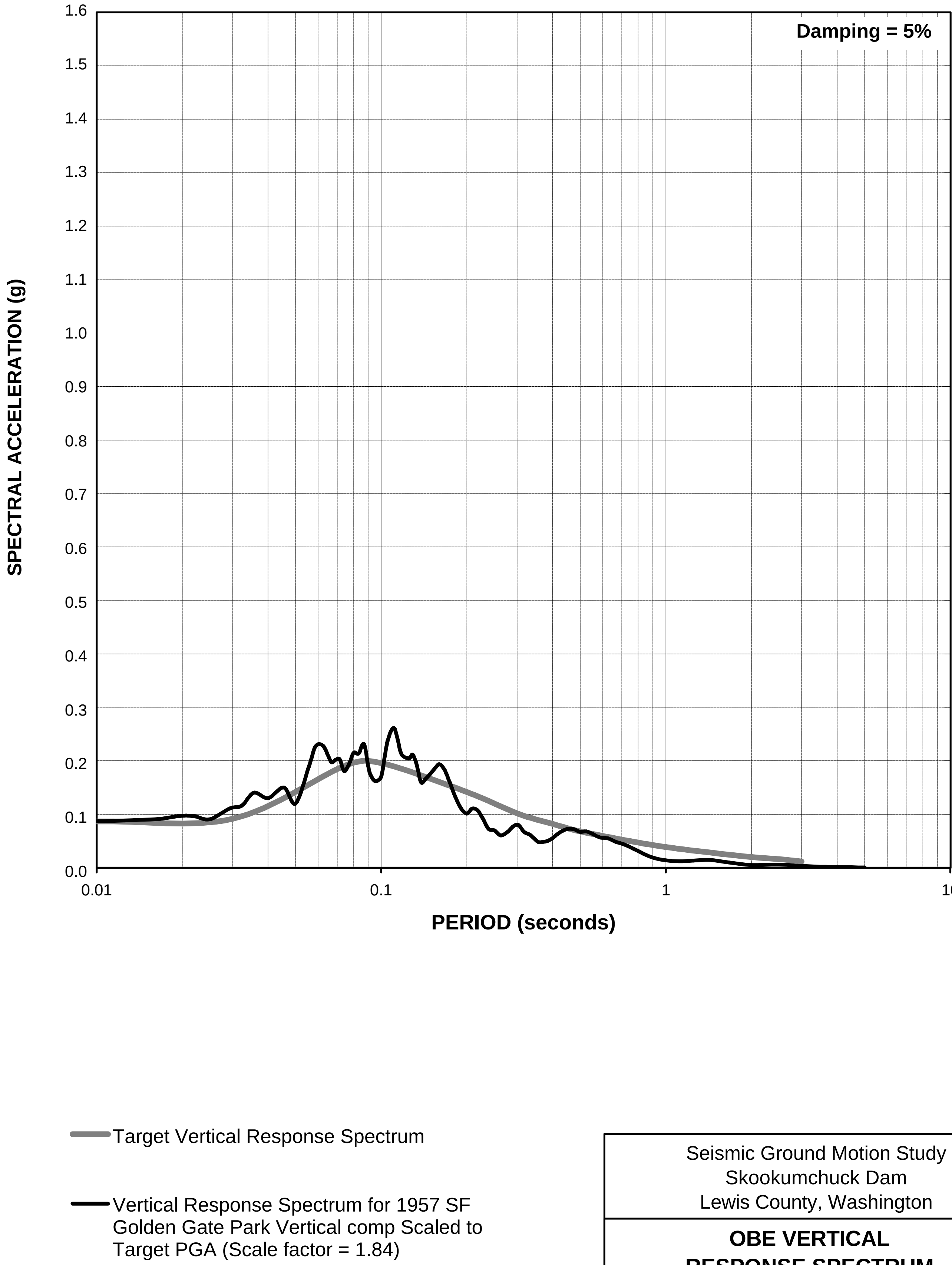

Seismic Ground Motion Study
Skookumchuck Dam
Lewis County, Washington

OBE VERTICAL RESPONSE SPECTRUM SCALED TIME HISTORIES

March 2001 21-1-08920-001

SHANNON & WILSON, INC.
Geotechnical and Environmental Consultants

FIG. B-30